

Development of an Aerobic Biocathode for Microbial Fuel Cells

Edward Michael Milner

A thesis presented for the degree of
Doctor of Philosophy

Chemical Engineering and Advanced Materials
Newcastle University

October 2015

Abstract

Microbial fuel cells (MFCs), which convert organic waste to electricity using microbes, could be used to make the wastewater infrastructure more energy efficient and sustainable. However, the chemical catalysts which catalyse the oxygen reduction reaction (ORR) at the cathode of MFCs are expensive and unsustainable. Mixed community aerobic biocathode biofilms are an alternative to chemical catalysts. However, little is known about the bacteria, their metabolism, and their mechanisms of electron transfer with the electrode.

A novel 4-electrode method was used to determine the minimum potential for production of peroxide on a porous carbon felt biocathode support. Biocathodes with a high onset potential for the ORR of +0.4 V vs Ag/AgCl were then cultivated in poised-potential half-cells at working electrode potentials of -0.1 and +0.2 V vs Ag/AgCl. These biofilms show what may be an electrode potential-dependent switch in an electron transfer mechanism from -0.1 to +0.2 V vs Ag/AgCl. The biofilms were dominated by unidentified *Gammaproteobacteria*, not present in unpolarised controls, which were most likely responsible for the ORR catalysis. This is the first time that a link has been made between a high onset potential for ORR catalysis of +0.4 V vs Ag/AgCl, and the bacteria responsible for this catalysis.

Using half-cells, the aerobic biocathodes were enriched and used to replace existing abiotic Pt cathodes in operational MFCs. MFC performance was found to be limited by high external resistance and oxygen mass transfer. The MFC with a biocathode achieved a 9-fold increase in peak power from 7 to 62 $\mu\text{W}/\text{cm}^2$ using a carbon electrode with a biocathode compared to a plain carbon electrode. A simple battery separator was shown to be as effective as an ion exchange membrane through novel abiotic analysis of this membrane, and the MFC with a battery separator was found to give similar performance to the MFC with an ion exchange membrane.

Acknowledgements

This work would not have been possible without the guidance, experience and friendship of a number of people. I would like to acknowledge them all here.

Thank you to my supervisors, Dr Eileen Yu, Professor Keith Scott, Professor Ian Head, Professor Tom Curtis, for giving me the opportunity to carry out research in an interesting and diverse area, and having patience with me whilst I learn a new field. I would especially like to thank Dr Eileen Yu, for her feedback on my research, and for having faith in my abilities.

Thanks go to the workshop team in CEAM, for their experience and help. I would especially like to thank Jamie Halliday for his skill and attention to detail in making the odd things which I needed through the years, and Simon Daley, for all of his hard work in building heat mats and setting up data loggers. Thanks go to Dorin Popescu, Angella Sherry, Julia R. de Rezende, Donna Swan and Sarah Jane Smith, for help and advice in community analysis. Thanks also go to David Race and Patrick Orme, for technical advice and support.

I would especially like to thank Martin Spurr and Dorin Popescu, for lively and informative discussions on different scientific topics, and for being good friends.

I dedicate this work to my family and my girlfriend Stephanie. Thank you for your love and support. I look forward to seeing you all a lot more!

Table of Contents

1	Introduction	1
1.1	Renewable Energy, Wastewater treatment and Microbial Fuel Cells	1
1.2	Why Aerobic Biocathodes for Microbial Fuel Cells?	2
1.3	Aims and Objectives	3
1.4	Contention	4
1.5	Chapter Summary	4
2	Literature Review on Aerobic Biocathodes	6
2.1	Microbial Fuel Cells	6
2.1.1	Background	6
2.1.2	Basis of electrical power production in an MFC	7
2.1.3	The chemical ORR catalysts used in MFCs	9
2.2	The Aerobic Biocathodes used in MFCs	10
2.2.1	Background	10
2.2.2	Aerobic chemolithotrophic bacteria	11
2.2.3	Direct application of known aerobic chemolithotrophic bacteria as aerobic biocathodes in MFCs	13
2.2.4	Mixed-community aerobic biocathodes in MFCs	15
2.3	The Bacteria Responsible for ORR Catalysis in Mixed Community Aerobic Biocathodes	20
2.4	Mechanism of Electron Transfer in Aerobic Biocathodes	24
2.4.1	Background	24
2.4.2	Direct ORR catalysis by direct electron transfer	25
2.4.3	Direct ORR catalysis by mediated electron transfer	26
2.5	The Effect of Poised-potential on Aerobic Biocathodes	27
2.5.1	Background	27
2.5.2	Aerobic biocathode poised-potential studies	28
2.5.3	Evaluation of carbon materials for poised-potential aerobic biocath- ode half-cells	29

2.6	Conventional MFC Systems and MFC Systems with an Aerobic Biocathode	31
2.7	Operation of Aerobic Biocathode MFC Systems	33
2.7.1	The effect of light on the performance of acetate-fed MFCs	33
2.7.2	The effect of external resistance on aerobic biocathode MFC performance	34
2.7.3	The effect of oxygen mass transfer on aerobic biocathode MFC performance	36
2.8	Electrode Materials for Aerobic Biocathode MFC Systems	36
2.8.1	Planar carbon electrodes for MFCs	36
2.8.2	Porous carbon electrodes for MFCs	38
2.8.3	Surface treatments and coatings	40
2.8.4	Oxygen diffusion electrodes	41
2.9	Membranes for Aerobic Biocathode MFC Systems	45
2.9.1	Fundamental properties and ion-selective membranes	45
2.9.2	Non-ion selective separators	47
2.10	Scale-up of Aerobic Biocathode MFC Systems	52
2.11	Summary	54
3	Materials and Methods	57
3.1	Electrochemical Methods	57
3.1.1	Basic electrochemical theory	57
3.1.2	Open circuit potential	58
3.1.3	Potentiostatic methods	58
3.1.4	Sweep methods	59
3.1.5	Electrochemical methods for MFCs	60
3.2	Microbiological Methods	64
3.2.1	Sampling	64
3.2.2	Biofilm imaging	64
3.2.3	Biomass determination	65
3.2.4	Community analysis	65
3.3	Analytical Methods	69
3.3.1	Sampling	69
3.3.2	Dissolved oxygen concentration determination	70
3.3.3	Acetate concentration determination	70
3.3.4	pH measurement	70
3.3.5	Cation and anion concentration determination	70
3.4	Materials Characterisation for Aerobic Biocathode Half-Cells	71
3.4.1	Setup	71

3.4.2	Electrochemical characterisation	73
3.5	Setup, Operation and Characterisation of Aerobic Biocathode Half-Cells . . .	73
3.5.1	Setup	73
3.5.2	Operation	75
3.5.3	Electrochemical characterisation	75
3.5.4	Calculation of coulombic efficiency	76
3.5.5	Oxygen mass transfer experiment	77
3.5.6	Microbiological characterisation	77
3.6	Membrane Characterisation for Microbial Fuel Cells	78
3.6.1	Overview	78
3.6.2	Determination of membrane principal charge carriers	78
3.6.3	Determination of membrane diffusion coefficients for acetate and oxygen	80
3.6.4	Determination of membrane ohmic resistance	82
3.7	Setup, Operation and Characterisation of Microbial Fuel Cells	83
3.7.1	Setup and operation	83
3.7.2	Electrochemical characterisation	87
3.7.3	Calculation of coulombic efficiency	88
3.7.4	Membrane characterisation	88
4	A Novel 4-Electrode Method for the Electrochemical Investigation of Porous Carbon Felt Material as a Biocathode Support	89
4.1	Introduction	89
4.2	Experimental	90
4.3	Results and Discussion	91
4.3.1	Potentials for the formation of peroxide on HNO ₃ -treated and un- treated carbon felts	91
4.3.2	Mathematical model describing the solution peroxide concentration with time	95
4.4	Conclusions	97
5	Aerobic Biocathodes with a High Onset Potential for the Oxygen Reduction Re- action of +0.4 V vs. Ag/AgCl are Dominated by Unidentified Gammaproteobac- teria	99
5.1	Introduction	99
5.2	Experimental	100
5.3	Results and Discussion	104
5.3.1	Development of aerobic biocathodes	104

5.3.2	Electrochemical performance of aerobic biocathodes grown at -0.1 and +0.2 V poised-potential	115
5.3.3	The mechanism of electron transfer in aerobic biocathodes grown at -0.1 and +0.2 V poised-potential	126
5.3.4	Bacterial community analysis of aerobic biocathode biofilms grown at -0.1 and +0.2 V poised-potential	135
5.4	Conclusions	141
6	The Effect of Light on the Performance of Acetate-fed Microbial Fuel Cells	145
6.1	Introduction	145
6.2	Experimental	146
6.3	Results and Discussion	148
6.3.1	Electrochemical characterisation of three identical MFCs exposed to alternating light and dark conditions	148
6.3.2	Electrochemical characterisation of an MFC kept in the dark and an identical MFC kept in the light	151
6.4	Conclusions	157
7	The Effect of External Resistance and Oxygen Mass Transfer on the Performance of Aerobic Biocathode Microbial Fuel Cells	159
7.1	Introduction	159
7.2	Experimental	160
7.3	Results and Discussion	162
7.3.1	The effect of external resistance	162
7.3.2	The effect of oxygen mass transport	172
7.3.3	Comparison of biocathode performance with a Pt cathode and an unmodified carbon electrode	175
7.4	Conclusions	178
8	The Effect of the Membrane on the Performance of Aerobic Biocathode Microbial Fuel Cells	181
8.1	Introduction	181
8.2	Experimental	183
8.3	Results and Discussion	184
8.3.1	Principal charge carriers and oxygen/acetate diffusion coefficients for a CEM, AEM and a BS	184
8.3.2	The effect of membrane-type on MFCs with an aerobic biocathode . .	195
8.4	Conclusions	208

9 Conclusions **211**

9.1 Summary 211

9.2 Materials Cost 213

9.3 Recommendations for Further Work 215

9.4 Closing Comments 216

Appendix A Additional material **217**

List of Figures

2.1	MFC diagram (a) and a hypothesised, simplified metabolic pathway for an anode respiring bacterium (b).	7
2.2	Aerobic biocathode MFC diagram (a) and a hypothesised, simplified metabolic pathway for an electrotroph (b).	11
2.3	Potential window over which an aerobic biocathode biofilm can be cultivated on a carbon support	30
3.1	CV and peak analysis for a 1 cm ² carbon felt electrode immersed in a solution containing 10 mM FeCN ₆ ³⁻ and 100 mM phosphate buffer. Graph a) shows the CV at different scan rates, whilst graph b) shows the oxidation and reduction peak heights plotted against $\sqrt{\nu}$	61
3.2	Example polarisation curve for an MFC	62
3.3	4-electrode setup for the detection of H ₂ O ₂ from porous CF electrodes, incorporating a primary working electrode (PWE) of the carbon felt material held at different CA potentials, a Pt secondary sensing electrode (SSE) held at +0.6 V, a reference electrode (RE) and a counter electrode (CNE).	72
3.4	Setup diagrams showing side (a) and top (b) views of the half-cell. The PTFE window with front and backing plate used to hold the carbon felt WE is given in (c).	74
3.5	Experimental setup for determining $C_E(O_2)$. The WE with biocathode is sealed into the right hand chamber with the DO probe and RE, and separated from the CNE with a membrane.	77
3.6	Setup diagrams for membrane experiments	79

3.7	MFC setups used in this thesis. A general setup is given in (a) with setup details common to all of the studies. Setups (b) and (c) were used to study the effect of light on MFC performance. Setup (d) was used to study the effect of external resistance. Setup (e) was used to study the effect of membrane-type on MFC performance. Additionally setup (e) was also used to study the effect of O ₂ mass transport on MFC performance with a biocathode, and to compare MFC performance using; a carbon felt electrode with a biocathode (1.), a plain carbon felt electrode with no biocathode (2.), and a carbon paper cathode with a Pt loading of 0.57 mg/cm ² (3.).	85
4.1	The average PWE and SSE current against time (two runs) for the HNO ₃ -treated carbon felt. The experiments were run for 1 hour, and the time-axis is in kilo seconds (ks). (a) and (b) show the average PWE and SSE currents against time, whilst (c) and (d) show the SSE currents against time for runs 1 and 2. Error bars are equal to the difference from the mean.	92
4.2	The average PWE and SSE current against time (two runs) for the untreated carbon felt. The experiments were run for 1 hour, and the time-axis is in kilo seconds (ks). (a) and (b) show the average PWE and SSE currents against time, whilst (c) and (d) show the SSE currents against time for runs 1 and 2. Error bars are equal to the difference from the mean.	93
4.3	The SSE current (solid lines) and the modeled solution H ₂ O ₂ concentration (dashed lines) against time for HNO ₃ -treated carbon felt (a) and untreated carbon felt (b). On each graph, the left hand axis is the SSE current against time, whilst the right hand axis is the modeled H ₂ O ₂ concentration against time. The curves are labeled according to the PWE potential.	96
5.1	Average CA and OCP against time for primary inoculated half-cells poised at -0.1 V (A and B) over their 266 day period of operation. Error bars are one standard deviation.	105
5.2	CV ($\nu = 5$ mV/s) for a primary inoculated half-cell (A) taken at 26, 34, 61, 132, 166 and 255 days of operation (in air).	106
5.3	CV ($\nu = 5$ mV/s) for a primary inoculated half-cell (B) taken at 25, 34, 61, 132, 166 and 255 days of operation (in air).	107

5.4	Control data for the half-cell study. Graphs (a) and (b) are the CA and CV ($\nu = 5$ mV/s) data respectively for a non-inoculated abiotic control half-cell poised at -0.1 V using normal biocathode medium. Graphs (c) and (d) are the CA and CV ($\nu = 5$ mV/s) data for a half-cell poised at -0.1 V using normal biocathode medium with micro nutrients at x 10 the normal concentration. Graph (e) contains the CV ($\nu = 5$ mV/s) data for the nutrient solutions used to make the biocathode medium; macro, metals and vitamin solutions at x 500, x 1000 and x 1000 times the normal concentration in the biocathode medium. Graph (f) contains the CV ($\nu = 5$ mV/s) data for normal biocathode medium with/without the addition of 1 ml/L of a 2% NaN_3 stock solution.	110
5.5	CA and CV ($\nu = 5$ mV/s) data for two secondary inoculated half-cells (K and L), one polarised at -0.1 V, the other at -0.2 V, over 20 days of operation. The CV ($\nu = 5$ mV/s) are recorded on both half-cells at 0 and 7 days of operation.	112
5.6	Gel documentation system images of the front (a) and back (b) of the carbon felt working electrode used in a secondary inoculated half-cell poised at -0.1 V (half-cell C), using an excitation wavelength of 365 nm and an exposure time of 1 min and 29 seconds. Fluorescence is shown in white. The contrast between white and black has been enhanced using InfranView 3.97.	113
5.7	Epifluorescence microscope images of a cross-section of the carbon felt working electrode of a secondary inoculated half-cell poised at -0.1 V (half-cell C). The images are ordered as consecutive frames starting from the electrode surface (a) and going into the cross-section, in the order of (a), (b), (c) then (d). The images are taken at x 100 magnification and a scale bar is included on all 4 images.	114
5.8	LSV ($\nu = 1$ mV/s) spectra for duplicate half-cells covering the three different treatments; -0.1 primary inoculum ((a) and (b)), -0.1 V secondary inoculum ((b) and (c)) and +0.2 secondary inoculum ((d) and (e)). For each half-cell, the LSV at $t = 0$ days and at the end of the half-cell operation period are presented.	119
5.9	Variation of current with changing electrolyte DO concentration for a secondary inoculated half-cell poised at -0.1 V (D). Graph (a) is a plot of DO concentration and flow rate against time, where the flow rate from the air pump sparging the electrolyte was changed in 0.4 LPM increments. Graph (b) is a plot of current versus time for the half-cell over the same time period. Graph (c) is a plot of current versus DO concentration taken by combining the data from (b) and (c).	121
5.10	O_2 coulombic efficiency at different points through time for secondary inoculated half-cells poised at -0.1 V (G and H) and +0.2 V (I and J).	123

5.11	Performance of primary inoculated half-cells grown at -0.1 V poised potential (A and B) with changing solution pH. LSV curves taken at 2-3 day intervals at pH 6.1/6.2, 7.3 and 8.5/8.6 are presented in graphs (a) and (c) for both half-cells. LSV curves at pH 6.3 taken immediately after the LSV at pH 8.5/8.6 are presented in (b) and (d). The variation of average OCP and pH for both half-cells at 132, 134 and 137 days is presented in graphs (c) and (d) respectively. Media changes are indicated on graph (f).	125
5.12	CV ($\nu = 5$ mV/s) spectra recorded in the presence and absence of O ₂ for primary (A and B) and secondary (E and F) inoculated half-cells poised at -0.1 V, and secondary inoculated half-cells poised at +0.2 V (I and J)	128
5.13	Peak analysis of the reversible redox couple with $E_{1/2} = +100$ mV in the absence of oxygen for a secondary inoculated half-cell poised at -0.1 V (F) at 41, 50, 103 and 104 days with $\nu = 1-100$ mV/s. Graph (a) shows the reversible redox peak at $\nu = 1$ mV/s on all occasions that the peak analysis was undertaken. Graph (b) shows the variation of the peak height with increasing ν at 104 days. Graphs (c) and (d) show the oxidation peak heights plotted against ν and $\sqrt{\nu}$, whilst graphs (e) and (f) show the reduction peak heights plotted against ν and $\sqrt{\nu}$	129
5.14	CV at $\nu = 5$ mV/s for electrolyte and bore samples taken from primary (A and B) and secondary (E and F) inoculated half-cells poised at -0.1 V at the end of their operational periods.	130
5.15	CV ($\nu = 5$ mV/s) in the presence and absence of azide for primary inoculated half-cells polarised at -0.1 V (A and B), and secondary inoculated half-cells polarised at +0.2 V (I and J).	132
5.16	Stacked-bar chart giving the total number of sequences (%) for a particular taxon, classified according to phylum and class for the polarised/unpolarised half-cell communities.	137
5.17	Stacked-bar chart giving the total number of sequences (%) for a particular taxon, classified according to order and family for the polarised/unpolarised half-cell communities.	138
5.18	Stacked-bar chart giving the total number of sequences (%) for a particular taxon, classified according to genus for the polarised/unpolarised half-cell communities.	139

5.19	Principal coordinates analysis for weighted ((a) and (b)) and unweighted ((c) and (d)) beta diversity (UniFrac) for the 4 different treatments; non-polarised controls (blue squares), primary inoculated half-cells polarised at -0.1 V (red circles), secondary inoculated half-cells polarised at -0.1 V (green triangles), and secondary inoculated half-cells polarised at +0.2 V (purple diamonds). Graphs (a) and (b) show the first 4 axes representing 95 % of the variation for the weighted beta diversity, whilst graphs (c) and (d) show the first 4 axes representing 66 % of the variation for the unweighted beta diversity.	142
6.1	E(cell)/mV for t = 0-150 days for triplicate acetate-fed batch MFC H-cells, MFCA (solid line), MFCB (dashed line) and MFCC (dotted line). Media changes are indicated as symbols along the time axis for MFCA (square), MFCB (triangle), MFCC(circle) and for when the media was changed on all of the MFCs simultaneously (crosses). Batch cycle lengths and numbers are indicated on the graph with arrows. The shaded area indicates the period when the MFCs were kept in the dark, the light area indicates the period when all three MFCs were exposed to the lab light.	149
6.2	Photos of triplicate acetate-fed batch MFC H-cells (MFCA, MFCB and MFCC) during the 2nd batch cycle at 21 (a) and 41 (b) days of operation. MFCA has been highlighted with a red circle in both photos.	150
6.3	Cell voltage (a) and anode potentials (b) for two acetate-fed batch MFC H-cells, one kept in the dark (solid lines), one kept in the light (dashed lines). Anode media changes are indicated for the dark cell (circles) and the light cell (triangles).	152
6.4	Anode LSV (a) and cathode LSV (b) and polarisation curves (c), for two acetate-fed batch MFC H-cells, one kept in the dark (solid lines) and one kept in the light (dashed lines).	154
6.5	Cell voltage data with accompanying photos taken at different points during operation of two acetate-fed batch MFC H-cells, one kept in the dark (a), one kept in the light (b). Anode media changes are indicated for the dark cell (circles) and the light cell (triangles).	156

7.1	Cell voltage against time (a), cathode potential against time (b), and cathode and anode pH against time (c), for the three cells at 100 Ω , 1000 Ω and 5480 Ω , for t = 0-63 days of cell operation. For the cell voltage (a) and cathode potential (b) graphs, 100 Ω = solid line, 1000 Ω = dashed line and 5480 Ω = dotted line. For the pH graph (c), anode pH = solid lines, cathode pH = dashed lines, 100 Ω = square, 1000 Ω = circle and 5480 Ω = triangle. Media changes are indicated on graphs (a) to (c) (crosses), and batch cycle numbers with cycle lengths are indicated in graph (a).	163
7.2	Polarisation curves taken for all 3 cells at (a) 7, (b) 27, (c) 32 and (d) 61 days of operation. Dashed lines represent cell voltages and solid lines represent power. Both Curves are given at each time for each of the 3 cells at 100 Ω (square), 1000 Ω (circle) and 5480 Ω (triangle).	165
7.3	Cathode and anode potentials during the polarisation curves taken for all 3 cells at (a) 7, (b) 27, (c) 32 and (d) 61 days of operation. Solid lines represent cathode potentials and dashed lines represent anode potentials. Both curves are given at each time for each of the 3 cells at 100 Ω (square), 1000 Ω (circle) and 5480 Ω (triangle).	166
7.4	Linear best fits of the linear region of the cell voltage from the polarisation curves taken for all 3 cells at (a) 7, (b) 27, (c) 32 and (d) 61 days of operation. The best fits are given at each time for each of the 3 cells at 100 Ω (square), 1000 Ω (circle) and 5480 Ω (triangle).	167
7.5	EIS taken for all 3 cells at (a) 7, (b) 27, (c) 32 and (d) 61 days of operation (immediately after the polarisation curves). The EIS are given at each time for each of the 3 cells at 100 Ω (square), 1000 Ω (circle) and 5480 Ω (triangle).	168
7.6	Anode and cathode LSV for all 3 cells at 0 and 34 days of operation; cell at 100 Ω (solid lines), cell at 1000 Ω (dashed lines) and cell at 5480 Ω (dotted lines).	172
7.7	Cathode dissolved oxygen concentration against time (a), cell voltage and cathode potential against time (b), and cell voltage and cathode potential against cathode dissolved oxygen concentration (c), for the cell previously operated at 100 Ω , operated at peak power with $R_{ext} = 510 \Omega$ (The measurements were taken at 518 days of continuous operation for this cell).	174
7.8	Potential step voltammetry on a biocathode grown at a poised-potential of -0.1 V, a Pt cathode and a carbon cathode. The potential-step voltammograms were taken under conditions of continuous sparging with air from an air pump, and using biocathode medium buffered to pH 7. The steady-state current was taken at 10 minutes at each potential.	175

7.9	Polarisation curves taken for the cell previously operated at 5480Ω , at peak power density with $R_{ext} = 510 \Omega$ (the curves were taken at 624-626 days of continuous operation for this cell), using a biocathode grown at a poised potential of -0.1 V (a and b), a Pt cathode (c and d) and a carbon cathode (e and f). The power (solid lines) and cell voltage (dotted lines) are given in graphs (a), (c) and (e), whilst the corresponding cathode (solid line) and anode potentials (dashed lines) are given in graphs (b), (d) and (f).	177
8.1	Average charge transfer across the CEM, AEM and BS across the 1st and 2nd runs of the ionic charge carriers experiment. ΔQ is the charge attributed to each measured ion assuming a specific ionic charge (z), whilst Q_{pass} is the charge passed in the external circuit of the cell. The ratio between the two is $\Delta Q/Q_{pass}$, expressed as a $\%$. Empty bars are for charge changes at the WE, filled bars are for charge changes at the CNE. The error bars are equivalent to the differences from the mean.	191
8.2	Cell voltage against time, cathode potential against time, and anode/cathode pH against time during the first operational period of 40 days for the three acetate-fed batch aerobic biocathode MFCs, fitted with AEMs (cells A-C). Media changes are given by circles along the time axes. Batch cycles are numbered.	196
8.3	Cell voltage against time, cathode potential against time, and anode/cathode pH against time during the second operational period of 40 days for the three acetate-fed batch aerobic biocathode MFCs, fitted with different membranes; a CEM (cell A), a new AEM (cell B) and a BS (cell C). Media changes are given by circles along the time axes. Batch cycles are numbered.	197
8.4	Polarisation curves with corresponding electrode potentials taken for the three aerobic biocathode MFCs at the end of the two operational periods; 1st 40 day operational period when the three cells had AEMs (cells A-C) (empty symbols), and the 2nd 40 day operational period when the cells had a CEM (cell A), a new AEM (cell B) and a BS (cell C) (filled symbols). Therefore, cell A is defined as AEM to CEM, cell B as AEM to AEM, and cell C as AEM to BS.200	200
8.5	EIS taken for the three aerobic biocathode MFCs at the end of the two operational periods; 1st 40 day operational period when the three cells had AEMs (cells A-C) (empty symbols), and the 2nd 40 day operational period when the cells had a CEM (cell A), a new AEM (cell B) and a BS (cell C) (filled symbols). Therefore, cell A is defined as AEM to CEM, cell B as AEM to AEM, and cell C as AEM to BS.	201

8.6	Biocathode and bioanode LSV taken for the three aerobic biocathode MFCs at the end of the two operational periods; 1st 40 day operational period when the three cells had AEMs (cells A-C) (solid lines), and the 2nd 40 day operational period when the cells had a CEM (cell A), a new AEM (cell B) and a BS (cell C) (dashed lines). Therefore, cell A is defined as AEM to CEM, cell B as AEM to AEM, and cell C as AEM to BS.	202
8.7	Images of biofouling on the AEM of cell A at the end of the 1st operational period on the anode-facing side (a) and cathode-facing side (b), and on the BS of cell C at the end of the 2nd operational period on the anode-facing (c) and cathode-facing side (d). A fresh AEM (e) and BS (f) are presented for comparison.	205
8.8	% charge transfer at the anode and cathode for cell A (CEM), cell B (AEM) and cell C (BS) during batch cycle 1 of the second operational period. ΔQ is the charge attributed to each measured ion assuming a specific ionic charge (z), whilst Q_{pass} is the charge passed in the external circuit of the MFC. The ratio between the two is $\Delta Q/Q_{\text{pass}}$, expressed as a % . Empty bars are for charge changes at the anode, filled bars are for charge changes at the cathode.	207
A.1	Image of a graticule slide taken at x100 magnification using an epifluorescence microscope (Olympus BX40) fitted with a digital camera (Olympus E-400). The rule has 1mm/0.01 divisions (10 μm). From this image, the image height has been determined as 0.55 mm.	217
A.2	BSA standard curve obtained using 0, 25, 125, 250, 500 and 1000 $\mu\text{g}/\text{ml}$ BSA dilutions from a 2 mg/ml BSA stock. The curve was fitted using a quadratic function. Absorbance was measured at 562 nm.	217
A.3	TOC calibration using x 3.5, 5, 10 diluted bioanode medium (1 g/L sodium acetate, 50 mM pH 7.0 phosphate buffer, nutrient solutions) and DI water.	218
A.4	CA data for half-cells A-F	219
A.5	CA data for half-cells G-L	220
A.6	CA data for control half-cells.	221
A.7	LSV data for half-cells A-F	222
A.8	LSV data for all half-cells G-L	223
A.9	LSV data for the control half-cell	224

A.10 2-electrode EIS spectra of the membrane ohmic resistance testing cell without a membrane, with a CEM (Nafion), with an AEM (Fumasep FAD) and with a BS (RhinoHide), using pH 7.0 anode medium as electrolyte (pH 7.0 phosphate buffer, 1 g/L sodium acetate, trace solutions). Graph (a) shows the EIS spectra over the complete frequency range (1-8 k Ω real impedance), whilst graph (b) gives the same EIS spectra between 40-50 Ω , real impedance. 224

List of Tables

2.1	Standard reduction potentials vs. Ag/AgCl of chemical species and biological electron transport proteins relevant or potentially-relevant to aerobic biocathodes.	13
2.2	Aerobic biocathode studies ranked according to E_{ORR} , where available. AS = activated sludge, AnS = anaerobic sludge, DW = domestic wastewater, PEC = Previously enriched consortium, NS = nitrifying sludge, MBR = membrane bioreactor, CC = carbon cloth, CF = carbon felt, CP = carbon paper, CB = carbon brush, AC = activated carbon, GAC = granular activated carbon, CG = carbon granules, CNT = carbon nanotubes, GCE = glassy carbon electrode, GG = graphite granules, GG = graphite brush, GF = graphite felt, GP = graphite plate, RVC = reticulated vitreous carbon, SS = stainless steel, SSM = stainless steel mesh. $*E_{1/2} = 0.15 \text{ V}$	16
2.3	Dominant bacteria / bacteria identified with ORR catalysis in different aerobic biocathode communities, ranked according to E_{ORR} . The types of BES are MFC, half-cell (HC), microbial solar cell (MSC), sediment microbial fuel cell (SMFC). The method of community analysis are clone libraries (CL), illumina-dye sequencing (IDS), pyrosequencing (PS) and denaturing gradient-gel electrophoresis (DGGE). $*E_{1/2} = 0.15 \text{ V}$	21
3.1	Composition of electrolyte consisting of 50 mM pH 7.0 phosphate buffer, 1 g/L of sodium acetate, and nutrients (nutrients are described in Subsection 3.5.1). Ions with a lower concentration than 0.04 mM are not included. Ac^- is the acetate anion.	79
4.1	Results summary for the 4-electrode electrochemical tests. The PWE potentials used and the minimum potential (E_{min}) at which an oxidation current is first detected at the SSE are listed for both the HNO_3 -treated and untreated carbon felts.	94

5.1	Experimental matrix of operational parameters and analyses for all half-cells in the study. The half-cells are labeled A-L, with control half-cells (CONT) given as a second grouping at the bottom of the table. The analyses are chronoamperometry (CA), cyclic voltammetry (CV) in air/N ₂ /azide, linear sweep voltammetry (LSV) in air, coulombic efficiency (CE), dissolved oxygen (DO), imaging, biomass determination and community analysis. *Inoculated at the same time using the same effluent. **The three different nutrient solutions used to make the biocathode media.	103
5.2	CA and OCP data summary; average current after the acclimatisation period, average I, calculated from the CA for each half-cell, and the OCP for each half-cell at the start and end of the operation period. The acclimatisation period for each half-cell is also given (Ac. time). Operational parameters for each half-cell have been included; poised potential (E _{poised}), type of inoculation (primary or secondary), and the operation time.	117
5.3	LSV ($\nu = 1$ mV/s) data summary; current, I, at +0.2 V, and the onset potential for ORR, E _{ORR} , for each half-cell in the study, at t = 0 days and at the end of the half-cell operation period. Operational parameters for each half-cell have been included; poised potential (E _{poised}), type of inoculation (primary or secondary), and the operation time.	118
5.4	Biomass data for the polarised/unpolarised half-cell communities. Operational parameters are also given.	135
6.1	1 st and 2 nd light studies with light exposure conditions for each of the MFCs .	147
6.2	Coulombic efficiencies of triplicate acetate-fed batch MFC H-cells (MFCA, MFCB and MFCC) for their 2nd and 4th batch cycles	150
6.3	Coulombic efficiency values of different batch cycles for two acetate-fed batch MFC H-cells, one kept in the dark and one kept in the light.	153
7.1	Coulombic efficiencies for cycles 4 and 5 for all three cells at 100 Ω , 1000 Ω , and 5480 Ω . The average of both cycles has been calculated with the standard deviation.	164
7.2	Summary of peak power densities and internal resistances determined from the polarisation curve data given in Figures 7.2 and 7.4, and the ohmic resistances determined from the EIS given in Figure 7.5, for all 3 cells at 100 Ω , 1000 Ω , and 5480 Ω external resistance, at 7, 27, 32 and 61 days of operation. Corresponding polarisation resistances (R_p) and ratios of ohmic resistance to internal resistance (R_Ω/R_{int}) have been calculated. Average values and standard deviations (SD) have also been calculated.	170

8.1	Cost of the CEM, AEM and BS used in this study	183
8.2	The two different periods of operation for the three acetate-fed batch aerobic biocathode MFCs. For the second period of operation, the three MFCs used different membrane types.	184
8.3	Cell ohmic resistances as determined by EIS using the membrane ohmic resistance testing cell given in materials and methods. Ohmic resistances are given for the cell, without a membrane, for with a CEM, AEM and BS membrane, with anode medium as electrolyte (50 mM pH 7.0 phosphate buffer, 1 g/L sodium acetate, nutrients).	186
8.4	Calculated area resistance, resistivity and conductivity, for a CEM, AEM and BS in anode medium (50 mM pH 7.0 phosphate buffer, 1 g/L sodium acetate, nutrients), using the cell ohmic resistances determined in Table 8.3. Membrane thicknesses were determined for the hydrated form of the membrane.	186
8.5	1st run results for the abiotic electrolysis experiment using a H-cell with a 1cm diameter membrane and 3 different membrane types; CEM, AEM and BS. Ion concentrations at the start and end of the experiment and % changes in charge for each ion after passing 2mA of current for 92.00 hours (662C) are presented. ΔQ is the change in charge in coulombs for each ion assuming a specific ionic charge (z), and Q_{pass} is the charge passed in the external circuit, equal to 662C.	187
8.6	2nd run results for the abiotic electrolysis experiment using a H-cell with a 4 cm diameter membrane and 3 different membrane types; CEM, AEM and BS. Ion concentrations at the start and end of the experiment and % changes in charge for each ion after passing 2mA of current for 76.15 hours (548C) are presented. ΔQ is the change in charge in coulombs for each ion assuming a specific ionic charge (z), and Q_{pass} is the charge passed in the external circuit, equal to 548C.	190
8.7	CEM, AEM and BS diffusion, D_{O_2} , and mass transfer, k_{O_2} , coefficients for O_2 in 50 mM phosphate buffer solution. Concentration changes have been given in both chambers of the testing H-cell.	193
8.8	CEM, AEM and BS diffusion, D_{Ac} , and mass transfer, k_{Ac} , coefficients for acetate in deionised water. Concentration changes have been given for both chambers of the testing H-cell.	194
8.9	Cathode and Anode ion concentrations in cells A (CEM), B (AEM) and C (BS) at the start and end of cycle 1 of the second operational period, and % changes in charge for each ion. ΔQ is the change in charge in coulombs for each ion assuming a specific ionic charge (z), and Q_{pass} is the charge passed in the external circuit for each MFC.	206

9.1 A simple comparative MFC capital cost analysis. The cost of the MFCs using a biocathode, Pt (5.7 g/m²) cathode and a plain carbon cathode are given. Price/Power is a ratio used for comparison, in order to factor in power performance. The cost analysis is with a RhinoHide BS. 214

List of Abbreviations

AC	Activated Carbon
ACNQ	2-amino-3-dicarboxy-1,4-naphthoquinone
AEM	Anion Exchange Membrane
AnS	Anaerobic Sludge
AOB	Ammonia Oxidizing Bacteria
ARB	Anode Respiring Bacteria
AS	Activated Sludge
ATP	Adenosine Triphosphate
BCA	Bicinochoninic Acid
BES	Bioelectrochemical System
BOD	Biological Oxygen Demand
BS	Battery Separator
BSA	Bovine Serum Albumin
CA	Chronoamperometry
CC	Carbon Cloth
CE	Coulombic Efficiency
CEM	Cation Exchange Membrane
CNE	Counter Electrode
CF	Carbon Felt
CG	Carbon Granules

CL	Clone Libraries
CNT	Carbon Nanotubes
COD	Chemical Oxygen Demand
CONT	Control
CoTMPP	Cobalt Tetramethoxyphenylporphyrin
CP	Carbon Paper
CV	Cyclic Voltammetry
DET	Direct Electron Transfer
DGGE	Denaturing Gradient Gel Electrophoresis
DNA	Deoxyribonucleic Acid
dNTP	Deoxynucleoside Triphosphate
DO	Dissolved Oxygen
DW	Domestic Wastewater
EIS	Electrode Impedance Spectroscopy
EPS	Extracellular Polysaccharides
ET	Electron Transfer
FePc	Iron Phthalocyanine
GAC	Granular Activated Carbon
GB	Graphite Brush
GCE	Glassy Carbon Electrode
GDE	Gas Diffusion Electrode
GF	Graphite Felt
GG	Graphite Granules
GP	Graphite Plate
HC	Half Cell

HOB	Hydrogen Oxidizing Bacteria
IC	Inorganic Carbon
ICP-AES	Inductively Coupled Plasma Atomic Emission Spectrometer
ICS	Ion Chromatography System
IDS	Illumina Dye Sequencing
IEM	Ion Exchange Membrane
IOB	Iron Oxidizing Bacteria
LSV	Linear Sweep Voltammetry
MBR	Membrane Bioreactor
MEC	Microbial Electrolysis Cell
MET	Mediated Electron Transfer
MFC	Microbial Fuel Cell
MIC	Microbiologically Influenced Corrosion
MOB	Manganese Oxidising Bacteria
MSC	Microbial Solar Cell
NADH	Nicotinamide Adenine Dinucleotide
NOB	Nitrite Oxidizing Bacteria
NS	Nitrifying Sludge
OCP	Open Circuit Potential
OMC	Outer Membrane Cytochrome
ORR	Oxygen Reduction Reaction
OTU	Operational Taxonomic Unit
PAN	Polyacrylonitrile
PCoA	Principal Coordinates Analysis
PCR	Polymerase Chain Reaction

PEC	Previously Enriched Consortium
PES	Poltethylenesulfone
PNS	Purple Non-Sulphur Bacteria
PQQ	Pyrroloquinoline Quinone
PS	Pyrosequencing
PTFE	Polytetrafluoroethylene
PWE	Primary Working Electrode
QIIME	Quantitative Insights Into Molecular Ecology
rDNA	Ribosomal DNA
RE	Reference Electrode
RNA	Ribonucleic Acid
RRDE	Rotating Ring Disk Electrode
rRNA	Ribosomal RNA
RVC	Reticulated Vitreous Carbon
SMFC	Sediment Microbial Fuel Cell
SOB	Sulphur Oxidizing Bacteria
SS	Stainless Steel
SSE	Secondary Sensing Electrode
SSM	Stainless Steel Mesh
TC	Total Carbon
TEA	Terminal Electron Acceptor
TOC	Total Organic Carbon
WE	Working Electrode

Chapter 1. Introduction

1.1 Renewable Energy, Wastewater treatment and Microbial Fuel Cells

The use of finite fossil fuels is contributing to global CO₂ emissions and irreversible climate change. Therefore, their use must be minimised and phased out if the worst of predicted climate change is to be avoided. In this context, a lot of research is now focused on the development of renewable forms of energy and sustainable technologies which can reverse this global trend of increasing CO₂ gas emissions. One of these sustainable technologies is the microbial fuel cell (MFC).

MFCs are a technology in which biodegradable organic chemicals are converted into electricity using bacteria. The strength of the MFC is that they are able to efficiently convert organic substrates directly into electricity, which cannot currently be achieved by any other technology. MFCs may find an application in the treatment of wastewaters rich in biodegradable organics, allowing direct conversion of these substrates into electricity. Wastewaters such as domestic wastewater and urine, as well as wastewater discharges from the brewery and woodpulp industries, could potentially be used. Additionally, MFCs may also serve as biological oxygen demand and toxicity sensors in domestic wastewater treatment, as the effluent must meet certain criteria for biological oxygen demand (BOD) content and heavy metals before it can be discharged into the environment. MFCs may also have applications in renewable energy, providing a route for the conversion of plants and algae into electricity [1–5], and as power sources for remote sensors [6–8] or autonomous robots [9–11] in the environment.

One potential application of MFCs is for energy recovery and treatment of domestic wastewater, although much work needs to be done to optimise performance and lower costs [12]. Wastewater treatment is a huge user of energy, with the UK wastewater industry being the fourth largest user of energy in the UK, with 1 % of the electricity consumed in England and Wales being for wastewater treatment purposes [12]. Pumps and energy intensive aeration account for most of this energy consumption, yet according to some estimates, up to 9.3 times the energy that is required to treat domestic wastewater is contained within the wastewater it-

self [13]. Therefore, new energy recovery technologies, such as MFCs, may be one day used to treat and extract energy from wastewater in order to make the energy wastewater treatment infrastructure more energy efficient and sustainable. One of the hurdles to implementation for domestic wastewater treatment is that electrical current generation decreases below a certain organic matter concentration threshold [14]. In order to overcome this problem, better materials and designs are sought for the MFC system.

1.2 Why Aerobic Biocathodes for Microbial Fuel Cells?

MFCs work by coupling the oxidation of organic matter by bacteria at the anode with the reduction of oxygen at the cathode, with electrons flowing through the external circuit and protons moving through solution, generating electrical power [13, 15, 16]. If the MFC technology is to be adopted, then capital costs must be lowered, particularly given the much lower instantaneous power outputs of these devices. Many of the biggest costs in the MFC system arise from the membrane and cathode chemical catalyst. In particular, Pt catalysts, which are commonly used at the cathode to catalyse the oxygen reduction reaction (ORR), are expensive, environmentally unsustainable, and are easily poisoned by contaminants and sulphides present in wastewater. At the time of writing, the base price of Pt is 28.4 £/g, compared with 14.7 £/g at the beginning of 2000 (adjusted for inflation), and world prices should continue to increase as Pt becomes more scarce. The ORR at the cathode can also be catalysed by non-noble transition metal macrocycles such as cobalt tetramethoxyphenylporphyrin (CoTMPP) and iron phthalocyanine (FePc) [17–19], by metal oxide catalysts such as MnO₂ [19], and by modified and unmodified carbon materials [19–21]. However, both non-noble transition metal macrocycles and metal oxides still have associated costs and sustainability issues, whilst carbon materials show low catalytic activity toward the ORR in comparison to modification with chemical catalysts.

Mixed-community aerobic biocathode biofilms catalysing the ORR, are a good substitute for chemical catalysts at the cathode, being both completely free and sustainable, and with potentially excellent catalytic activity. However, little is understood about the bacteria responsible for catalysis, the factors which effect their performance, and the mechanisms whereby they perform catalysis. An understanding of these areas is vital if these catalysts are to be used in the MFC technology to lower capital and operational costs.

1.3 Aims and Objectives

In the literature, the best performing aerobic biocathodes to date have an onset potential for the ORR of approximately +0.4 V vs. Ag/AgCl (all potentials in this thesis are against Ag/AgCl), and have been developed in poised-potential half-cells. Higher onset potentials for the ORR imply a better performing ORR catalyst, and an increased MFC power output. However, the bacteria which catalyse the ORR at a high onset potential of +0.4 V have not been identified, and little is understood about the mechanism of ORR catalysis by these bacteria. Indirect ORR catalysis by the bacteria, as well as direct catalysis in which the bacteria use the electrode as the sole electron donor for energy and growth, are both possibilities. Direct catalysis may involve direct electron transfer and/or mediated electron transfer from the cathode to the bacteria. A fundamental understanding of these mechanistic behaviors, and an identification of the organisms involved in ORR catalysis, is essential to selecting better-performing aerobic biocathodes in order to improve MFC performance.

It is also predicted that the mechanisms of ORR catalysis, as well as the community composition, will vary as the electrode potential is varied. Variation of the electrode potential is therefore an important investigative tool for studies into both mechanism and bacterial community. In particular, if the mechanism of ORR catalysis is direct, then the bacteria may use different pathways of electron transfer in order to maximise their energy gain from the electrode, which may select for different bacteria within the mixed community.

Further to these fundamental investigations in poised-potential half-cells, the performance of aerobic biocathodes in full MFC systems must also be investigated in order to understand the factors which effect performance, so the system can be further optimised for power generation. Important external factors which can be controlled include light, external resistance and oxygen mass transfer to the biocathode. Additionally to these external factors, the membrane separating the anode and cathode electrodes in this system is predicted to play an important role. Membranes have different selectivity for oxygen, anode substrate, and charge carrying ions, and suitable membranes for aerobic biocathode MFCs need to be identified.

There are two main aims in this thesis. The first main aim is to improve the fundamental understanding of aerobic biocathodes in general, and in particular, aerobic biocathodes with an onset potential for ORR of +0.4 V. The latter are distinct from other aerobic biocathodes in the literature, given their high ORR onset potential. The knowledge acquired by these fundamental studies of aerobic biocathode biofilms will be applied to their use in full MFCs. The second main aim of this thesis is to investigate the performance of MFCs using an aerobic biocathode under different conditions/external factors, in order to improve system performance/cost/stability. It will therefore be possible to see whether the aerobic biocathode is a

good substitute for a conventional chemical ORR catalyst.

Using poised-potential half-cells, aerobic biocathode biofilms with an onset potential for ORR of +0.4 V will be developed, with the following specific objectives;

1. To identify the mechanism of ORR catalysis using electrochemical methods
2. To identify the bacteria responsible for ORR catalysis using bacterial community analysis
3. To determine the effect of applied potential on performance, of the ORR catalysis mechanism and bacterial community

Before the aerobic biocathodes can be grown in poised-potential half-cells, a potential window over which aerobic biocathode growth is possible needs to be determined. This is because carbon materials catalyse the ORR at specific potentials, producing peroxide, which sterilises bacteria. Once the aerobic biocathode is developed, it will be integrated into a full MFC system, and the effect of different external variables on aerobic biocathode MFC performance will be assessed. Therefore, the effect of the following factors on aerobic biocathode MFC performance will be determined;

1. Light
2. External resistance
3. O₂ mass transfer
4. Membrane

1.4 Contention

In this thesis, I will seek to determine whether aerobic biocathodes are a suitable alternative to conventional chemical ORR catalysts in MFCs.

1.5 Chapter Summary

This thesis is split into 10 chapters. These ten thesis chapters, along with a brief description of each chapter, where applicable, is given below;

1. Introduction
2. Literature Review on Aerobic Biocathodes

3. Materials and Methods
4. Evaluation of Carbon Materials for Biocathode Supports in Aerobic Biocathode Half-Cells
 - Using a novel 4-electrode half-cell setup, a potential window over which to grow aerobic biocathodes on a porous carbon support was determined.
5. The Electron Transfer Mechanism and Bacterial Community in Aerobic Biocathodes with an Onset Potential for ORR of +0.4 V vs. Ag/AgCl
 - Using half-cells poised at -0.1 and +0.2 V, aerobic biocathode biofilms with an onset potential for ORR of +0.4 V were grown and investigated in terms of electron transfer mechanism and bacterial community, using different electrochemical, analytical and microbiological methods. Additionally, aerobic biocathode performance under different conditions of pH and O₂ mass transfer was also assessed.
6. The Effect of Light on the Performance of Acetate-fed Microbial Fuel Cells
 - The effect of light on MFC performance was assessed using acetate-fed batch MFCs exposed to light and dark conditions. The investigation was carried out using different electrochemical/analytical methods.
7. The Effect of External Resistance and Oxygen Mass Transfer on the Performance of Aerobic Biocathode Microbial Fuel Cells
 - The effect of external resistance on the performance of aerobic biocathode MFCs was assessed by using a combination of different external resistances, and electrochemical/analytical methods. Additionally, the effect of O₂ mass transfer to the biocathode on MFC performance was also assessed.
8. The Effect of the Membrane on the Performance Aerobic Biocathode Microbial Fuel Cells
 - The effect of three different membrane types on the performance of aerobic biocathode MFCs was assessed using different electrochemical/analytical methods.
9. Conclusions
10. Additional Material

Chapter 2. Literature Review on Aerobic Biocathodes

2.1 Microbial Fuel Cells

2.1.1 Background

MFCs utilise bacteria to produce electricity from organic waste [22]. The first MFC was developed by Potter in 1911 [23], and the last decade has seen significant activity in the area [13, 15, 16, 16, 22, 24–33]. In MFCs, specialised bacteria called anode respiring bacteria (ARB)¹, oxidise organic substrates and release the electrons in these substrates to an insoluble anode electrode. The electrons then travel through an external circuit, before combining with protons and oxygen to form water at a chemically catalysed cathode electrode. The circuit is completed by the passage of protons from the anode to the cathode electrode, generating electrical power. Most MFCs also include a membrane, which separates the anode from the cathode, limiting O₂ diffusion from the cathode to the anode, which otherwise lowers the efficiency of the device. This membrane is typically a cation exchange membrane (CEM), which is designed to only permit the passage of protons from the anode to the cathode chambers. The principle of operation behind an MFC is presented in Figure 2.1a, along with a hypothesised, simplified metabolic pathway for an anode respiring bacterium in Figure 2.1b.

MFCs generally come in single- and dual- chamber variants. The two chamber designs have a liquid anode chamber and a liquid cathode chamber, both filled with electrolyte solutions and separated by a membrane. The anode chamber contains the conductive, usually carbon anode electrode, the bacterial biofilm which grows on this, and the organic substrate for the bacteria. The anolyte containing the ARB must be conductive and must also have some buffering capacity to allow the passage of charge through solution and to maintain the pH respectively, as well as being non-toxic to the bacteria. Phosphate buffer fulfills these requirements, and is

¹Throughout this thesis, the term ARB, will be adopted to describe bacteria which are able to donate electrons to an insoluble anode, and therefore produce electricity in an MFC. In the natural environment, however, these bacteria reduce iron oxides, in a process called dissimilatory metal reduction [13], and it is this process which they are evolved to carry out. The term ARB is used to denote bacteria which are able to use the insoluble anode as their terminal electron acceptor.

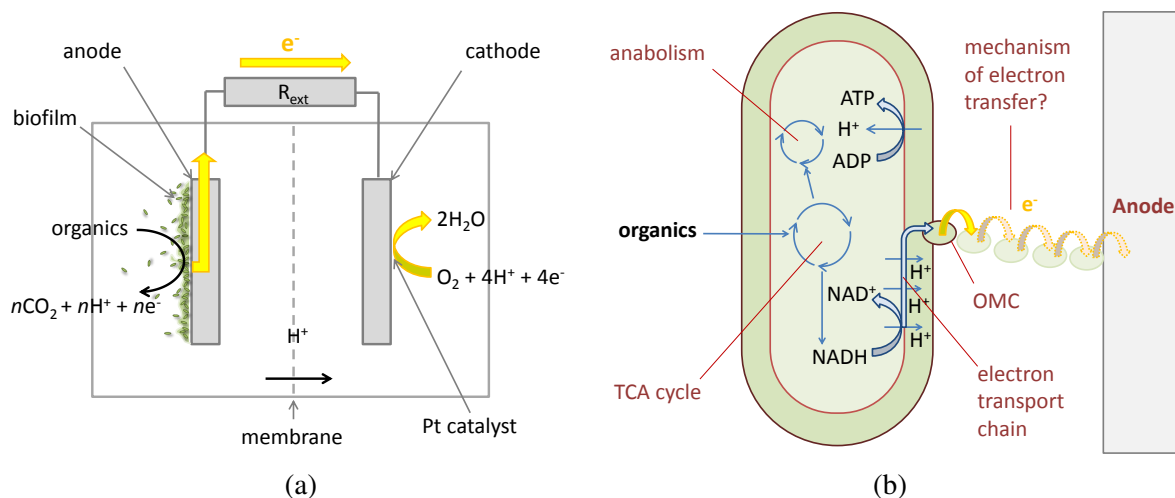


Figure 2.1: MFC diagram (a) and a hypothesised, simplified metabolic pathway for an anode respiring bacterium (b).

used in the anolyte of a large number of lab-scale MFCs. At the cathode, oxygen is usually used as the cathode reactant, and its reduction is typically catalysed with a chemical catalyst such as Pt supported on carbon.

In dual-chamber designs, oxygen solubility is a limiting factor for the submerged cathode electrode, so these designs have largely been superseded by single-chamber designs using gas diffusion electrodes (GDEs), which allow passive oxygen mass transfer from the air to the cathode surface to the catalyst [13]. In single-chamber MFCs, the membrane can be directly pressed onto the solution-facing side of the GDE, or alternatively, the membrane can be dispensed with in order to lower the internal resistance of the MFC [34].

Power outputs for MFCs vary in the order of tens to hundreds of mW/m^2 , normalised to the anode electrode area, depending on a large number of different factors. Very high power outputs of the order of W/m^2 are sometimes reported for MFC systems using ferricyanide as a catholyte [13], although ferricyanide is an unsustainable chemical which has to be continuously replenished. Much of the research in the MFC area is application driven [24,25,27,35–41], typically using lab-scale MFCs, or focuses on fundamental aspects of the ARB.

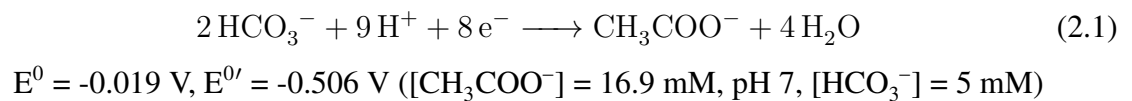
2.1.2 Basis of electrical power production in an MFC

Under anaerobic conditions, complex organic polymers, cellulose and proteins are broken down into simpler molecules through hydrolysis, fermentation and acetogenesis [42]. The anaerobic digestion of organic matter then terminates with methanogenesis or sulphate reduction [42]. Acetate occupies a central position in the anaerobic degradation of organic matter, and for microbial metabolism in general, as it is a precursor in anaerobic, as well as aerobic

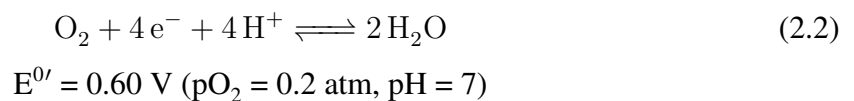
respiration. It is converted to acetyl coenzyme A, which is converted to various biosynthetic precursors for anabolic pathways via the tricarboxylic acid cycle, as well as to adenosine triphosphate (ATP) and nicotinamide adenine dinucleotide (NADH) for catabolism [43]. It is NADH which is the electron donor into an electron transport chain terminating in the reduction of an electron acceptor such as oxygen, and the production of proton motive force for ATP synthesis [43].

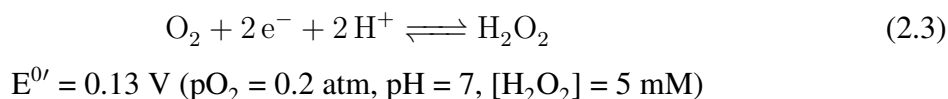
For the ARB, the terminal electron acceptor (TEA) in the electron transport chain is the anode. ARB, such as *Geobacter* and *Shewanella* species, are able to form a biofilm on the anode electrode of an MFC, and use this as an electron sink, allowing them to oxidise NADH to NAD⁺ for energy generation [22]. In the case of the MFC, the potential of the anode electrode in theory controls how much energy the bacteria may gain by oxidising acetate, although this is dependent on the exact potential at which electrons exit the respiratory chain [22]. The remaining redox potential difference between the anode potential and the cathode potential can then be used to produce electrical power in the MFC [22].

One important aspect of MFC anodes is that the greatest power outputs are observed for mixed community biofilms as opposed to monocultures [13]. The reasons for this are likely due to the complex nature of the biofilm and cooperative interactions between different bioanode bacteria. Considering acetate oxidation by bacteria at the anode, the theoretical potential for acetate oxidation is [22];



Oxygen has a high reduction potential, and is a readily available oxidant for use in MFCs. At the cathode, the electrochemical reduction of O₂ to either water or H₂O₂ occurs, depending on the catalyst/electrode material [44]. At neutral pH, 2 e⁻ oxygen reduction to H₂O₂, and 4 e⁻ oxygen reduction to water are described by the following equations [44];





Therefore, the maximum theoretical MFC voltage is $0.60 \text{ V} - -0.51 \text{ V} = 1.1 \text{ V}$, assuming 4e^- ORR, neutral pH and $[\text{CH}_3\text{COO}^-] = 16.9 \text{ mM}$. This is the maximum voltage which can be achieved using acetate oxidation at the anode and oxygen reduction at the cathode. However, at the anode electrode, a complex bacterial community controls the anode potential, and at the cathode electrode, there is a large overpotential for the ORR. Both of these factors mean that the real anode and cathode potentials are more and less positive respectively than the theoretical anode and cathode potentials, which reduces the MFC cell voltage. Using a catalyst at the cathode significantly decreases the overpotential for ORR, increasing the MFC cell voltage. Chemical catalysts such as Pt are typically used, but biological catalysts, such as enzymes and bacteria, are also able to catalyse the ORR.

2.1.3 The chemical ORR catalysts used in MFCs

Many different types of chemical catalyst have been investigated in MFCs. ORR catalysts which are cheap, sustainable, robust, can be mass-manufactured and scaled-up, are much sought for. Pt catalysts supported on carbon are commonly used at the MFC cathode to catalyse the ORR, given their high activity toward the ORR. An additional advantage of Pt catalysts is that they carry out the ORR by a 4e^- and not a 2e^- pathway. The latter pathway produces peroxide, which causes membrane degradation and corrosion of the cathode [45]. However, Pt catalysts are both expensive and environmentally unsustainable, and are easily poisoned by the contaminants present in wastewater, such as sulphides. Therefore, MFC research in the area of ORR catalysis looks toward alternative chemical or biological catalysts.

Cobalt tetramethoxyphenylporphyrin (CoTMPP) and iron phthalocyanine (FePc) catalysts [17–19], are non-noble, metal macrocycle catalysts, which incorporate a porphyrin ring. CoTMPP and FePc show good catalytic activity toward the ORR, with open circuit potentials (OCPs) of 300 mV at pH 7.0 on graphite supports [17], and are cheaper than Pt catalysts. However, whether these catalysts are robust in the MFC system and can be mass-manufactured [16], has yet to be determined.

MnO_2 has also been shown to improve the power output of MFCs [19, 45]. Roche *et al.* found that a carbon-supported MnO_x catalyst gave a comparable performance to a carbon-

supported Pt catalyst (both at 0.82 mg/cm^2 loading on gas diffusion electrodes) in MFCs, with cathode potentials in the region of 300 mV for MnO_x as compared to 400 mV for Pt at pH 7.0 [45], whilst the cathode potentials in the MFC for the carbon support were lower than this, in the region of 100 mV. MnO_x is a cheap and sustainable catalyst for MFCs, although Mn chemistry is complex and more research is needed to see how robust this catalyst is in the MFC system [19,45].

Carbon itself catalyses the ORR, and modified and unmodified carbon materials have been developed for MFCs [19–21]. The catalytic activity of modified/unmodified carbon materials is lower than with carbon-supported chemical catalysts; the onset potential for ORR, E_{ORR} , is lower than $< 200 \text{ mV}$ [19,45–48], and the Tafel slope for unmodified carbon is 120 mV/dec at pH 7.0 [44]. Additionally, unmodified carbon materials produce peroxide through $2e^-$ reduction of O_2 to water, which degrades membranes and materials in MFCs. Improvements in ORR catalysis can be made through modification of the carbon surface through NH_3 gas [46] and nitric acid treatment [47], or the use of activated carbon materials with a high surface area [48]. Additionally, NH_3 gas surface treatment has also been shown to increase $4e^-$ ORR over $2e^-$ ORR, therefore reducing peroxide [46]. Modified carbon is therefore an improvement on unmodified carbon, although carbon-supported chemical catalysts have better performance than either of the two.

Pt is very expensive and not environmentally sustainable. Non-noble transition metal macrocycles and metal oxides are much cheaper, but still have associated costs and sustainability issues. Modified and unmodified carbon materials are cheap and sustainable, although they have lower catalytic activity than for carbon-supported catalysts. In the case of the majority of these abiotic cathodes, $4e^-$ ORR is in competition with $2e^-$ ORR. Given the low current and power densities typical of MFCs, biocathodes have a distinct advantage, being completely free, environmentally sustainable, robust, scalable, and do not need to be manufactured. Additionally, their ORR catalysis does not produce peroxide, as in the case of a chemical catalyst. However, little is currently understood about aerobic biocathode bacteria. In particular, what the mechanism of ORR catalysis is, and which bacteria are responsible for the catalysis.

2.2 The Aerobic Biocathodes used in MFCs

2.2.1 Background

Biocathodes are based on a biofilm of bacteria which catalyse a specific cathodic reaction. The type of reaction that the bacteria catalyse dictates the type of Bioelectrochemical System

(BES) which can be operated, broadly falling into two different categories; MFCs and microbial electrolysis cells (MECs). MFCs produce a voltage and therefore power, whereas MECs require an additional voltage input, utilising the energy available from the anode substrate for some useful cathode reaction, such as hydrogen production or metal recovery. Bacteria can be used to catalyse a wide-range of cathode reactions in a wide-range of different MFC and MEC systems, lowering the cathode overpotentials required [49, 50].

For MFCs, oxygen and nitrate -reducing biocathodes are attractive TEAs given their high reduction potentials and availability in the environment. Oxygen has the highest reduction potential (+0.60 V), but can require energy intensive aeration of the catholyte. Nitrate has a lower reduction potential (+0.54 V) than oxygen, but does not have the same solubility issues, removing the need for energy intensive aeration. Additionally, denitrification is an important step in wastewater treatment. The use of algae at the cathode which produce oxygen *in situ* is also an active area of MFC biocathode research [51–53]. Algae at the cathode can overcome problems associated with oxygen solubility at abiotic cathodes, but require a source of light. The aerobic biocathodes discussed in this thesis catalyse the ORR using biofilms of aerobic bacteria. A diagram of an MFC utilising an aerobic biocathode is presented in Figure 2.2a, along with a hypothesised, simplified metabolic pathway for an electrotroph in Figure 2.2b.

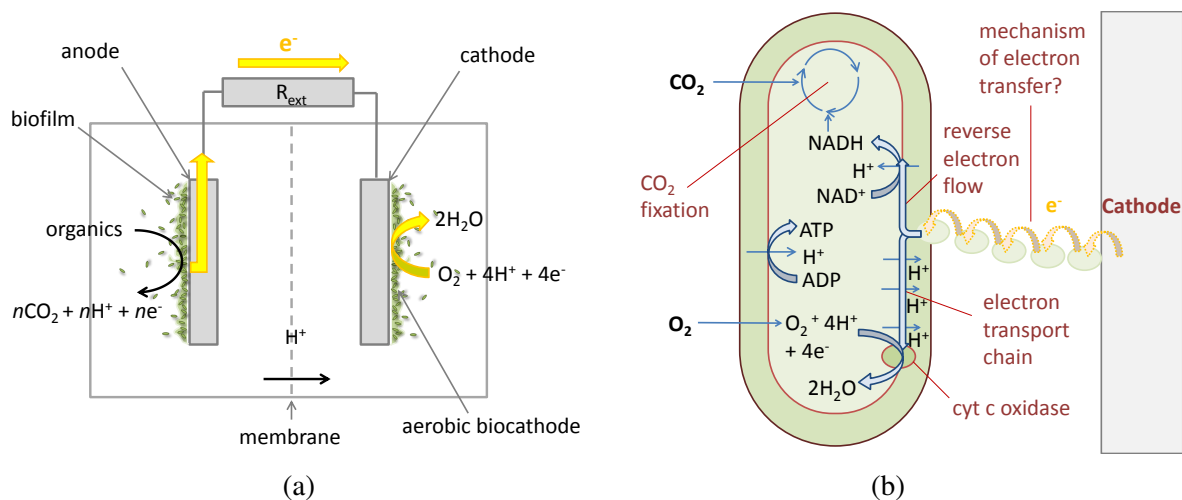


Figure 2.2: Aerobic biocathode MFC diagram (a) and a hypothesised, simplified metabolic pathway for an electrotroph (b).

2.2.2 Aerobic chemolithotrophic bacteria

Catalysis of the ORR at MFC cathodes by bacteria may occur indirectly or directly; the bacteria may produce a protein or chemical which catalyses the reaction abiotically or the bacteria may derive energy directly from the electrode for metabolism and growth. Known

groups of bacteria which derive energy directly for metabolic energy are collectively called chemolithotrophs. Aerobic chemolithotrophic bacteria can be classified according to the type of oxidation they undertake. The main types are iron oxidising bacteria (IOB), sulphur oxidising bacteria (SOB), ammonia oxidising bacteria (AOB), nitrite oxidising bacteria (NOB), manganese oxidising bacteria (MOB) and hydrogen oxidising bacteria (HOB, 'Knallgas bacteria'). Most of these groups of bacteria couple substrate oxidation with oxygen reduction through electron transport chains, with the generation of proton motive force and ATP. Most chemolithotrophs are also autotrophic, and fix CO₂ for biomass using the Calvin cycle [43]. Because NADH is required for reducing power in the Calvin cycle and most chemolithoautotrophs oxidise substrates with reduction potentials higher than that for NADH/NAD⁺, proton motive force is consumed through reverse electron transport, and ATP yields for chemolithoautotrophs are low [43]. This is also the case for HOB, even though the reduction potential for hydrogen is more negative than that for NADH; HOB do not usually possess the NAD⁺ hydrogenase required to generate NADH [54]. In the case of MOB, the reasons for Mn oxidation are not well-established, and many of the proposed mechanisms of Mn oxidation are indirect [55].

With the ARB found in bioanode biofilms, an ability to reduce insoluble Fe(III) oxides has been found to be important [56]. Given this, it may be that an ability to oxidise insoluble inorganic electron donors, such as reduced Fe and S minerals, is important for electrotrophs which use the electrode as the sole electron donor for metabolism and growth. Iron oxidation coupled with oxygen reduction by bacteria has been studied in the literature at acid and neutral pH, and the bacteria involved have been shown to derive energy directly for metabolism [57]. At low pH, Fe²⁺ is stable as aqueous ions, and acidophilic Fe oxidisers are able to couple soluble ferrous Fe oxidation with oxygen reduction, which yields approximately 30 kJ/mol (pH 2) for energy and growth [57]. At neutral pH, neutrophilic IOB are able to oxidise Fe(II) present as different minerals, Fe(II) complexes, or as the free ion at oxic/anoxic interfaces, to an insoluble Fe(III) precipitate [57]. This oxidation takes place on the outer membrane to prevent internal precipitation in the periplasmic space [57]. Apart from Fe oxidation, SOB are able to couple the oxidation of various reduced forms of S, including H₂S, S(0), SO₃²⁻ and S₂O₃²⁻, with oxygen reduction, producing sulfate [58]. This form of metabolism may be important for aerobic biocathodes, given that S(0) is insoluble in water and sulphide is present as various minerals in the natural environment, such as pyrite (FeS₂). Other forms of chemolithotrophy, which do not involve the oxidation of a reduced insoluble electron donor, may yet turn out to be involved in ORR catalysis at aerobic biocathodes, such as hydrogen oxidation, though this would not be a natural analogue of the insoluble cathode electrode. Many of the reduction potentials, important, or potentially-important, for aerobic biocathodes have been collected in Table 2.1.

Redox couple	E ⁰ (V)	E ^{0'} (V)	Conditions	Ref.
0.5O ₂ /H ₂ O	1.229	0.60	pH 7.0, pO ₂ = 0.2 atm	[59]
Fe ³⁺ /Fe ²⁺	0.77	0.57	[Fe ²⁺] = [Fe ³⁺]	[59]
NO ₃ ⁻ /0.5N ₂	-	0.54	pH 7.0	[22]
Cyc2	-	0.36	pH 4.8	[60]
MnO ₂ (s)/Mn ²⁺	1.229	0.26	pH 7.0, [Mn ²⁺] = 5mM	[59]
NO ₃ ⁻ /NO ₂ ⁻	-	0.22	pH 7.0	[22]
Cytochrome a3	-	0.15	pH 7.0	[61]
O ₂ /H ₂ O ₂	0.695	0.12	pH 7.0, pO ₂ = 0.2 atm, [H ₂ O ₂] = 5 mM	[59]
Cytochrome a	-	0.09	pH 7.0	[61]
Cytochrome c	-	0.05	pH 7.0	[61]
Fe(OH) ₃ (s)/FeCO ₃ (s)*	-	0.00	pH 7.0	[57]
FeOOH(s)/FeCO ₃ (s)*	-	-0.26	pH 7.0	[62]
FAD/FADH ₂	-	-0.42	pH 7.0	[63]
S(0)/HS ⁻	-	-0.48	pH 7.0	[63]
CH ₃ COO ⁻ /2 HCO ₃ ⁻	0.187	-0.51	pH 7.0, [CH ₃ COO ⁻] = 16.9 mM, [HCO ₃ ⁻] = 5 mM	[22]
NAD ⁺ /NADH	-	-0.53	pH 7.0	[63]
2 H ⁺ /H ₂	0	-0.62	pH 7.0	[59]

Table 2.1: Standard reduction potentials vs. Ag/AgCl of chemical species and biological electron transport proteins relevant or potentially-relevant to aerobic biocathodes.

2.2.3 Direct application of known aerobic chemolithotrophic bacteria as aerobic biocathodes in MFCs

Isolates of Fe and Mn oxidising aerobic bacteria have been used in poised-potential half-cells and as biocathodes in MFCs, utilising Fe³⁺/Fe²⁺ or MnO₂(s)/Mn²⁺ as an electron shuttle between the electrode and the bacteria. This is because both MnO₂ and Fe³⁺ have better reduction kinetics than the ORR at plain non-catalysed electrodes [64–66]. In this type of aerobic biocathode, Fe³⁺ or MnO₂(s) are electrochemically reduced, then re-oxidised back to Fe²⁺ or Mn²⁺, thus mediating/catalysing electron transfer between the electrode and the bacteria, and improving cathode performance.

Lopez *et al.* developed a system for the electrochemical oxidation of organic contaminants present in industrial effluents which could not be treated with conventional microbiologically-based wastewater treatment processes [67]. In this system, they coupled the oxidation of methanol with the electrochemical reduction of Fe(III) at the cathode electrode at low pH, using an external microbial culture vessel containing *Acidithiobacillus ferroxidans* to biologically regenerate the Fe(III). This system was not an MFC, but demonstrated how fuel cell cathode performance could be improved by using an acidophilic IOB bacterium. Subsequently, an MFC was developed using the same cathode system, but with acetate oxidation

by a bioanode biofilm instead of abiotic methanol oxidation at the anode [66, 68, 69]. A high cathode potential of 0.448 V was achieved for the lab-scale systems, with an MFC peak power density of 120 $\mu\text{W}/\text{cm}^2$. However, this MFC system required the use of both a bipolar membrane and an external recirculation vessel.

It has also been shown that certain strains of IOB are able to use the electrode as the sole electron donor for energy and growth. Cultivation of the neutrophilic Fe oxidiser *Mariprofundus ferrooxydans* PV-1 at a potential of -0.286 V gave a small increase in the ORR catalytic activity, with an onset potential for ORR of approximately -0.2 V determined by cyclic voltammetry (CV) [70]. Additionally, a half-cell containing a graphite working electrode poised at -0.045 V in pH 2 minimal media inoculated with *Acidithiobacillus ferrooxidans* was shown to significantly increase the chronoamperometry (CA) reduction current over time in comparison to non-inoculated controls, which was interpreted as the bacteria using the electrode as the sole electron donor for metabolism and growth [71]. In this study, electron transfer to the bacteria was thought to be mediated by a redox compound with a formal potential of 0 V [71].

The use of MOB at the cathode of an MFC has also been demonstrated. Rhoads *et al.* used the Mn^{2+} oxidising bacterium *Leptothrix discophora* to increase the cathode potential of their MFC to 0.34 V, achieving a peak power density of 13 $\mu\text{W}/\text{cm}^2$ over 500 hours of operation [65]. The cathode potential was a full 300 mV higher than the unmodified electrode, and it was concluded that the ORR catalysis was occurring through the cycling of $\text{Mn}^{2+}/\text{MnO}_2(\text{s})$ on the electrode surface through microbial oxidation of Mn^{2+} and electrochemical reduction of $\text{MnO}_2(\text{s})$.

The ability of well-known single species of IOB and MOB bacteria to oxidise Fe and Mn respectively has been exploited to improve catalysis at the cathode of MFCs. The use of acidophilic IOB requires expensive external recirculation vessels and both expensive and higher-resistance bipolar membranes for the MFC system, whereas neutrophilic IOB are very difficult to isolate. Individual strains of MOB which oxidise Mn at neutral pH may be a good solution for the MFC, although more needs to be understood about the mechanism of electron transfer for these bacteria. Some of these bacteria have been shown to be able to use the electrode as the sole electron donor for metabolism and growth, catalysing the ORR in the process. Therefore, the electrode might provide an ecological niche allowing the bacteria to compete with other metabolic pathways and form a stable, ORR catalysing biofilm. One strategy for enriching for an efficient ORR catalysing biofilm is therefore to provide the right conditions in order to select for the best bacteria to perform the catalysis. Various studies from the literature utilising this strategy of enrichment are discussed in the following sections.

2.2.4 Mixed-community aerobic biocathodes in MFCs

In the field of microbiologically influenced corrosion (MIC), it has long been established that the corrosion of stainless steel and other metals in seawater is accelerated by the formation of mixed community biofilms of aerobic bacteria which catalyse the ORR via direct or indirect means [72]. In particular, stainless steel materials exposed to seawater or freshwater undergo a process called ennoblement, where the OCP of the electrode increases over time [72]. This ennoblement process is important, as it causes the stainless steel to corrode [72]. After the first MFC study by Potter in 1911 [23], research in the general area of BES continued during the 1960s due to an interest in MIC, with several studies coupling a magnesium anode with an iron cathode colonised by sulphate-reducing bacteria [73]. Later, in 1997, MIC was exploited in an underwater battery in which a magnesium anode was coupled to a graphite cathode exposed to seawater and on which an aerobic biocathode developed [74]. Since these early studies, a number of sediment-type MFCs have been developed which couple a bioanode oxidising organics in the anaerobic sediment beneath a fresh or seawater body to an aerobic biocathode positioned in the overlying water, which catalyses the ORR [75]. These are sometimes called benthic MFCs.

Much of the recent interest in using aerobic biocathodes for MFCs came in 2007 and 2008, with papers by Clauweart *et al.* and Rabaey *et al.* using reactor-type MFCs [76,77]. Clauweart *et al.* obtained an aerobic biocathode catalysing the ORR in an MFC under fresh water conditions by using a mixed sludge/sediment inoculum [76], whereas Rabaey *et al.* used a mixture of environmental samples obtained from rusted metal poles, sediments and activated sludge from a wastewater treatment plant to inoculate their MFC reactors [77]. Clauweart *et al.* inferred the presence of an aerobic biocathode in their MFCs by using autoclaved controls [76], whereas Rabaey *et al.* attributed a sudden decrease in anode potential, but a considerable increase in MFC cell voltage over a much-longer period to formation of an aerobic biocathode catalysing the ORR at the cathode [77]. Further MFC studies followed, forming the bulk of the aerobic biocathode literature. In this literature, many different types of MFC system have been engineered and investigations undertaken using environmental samples as inoculum to generate biofilms which catalyse the ORR at the cathode. A summary of these studies is provided in Table 2.2.

In terms of the engineering of these systems, there have been a number of different investigations. Freguia *et al.* used the anode effluent as influent for the biocathode, purportedly solving the pH splitting problem between the anode and cathode, although the organic loading of the anode effluent may have impacted on the performance of the biocathode [111]. There have also been a few of studies where an organic electron donor, such as acetate [99, 101] or azo dye [102], have been used in the cathode chamber. In the former studies, it was claimed

System type	Inoculum	Electrode	E_{ORR} V	Peak power $\mu\text{W}/\text{cm}^2$	Year	Community analysis	Ref.
MFC	Non-inoculated	CC	0.40	57	2011	Y	[78]
MFC	NS	GF	0.40	-	2011	N	[79]
Half-cell	AS	GP	0.40	-	2013	N	[80]
Half-cell	AS	CC gas diffusion electrode	0.40	-	2013	N	[81]
Sediment MFC	Seawater	CC	0.40	-	2014	N	[82]
MFC	AS	GF	0.40	68	2015	N	[1]
Sediment MFC	Seawater	GP	0.40	3	2006	Y	[75]
Sediment MFC	Freshwater/Brackish	CF and SS	0.35	12	2010	Y	[83]
Half-cell	NS	GP	0.35	-	2010	N	[84]
Half-cell	NS	GP	0.35	-	2011	N	[85]
MFC	PEC	GAC	0.35	-	2011	N	[86]
Sediment MFC	Seawater	SS	0.30	2	2007	N	[87]
MFC	Various	CF	0.30	-	2007	Y	[76]
Half-cell	AS and PEC	CP	0.25	-	2012	Y	[88]
Microbial solar cell	PEC	GP	0.25	-	2013	Y	[89]
Marine floating MFC	Seawater	SS	0.20	2	2013	N	[90]

Table 2.2: Aerobic biocathode studies ranked according to E_{ORR} , where available. AS = activated sludge, AnS = anaerobic sludge, DW = domestic wastewater, PEC = Previously enriched consortium, NS = nitrifying sludge, MBR = membrane bioreactor, CC = carbon cloth, CF = carbon felt, CP = carbon paper, CB = carbon brush, AC = activated carbon, GAC = granular activated carbon, CG = carbon granules, CNT = carbon nanotubes, GCE = glassy carbon electrode, GG = graphite granules, GF = graphite brush, GP = graphite felt, GP = graphite plate, RVC = reticulated vitreous carbon, SS = stainless steel, SSM = stainless steel mesh. * $E_{1/2} = 0.15$ V.

System type	Inoculum	Electrode	E_{ORR} V	Peak power $\mu\text{W}/\text{cm}^2$	Year	Community analysis	Ref.
MFC	AS	CC	0.20	10	2013	Y	[91]
MFC	DW	CB	0.20	119	2014	Y	[92]
MFC	AnS	SSM and CNT coated SSM	0.15	15	2013	N	[93]
Marine PEM fuel cell	Seawater	SS	0.10	32	2005	N	[94]
MFC	ANS	GF	0.05	11	2012	N	[95]
MFC-MBR	DW	Ultrafiltration membrane	0.00	38	2013	N	[96]
Marine half-cell	Seawater	GP	-0.10	-	2010	N	[97]
MFC	AS	Graphene	-0.10	32	2012	N	[98]
MFC	Various	GF and CC	-0.10	30	2008	Y	[77]
HC	Garden compost	CC	-0.10	-	2014	Y	[99]
MFC	DW	CC and CP	-0.10	50	2013	N	[100]
MFC	PEC	GG	-0.15	-	2010	N	[101]
MFC	As and AnS	CP	-0.20	5	2011	N	[102]
MFC-MBR	AS	SS	-0.20	-	2013	N	[103]
MFC	AnS	SSM	-	-	2010	N	[104]
Seawater battery	Seawater	CB	-	-	1997	N	[74]

Table 2.2 (continued)

System type	Inoculum	Electrode	E_{ORR} V	Peak power $\mu\text{W}/\text{cm}^2$	Year	Community analysis	Ref.
Sediment MFC	Freshwater	GF	-	-	2012	N	[105]
MFC	AS and AnS	GG	-	-	2010	Y	[106]
MFC	AS	GG and GB	-	-	2011	Y	[107]
MFC	PEC	GAC	-	-	2012	Y	[108]
MFC	Soil	GG	-	-	2012	Y	[109]
MFC	Various	CF	-	3	2013	Y	[110]
MFC	Anode effluent	GG	-	-	2008	N	[111]
MFC	AS	GB	-	-	2008	N	[112]
MFC	AnS	CP	-	-	2009	N	[113]
MFC	AS	GF	-	-	2010	N	[114]
MFC	AS	GC	-	-	2010	N	[115]
MFC	AnS	CNT-chitosan composite	-	19	2011	N	[116]
MFC	AS	GP	-	4	2011	N	[117]
MFC	Soil	GG	-	-	2012	N	[118]
Half-cell	AS	CF	-	-	2009	N	[119]
MFC	AS and AnS	GG	Redox peak*	-	2008	Y	[120]

Table 2.2 (continued)

that the acetate-oxidising biofilm was able to catalyse the ORR. However, such environments will not select for autotrophic bacteria which are able to use the electrode as the sole electron donor for energy and growth. Other studies have examined the use of air biocathodes in order to solve the oxygen solubility issue [76, 81, 100, 116], and the use of cheap electrode materials [86, 93, 95, 98, 104, 107] and membranes [104] has also been explored. Recently, an aerobic biocathode was coupled to a bioanode using the rhizodeposits from a species of grass to provide the substrate, therefore using the aerobic biocathode as a free and sustainable alternative to an expensive chemical catalyst, such as Pt [1]. With many of these studies, it is important to bare in mind that having bacteria at the biocathode does not necessarily mean that they are catalysing the ORR. This must be proven by using controls coupled to cathode polarisation tests.

Mixed-community aerobic biocathodes have also been used to improve MFC performance for wastewater treatment applications. Different types of wastewater have been used, such as synthetic wastewater containing glucose [112, 117], sewage sludge collected from the secondary sedimentation tank of a domestic wastewater treatment plant [118] and dairy manure [109]. Additionally, different wastewater treatment systems which incorporate an MFC have also been developed, such as an aerobic biocathode MFC coupled to a denitrifying biocathode MFC [79], an aerobic biocathode MFC submerged in the AS aeration tank of a wastewater treatment plant [114], and a coupled MFC-membrane bioreactor (MFC-MBR) [96, 103]. In the MFC-MBR systems, the effluent from the MFC is used as influent for the MBR, with the energy from the MFC offsetting energy intensive aeration costs in the MBR and the MBR improving the effluent quality of the MFC.

The remaining studies in the literature on mixed-community aerobic biocathodes have some component of fundamental investigation, examining performance under different conditions. Investigations have been carried out on the bacterial communities and mechanisms of electron transfer to the electrode. Additionally, different studies have looked at the effect of poised-potential [84, 85, 88, 119], oxygen mass transfer [85] and pH/temperature [80]. The mechanism of electron transfer is unknown, but discussed to a small extent in different papers which have some component of electrochemical analysis [89, 92, 93, 95, 98, 106, 120]. The remaining aerobic biocathode investigations have some element of discussion on community analysis, which is of fundamental importance in efforts to identify the bacteria responsible for ORR catalysis [76–78, 88, 89, 91, 92, 99, 106–110, 120, 121]. The community analysis studies will be discussed in the next section.

2.3 The Bacteria Responsible for ORR Catalysis in Mixed Community Aerobic Biocathodes

The community composition of aerobic biocathodes has been determined in different studies, and these are compiled in Table 2.3. The aerobic biocathodes have been ranked according to the onset potential for ORR (E_{ORR}), determined from cathode polarisation, as this is a key parameter used to characterise any chemical or biological ORR catalyst, being a measure of catalytic activity of the ORR catalyst. Using this parameter, it becomes readily apparent how different the aerobic biocathodes from different studies are. These differences are likely due to differences in the mechanism of ORR catalysis and the bacteria catalysing the reaction.

Table 2.3 gives the bacteria which have been associated with ORR catalysis or were found to be dominant in the mixed-community aerobic biocathodes of MFCs and SMFCs, as well as in one half-cell study. The aerobic biocathodes with a high onset potential for the ORR cluster at the top of the table. Of the three studies where the aerobic biocathode had an onset potential of 0.35-0.40 V, two of the MFCs were SMFCs [75,83], whilst one was an MFC [78]. In the MFC study, the cathode electrode was loaded with 4 mg/cm² of Pt, therefore the catalytic activity may or may not have been associated with ORR catalysis by microorganisms. In the SMFC study by Schamphelaire *et al.*, a comparison with an unpolarised control electrode was included, allowing the authors to identify with increased confidence that an uncultured proteobacterium was likely responsible for the ORR catalysis [83]. This bacterium was 100 % similar to an uncultured *Gammaproteobacterium* found in some steel waste. In the other SMFC study, Reimers *et al.* found *Pseudomonas* species were dominant in their aerobic biocathodes, but there was no comparison to a non-polarised control, therefore these species were not necessarily responsible for the ORR catalysis in their biofilms [75]. As *Pseudomonas fluorescens* was present in the biofilm, the authors inferred that MnO_x, oxyhydroxides and phenazines were playing a role in ORR catalysis [75], though this was not proven.

Of the aerobic biocathodes with a lower onset potential for ORR catalysis, various species have been detected, as indicated in Table 2.3. Generally, many of the authors relate an ability to oxidise hydrogen with ORR catalysis, which stems from the study by Rabaey *et al.* in which all of the dominant bacteria had an ability to oxidise hydrogen [77]. Community analysis using the 16S rRNA gene gave the dominant bacteria in the community as *Sphingobacterium*, *Acinetobacter* and *Acidovorax* species, all with a known ability to oxidise hydrogen [77]. Subsequently, the authors tested isolates enriched from biofilm samples using a culture method for isolating H₂-oxidising bacteria aerobes, obtaining 6 isolates closely related to *Sphingobacterium multivorum*, and one closely related to *Acinetobacter calcoaceti-*

Type	Phylum	Class	Order	Family	Genus	E_{ORR} V	Method
MFC	<i>Proteobacteria</i>	<i>Gammaproteobacteria</i>	<i>Xanthomonadales</i>	<i>Xanthomonadaceae</i>		0.40	CL [78]
	<i>Proteobacteria</i>	<i>Gammaproteobacteria</i>	<i>Xanthomonadales</i>	<i>Xanthomonadaceae</i>	<i>Xanthomonas</i>		
SMFC	<i>Proteobacteria</i>	<i>Gammaproteobacteria</i>	<i>Pseudomonadales</i>	<i>Pseudomonadaceae</i>	<i>Pseudomonas</i>	0.40	CL [75]
	<i>Proteobacteria</i>						
MFC	<i>Proteobacteria</i>	<i>Gammaproteobacteria</i>	<i>Pseudomonadales</i>	<i>Pseudomonadaceae</i>	<i>Pseudomonas</i>	0.30	CL [76]
	<i>Proteobacteria</i>	<i>Gammaproteobacteria</i>	<i>Xanthomonadales</i>	<i>Xanthomonadaceae</i>	<i>Hydrocarboniphaga</i>		
	<i>Proteobacteria</i>	<i>Alpha Proteobacteria</i>	<i>Sphingomonadales</i>	<i>Sphingomonadaceae</i>	<i>Sphingopyxis</i>		
	<i>Proteobacteria</i>	<i>Alpha Proteobacteria</i>	<i>Rhizobiales</i>	<i>Hyphomicrobiaceae</i>	<i>Xantobacter</i>		
MSC	<i>Proteobacteria</i>	<i>Gammaproteobacteria</i>	<i>Alteromonadales</i>	<i>Alteromonadaceae</i>	<i>Marinobacter</i>	0.25	CL [89]
HC	<i>Proteobacteria</i>	<i>Gammaproteobacteria</i>	<i>Chromatiales</i>	<i>Chromatiaceae</i>		0.25	IDS [121]
HC	<i>Bacteroidetes</i>					0.25	CL [88]
MFC	<i>Proteobacteria</i>	<i>Alpha proteobacteria</i>	<i>Rhizobiales</i>	<i>Bradyrhizobiaceae</i>	<i>Nitrospira</i>	0.20	CL [92]
	<i>Proteobacteria</i>	<i>Beta proteo bacteria</i>	<i>Nitrosomonadales</i>	<i>Nitrosomonadaceae</i>	<i>Nitrosomonas</i>		
	<i>Proteobacteria</i>	<i>Gammaproteobacteria</i>	<i>Chromatiales</i>	<i>Ectothiorhodospiraceae</i>	<i>Alkalilimnocola</i>		
MFC	<i>Bacteroidetes</i>					0.20	DGGGE [107]
	<i>Proteobacteria</i>	<i>Gammaproteobacteria</i>	<i>Pseudomonadales</i>	<i>Moraxellaceae</i>	<i>Acinetobacter</i>		
	<i>Proteobacteria</i>	<i>Alpha proteobacteria</i>	<i>Rhizobiales</i>	<i>Bradyrhizobiaceae</i>	<i>Nitrobacter</i>		
	<i>Proteobacteria</i>	<i>Beta Proteobacteria</i>	<i>Burkholderiales</i>	<i>Alcaligenaceae</i>	<i>Achromobacter</i>		
MFC	<i>Proteobacteria</i>	<i>Alpha proteobacteria</i>	<i>Rhizobiales</i>			0.20	PS [91]
	<i>Proteobacteria</i>	<i>Gammaproteobacteria</i>	<i>Pseudomonadales</i>				
	<i>Bacteroidetes</i>	<i>Sphingobacteria</i>	<i>Sphingobacteriales</i>				

Table 2.3: Dominant bacteria / bacteria identified with ORR catalysis in different aerobic biocathode communities, ranked according to E_{ORR} . The types of BES are MFC, half-cell (HC), microbial solar cell (MSC), sediment microbial fuel cell (SMFC). The method of community analysis are clone libraries (CL), illumina-dye sequencing (IDS), pyrosequencing (PS) and denaturing gradient-gel electrophoresis (DGGGE). * $E_{1/2} = 0.15$ V.

Type	Phylum	Class	Order	Family	Genus	E _{ORR} V	Method
MFC	<i>Proteobacteria</i> <i>Bacteroidetes</i>	<i>Betaproteobacteria</i>	<i>Rhodocyclales</i>	<i>Rhodocyclaceae</i>	<i>Azovibrio</i>	0.15*	CL [120]
MFC	<i>Proteobacteria</i> <i>Uncultured</i> <i>Bacteroidetes</i>	<i>Gammaproteobacteria</i>	<i>Xanthomonadales</i>	<i>Xanthomonadaceae</i>	<i>Xanthomonas</i>	0.15*	CL [106]
HC	<i>Deinococcus-Thermus</i> <i>Gemmatimonadetes</i>					0.00	PS [122]
MFC	<i>Proteobacteria</i> <i>Bacteroidetes</i> <i>Proteobacteria</i>	<i>Gammaproteobacteria</i> <i>Sphingobacteria</i> <i>Beta Proteobacteria</i>	<i>Pseudomonadales</i> <i>Sphingobacteriales</i> <i>Burkholderiales</i>	<i>Moraxellaceae</i> <i>Sphingobacteriaceae</i> <i>Comamonadaceae</i>	<i>Acinetobacter</i> <i>Sphingobacterium</i> <i>Acidovorax</i>	-0.10	CL [77]
MFC	<i>Chloroflexi</i>	<i>Chloroflexi</i>	<i>Chloroflexales</i>	<i>Chloroflexaceae</i>	<i>Chloroflexus</i>	-0.15	PS [99]
MFC	<i>Proteobacteria</i> <i>Proteobacteria</i>	<i>Betaproteobacteria</i> <i>Gammaproteobacteria</i>				-	PS [110]
MFC	<i>Proteobacteria</i> <i>Proteobacteria</i> <i>Proteobacteria</i> <i>Proteobacteria</i>	<i>Betaproteobacteria</i> <i>Beta Proteobacteria</i> <i>Beta Proteobacteria</i> <i>Beta Proteobacteria</i>	<i>Burkholderiales</i> <i>Burkholderiales</i> <i>Burkholderiales</i> <i>Burkholderiales</i>	<i>Comamonadaceae</i> <i>Comamonadaceae</i> <i>Comamonadaceae</i> <i>Comamonadaceae</i>	<i>Comamonas</i> <i>Comamonas</i> <i>Comamonas</i> <i>Acidovorax</i>	-	CL [108]
MFC	<i>Proteobacteria</i> <i>Bacteroidetes</i> <i>Proteobacteria</i>	<i>Beta Proteobacteria</i> <i>Sphingobacteria</i> <i>Gammaproteobacteria</i>	<i>Burkholderiales</i> <i>Sphingobacteriales</i> <i>Pseudomonadales</i>	<i>Alcaligenaceae</i> <i>Sphingobacteriaceae</i> <i>Moraxellaceae</i>	<i>Achromobacter</i> <i>Sphingobacterium</i> <i>Acinetobacter</i>	-	PS [109]

Table 2.3 (continued)

cus [77]. These isolates had a catalytic effect, but at current densities which were a 1/3 of the mixed community [77]. Though the onset potential for ORR was not determined for the isolates, examination of the cathode polarisation curve for the mixed community shows an E_{ORR} of -0.1 V [77]. Further to this study, Freguia *et al.* tested *Acinetobacter calcoaceticus* in a poised potential half-cell, finding ORR catalytic activity with an onset potential for the ORR of 0.0 V [123].

Since the study by Rabaey *et al.*, HOB are thought to play an important role in mixed community aerobic biocathodes, with researchers either inoculating their MFC reactors with environmental samples thought to be enriched in HOB [107], and/or subsequently identifying bacteria from community analysis of biofilms generated from diverse inocula with a known ability to oxidise hydrogen as responsible for the ORR catalytic current [91, 107, 109]. Additionally, an ability to oxidise Mn/Fe is suggested as being important in the literature [115], although no known Fe/Mn oxidising bacteria have yet been identified through community analysis, or an ability to oxidise Fe/Mn tested for. In a study by Mao *et al.*, Fe/Mn deposits on the electrode were identified by surface analysis techniques, but no link between Fe/Mn oxidation and ORR catalysis was proven [115]. Recently, it has also been proposed that there is an association between the nitrification activity of the biofilm and ORR catalysis by the biofilm [92]. Finally, it has been proposed that c-type cytochromes are important for direct electron uptake by cathode bacteria from insoluble electron donors [124]. These c-type cytochromes may turn out to be similar to the multihæm c-type cytochromes used by *Geobacter sulfurreducens* and *Shewanella oneidensis* MR-1 species to carry dissimilatory reduction of metal hydr(oxides) [125].

Investigations using isolates of bacteria have shown that a large number of different bacteria are able to catalyse the ORR, but all of these studies give E_{ORR} values much less than +0.4 V, indicating a different type of ORR catalysis [126–128]. Erable *et al.* isolated 19 different strains spanning the *Actinobacteria*, *Gammaproteobacteria*, *Alphaproteobacteria*, *Firmicutes* and *Flavobacteriaceae* from mixed-community aerobic biocathodes grown at poised potential on SS electrodes in seawater, but did not obtain any cathode polarisation curves [126]. Employing the same approach, Parot *et al.* tested 7 isolates from stainless steel electrodes in seawater at a poised potential of -0.2 V, but the onset potential for ORR was no more than -0.2 V across all strains and could not be sustained under constant polarisation [127]. Cournet *et al.* also found transitory catalysis, testing the catalytic activity of 20 different Gram-negative and Gram-positive strains by CV on GCE electrodes and finding onset potentials of the ORR which were no greater than -0.2 V. They suggested that the transitory nature of the ORR catalysis was likely due to a redox active metabolite secreted by the bacteria [128].

To date, mixed-community aerobic biocathodes with the highest onset potentials for the

ORR ($> +0.35$ V) have been enriched from activated sludge in poised-potential systems [80, 81, 84, 85]. However, little community analysis has been carried out on these type of aerobic biocathodes, and only using clone libraries and DGGE community analysis techniques. The long-term effect of poised potential on aerobic biocathodes using half-cells inoculated with activated sludge was examined by Xia *et al.* [88], however, the resulting aerobic biocathodes had E_{ORR} values of $+0.25$ V and were dominated by species related to *Bacteroidetes*. Therefore, there is a need to identify the community composition and the bacteria responsible for ORR catalysis in high-performing aerobic biocathodes with high E_{ORR} values ($> +0.35$ V). The different onset potentials for biologically catalysed ORR likely indicate different mechanisms of catalysis by the bacteria. Details about these mechanisms of ORR are vital for better understanding aerobic biocathodes, and will be discussed in the next section.

2.4 Mechanism of Electron Transfer in Aerobic Biocathodes

2.4.1 Background

Only one study currently exists which examined the mechanism of electron transfer (ET) for aerobic biocathode bacteria [123]. These were two aerobic biocathode bacteria, *Acinetobacter calcoaceticus* and *Shewanella putrefaciens*, which were chosen on the basis of previous ORR catalytic activity and having a number of different pathways for ET in bioanodes respectively [123]. In this study, there was an increase in E_{ORR} to -0.1 V for *Acinetobacter calcoaceticus* and 0 V for *Shewanella putrefaciens* on a plain carbon paper electrode, which was attributed to ORR catalysis by the bacteria. In the same study, similar increases in onset potential for ORR were also observed for a plain carbon electrode immersed in solutions containing hemin at 1 μM concentration, and 2-amino-3-dicarboxy-1,4-naphthoquinone (ACNQ) at 1 μM , which both catalyse $2 e^-$ ORR to peroxide, although no increase in catalytic current was observed for 0.1 mg/L of catalase enzyme [123]. These controls approximated the effect of heme proteins, quinones and catalase enzyme [123]. Heme proteins may result from cell lysis within the biofilm, whilst quinones and catalase can be secreted by bacterial cells [123]. This is important, as it is possible that catalysis by the bacteria in aerobic biocathodes is indirect and not associated with energy metabolism. The mechanisms proposed for indirect ORR catalysis by bacteria include;

1. ORR catalysis by extracellular enzymes, such as superoxide dismutase, catalase and peroxidase [72]
2. ORR catalysis by extracellular porphyrins [72]

3. ORR catalysis by metal ions complexed within extracellular polymeric substances (EPS) [72]

However, in the study by Freguia *et al.*, the E_{ORR} at a plain carbon electrode for ACNQ and hemin increased to no more than -0.1 V, and catalase exhibited no ORR activity [123]. It is therefore unlikely that these compounds secreted by bacteria are responsible for the large increase in E_{ORR} to +0.4 V which has been observed in some of the aerobic biocathode studies so far. The mechanism of ORR catalysis for these aerobic biocathodes remains to be determined, but mechanisms of ET involving electron uptake by the bacteria for energy and growth remain the likeliest candidates. Analogy with bioanodes might provide a starting point for discussion. The ARB found at the bioanode which are able to donate electrons to solid anode electrodes or insoluble Fe(III) oxides via direct electron transfer (DET) and mediated electron transfer (MET) mechanisms [56]. DET mechanisms include direct electrode contact of outer-membrane cytochromes (OMCs) or the use of conductive pilli called nanowires [56]. MET mechanisms rely on the shuttling of electrons from the bacterial electron transport chain to the electrode via endogenous (excreted by the bacteria) or exogenous (artificially or environmentally available) mediators [56].

2.4.2 Direct ORR catalysis by direct electron transfer

DET mechanisms reported in the literature for *Geobacter sulfurreducens* are thought to involve networks of c-type OMCs or conductive nanowires attached to interfacial c-type cytochromes, which allow electrical contact for bacteria at a distance within the biofilm [129]. These DET mechanisms should allow dead biomass to accumulate at the electrode surface and for the ARB to expand beyond a monolayer of cells at the electrode surface.

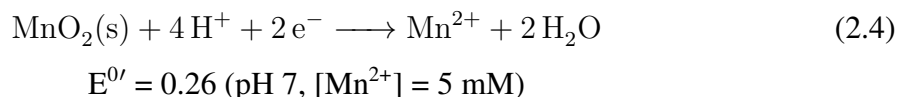
Geobacter species, which are able to form anode biofilms and use DET mechanisms for ET to the insoluble anode, have also been shown to accept electrons from poised-potential electrodes for respiration [130]. In particular, *Geobacter sulfurreducens* was able to reduce the periplasmic electron acceptor nitrate to nitrite, using the electrode as the electron donor [130]. Additionally, CV on purified *Geobacter* c-type cytochromes shows that these enzymes are electrochemically reversible, so they may also be involved in direct electron uptake from poised-potential cathodes [124]. If these c-type OMCs are coupled to an electron transport chain comprising periplasmic ET proteins, for example, then electrons could be shuttles to cytochrome c oxidase located on the inner membrane, and ultimately to intracellular O_2 . A similar electron transport chain is already found in *Acidithiobacillus ferrooxidans* [60]. For this chemolithoautotroph, electron uptake is thought to occur via oxidation of soluble Fe(II) on the outer-membrane by Cyc2, which transfers electrons via periplasmic ET proteins to

cytochrome c oxidase located on the inner membrane [60].

2.4.3 Direct ORR catalysis by mediated electron transfer

Shewanella oneidensis MR1 is able to utilise both DET and MET mechanisms for ET to anode electrodes. For MET, *Shewanella oneidensis* MR1 is reportedly able to utilise endogenous redox shuttles such as riboflavin, flavin mononucleotide and 9,10-anthraquinone-2,7-disulphonic acid (AQDS) [131], and exogenous redox shuttles such as humic acids [132,133] and phenazines [15,134]. However, electron shuttles represent an energy investment for an individual species [135], they may be used by other species of bacteria within the biofilm [136], low rates of shuttle flux to the electrode surface can potentially limit the current density [137], and they may diffuse out of the biofilm [137]. However, with regards to the last point, it has been shown that a portion of soluble flavins involved in ET in *Shewanella oneidensis* MR1 were absorbed on the electrode surface, which may aid their retention in the biofilm [135].

Hydrogen can also act as an electron donor for microbial metabolism, but only at electrode poised-potentials more negative than -0.62 V (pH 7). Additionally, carbon electrodes require a large electrode overpotential for the hydrogen evolution reaction [138]. Hydrogen is therefore unlikely to mediate ET from the cathode to an aerobic biocathode in the vast majority of aerobic biocathode studies discussed so far. One other MET mechanism is using biomineralised MnO_x as an electron shuttle, which is a mechanism implicated in the ennoblement of stainless steel electrodes [72], and which has also been shown to increase the cathode potential of an MFC using a pure strain of MOB called *Leptothrix discophora* [65]. The overall half-cell reaction for $\text{MnO}_2/\text{Mn}^{2+}$ is;



In this case, electrons are passed from the electrode to the bacteria through the bacterial oxidation of Mn^{2+} to MnO_2 , and the subsequent electrochemical reduction of MnO_2 to Mn^{2+} .

MET was been proposed to be a possible pathway of ET to the bacterium *Acinetobacter calcoaceticus*, which was shown to catalyse the ORR at a plain carbon paper electrode, whilst also producing an unidentified reversible redox active peak with a mid-point potential of -0.14 V, which was observed in the absence of oxygen [123]. This spectrum was compared to CV on a plain carbon paper electrode immersed in a solution containing pyrrollquinone quinone

(PQQ) at 2 μM on a plain carbon electrode, and the two CV were found to be identical. Further tests showed an enhancement in electrical current for *Acinetobacter calcoaceticus* in the presence of PQQ, which was interpreted as MET from the electrode to the bacteria as part of an electron transport chain, though this was not proven. Indirect 2e^- ORR to peroxide through the autooxidation of PQQ was ruled out as the principal mechanism of ORR catalysis given the negligible currents associated with a control [123].

2.5 The Effect of Poised-potential on Aerobic Biocathodes

2.5.1 Background

The use of poised-potentials allows for the controlled enrichment of aerobic biocathode bacteria from environmental samples and investigations on the community composition and ORR catalysis. In the case of bioanodes, changing the anode potential may select for bacteria using different terminal cytochromes with different mid-point potentials, which may change the energy gain for the bacteria when using the anode. However, this would be dependent on the exact mechanism, as it is the electron transport proteins in the electron transport chain which translocate protons across a membrane, thereby establishing the proton gradient necessary for ATP synthesis. Additionally, changing the anode potential also changes the rate of ET for any given ET protein. Within an individual species, this could allow the bacterium to increase its rate of respiration, or to gain more energy from using the anode as the TEA. Across a mixed-community, the anode may therefore apply selective pressure for different species.

For example, Zhu *et al.* inoculated bioanode half-cells with wastewater using acetate as the organic donor, and poised them at a range of different anode potentials [139]. At all potentials, the biofilms were dominated by *Geobacter sulfurreducens* ($75 \pm 6\%$ of all sequences), and 4 different reversible redox peaks were detected in the non-turnover CV with different mid-point potentials, with their occurrence dependent on the applied potential used. Only one of these reversible redox peaks was identified with either OmcZ or OmcB of *Geobacter sulfurreducens*, with mid-point potentials of -0.42 and -0.39 respectively. The non-turnover CV used in this study gave many of the same peaks and behaviour as observed with a pure strain of *Geobacter sulfurreducens*, and it was proposed that the poised-potential selects for different ET mechanisms in this bacterium [140]. This result is perhaps not surprising, given that *Geobacter sulfurreducens* reportedly has 111 genes for c-type cytochromes, which may allow it to regulate its ET mechanisms in response to different applied potentials [141]. The same use of non-turnover CV to yield information about ET pathways in aerobic biocathode biofilms grown at different poised-potential has not yet been carried out in the litera-

ture.

2.5.2 Aerobic biocathode poised-potential studies

Early poised-potential half-cell studies demonstrated that lower cathode potentials decreased the start-up period for enrichment and increased the CA reduction current. For example, Bergel *et al.* enriched marine cathode biofilms catalysing the ORR on stainless steel electrodes polarised at -0.45, -0.30 and -0.15 V for use in polymer electrolyte membrane (PEM) fuel cells [94], and found that the aerobic biocathodes polarised at -0.45 and -0.30 took half the time to enrich (4 days) than the aerobic biocathode polarised at -0.15 V (8 days) [94]. Similar trends in enrichment period have since been observed for aerobic biocathodes cultivated from AS in poised potential half-cells [84, 119]. This effect has been attributed to an increased metabolic energy gain for the bacteria, although manipulation of the poised-potential in this way may change the kinetics of ET for any given ET protein or reversible redox shuttle.

In the literature, poised-potential studies have been undertaken, which show different trends in biocathode performance for a series of aerobic biocathodes grown at different poised potentials [84, 88, 119]. Liang *et al.* inoculated half-cells containing carbon felt working electrodes with AS and polarised them at -63, 37, 137, 237 and 337 mV for 27 days, finding a maximum in the CA current at 37 mV [119]. The half-cell poised at 37 mV also had the highest power when a polarisation curve was taken in a fuel cell setup using sodium sulfite as the anode electron donor, although no further electrochemical or community analysis was undertaken. Heijne *et al.* inoculated half-cells containing graphite plate working electrodes with AS and polarised them at 50, 150 and 250 mV, finding a maximum in the CA current at a higher poised-potential of 150 mV, and smaller enrichment periods for the half-cells polarised at 50 and 150 mV [84]. When analysed by CV, there was a trend in E_{ORR} , although no community analysis was undertaken to determine if there were any differences in community composition between the different half-cells.

In contrast to the study by Heijne *et al.*, Xia *et al.* inoculated half-cells containing carbon felt electrodes with AS and polarised them at -144, 16 and 156 mV, and found that all three half-cells had an identical enrichment period of 10 days and E_{ORR} of 0.25 V when analysed by CV [88]. The average CA currents were 3.39 ± 0.89 mA, 3.53 ± 0.97 mA and 2.32 ± 0.46 , therefore the current was significantly higher for those aerobic biocathodes grown at potentials of -144 and 16 mV [88]. Community analysis data showed a strong selection for bacteria 98 % similar to an uncultured *Bacteroidetes* bacterium, which accounted for between 80 and 75 % of sequences on the electrodes poised at -144 and 16 mV respectively, but was

lower at 46 % in the half-cell polarised at 156 mV [88].

Given the differences in E_{ORR} for the aerobic biocathodes in the Heijne study [84], there may have been some selection for different electroactive bacteria and mechanisms of ET, therefore community analysis would have been a useful tool in this context. In the Xia study, cultivation at 156 mV yielded a lower average CA current than at -144 and 16 mV, however all biocathodes had the same E_{ORR} of 0.25 V, and all three were dominated by an uncultured *Bacteroidetes* species [88]. In the latter case, if the community is dominated by one electroactive species which is largely responsible for the catalytic current using only one ET mechanism, then the effect of the applied potential is only likely to influence the ET kinetics of this one ET mechanism. In the Xia study [88], both of the poised potentials of -144 and 16 mV with higher average CA current were in the oxygen mass transfer region of the CVs, whilst the half-cell poised at 156 mV was a potential in the kinetically limited region of the CV for the bacteria, therefore introducing a limitation in the metabolic rate for the bacteria. This analysis helps to explain the much higher proportion of *Bacteroidetes* at -144 and 16 mV, in comparison to 156 mV. However, no non-polarised control was included in this study, meaning this dominant bacterium may or may not have been the species primarily responsible for the ORR catalysis.

The above investigations studied the long-term effect of applied potential on the development and performance of the aerobic biocathode. The effect of the electrode potential on an aerobic biocathode grown at +0.15 V has been studied by electrode impedance spectroscopy (EIS) [85]. In this study, a minimum in the total resistance (R_{tot}) determined from the EIS plot was observed at +0.28 V, due to a minimum in the charge transfer resistance (R_{ct}) and a decrease in the diffusion resistance (R_{diff}) with increased electrode overpotential [85]. This result was modeled using the Butler-Volmer-Monod model, which predicts a minimum in R_{ct} with increasing electrode over-potential due to a combination of electron transfer kinetics and bioelectrochemical kinetics [85]. Therefore, for a given electron aerobic biocathode ET mechanism, a minimum in R_{tot} should be observed. In particular, this is consistent with the clear kinetically limited aerobic biocathode grown at 156 mV in the Xia study, which was much less enriched in *Bacteroidetes* species, the presumed electro-trophs [88].

2.5.3 Evaluation of carbon materials for poised-potential aerobic biocathode half-cells

Cheap, conductive, biocompatible electrode materials are predicted to improve bioanode performance [22]. Additionally, these bioanode materials should have large surface areas, and should be designed to allow the efficient mass transfer of substrates to the biofilm [22]. For bioanodes, porous carbon electrodes such as carbon felt, carbon cloth, carbon veil or carbon

brush fit these criteria and are usually used, and the same rationale has been applied to biocathodes in the literature. However, electrochemical cultivation of aerobic biocathodes on such carbon materials could potentially be complicated by the abiotic formation of H_2O_2 on carbon which occurs at different potentials depending on the carbon material. H_2O_2 kills bacteria through the generation of reactive oxygen species, such as superoxide, and the damage caused to the bacterial cells by these species is known as oxidative stress. Enzymes, such as catalase and superoxide dismutase, mitigate the harmful effects of oxidative stress by catalysing the decomposition of H_2O_2 to oxygen and water, and catalysing the disproportionation of superoxide (O_2^-) to oxygen and H_2O_2 respectively. Therefore, a means of determining the potential at which H_2O_2 is first produced on a porous carbon electrode would be advantageous in understanding how H_2O_2 production affects the growth of aerobic biocathode biofilms, and for determining a potential window over which the aerobic biocathode can be safely cultivated in poised potential half-cells, without the possibility of oxidative stress. This information is summarised in Figure 2.3.

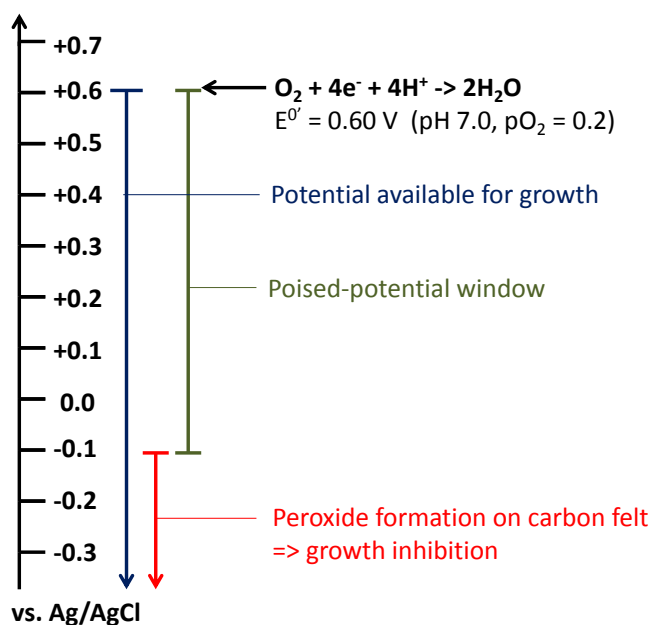


Figure 2.3: Potential window over which an aerobic biocathode biofilm can be cultivated on a carbon support

The degree to which the ORR occurs via the 4e^- or 2e^- reduction pathways is given by the average electron number, n_{e^-} , for the carbon electrode material, which varies between 2 and 4. This is calculated using the data obtained from rotating ring disk electrode (RRDE) experiments. In RRDE, the ORR catalyst is immobilised onto a special RRDE electrode which comprises a disk and a Pt ring surrounding the disk. Both the disk and ring are polarised simultaneously, and the RRDE is rotated at high speed. The ring is usually polarised at a potential at which peroxide is oxidised on Pt, therefore any peroxide produced at the disk

is detected at the ring, giving an oxidation current response. Using the following equation, the average electron number, n_{e^-} , for the carbon supported catalyst can be calculated at any given disk potential [44];

$$n_{e^-} = \frac{4I_D}{I_D + I_R/N} \quad (2.5)$$

Where I_D is the disk current, I_R is the ring current, and N is the collection efficiency. This type of experiment is only possible for carbon powders or carbon supported catalysts which can be immobilised as inks onto the supporting glassy carbon disk electrode [44]. For graphite, pyrolytic graphite, and carbon nanotubes, ORR occurs via $4e^-$ and $2e^-$ pathways, leading to n_{e^-} numbers that lie between 2 and 4 [44]. Further reduction of H_2O_2 to OH^- or H_2O is also possible, dependent on several factors, such as the applied potential and the pH [44]. For example, Watson *et al.* tested various ammonia and non-ammonia treated activated carbon powders with varying nitrogen and oxygen content by RRDE [46]. The different carbon powders had n_{e^-} numbers ranging between 2 and 4, with some potential-dependance with the disk applied potentials, tested between -1 and +0.2 V [46].

RRDE experiments are ideal for the assessment of carbon powders and carbon-supported catalysts that can be made into inks and immobilised onto glassy carbon disc electrodes, but this experiment cannot be used to characterise porous carbon felts, brushes or cloths, which may have unique surface chemistry. These unique surface properties arise because of the different ways in which porous carbon materials are manufactured. For example, porous carbon felt can be manufactured by carbonising viscose rayon or polyacrylonitrile (PAN) felts, and is likely to have a different surface chemistry to a graphite plate. Given the varying potential-dependent n_{e^-} numbers for carbon powders, it is unsurprising that it can be difficult to predict at which potential, on a given porous carbon electrode, H_2O_2 is generated. This information is important for determining the minimum potential at which it is possible to cultivate aerobic biocathode biofilms in poised-potential half-cells.

2.6 Conventional MFC Systems and MFC Systems with an Aerobic Biocathode

Conventional MFC systems can be either dual- or single- chamber devices. Dual-chamber devices use a membrane, whereas single-chamber devices may or may not use a membrane. In general, for the aerobic biocathode MFC, single-chamber devices cannot be used as we seek autotrophic metabolisms at the cathode electrode deriving energy from the cathode electrode, and which will otherwise be out-competed by heterotrophic metabolisms respiring using oxygen and oxidising organic substrate. For example, Xia *et al.* attempted to combine

an acetate-oxidising bioanode with a high-performing potentiostatically-grown biocathode in a single-chamber MFC, but the cell voltage dropped from more than 600 mV to less than 300 mV over the space of just 300 hours of operation [81]. The authors attributed this to heterotrophic growth at the biocathode [81], which is an unsurprising result given that autotrophic growth typically derives much less energy for bacteria than heterotrophic growth using carbon as the electron donor. Therefore, any aerobic biocathode MFC system must use a separator to separate bioanode and biocathode electrodes, and is therefore a dual-chamber device. MFC H-cells can be used to do this, but are known to suffer from high internal resistance due to a high cell ohmic resistance. This is principally due to a small membrane area relative to much larger cathode and anode areas, as well as a large anode-cathode distance. This also makes studying other system variables, such as the anode and cathode, more difficult, as the high ohmic resistance becomes system limiting. Additionally, an optimised cell architecture is preferable from the point of view of assessing the true performance of the developed system at lab scale, in order to examine system feasibility before scale-up. In this thesis, the H-cell architecture was used to couple pre-enriched bioanodes and biocathodes in order to study performance of the full aerobic biocathode MFC system, as this was an available and established cell architecture. This was due to time constraints, as much effort went into developing the aerobic biocathode, and a better optimised cell architecture would have been preferable for all of the reasons discussed above.

Many different cell architectures are available [22, 142]. These include, flat plate reactor designs which allow small electrode separation, and which can be stacked and connected electrically in parallel to increase the voltage [22, 142]. Tubular packed bed reactors are another option, but are often packed with granular materials, which are not a good anode material, suffering from high ohmic resistance between particles [22]. Recently, efficient tubular reactor designs have been developed made from ceramic materials which also function as anode-cathode separator [39, 143].

The different substrates used at the anode of MFCs are many and varied, as well as the different types of real and synthetic wastewaters used at the bioanode of MFCs. Typically, more complex substrates and types of wastewaters give much lower MFC performance, due to competitive processes such as fermentation. Within these biofilms, acetate is derived as a product from fermentation of more complex substrates, such as glucose, and is an important intermediate organic compound in the anaerobic degradation of organic matter. When acetate is the only organic substrate, this tends to select for *Geobacter* species at the anode, which gives much higher MFC performance. Therefore, acetate is often used as a benchmark organic substrate in the literature, and is particularly useful for researchers looking at other aspects of the MFC, due to its ease of use and consistency in performance in comparison to complex wastewaters or substrates. In this thesis examining MFCs with an aerobic biocathode,

acetate was chosen as the substrate at the MFC anode, in order to obtain a high-performing and consistent bioanode performance.

The performance of aerobic biocathode MFCs is predicted to be dependent on the dynamic nature of the bioanode and biocathode biofilms, and their response to different conditions. Therefore, conditions which may be important in order to optimise aerobic biocathode MFC performance include the degree of light, the external resistance, the rate of oxygen mass transfer to either biofilm, the temperature, and organic substrate/oxygen levels in both chambers. Certain conditions within each chamber of the MFC favour either the bioanode or the biocathode, and the roles that these different conditions play can be understood and optimised through separate investigations.

2.7 Operation of Aerobic Biocathode MFC Systems

2.7.1 The effect of light on the performance of acetate-fed MFCs

In the literature, MFCs utilising light at the anode have been developed and investigated. These include MFCs fed the products of photosynthesis at the bioanode, and MFCs utilising *Cyanobacteria*, algae and purple non-sulphur bacteria (PNS) at the bioanode. MFC bioanodes using algae biomass [1, 4, 5] and the rhizodeposits (carbohydrates) on the roots of plants [2, 3, 144] as substrates, allow the conversion of light energy into chemical energy via photosynthesis, from which electrical energy can be produced using ARB in the MFC. Current generation using isolates of algae and *Cyanobacteria* is also possible with added mediator [145, 146] and without added mediators [147, 148], and via photosynthetic production of H₂ at Pt catalysed electrodes [149]. In the anaerobic conditions found at the anode of MFCs, strains of PNS have also been used to produce H₂ which can be oxidised at Pt catalysed electrodes to produce current [150, 151].

A couple of studies on the effect of light on mixed-community anode acetate-fed MFCs have found that light enhances power output. These papers hypothesise that certain PNS bacteria in the biofilm are able to act like ARB and deliver electrons to carbon electrodes without H₂ as an electron mediator, and that this process is enhanced in the presence of light. In the paper by Cao *et al.*, two H-cell MFCs with carbon electrodes, one at open-circuit, the other at closed-circuit, were inoculated with domestic wastewater and exposed to light [152]. They reported an 8-fold increase in power under closed-circuit as opposed to open-circuit conditions to 2650 mW/m² (using 50mM potassium ferricyanide at the cathode), which they attributed to the community at the electrode containing 51.2 % of alpha-proteobacteria 16S rDNA sequences under closed-circuit conditions as opposed to 15.3 % under open-circuit

conditions [152]. Of the 51.2 % of *Alphaproteobacteria* 16S rDNA sequences, 62 % were found to belong to *Rhodobacter* and *Rhodopseudomonas*, both genera of PNS bacteria. The authors proposed that the phototrophic consortium produced an electron shuttle which catalysed ET to the anode [152]. A further study by Xing *et al.* using acetate- and glucose-fed H-cell MFCs utilising carbon electrodes supported this conclusion, with 8-10 % increase in power densities for glucose-fed MFCs, and 34 % for acetate-fed MFCs [153]. The authors attributed this power increase to a significant presence of *Rhodopseudomonas palustris* and *Geobacter sulfurreducens* in the biofilms, as analysed by DGGE using the 16S rRNA gene of bacteria/archaea [153].

H₂ production from short-chain carboxylic acids, such as acetate, in the presence of light is a known metabolic pathway for PNS, such as *Rhodobacter* sp., *Rhodopseudomonas* sp. and *Rhodospirillum* sp. [154, 155]. As this metabolism is not electrode dependent, growth anywhere in the anolyte and at the electrode surface should be possible. Given that carbon has no H₂ oxidation activity at all [138, 156], this metabolic pathway cannot contribute to MFC bioanode current when carbon is the electrode support. Although studies by Xing *et al.* and Cao *et al.* suggest an increase in bioanode performance on exposure to light attributed to anode respiring PNS, the presence of PNS may cause a lowering of coulombic efficiency and bioanode performance, as acetate in the medium is used for H₂ production and not for anode respiration, under anaerobic conditions. Therefore, it is hypothesised that exposing acetate-fed MFCs to light will cause a drop in MFC power output and coulombic efficiency. A further point to make is that in these studies, the experiments were not replicated, in order to confirm the results.

2.7.2 The effect of external resistance on aerobic biocathode MFC performance

The effect of MFC external resistance (R_{ext}) has been studied in the literature for conventional MFCs, but not for MFCs with an aerobic biocathode. With conventional MFCs fed with acetate, variation of R_{ext} has been observed to affect the coulombic efficiency (CE), peak power and anode charge transfer resistance (R_{ct}) [157–159]. Lyon *et al.* looked at the effect of R_{ext} on peak power density by operating separate 1g/L acetate-fed batch MFCs at 10,000, 1000, 470, 100 and 10 Ω [157]. They found that the peak powers for the MFCs clustered between 30 and 35 mW/m², apart from the MFC operated at 10,000 Ω , which had a lower peak power of 25 mW/m². The authors did not calculate CE values for their MFCs. Ren *et al.* operated separate 1 g/L acetate-fed batch MFCs at $R_{ext} = 10, 50, 265, 1000$ and 5000 Ω [158], finding that the peak powers of the MFCs were consistently between 140 and 160 mW/m². Although there was no trend in the peak power measurements, the anode R_{ct} values were 0.72, 1.04, 1.62, 1.79 and 3.55 k Ω /cm², in order of increasing R_{ext} , and the CE values

were 45.0, 42.5, 28.2, 10.8 and 6.1 %, also in order of increasing R_{ext} . Finally, Zhang *et al.* operated 4 separate 2.7 g/L acetate-fed continuous flow MFCs which each used 50 mM potassium ferricyanide as catholyte at $R_{\text{ext}} = 10, 50, 250$ and 1000Ω , giving peak powers of 1.25, 2.61, 1.53 and 0.93 W/m^2 respectively [159], and therefore a maximum in the peak power at 50Ω . From these studies on acetate-fed MFCs, it can be seen that lower R_{ext} values favour higher CE, higher peak power, and lower anode R_{ct} . This is likely due to a higher metabolic rate for the ARB over lower R_{ext} , increasing the density of ARB and the fraction of the substrate which they use in comparison to parasitic processes.

The same analysis has also been carried out for conventional MFCs using complex anode substrates [160–162]. Jadhav *et al.* looked at the effect of R_{ext} on chemical oxygen demand (COD) removal efficiency for a continuous flow MFC system using synthetic wastewater at an influent flow rate of 1.3 L/day (giving a set hydraulic retention time of 24.55 hours, which was the same for all experiments) [160]. They tested 50, 100, 500 and 1000 ohm external resistors at 30 minute intervals over a 2 hour period, and found a decrease in COD removal efficiency with the decreasing current from 71 to 65 %. Although the CE values were not also calculated during this experiment, they were no higher than 6% from other experiments using the same system. Katuri *et al.* examined the effect of external resistance on duplicate glucose-fed batch MFCs operated at $R_{\text{ext}} = 0.1, 1, 10, 25, 50 \text{ k}\Omega$, obtaining CE values of 6.15, 3.83, 0.81, 0.47 and 0.44 % respectively, whilst the peak powers were similar and clustered between $25\text{--}30 \text{ mW/m}^2$ [161]. Finally, Rismani-Yazdi *et al.* operated cellulose-fed batch MFCs at $R_{\text{ext}} = 20, 249, 480$ and 1000Ω , giving peak power densities of 66, 57.5, 27 and 47 mW/m^2 respectively, and CE values of 19, 14, 14 and 12 % respectively [162]. For this study therefore, the highest peak power density and CE was observed for the MFC operated over 20Ω , and the CE decreased with increasing R_{ext} . For the MFC resistor studies using complex anode substrates, the CE values are much lower than for the acetate-fed MFCs, as expected, given that an increased fraction of substrate is likely used for purely fermentative metabolism. However, the same dynamic exists for complex substrate-fed MFCs as with acetate-fed MFCs, with higher currents and rates of substrate utilisation for the ARB at lower R_{ext} values, leading to increased CE and power.

For aerobic biocathode MFCs, it is anticipated that changing R_{ext} will exert an effect on both the bioanode and biocathode biofilms. Operation over higher R_{ext} should cause a decrease in CE and bioanode performance. This is because the current is reduced, which means a lower metabolic rate for the bioanode bacteria, making anode respiration less competitive with competing pathways utilising acetate, such as methanogenesis. For the same reasons, biocathode performance is also anticipated to decrease over higher R_{ext} , with lower currents and metabolic rates for the bacteria.

2.7.3 The effect of oxygen mass transfer on aerobic biocathode MFC performance

The effect of O₂ mass transfer on high-performing aerobic biocathodes has been studied in the literature for a continuous flow, poised-potential system [84, 85], and briefly studied in aerobic biocathode MFCs [112, 116]. In the poised-potential studies, the mass transfer of oxygen was found to have an effect on the observed current, with higher flow rates increasing the current at fixed applied-potential [84, 85]. In the aerobic biocathode MFC study by Liu *et al.*, the biocathode chamber was sealed and the dissolved oxygen (DO) measured, and both the current density and DO decreased with time [116]. However, the authors did not measure the cathode potential, and the DO and current were not measured under normal operating conditions. In the study by Zhang *et al.*, the aeration rate into the cathode chamber was changed from 0 to 400 ml/min, and the anode, cathode and cell potential were measured [112]. From 0 to 300 ml/min, the authors observed a fairly constant anode potential, but the cathode potential increased from -0.20 to 0.10 V, and the cell voltage increased from 0.10 to 0.35 V. At flow rates above 300 ml/min, the anode potential increased sharply, and the cathode potential and cell voltage then decreased, which was attributed to oxygen influx into the anode chamber. In this study, DO was not measured, and the aerobic biocathode was lower performing than in other aerobic biocathode studies, exhibiting a maximum cathode potential of +0.1 V over a 500 Ω external resistance [112]. Therefore in full aerobic biocathode MFCs, there is room to explore the effect of oxygen mass transfer on performance, which is vital given how potentially important it is to system performance, and for making an assessment of the feasibility of the technology. DO, cell voltage and cathode potential are all important variables to measure simultaneously as the air flow rate is changed so that a full picture of the effect of oxygen mass transfer on performance can be obtained.

2.8 Electrode Materials for Aerobic Biocathode MFC Systems

2.8.1 Planar carbon electrodes for MFCs

The anode materials used in MFCs must be non-corroding, conductive, sustainable, cheap, and have a high surface area. Most importantly for MFC applications, the anode electrode must support an anode biofilm, and so must have good bacterial adhesion. Supporting materials that meet the requirement of having good conductivity are carbon and metals. The conductivities (S/cm at 20 °C) are 6.29×10^2 for polycrystalline graphite [163], 1.28×10^4 for 316 stainless steel [164], 2.85×10^4 for titanium [165], 5.92×10^5 for copper [165], 4.55×10^5 for gold [165], and 6.13×10^5 for silver [165]. Metals typically have the highest conductivities, and therefore should be excellent materials for use as MFC anodes. However,

many metals also corrode under normal MFC operating conditions. For example, copper and silver corrode to produce Cu^{2+} and Ag^+ ions respectively, which may also be toxic to bacteria. Non-corroding metals such as stainless steel [87] and titanium [166] have been used for MFC bioanodes, although low power/current densities are observed. In a sediment MFC study, a low power density of 4 mW/m^2 was observed for a cell using a stainless steel plate bioanode [87], compared to 28 mW/m^2 for a typical sediment MFC system using a graphite plate bioanode [167]. Similarly, a stainless steel electrode was compared to a graphite plate electrode as a biocathode support in a freshwater sediment MFC, and it was found that the power output of the cell was greatest with the graphite plate ($28 \text{ } \mu\text{W/cm}^2$) than with the stainless steel plate ($2 \text{ } \mu\text{W/cm}^2$) [83]. Both stainless steel and titanium are conductive and corrosion resistance, but bacteria do not adhere well to their smooth surfaces [168]. Titanium and many other metals are also expensive and non-sustainable.

Carbon is a good candidate for use in MFCs, meeting many of the criteria discussed above; it is cheap, environmentally sustainable, does not corrode, has good electrical conductivity, and good bacterial adhesion properties. However, there are many different forms of carbon with different structures, and these structures can significantly effect how the materials perform. Additionally, material comparisons between different studies can be challenging due to difficulty in isolating the effect of the material from the numerous other factors that determine the peak power density of an MFC, such as cell geometry, cathode reaction (e.g. ferricyanide versus O_2), membrane, and different and dynamic anode communities fed different substrates. Planar carbon materials include carbon cloth, carbon mesh, carbon paper, carbon fiber veil and graphite plate, with varying porosities. One significant advantage of planar electrodes is that the anode-cathode electrode spacing can be made to be very small, therefore reducing MFC internal resistance. Wang *et al.* compared NH_3 gas treated carbon cloth and carbon mesh using a single chamber acetate-fed MFC with an air cathode, finding similar peak power outputs for the two materials; 988 mW/m^2 (49 W/m^3) and 1015 mW/m^2 (51 W/m^3), respectively [169]. Despite having similar peak power outputs, the materials costs are significantly different; $350 \text{ } \text{£/m}^2$ for carbon cloth [170] and $17 \text{ } \text{£/m}^2$ for carbon mesh [171]. This would significantly effect MFC capital costs. Another planar carbon electrode material is carbon fiber veil, which is formed from continuous carbon strands randomly matted together using a binder, such as polyvinyl alcohol, and has a cost of $12 \text{ } \text{£/m}^2$ [172] (a lower cost of $6.70 \text{ } \text{£/m}^2$ has also been reported for this material [39]). This material has been used less extensively for MFC applications [173], although it's low cost is an attractive feature of the material. Further comparative studies with this material would be useful in assessing performance against other planar materials, such as cloths and meshes. Additionally, polyvinyl alcohols are known to biodegrade [174, 175], therefore the integrity of carbon fiber veil using this as a binder would need to be assessed over time.

2.8.2 Porous carbon electrodes for MFCs

Carbon/graphite felts are significantly more porous than the carbon materials discussed above, produced as a thick planar sheet of tangled carbon fibers. In theory, the bacteria can penetrate the material through the voids between strands, giving a higher specific surface area for the biofilm. However, the bacteria may become limited by the transfer of substrates to the inner surfaces [168]. Chaudhuri *et al.* compared graphite felt to graphite rods using *Rhodospirillum rubrum* in a poised-potential system, finding a three-fold increase in current density using the felt [176], although the total accessible geometric surface area was 3-fold higher for the felt in comparison to the rods. Therefore, for porous carbon materials, knowing the specific surface area is an important factor in attempts to compare materials. Aerobic biocathode MFC systems utilising carbon felts have also been investigated. The performance of a biocathode MFC using either graphite felt, carbon paper and stainless steel mesh (all of equal geometric area, 7 cm²) was assessed, giving peak powers of 109.5, 32.7 and 3.1 mW/m² respectively [95]. Similarly, graphite felt was also found to compare favorably with carbon cloth, with aerobic biocathode MFCs setup using various combinations of carbon cloth and graphite felt for the bioanode and biocathode [114]. In this study, a maximum power density of 16.7 W/m³ was observed for the MFC with graphite felt as both bioanode and biocathode support [114]. However, one of the major drawbacks of carbon felt is the prohibitive cost at 417 £/m² [177], which therefore makes this material unattractive for use in MFCs.

Other porous materials include granular forms of graphite and activated carbon, which can be packed to form a fixed anode bed. Granular materials tend to have porosities ranging from 30-50 % [168], and graphite granules of diameters ranging from 1.5 to 5.0 mm have been tested in MFCs [22]. With a granule bed porosity of 53 % and granule diameter of 3 mm, the specific surface area has been calculated as 1100 m²/m³ [22], giving a high surface area for biofilm growth. Aelterman *et al.* compared granular graphite of different sizes to graphite and carbon felts, packed into equal anode volumes using a dual-chamber acetate-fed MFC with a ferricyanide catholyte [178]. Peak volumetric power outputs ranged from 356-386 W/m³ for the felts, compared with 143 and 257 W/m³ for 2 and 5 mm diameter granules respectively, and high ohmic resistances were determined for the granular materials [178]. The use of granular materials has also been reported for aerobic biocathode MFCs. Wei *et al.* compared granular semicoke (GS), granular activated carbon (GAC), graphite granules (GG) and carbon felt (CF) as biocathode materials, with diameters ranging between 2 and 5 mm, and total surface areas of 1.44 x 10⁴ m², 3.43 x 10⁴ m², 60.7 m² and 10.6 m² in the cells [86]. The 1000-fold larger total surface area for the GS and GAC materials did not translate into MFC peak power outputs of the same order of magnitude, with values of 24.3, 20.1, 17.1 and 14.4 W/m³ in the order GAC > GS > CFC > GG, respectively [86]. This may have been

due to smaller differences in bio-available surface areas. With the use of granular materials at the bioanode/biocathode, the chief disadvantage is that individual granules need to make good electrical contact with each other, and can only connect at a small fraction of their total surface area [22, 178]. It is also anticipated that dead zones may develop after long-term operation [168].

Brush electrodes with high porosity and specific areas, have also been reported as bioanode supports in conventional MFCs [179–181]. They are manufactured by twisting two titanium wires to form a central core from which small diameter graphite fibers (7.2 μm) protrude outwards [22]. As each individual graphite fiber strand is connected to the central titanium wire current collector, this allows for efficient current collection, which is not possible in granular carbon beds. Logan *et al.* carried out the first study using two different sizes of carbon brush electrode in a single chamber air-cathode MFC configuration [179]. The larger brush used in the study ($d = 5$ cm, $l = 7$ cm) had an estimated surface area of 7170 m^2/m^3 with a porosity of 98 % porosity, reaching a peak power output of 2400 mW/m^2 (73 W/m^3) using acetate as anode substrate [179]. This was reportedly the highest power output achieved so far using an air-cathode MFC [22], with the power measurements normalised to air-cathode geometric area. Recently, Lanas *et al.* further investigated brush sizes using an air-cathode MFC fed acetate, comparing 3 large brushes ($d = 25$ mm), 5 medium brushes ($d = 12$ mm) and 8 small brushes ($d = 8$ mm) [181]. The MFC with three large brushes gave the highest peak power output of 1240 mW/m^2 , whilst the MFC with 8 small brushes achieved the lowest peak power output of 600 mW/m^2 . However, for the MFC with small brushes, decreasing the spacing between the centre of the brushes and the air-cathode increased the peak power density significantly to 1030 mW/m^2 , indicating that this was a crucial factor in power generation [181].

Aerobic biocathode MFCs have also been reported using carbon brush electrodes as biocathode supports [107, 109, 112, 118]. The first such system was developed as a continuous flow MFC oxidising glucose at the anode, and utilising an aerated biocathode with an E_{ORR} value of approximately +0.1 V [112]. This MFC had a peak power of 25 W/m^3 (normalised to anode volume). A combination of both graphite granules and brushes have also been employed as a biocathode support for an MFC [107, 109, 118]. Zhang *et al.* reported that performance of an aerobic biocathode MFC fed glucose was improved using a combination of both graphite granules and a graphite brush at the cathode (99.83 W/m^3), instead of either graphite granules (72.84 W/m^3) or a graphite brush (72.35 W/m^3) alone [107].

Other porous electrode materials have been less extensively studied, such as reticulated vitreous carbon (RVC) [22]. This material has high porosity (97% [22, 168]), conductivity (200 S/cm [22]) and specific surface area (6070 m^2/m^3 [182]), but is very brittle [22, 168].

Additionally, biofilms of E-coli have been tested with a 3D scaffold comprising carbon nanotubes synthesised in the lab using ice segregation induced self-assembly, with internal micro-channels allowing for high surface area for bacterial attachment [183]. A mesoporous polyaniline/TiO₂ composite electrode [184] and an ordered mesoporous carbon composite electrode [185] were also developed, having uniform pore structures and large internal surface areas. The polyaniline/TiO₂ composite had a high specific surface area (>150 m²/g), which was determined to be 300 times larger than for graphite felt (0.5 m²/g) [184]. 3D scaffolds and mesoporous carbon composite electrodes could potentially be excellent for use as biocathode supports, although further tests will be needed to establish whether electroactive biofilms occupy the internal structure effectively, and whether they are robust and can be scaled-up.

2.8.3 Surface treatments and coatings

An important strategy in electrode development is to modify the electrode surface in order to increase conductivity, surface area, improve bacterial adhesion and facilitate bacterial electron transfer. One form of modification for MFC bioanodes has been to coat with metals or metal oxides. Examples include coating with iron oxide [186], gold and Pd nanoparticles [187], graphite paste containing either Fe₃O₄ [188], Fe₃O₄ plus Ni²⁺ [188], and a graphite-ceramic mixture containing Mn²⁺ plus Ni²⁺ [188]. Some of these improvements could potentially be due to metal oxidation, and so long-term stability tests are important, and the addition of precious metals may not be cost efficient or sustainable. An alternative to this is surface treatment using high temperature NH₃ gas treatment (5% NH₃ gas at 700 °C) [169,189] or combined acid/heat treatment [180]. For air-cathode acetate-fed MFCs, substantial performance increases have been observed for these modified electrode materials. For example, Cheng *et al.* increased performance of an air-cathode MFC fed acetate from 1640 to 1970 mW/m² on modification of the carbon cloth anode with high temperature NH₃ gas treatment [189]. Analysis of these modified surfaces using X-ray photoelectron spectroscopy (XPS) has shown an increase in atomic N/C ratio, suggesting the presence of nitrogen functional groups which improved bacterial adhesion and/or electron transfer [169].

In addition to these surface treatments, nanomaterials have been deposited onto carbon electrodes. The most commonly used are CNTs [168]. CNTs have good electrical conductivity and high surface area, although it is unclear whether they improve bacterial adhesion or facilitate electron transfer to the anode [168]. Similarly, modification of carbon anodes with conductive polymers, such as polyaniline nanofibers and polypyrrole, and nitric acid treatment, have also been investigated. These modifications may increase bacterial adhesion through the introduction of surface groups, such as quinone (O=C=O) and quinoid groups

(N=C=N) [190]. Surface treatments specifically designed for electrodes supporting aerobic biocathode biofilms have also been carried out, but less extensively. In order to enhance the biofilm coverage of stainless steel, Zhang *et al.* coated SS mesh with CNTs, enhancing ORR catalysis for the electrodes with a biocathode 49-fold from 3 to 147 mW/m² [93]. Similarly, Liu *et al.* electrodeposited chitosan and CNTs onto carbon paper, observing an improvement in ORR activity of the electrode [116]. However, for both studies, it was not clear whether the improvements were due to improvements in abiotic ORR catalysis, or biotic ORR catalysis through e.g. improved biofilm surface coverage. Another strategy employed to improve biocathode performance in a dual-chamber acetate-fed MFC was to impregnate the granular carbon electrode with iron and manganese oxides with the aim of selecting for metal oxidising bacteria, although this study lacked control cells to assess the effect of electrode modification [115].

2.8.4 Oxygen diffusion electrodes

Apart from all of the requirements of an electrode support discussed above, the electrode material for the aerobic biocathode must also allow the efficient mass transfer of O₂ to the biofilm/electrode surface. In aerobic biocathode sediment MFCs, mass transport of O₂ to the biocathode occurs through the continual mixing of the water above the sediment. More generally, in lab-scale aerobic biocathode MFCs, the mechanism of mass transfer of O₂ to the aerobic biocathode biofilm imposes design constraints on the electrode material. In the vast majority of studies, the electrolyte is sparged insitu like in a conventional bioreactor, or recirculated under constant flow conditions from a sparged external recirculation vessel. In addition to these methods, Clauwaert *et al.* investigated an alternative method of aeration using a tubular up-flow MFC configuration [76]. In this configuration, graphite granules in the centre of a vertical tube were used to support a bioanode biofilm, and were surrounded by a tubular membrane and a graphite felt cathode [76, 191]. The catholyte was pumped to the top of the tube at a flow rate of 0.6 L/hr and dripped over the graphite felt supporting a biocathode biofilm, trickling over the electrode with the aid of gravity [76]. Catholyte collected at the bottom of the tube was recirculated, and the anolyte was pumped up through the middle of the graphite granule bed from the bottom of the tube. The system reached a peak volumetric power of 65 W/m³ when fed acetate. Notably, catholyte in the external recirculation vessel was not actively aerated, with O₂ dissolving from the air to the cathode over the high air-solution contact interface, in a similar way to a trickling filter. As wastewater is already pumped through a wastewater treatment plant, this system would not introduce any additional energy cost.

Mass transfer of O₂ to the cathode electrode surface can also occur using a GDE, which

allows the passive transfer of O₂ to the cathode surface, therefore also eliminating the need for energy intensive aeration. The GDE is specially designed to give a 3-phase interface of solid, water and gas, which overcomes the problem of low O₂ solubility in the catholyte. At the 3-phase interface, oxygen diffuses from the air and protons are transported from the electrolyte, combining at the solid catalyst surface to produce water/peroxide. In the MFC literature, they have been used in conjunction with chemical catalysts, such as Pt, which form the catalyst layer of the GDE. The catalyst layer is typically deposited as an ink onto the side of the GDE facing the cell solution, which is formed by mixing a binder, such as Nafion or PTFE, with a catalyst supported on carbon black powder. The GDE itself is based on either carbon paper or carbon cloth, and can be purchased commercially with different conductivity, hydrophobicity, porosity and gas permeability.

The catalyst layer on the solution-facing side, significantly increases cathode potential and MFC performance. Experimentally, Cheng *et al.* found that varying Pt loadings from 0.1 to 2.0 mg/cm² for a carbon cloth-based GDE did not significantly effect the cathode potential in chronopotentiometry tests at current densities ranging from 0-2 mA/cm², with cathode potential differences found to be within a 10-20 mV range [192]. Using the same electrochemical cell setup, they found that at a fixed Pt loading of 0.5 mg/cm², the GDE cathode with Nafion binder had a cathode potential which was 12 % more positive than with PTFE binder at the same binder loading and a current density of 1 mA/cm² [192]. The use of metal porphyrin catalysts, at similar loadings to Pt, have also been found to give comparable performances [18, 192]. The O₂ mass transfer limiting reduction current density for Pt on carbon black at a loading of 0.5 mg/cm² was found to be 1.2 mA/cm² (1200 μA/cm²) using an RRDE at 2100 rpm (linear sweep voltammetry (LSV) at 1 mV/s scan rate) [46], which sets an upper limit for the O₂ mass transfer limited current possible for a GDE with a Pt catalyst.

Of more relevance to aerobic biocathodes is how the GDE is constructed. A GDE for use in MFCs was constructed in the lab based on carbon cloth, requiring the addition of gas diffusion layers to lower the rate of O₂ flux to the solution-facing side of the GDE, and to prevent water loss through evaporation to the air-facing side of the GDE, both of which can lower MFC coulombic efficiency [193]. Cheng *et al.* took plain carbon cloth, adding first a mixture containing carbon powder and PTFE solution to form a base diffusion layer, then adding successive coatings of PTFE solution to form successive numbers of diffusion layers (DLs) [193]. Experimentally, they found that the mass diffusion coefficient for O₂, k (10⁻³ cm/s), varied with the number of DLs; 3.3 for no DL, 3.9 with the base DL, and for 2,4,6 and 8 additional DLs, the values were 2.9, 2.3, 1.5 and 0.6 respectively. When these GDEs were tested in single chamber membraneless MFCs fed on acetate, a maximum in the cathode potential and peak power of 766 mW/m² was observed for the MFC with 4 additional DLs,

compared to 538 mW/m^2 without a DL. Coulombic efficiency increased in proportion to the number of additional DLs, from 13-20 % for no DL, 20-27% for 4 additional DLs, up to a maximum of 32 % for 8 additional DLs. The GDE with 4 DLs with a k value of 2.3 gave the right balance between the rate of O_2 mass transfer to the cathode and to the bioanode. At 30°C , volumetric water loss was 20 % for the MFC with no DL (plain carbon cloth), 5 % for 2 additional DLs, and it was not detectable for 4 additional DLs.

GDEs have also been constructed from stainless steel mesh coated with 1 to 5 DLs formed from a mixture of 6.25 mg/cm^2 poly(dimethylsiloxane) (PDMS) and 1.56 mg/cm^2 of carbon black on the air-facing side, in addition to a Pt catalyst layer on the solution-facing side (0.5 mg/cm^2 Pt loading) [194]. In membraneless air-cathode MFCs fed acetate, it was found that the MFC with an SS GDE with 2 DLs performed best with a k value of $1.1 \times 10^{-3} \text{ cm/s}$ for O_2 mass transfer, a peak power density of 1610 mW/m^2 , and a coulombic efficiency of 80 % [194]. In this study, GDEs constructed from carbon cloth using exactly the same method with 1-5 DLs gave comparable performances in identical MFCs, with the best-performing MFC having a GDE with 3 DLs, a peak power density of 1635 mW/m^2 , and a coulombic efficiency of 57 %. The authors highlighted the lower cost for PDMS in comparison to PTFE as a hydrophobic polymer for forming DLs, and the advantage of lower electrode ohmic resistance on system scale-up when the current collector is integral to the GDE. In a separate study using acetate-fed batch MFCs with SS GDEs, it was found that coarser SS mesh GDEs produced higher peak power densities (up to 1616 mW/m^2 with a 0.53 mm opening size), whilst finer SS mesh GDEs produced lower peak power densities (down to 599 mW/m^2 with a 0.12 mm opening size) [195]. This trend correlated with increased diffusion resistances and decreasing O_2 mass transfer coefficients ($2.1 \times 10^{-3} \text{ cm/s}$ for the 0.53 mm mesh, $1.7 \times 10^{-3} \text{ cm/s}$ for the 0.12 mm mesh) [195].

For high-performing aerobic biocathodes with an E_{onset} value of $+0.4 \text{ V}$, the O_2 mass transfer limited current densities have been well-established for roughened graphite plate electrodes using a poised-potential half-cell flow-through system. In this system, aerated catholyte from an external recirculation vessel was flowed pass the biocathode at 12 L/hr , and the O_2 mass transfer limited reduction currents were determined by sweeping the potential of the electrode from positive to negative values at slow scan rates. The currents were found to be dependent on the conditions of cultivation, such as pH, temperature and poised-potential [80, 84, 85]. A value of 660 mA/m^2 ($66 \text{ }\mu\text{A/cm}^2$) was determined for a biocathode cultivated at $+0.15 \text{ V}$ poised-potential, pH 5, and 31°C [80], whilst values of $244 \pm 53 \text{ mA/m}^2$ ($24 \text{ }\mu\text{A/cm}^2$) [85] and 313 mA/m^2 ($31 \text{ }\mu\text{A/cm}^2$) [84] were found for biocathodes cultivated at neutral pH and a poised-potential of $+0.15 \text{ V}$ in separate studies. These studies provide a good comparison with the same type of high-performing (E_{onset} of $+0.4 \text{ V}$) aerobic biocathode cultivated on a GDE.

Xia *et al.* cultivated an aerobic biocathode on a carbon cloth GDE with 4 PTFE DLs [81]. The GDE was made in the lab using the method developed by Cheng *et al.* [193], and the aerobic biocathode biofilm was grown on the GDE under conditions of active aeration using a half-cell at a poised-potential of approximately +0.1 V. The GDE supported biocathode was then assessed by LSV (at $\nu = 1$ mV/s from -150 to +450 mV) as a GDE under conditions of passive aeration, giving an onset potential for ORR of +400 mV, and an O₂ mass transfer limited current density of 1.2 A/m² (120 μ A/cm²) [81]. An O₂ mass transfer limited reduction current of 120 μ A/cm² is significantly higher than the 24-66 μ A/cm² found for aerobic biocathodes grown on roughened graphite plates under continuous flow conditions discussed above [80, 84, 85]. Therefore, the carbon cloth GDE performs much better than a roughened graphite plate under continuous flow conditions (12 L/hr), although high-performing aerobic biocathodes grown on porous carbon materials, such as carbon felt, may also have the effect of increasing current density in comparison to planar graphite due to an increase in surface area.

In the Xia *et al.* aerobic biocathode GDE study, the GDEs were transferred to full dual-chamber membrane, and single chamber membraneless MFC configurations, after initial poised-potential half-cell enrichment, and operated over 1000 Ω external resistances for at least two weeks. They reached peak power densities of 554 mW/m² and 199 mW/m², respectively. The cell voltage in the dual-chamber MFC was initially 609 mV, more positive than the cell voltage for the same cell with a Pt cathode at 557 mV (0.5 mg/cm² Pt loading). As described above, Cheng *et al.* found that 4 DLs were optimal for the carbon cloth GDE in their membraneless single chamber MFC with Pt catalyst, yet GDEs with fewer DLs increased the k value for O₂ mass transfer of the GDE [193]. Therefore, in the dual-chamber biocathode MFC configuration tested by Xia *et al.*, an increased flux of O₂ to the biocathode may have increased the current density, given that a membrane was already in place to reduce O₂ transfer from the cathode to the anode. The addition of more PTFE layers to the GDE may also make the solution facing side increasingly hydrophobic, which would reduce bacterial attachment. A GDE with increased porosity and low hydrophobicity to improve bacterial attachment, as well as a high k value for increased O₂ mass transfer would be desirable for an aerobic biocathode GDE support.

To increase O₂ mass transfer to the aerobic biocathode and to lower hydrophobicity, Wang *et al.* constructed a GDE from carbon cloth according to the method developed by Chen *et al.* [193], but with only 2 DLs and using only 10 % wt PTFE instead of 30 % [91]. The GDE was used as the WE in a poised-potential half-cell with the WE potential set at -0.3 V in order to cultivate an aerobic biocathode biofilm [91], before incorporation into an acetate-fed dual chamber MFC with a CEM separating anode and cathode. LSV from positive to negative potential at a scan rate of 10 mV/s gave an E_{onset} for ORR of +0.2 V and an O₂ mass transfer

limited reduction current of approximately 5 mA, or 0.31 mA/cm² (313 μA/cm²) normalised to a projected GDE area of 16 cm². This value was considerably higher than that the 120 μA/cm² found by Xia *et al.* for their aerobic biocathode GDE [81], although at an LSV scan rate of 10 mV/s, capacitive currents may have contributed significantly to the measured current. Assuming that the value determined is close to the true value, this may indicate that the GDE was better optimised for the system. However, for this study, it is important to note that the onset potential for ORR was some 200 mV more negative than that determined for the aerobic biocathode GDE with an E_{onset} for ORR of +0.4 V described by Xia *et al.* [81]. This indicates a less efficient ORR mechanism for the former biocathode, and the bacteria associated with ORR catalysis by the authors from community analysis were found to be *Pseudomonadales*, *Rhizobiales* and *Sphingobacteriales* (according to Order). The system had a peak power output of 103 mW/m² [91], which was lower than 554 mW/m² reported by Xia *et al.* for their dual-chamber MFC with an aerobic biocathode GDE [81].

From the analysis of the studies described above, it should be noted that aerobic biocathode GDEs could be optimised for better performance by engineering conditions in order to cultivate the right bacteria, but also by coupling that with efforts in improving the GDE itself. Only two studies so far have tested aerobic biocathodes grown on GDEs [81, 91], and both constructed the GDE using a method developed for use with a Pt catalyst. GDEs perform well as a replacement to energy-intensive aeration of the catholyte, although scale-up of this type of system may be problematic due to the increased pressure exerted from the liquid side as the GDE increases in size. With conventional GDEs using a chemical catalyst, formation of a non-electroactive biofilm, using substrate from the electrolyte and O₂ diffusing through the GDE, can have a detrimental effect on performance, reducing O₂ diffusion and transport of H⁺ to the catalyst surface, and this is also likely to be a problem for the aerobic biocathode GDE. With the aerobic biocathode MFC, the use of a membrane separator is essential to prevent organics cross-over from the anode, as the aerobic biocathode biofilm will be quickly out-competed by a proliferation of heterotrophic aerobic biomass oxidising organics.

2.9 Membranes for Aerobic Biocathode MFC Systems

2.9.1 Fundamental properties and ion-selective membranes

To date, no studies have looked at the effect of the membrane on aerobic biocathode MFC performance, however, a number of papers examine the use of membranes for conventional MFCs using an abiotic cathode. Typical membranes used in MFC research broadly fall into three different classes; cation exchange membranes (CEMs), anion exchange membranes (AEMs), and non-ion selective membranes. CEMs are designed to conduct only cations,

AEMs conduct only anions, whilst non-ion selective membranes, such as battery separators (BS), conduct all ions. In a conventional MFC, the membrane's principal function is to stop the cross-over of oxygen to the bioanode, which can promote heterotrophic bacterial growth using oxygen, therefore lowering MFC coulombic efficiency. Substrate loss from the anode over the membrane may also cause a lowering of the coulombic efficiency at the anode, and the passage of inhibitors from the anode such as sulphate can cause degradation of the cathode chemical catalyst. Therefore, the membrane acts as a barrier to the passage of oxygen from cathode to anode, the passage of substrate from cathode to anode, and the passage of inhibitors present in the wastewater from anode to cathode. Membranes should, in part, be chosen on the basis of having a low permeability for both oxygen and substrate. In the context of conventional MFCs, a couple of studies have investigated different membranes in terms of acetate and oxygen cross-over. Kim *et al.* determined oxygen and acetate diffusion coefficients for a cation, anion and ultrafiltration membrane [196], before testing each of them in dual-chamber MFC systems. They found that the ultrafiltration membrane gave the highest MFC internal resistance of the three membranes. The cation exchange membrane, which was Nafion, had the highest oxygen mass transfer coefficient of the three different membranes in this study with $K_0 = 1.3 \times 10^{-4}$ cm/s [196], although Chae *et al.* determined a value which was double this of $K_0 = 2.8 \times 10^{-4}$ cm/s in a separate study [197]. Both groups used the same method for measuring oxygen concentrations over a period of time to determine their K_0 values.

Apart from the cross-over of substrate, oxygen and inhibitors, the other major problem associated with the membrane in conventional MFC systems is pH increase at the cathode, and pH decrease at the anode over time for MFCs operated in batch mode, which causes performance losses at both bioanodes and chemical cathodes, as well as degradation of the bioanode. It has also been shown that for a poised-potential aerobic biocathode with an onset potential of +0.4 V at pH 7.0, the optimum pH was 5.0 [80]. pH splitting is therefore an issue related to long-term system stability, and is predicted to lower the performance of batch MFCs with long batch cycles, and continuous flow MFCs with high hydraulic retention time. pH splitting has been shown to occur due to preferential transfer of ions over the membrane other than H^+/OH^- , causing accumulation of H^+ at the anode and OH^- at the cathode, which are the products of the reactions at both electrodes respectively. The phenomenon is caused by the condition that charge neutrality must be maintained in the fuel cell, as for every mol of Coulombs that passes through the external circuit, an equal number of mols of charge must pass through the membrane.

In the literature, different membrane types have been assessed in phosphate buffered electrolytes by different means in order to investigate this process. For example, different studies have measured ionic concentrations [196, 198–200], as well as membrane potentials using a

4-electrode setup [201, 202]. In terms of the studies where ionic concentrations were measured, Kim *et al.* measured Na^+ and phosphate concentrations for CEM (Nafion 117), an AEM (AMI-7001, membrane international) and an ultrafiltration membrane, in single chamber MFCs, but did calculate values based on % charge transfer for these membranes [196]. Rozendal *et al.* tested a CEM (Nafion-117) and an AEM (Fumasep FAB, Fumatech) in MFCs, and found that 1/3 of the charge was transferred by K^+ and 1/3 by Na^+ in the case of Nafion-117, whilst 1/2 of the charge was transferred by OH^-/H^+ and 1/4 was transferred by phosphate in the case of the AEM [199]. Finally, Sleutels *et al.* looked at charge transferred across a CEM (Fumasep FKE, Fumatech) and an AEM (Fumasep FAA, Fumatech) in MFCs, finding approximately equal percentages of charge were transferred by OH^-/H^+ , Na^+ and K^+ for the CEM, whilst 80 % of the charge was transferred by H^+/OH^- in the case of the AEM [200]. However, in the literature, there has been no assessment of battery separators using these in-depth methods (although battery separators have been used in pilot scale MEC studies [203, 204]).

2.9.2 Non-ion selective separators

A wide-range of different porous materials can be used as ion-selective membrane separators for MFCs; ceramics, polymers, fabrics and glasses. In principal, any material which is electrically insulating and permits the passage of ions can be used. The simplest non ion-selective separators are salt bridges, which contain electrolytes in solid agar [205–209]. Very low rates of O_2 diffusion have been determined for this type of separator, which is advantageous in an MFC, but the use of salt bridges leads to very high MFC internal resistances. For example, Min *et al.* constructed an MFC with a phosphate buffered agar salt bridge in a 30 cm long, 0.6 cm diameter tube to connect the anode and cathode chambers, and compared this with a H-cell MFC with a Nafion CEM clamped between glass flanges with a total length of 8 cm, and a diameter of 1.3 cm [205]. The authors found that the internal resistance in the MFC with the salt bridge was 19920Ω , significantly larger than the 1286Ω found for the H-cell MFC with a CEM [205]. Therefore, salt bridges are not good separators to use in MFCs. J-cloth separators, which are cheap fabric separators, have also been investigated [210–212], and can perform well in comparison to a typical CEM [211]. They have also been found to increase the CE of a membraneless air-cathode single chamber MFC when pushed up against the air-cathode to form a membrane electrode assembly (MEA) [212]. However, J-cloths are prone to degradation over time [211], and can become easily biofouled. Additionally, due to a high k value for O_2 mass transfer ($290 \times 10^{-5} \text{ cm/s}$ for a J-cloth as compared to $9.4 \times 10^{-5} \text{ cm/s}$ for Nafion CEM), coulombic efficiencies for MFCs using J-cloths can be low (20-40%) [211].

Porous polymer membranes represent an improvement on J-cloths, as polymers with suitable properties can be tested from the wide range of these materials which are available. Biffinger *et al.* carried out a comparative study looking at four different non ion-selective polymer membranes; cellulose, cellulose acetate, polycarbonate and nylon [213]. Using a mini-MFC configuration with a 1.2 ml volume [182], *Shewanella oneidensis* was fed lactate at the anode, and ferricyanide was used at the cathode to test the membranes, and performances of the different polymer membranes were compared to a control cell using a Nafion CEM [213]. In this study, similar performances were observed for all membranes tested, although degradation of the cellulose nitrate membrane occurred. For the three membranes with 0.2 micron pore sizes (polycarbonate, cellulose nitrate and nylon), crossover of the ferricyanide catholyte was observed within 15 hours of operation, whilst no cross-over was observed for Nafion and cellulose membranes [213]. One problem with cellulose is that it is likely to biodegrade over time, whereas polycarbonate and nylon would seem to be promising for MFCs. A biodegradable bag made from starch and biodegrading polyester has also been used tested in an MFC and found to degrade [143]. The biodegradable bag eventually degraded after 8 months of continuous operation, but it was stable with a comparable power output to an MFC with a Nafion CEM before up until this point [143]. Ultrafiltration membranes are another type of non ion-selective membrane which have been tested in MFCs [214, 215]. Zuo *et al.* constructed a tubular cathode MEA using a polysulfone membrane on a composite polyester carrier coated with a graphite coating containing a CoTMPP catalyst, and tested this in different single chamber air-cathode MFC configurations [214]. The performance of these configurations compared favorably with a carbon GDE coated with Pt catalyst, but differences between cathode surface areas, and the very different geometries of these different configurations meant that direct membrane comparisons were not possible. A direct comparison between a Nafion CEM and a microfiltration membrane using the same single-chamber MFC configuration was made by Sun *et al.* [215]. These membrane were incorporated into MEAs, and it was found that the MFC with the microfiltration membrane exhibited a 2-fold increase in power in comparison to the MFC using a CEM. This increase was attributed to greater mass transfer of O₂ through the microfiltration membrane due to its 0.2 micron pore size in comparison to the CEM, although O₂ mass transfer was not measured directly. Recently, a battery separator (RhinoHide, Entek Ltd., UK) has been used in pilot-scale MEC studies [203, 204], although in-depth electrochemical characterisation has not yet been carried out.

Glass separators have also been used as separators in MFCs [211, 216]. Mohan *et al.* tested glass wool as a separator for an MFC based on an anaerobic tank design with an air cathode on the tank surface [216]. The glass wool was able to function as part of an MEA in the MFC system, although no comparisons were made against other separators using the same MFC system [216]. In a different study, comparisons were made between 1.0 and 0.4 mm thickness

glass fiber mats and a CEM as cathode MEAs using a single chamber aerobic cathode MFC configuration [211]. The MFCs with glass MEAs had peak power outputs of 791 and 623 mW/m² for 1.0 and 0.4 mm thicknesses, larger than the value for the MFC with the CEM, which was 267 mW/m². The CEM had a thickness 0.46 mm and a k value of 9.4×10^{-5} cm/s for O₂ mass transfer, which was higher than the values for the 1.0 and 0.4 mm glass fiber mats, which were 5.0 and 7.5×10^{-5} cm/s, respectively [211]. For the 1.0 and 0.4 mm glass fiber separators, the ohmic resistances were 2.26 and 2.39 Ω respectively, whilst the ohmic resistance of the CEM was 3.78 Ω . The lower O₂ flux and/or ohmic resistances for the glass separators likely increased MFC performance in comparison to the CEM. For the glasses, a 1.0 mm thickness was found to be optimal for power production, which may have meant that O₂ flux to the anode was relatively more important than membrane ohmic resistance. One significant advantage of glass is that it does not degrade over time, as is the case with some of the polymer membranes tested in the studies discussed above, which makes it a suitable membrane for MFCs. However, glasses may be expensive in comparison to other separators, and may not be robust when scaled up.

Ceramic materials have also been employed as porous separators in MFCs. The chief advantages of ceramic materials are that they are cheap, there is no biodegradation of the material, and the ceramic can serve as both the membrane and the cell walls, simplifying MFC construction. The first study looking at ceramic separators was by Park *et al.* [217]. They constructed an MFC with a 1 mm thick porcelain membrane made from 100 % kaolin, but did not compare the same configuration using a conventional Nafion CEM. Similarly, Seo *et al.* produce a novel 3 layer cathode MEA comprising cellulose acetate, a ceramic membrane, and a planar porous carbon electrode impregnated with MnO₂ as ORR catalyst for a single chamber air cathode MFC, but again, the same MFC configuration was not also tested with an MEA using a Nafion CEM for comparison [218]. Comparison with a CEM has been provided by Winfield *et al.*, who tested a ceramic membrane against a CEM using the same MFC architecture [143]. In this study, performance improved over an 8 month period for both MFCs using CEM and ceramic separators, with both cells reaching very similar power densities of approximately 4 W/m³. In this study, the ceramic had a thickness of 5 mm, whilst the thickness of the CEM was 0.16 mm.

Developments in constructing the entire MFC around the ceramic separator were made by Behera *et al.* in a number of different studies [104, 219, 220]. In these studies, the MFC was constructed from an earthenware pot, serving as both the MFC wall and the separator. In one study, the earthenware pot had a 4 mm wall thickness, 400 ml volume, and cost 6 pence to produce [104]. Stainless steel was used as the anode and inserted inside the pot, whereas a cathode assembly of graphite plate and stainless steel was wrapped around the external face of the pot. The pot was filled with anode medium containing acetate, and then

placed inside a plastic bucket containing aerated tap water as catholyte. During operation in batch mode, both bioanodes and biocathodes formed on their respective electrodes, and a peak power of 16.8 W/m^3 and CE of 31.3 % were achieved. With all the other components, the total cell cost of the MFC reactors was less than 64 pence, making this a very cheap cell. In a further study, the same cell was used to treat rice mill wastewater containing lignin and phenols, achieving a lower peak power of 2.3 W/m^3 , but a high COD removal efficiency of 96.5 %, with the anode influent adjusted to pH 8.0 with phosphate buffer [219]. Using the experimental setup, earthenware pots with different thicknesses and volumes were tested using sucrose as the anode medium [220]. These earthen pots had thicknesses of 3, 5, 7 and 8.5 mm, and volumes of 350, 350, 400 and 400 ml, respectively. The MFC based around the pot with 3 mm wall thickness gave the highest volumetric power of 1.04 W/m^3 and a CE of 7.7 %, and these values decreased as the pot wall thickness increased, to values of 0.78 W/m^3 and 6.1 %, respectively, for 8.5 mm. The MFC internal resistances increased in the reverse order, indicating an increased separator ohmic resistance with increased wall thickness. Additionally, a k value for O_2 mass transfer of $1.79 \times 10^{-5} \text{ cm/s}$ was determined for the pot with 3 mm wall thickness (an order of magnitude lower than for Nafion, which is $1.3 \times 10^{-4} \text{ cm/s}$ [196]).

Ceramic separator thickness was also investigated by Winfield *et al.* [221], using a small 6 ml volume single chamber design with a hydrated, open-to-air cathode, and using yeast extract and tryptone as anode substrate [173]. The ceramic separators were made in the lab by shaping either red terracotta or white earthenware clays with different thicknesses of 18, 8 and 4 mm, before firing in the oven to harden the material. Peak powers for the resulting MFCs were in order of separator thickness, with the thinnest separator thickness of 4 mm giving the highest peak power output. However, differences between the type of clay were significant, with the earthenware MFCs producing more power than the terracotta MFCs by 33, 31 and 59 % for the thicknesses of 18, 8 and 4 mm, respectively. From energy-dispersive X-ray spectroscopy, the elemental composition of the materials was determined, with the terracotta found to contain significantly more iron than the earthenware clay, but a lower % of silica. Additionally, earthenware was found to have higher water absorption at 16 % of the mass when hydrated, whilst the terracotta material had a value of 9.1 %, indicating a higher porosity in the former. Higher porosity is also likely to be important in terms of anolyte water loss via the ceramic separator, which occurs through a combination of electro-osmotic drag followed by evaporation from the cathode surface, and which was proposed to account for the increased anolyte loss for earthenware over terracotta as an MFC separator [221].

These material differences in clay have also been investigated by Ghadge *et al.* [222]. The MFCs in this study were built around ceramic pots made from red and black clays, and extensive chemical analysis of the raw clays was also provided. It was found that the ceramic

MFC built around a red clay pot performed best, with a higher CE and peak power [222]. In comparison to the black clay, the red clay was found to have a higher number of cationic sites, lower porosity, higher electrical conductivity and cation exchange capacity. Silica made over 50 % and aluminum over 20 % in both clays, with more silica and aluminium found in the red clay. The black clay contained more Ca^{2+} ions, Mg^{2+} ions, and iron. Porosity was determined using dry and wet weights, therefore it would also have been interesting to have measured porosity by N_2 gas absorption too [223], thereby giving a direct measure of material hydrophobicity. From these studies, it can be seen clearly that the type of clay is critical in how it will perform as a separator. Water porosity was found to be important for these ceramic materials, and can be controlled using sol-gel processing, which is a process which can also be used to prepare different ceramic materials e.g. TiO_2 , ZrO_2 [223].

In terms of reactors design integrating ceramic separators, a novel ceramic pot configuration with an air cathode was made by coating a ceramic terracotta pot with polyurethane and a conductive graphite paint to serve as a GDE [41]. The pot was first coated with the graphite paint, then the polyurethane layer was applied to act a DL and waterproof membrane, to prevent anolyte loss through evaporation. The anode electrode inside the pot was graphite felt, with the bioanode using acetate containing medium in batch mode, achieving a peak power of 33 mW/m^2 , and a cathode potential of 50 mV at OCP. The same system was also operated using hay extract with added NaCl, producing a stable 2 mA of current over a two week operational period, although no peak power was reported [41]. Winfield *et al.* also employed a cylindrical design with the ceramic separator forming an MEA with the anode and cathode, and using a hollow interior for medium [221]. This configuration achieved a peak power of $180 \text{ } \mu\text{W}$, with a 40 ml anode volume (4.5 W/m^3), and earthenware as the ceramic separator [221]. A similar cylindrical terracotta based MFC, this time with an internal air cathode, was developed, with three connected in parallel to power a DC electric fan [39]. This system produced liquid catholyte in the hollow internal cathode chamber through the electro-osmotic drag of anolyte through the ceramic [39], a phenomenon which was later exploited using the same configuration for the production of a caustic solution for CO_2 capture [224].

The use of a membrane increases the cost of the MFC system, and reduces the MFC power output due to an increased MFC ohmic resistance. For example, Liu *et. al* removed the CEM from a single chamber MFC, causing an increase in the power [34]. However, they also observed a decrease in CE which was likely due to O_2 cross-over, and removing the membrane from an aerobic biocathode MFC system is likely to degrade the aerobic biocathode catalyst due to heterotrophic growth at the cathode electrode. Therefore, with the aerobic biocathode MFC system, membranes with high rates of O_2 and substrate cross-over are predicted to degrade biocathode catalyst performance through heterotrophic growth at the cathode, promote

biofouling at the membrane/anolyte and membrane/catholyte interfaces, and lower overall MFC coulombic efficiency. pH splitting lowers the performance of both catalysts at the bioanode and cathode in conventional MFC systems, and degrades the bioanode catalyst. In the case of aerobic biocathode MFCs, there is the additional complication with pH increase at the cathode degrading the biocathode catalyst over time. Membranes which effectively separate substrate and oxygen, and minimise pH splitting are therefore predicted to be best for aerobic biocathode systems. Different membrane types can have quite different costs, and therefore the cheapest membranes are sought. However, lowering the capital cost of the MFC system must be weighed up against MFC system performance, which is dependent on oxygen/substrate cross-over, as well as the degree of membrane pH splitting and membrane ohmic resistance.

2.10 Scale-up of Aerobic Biocathode MFC Systems

Sediment MFCs are have already found practical application as power sources for remote sensors in the environment [7, 8, 167, 225]. However, the use of MFCs for electricity generation from wastewater has not yet reached the stage of practical application, although there have been some reports of pilot-scale studies [38]. One such pilot-scale MFC system was constructed at Foster's brewery (Yatalya, Queensland, Australia) for the treatment of brewery wastewater [38]. This system consisted of twelve, three meter high tubular modules with carbon fiber brush anodes and cathodes. The brewery wastewater effluent was pumped up through the anode chamber and flowed down over the outside of the tubular modules to hydrate the cathodes. No performance information has yet been given for the system, although it was reported that the anolyte had low conductivity, and that high anode effluent biochemical oxygen demand (BOD) caused a high degree of biofilm growth on the outside of the tubular modules [38]. A 20 L pilot scale reactor was setup and operated at a wastewater treatment plant by Jiang *et al.* for the treatment of domestic influent [226]. The system achieved a COD removal of 80 % at a high hydraulic retention time of 20 hours, a peak power of 500 mW/m², and CEs ranging from 0.30 - 0.04 % [226]. The system suffered from high internal resistance due to the use of graphite rods inserted into a graphite granule bed as anodes and a large average anode-cathode electrode spacing (15 cm) [226]. A scaled-up, 1 L single chamber air-cathode MFC has also been used to power an electric fan in a lab demonstration of the technology [38]. It has been suggested that to be competitive with anaerobic digestion, the MFC technology needs to reach a peak power of 400 W/m³ [227].

Most lab-scale studies use tubular or planar electrode configurations [24], and scale-up issues regarding single chamber air cathode MFCs have been discussed in the literature [227–229]. Factors such as substrate concentration, anode/cathode areas, electrode spacing, and anolyte

conductivity, all effect MFC performance. Cathode surface area [227] and electrode spacing [228], have been highlighted as being particularly important for scale up. With respect to cathode size, GDEs are unlikely to be scaled up above a certain size due to an increased pressure exerted on the GDE from the anolyte. Additionally, the relationship between anode surface area and anode current density on increasing anode size must be better understood, as it has been reported that this is not linear in studies where the cathode area was kept at 5 times the anode area [229].

Given the likely issues regarding scaling up of MFC reactor size, stacked configurations using series or parallel-series of smaller MFC units [37, 173, 230, 231], may represent the best way of circumventing these problems for efficient electrical energy production from wastewater. Additionally, series configurations are necessary when higher voltages are needed to power most electrical devices. Connecting MFCs in parallel has the disadvantage that the higher currents produced lead to greater ohmic losses through the connecting materials, whilst series connection can lead to the problem of cell voltage reversal [230]. The latter can be minimised by matching the internal resistances of individual cells more precisely [37], and in practice, series-parallel configurations have been found to work best, simultaneously increasing both the cell voltage and current [173]. Another stacking option is to use a series of bipolar plates in which the anode of one MFC unit and the cathode of another MFC unit are fixed to either side of a bipolar plate, and electrons transfer from the cathode of one MFC to the anode of another, giving a series connection [230]. Such a configuration minimises ohmic losses through electrical connections [230], and provides a simplified way for connecting MFCs in series. Dekker *et al.* constructed a stack of four, five L MFCs using titanium bipolar plates coated with metal oxide, achieving an OCP of 3.1 V, and a peak power density of 11 W/m³ for the 20 L stack [230]. However, the metal oxide coated titanium plates used for both anode and cathode as part of the bipolar plate are unlikely to have been optimal for the anode and cathode reactions, and the large cell anolyte volumes may not have been optimal for stacking. With respect to the latter, Ieropoulos *et al.* determined a peak power projection for 80 small 6.3 ml MFC units based on the peak power determined for 10 of these units of 10 W/m³, which was 50 times larger than the peak power output of a single 500 ml MFC unit with the same equivalent anode volume [173].

Further developments have been made in the area of stacked MFC systems, with the reporting of the first self-sustaining MFC stack treating artificial wastewater, using 40 individual MFC units arranged in 4 separate gravity cascades, each 10 MFC units high [37]. Individual 10 MFC unit cascades consisted of 5 series connected groups of 2 MFC units connected in parallel [37]. The electrical energy produced from the entire stack was used to power the peristaltic pumps for pumping the anolyte feed and catholyte for cathode hydration to the top of the stack, as well as the devices required for self-sensing and reporting of this data by

wireless radio transmission. The stack had a total voltage output of 13.03 V, and some excess energy was also produced, equivalent to 14.55 kWh per day. The reduction in the influent COD was high at 89.45 %, with 740 mg of COD per L remaining in the anode effluent, but a very low CE of 0.018 % was also reported, indicating a high amount of substrate lost to bacterial processes not associated with electricity generation. In this stack, individual MFC units were constructed without precious metal catalysts, which is important in making stack configurations as a whole cheaper and more sustainable.

2.11 Summary

In the literature, bioanode bacteria have been isolated and studied extensively. This has not been the case with aerobic biocathodes. Aerobic biocathode biofilms have been studied in different BESs, such as half-cells and MFCs, and a range of bacteria which catalyse the ORR have been isolated from mixed-community aerobic biocathodes. However, these mixed-community aerobic biocathodes have low catalytic activity toward the ORR ($E_{\text{onset}} < 0.1$ V), as do the bacteria isolated from them ($E_{\text{onset}} < 0.1$ V). Therefore, the bacteria and mechanisms involved of ORR catalysis in aerobic biocathodes with more positive E_{onset} values (0.1-0.4 V) are likely to be different. To date, *Leptothrix discophora*, a well-known Mn oxidiser, is the only bacterial isolate which has achieved a high E_{onset} potential for ORR, which was 0.34 V [65]. It may be that an ability to oxidise Fe/Mn is important in aerobic biocathodes, if the mechanism of ORR catalysis is direct, but this needs to be demonstrated. Indirect mechanisms of ORR catalysis, involving bacterial excretion of a compound that catalyses ORR for example, may also play a role in aerobic biocathode ORR catalysis, particularly if the increase in E_{onset} from abiotic ORR on carbon, for example, is only small. In the literature, the bacteria which catalyse the ORR with a high onset potential (+0.4 V), have not yet been identified. Identification of these bacteria will help in selecting for better performing mixed-community aerobic biocathodes, thereby improving MFC performance.

Very little is known about the mechanism of ORR catalysis in aerobic biocathodes. Indirect [72], as well as direct [124] ORR catalysis mechanisms have been proposed. The only mechanistic study to date has so far studied two bacterial isolates, *Acinetobacter calcoaceticus* and *Shewanella putrefaciens*, which were chosen on the basis of ORR activity in a previous study [77], and for being prevalent in bioanode biofilms, respectively [123]. In this study, there was an increase in E_{ORR} to -0.1 V for *Acinetobacter calcoaceticus* and 0 V for *Shewanella putrefaciens* on a plain carbon paper electrode. The authors determined that the bacteria utilised a self-produced diffusive redox compound analogous to PQQ, and outer-membrane redox compounds, respectively. However, direct ORR catalysis by the bacteria was not proven. Therefore, within the literature, there is a need to determine mechanistic in-

formation for aerobic biocathode biofilms. An understanding of whether the bacteria use the electrode for energy and growth, and how electrons are transferred to the bacteria will help in selecting for better performing mixed-community aerobic biocathodes, thereby improving MFC performance.

The use of poised-potential is a useful investigative tool for studies into mechanisms and communities, as the anode potential may have the effect of altering ET pathways, and also community composition. In the literature, the effect of cathode potential on aerobic biocathode community composition has not yet been studied. One further advantage of poised-potentials is that they allow predictions into how the aerobic biocathode will perform in the full MFC system e.g. with varying external resistance and conditions.

For aerobic biocathode MFCs, the effect of different system variables which can be controlled or engineered, has not so far been explored. These include the degree of exposure of the system to light, the effect of external resistance, and the effect of the membrane. In the literature, light has been found to enhance the performance of acetate-fed batch MFCs [152, 153], despite the well-known fact that certain PNS are able to utilise short chain carboxylic acids and light [154, 155], and are therefore likely to proliferate in the bulk anolyte solution away from the electrode, causing a drop in MFC performance. This is an important engineering parameter, as the degree of exposure to light can be easily controlled for the MFC system. The effect of membrane and external resistance on the performance of conventional MFCs has been studied extensively [34, 157–162, 196, 196–200]. However, how these factors affect the performance of aerobic biocathode MFCs is currently unknown. Both of these variables are known to affect the bioanode, and are also predicted to affect the biocathode too, and therefore performance of the whole aerobic biocathode MFC system. The external resistance is predicted to have an effect on both the bioanode and biocathode, due to the interplay between current and degree of pH splitting; two factors which have not before been considered together in any MFC study. Similarly, with regards to the membrane, the membrane has many properties which are important to consider for development of the system, such as selectivity for ions/O₂/acetate, as well as membrane cost. These membrane properties have a bearing on both the bioanode and biocathode, and therefore membranes should be tested in the aerobic biocathode MFC to see what effect their properties might have on system performance. The results of these studies can be used to improve the performance of aerobic biocathode MFCs, thereby significantly lowering the cost and increasing the sustainability of the MFC technology. Although a battery separator was tested in this thesis, a ceramic separator was not tested. These separators also represent a cost-effective separator for use in MFCs, with other added advantages, such as being able to construct the cell walls and membrane using the same material (e.g. a ceramic pot), as discussed in this literature review. Testing of ceramic separators using the same experimental setups and methodologies used in this thesis

for the testing of membranes would have been desirable, but due to time constraints, was not carried out.

Chapter 3. Materials and Methods

3.1 Electrochemical Methods

3.1.1 Basic electrochemical theory

A multi-step electron transfer reaction can be described using the following equation [232];



Where O is the oxidised species, R is the reduced species, and n is the number of electrons transferred. The bulk concentrations of O and R can be related to the electrode potential at equilibrium according to the Nernst equation [232];

$$E_{eq} = E^0 + \frac{RT}{nF} \ln \frac{C_0^*}{C_R^*} \quad (3.2)$$

Where C_0^* and C_R^* are the bulk concentrations of the oxidised and reduced forms, E^0 is the formal potential, E_{eq} is the electrode potential at equilibrium, F is the Faraday constant, R is the ideal gas constant and T is the temperature. At equilibrium, there is no net flow of current, and so the forward and reverse currents are equal. When the system moves away from equilibrium, there is a net flow of current in either the forward or the reverse directions. Deviation of the electrode potential from the equilibrium electrode potential is over-potential, and is given by the following expression [232];

$$\eta = E - E_{eq} \quad (3.3)$$

When the solution is well-stirred and the surface concentrations of O and R are equal their bulk values ($C_0 = C_0^*$ and $C_R = C_R^*$), the Butler-Volmer equation can be derived for a multi-step electron transfer reaction [44, 232, 233];

$$i = Ai_0 [e^{-\alpha n f \eta} - e^{(1-\alpha)n f \eta}] \quad (3.4)$$

Where A is the electrode area, i_0 is the exchange current density, $f = F/RT$ and α is a parameter relating to the symmetry of the transition state which has a value between 0 and 1. When the overpotential is greater than $118/n$ mV, there is no significant contribution from the reverse reaction, and one of the exponential terms in Equation 3.4 becomes negligible [232]. This allows derivation of the Tafel equation [232, 233];

$$\begin{aligned} i &= i_0 e^{n\alpha f \eta} \\ \eta &= a + b \log i \end{aligned} \quad (3.5)$$

Where $a = \frac{-2.3RT}{\alpha n F} \log i_0$ and $b = \frac{2.3RT}{\alpha n F}$. Therefore, a plot of $\log i$ vs η from values determined experimentally gives the Tafel plot for a given electrochemical reaction, with a Tafel slope equal to b . The Tafel equation only applies at high overpotential when the electrode kinetics are slow, as when the electrode kinetics are fast, mass transfer effects occur before the Tafel region is reached [232]. The abiotic ORR is a kinetically slow reaction, and Tafel slopes of 120 mV/dec and 60 mV/dec are observed for carbon and Pt electrodes respectively, depending on the rate determining step in the mechanism [44].

3.1.2 Open circuit potential

The open circuit potential (OCP) is the potential of an electrode or fuel cell when no current is flowing. For anodes or cathodes, the OCP was measured against a reference electrode (RE), whilst for MFCs, the OCP was measured between the anode and cathode electrodes when they were disconnected and there was no external resistor between the two. The specific setups used were dependent on the investigation, and are discussed later in Sections 3.7 and 3.5. The OCP was measured using either an ohm meter, potentiostat, or voltage data logger.

3.1.3 Potentiostatic methods

In chronoamperometry (CA), the potential of the electrode is controlled using a potentiostat, and the current measured over time. In a 3-electrode setup, the working electrode (WE) is maintained at a fixed potential using a reference electrode (RE) and a counter electrode

(CNE). The RE provides a reference potential, whilst the CNE acts as an electron source or sink, depending on the reaction occurring at the WE. The electrode potential can be stepped from a potential where no current flows, E_{eq} , to an electrode potential at which electrolysis occurs and net current flows. The rate of a cathodic or anodic electrochemical reaction is described by the following equation [232];

$$Rate(mol/s) = \frac{dN}{dt} = \frac{i}{nF} \quad (3.6)$$

Where N is the number of mols of oxidised or reduced species, depending on whether the reaction is anodic or cathodic. At a planar electrode for an electrochemical reaction occurring under diffusion control, the diffusion limited current, i_d , at time, t , is described by the Cottrell equation [232];

$$i_d(t) = \frac{nFAD_0^{1/2}C_0^*}{\pi^{1/2}t^{1/2}} \quad (3.7)$$

Where D_0 is the diffusion coefficient, and A is the electrode area.

For any electrochemical reaction, the CNE needs to be more electrochemically active than the WE. For a bioelectrochemical half-cell, this can be achieved by making the CNE at least as big as the WE, and by coating the CNE with Pt. Pt has excellent activity toward the ORR / O_2 evolution and H_2 oxidation / H^+ reduction, so CNEs coated with Pt can function in both aerobic and anaerobic environments in BESs. For the cultivation of bioanodes, a cathodic reaction at the CNE balances the anodic reaction at the WE, such as H_2 evolution or ORR, depending on conditions at the CNE. For aerobic biocathodes, an anodic current at the CNE balances the cathodic current at the WE, which is O_2 evolution from the electrolysis of water. As the product at the CNE is O_2 , a membrane separating the WE and CNE electrodes is not required, and the two electrodes can be positioned in the same half-cell chamber with air supplied through a gas sparger into the electrolyte.

3.1.4 Sweep methods

In linear sweep voltammetry (LSV), the electrode potential is scanned in a positive or negative direction from the OCP at a particular scan rate, ν , and the current measured [232]. At low overpotentials, the current is described by R_{ct} , whilst at higher overpotentials for electrochemical reactions with slow reactions kinetics, the current is described by the Tafel equation (Equation 3.5) [232]. As the potential is further increased, mass transfer effects begin to dominate the current response, and the current eventually peaks.

LSV were recorded for bioanodes and biocathodes to assess performance of the electrode. This was done by sweeping the potential at $\nu = 1$ mV/s, so as to minimise the current due to electrode capacitance (which is proportional to ν [232]). From the resultant LSV, mass transfer limited currents and onset potentials were identified.

In cyclic voltammetry (CV), the applied potential has a saw tooth waveform, and the potential is scanned in both positive and negative directions at a particular ν [232]. CV for aerobic biocathodes can be used to provide mechanistic information about the bioelectrochemical processes occurring at the electrode surface, such as the identification of catalytic waves or reversible redox features. Further to this, non-turnover CV can be obtained when the electroactive bacteria are not metabolising. For bioanodes, this can be achieved by removing the organic substrate, whilst for aerobic biocathodes, these conditions are achieved by removing O_2 . As the bacteria are no longer metabolising, processes decoupled from metabolism are observed in the CV, such as those belonging to adsorbed redox active proteins or diffusing electron shuttles involved in ET to the electroactive bacteria.

For a given reversible electrochemical reaction, the forward and reverse scans in the CV give anodic and cathodic peaks with corresponding peak potentials and peak currents. Taking either the cathodic or anodic peaks, if the kinetics of the electrochemical reaction are fast relative to ν , then the peak current, i_p , is proportional to ν , and the peak position, E_p , is invariant with ν [232]. For an electrochemical reaction with slow kinetics relative to ν , i_p varies with $\sqrt{\nu}$, and E_p varies ν (causing peak separation) [232]. An example of an electrochemical reaction with slow reaction kinetics, the ferricyanide/ferrocyanide redox couple ($[Fe(CN)_6^{3-}] + e^- \rightleftharpoons [Fe(CN)_6^{4-}]$), is given in Figure 3.1. In Figure 3.1a, the increasing separation between the anodic and cathodic peaks can be observed, whilst Figure 3.1b illustrates the linearity in the plot of i_p versus $\sqrt{\nu}$. For adsorbed redox active proteins confined to the electrode surface, a linear dependence of i_p versus ν is observed when the electrode kinetics are fast relative to ν , and analysis of the peak area gives the number of finite adsorbed redox active species [234].

Peak analysis of the type described above can be used to elucidate mechanistic details in electroactive biofilms by coupling with non-turnover CV.

3.1.5 Electrochemical methods for MFCs

At any given current, the MFC cell voltage, E_{cell} , is given by [235];

$$E_{cell} = E_{cat} - E_{an} \quad (3.8)$$

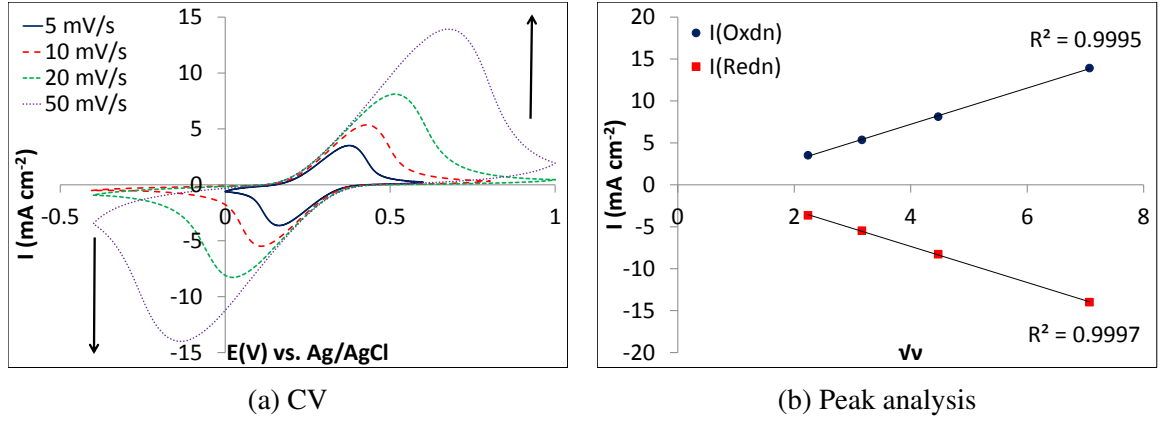


Figure 3.1: CV and peak analysis for a 1 cm² carbon felt electrode immersed in a solution containing 10 mM FeCN₆³⁻ and 100 mM phosphate buffer. Graph a) shows the CV at different scan rates, whilst graph b) shows the oxidation and reduction peak heights plotted against \sqrt{v} .

Where E_{cell} is the MFC cell voltage, E_{cat} is the cathode potential, and E_{an} is the anode potential. For the MFCs, E_{cell} and E_{cat} were logged at 15 minute intervals during operation, with E_{cat} measured using an RE in the cathode chamber. All MFC voltages, whether acquired during operation or a polarisation curve, were recorded using a voltage data logger (National Instruments multi-channel data logger with LabVIEW, UK).

MFC polarisation curves are used to assess MFC performance and determine peak power. Peak power is a measure of the amount of energy produced by the MFC, which is the ultimate goal in MFC research for power generation. The power, P , is related to E_{cell} and the MFC external resistance, R_{ext} , through the following equations [22];

$$P = IE_{cell} \quad (3.9)$$

$$P = \frac{E_{cell}^2}{R_{ext}} \quad (3.10)$$

Where I is the current flowing through the MFC. By varying R_{ext} and measuring E_{cell} , the power can be calculated at different resistances, known as an MFC polarisation curve. In the polarisation curve, a maximum in the power is observed, which is the peak power of the MFC system. An example is given in Figure 3.2. For an MFC, E_{cell} can also be written in the following way [22];

$$E_{cell} = E_{cell}^{0'} - (\eta_{cat} + \eta_{an} + IR_{\Omega}) \quad (3.11)$$

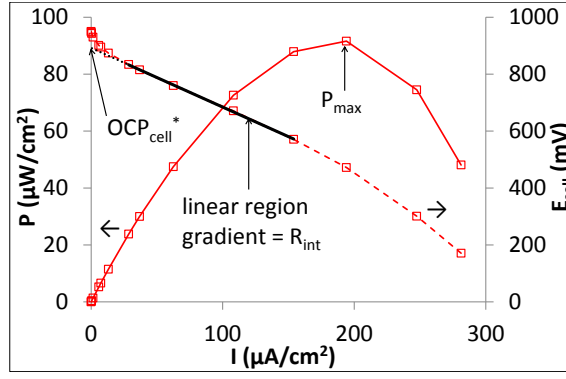


Figure 3.2: Example polarisation curve for an MFC

Where E_{cell}^0 is the theoretical MFC cell voltage (derived previously in the literature review as 1.1 V), η_{cat} and η_{an} are the overpotentials at the cathode and anode electrodes respectively, I is the current flowing through the MFC, and R_{Ω} is the ohmic resistance of the MFC. The overpotentials at the cathode and anode electrodes vary non-linearly with the current, whilst R_{Ω} varies linearly with the current and is constant for a given MFC system [22]. R_{Ω} is the sum of ohmic resistances from the solution (R_s), membrane (R_{mem}) and electrode contacts ($R_{contact}$), and can be expressed using the following equation;

$$R_{\Omega} = R_s + R_{mem} + R_{contact} \quad (3.12)$$

For polarisation plots of E_{cell} against I , there is a linear region with a gradient of constant resistance equal to the MFC internal resistance, R_{int} , which can be expressed using the following equation [22];

$$E_{cell} = OCP_{cell}^* - IR_{int} \quad (3.13)$$

Where OCP_{cell}^* is the y-intercept extrapolated from the linear region of the curve, and is not the true OCP_{cell} . R_{int} can be further expressed as a sum of ohmic and polarisation resistances [236];

$$R_{int} = R_p^{cat} + R_p^{an} + R_{\Omega} \quad (3.14)$$

Where R_p^{an} and R_p^{cat} are the polarisation resistances at the anode and cathode electrodes in the linear region of the MFC polarisation curve, respectively, and are themselves a sum of charge transfer and diffusion resistances [237]. From Equation 3.14, if both R_{int} and R_{Ω} are known for any given MFC system, then the sum of R_p^{cat} and R_p^{an} can be calculated. This gives

a measure of the combined activity of both anode and cathode electrodes in the MFC.

In practice, MFC polarisation curves were recorded in the following way; Firstly, the MFC was put into OCP for 2 hours, and at the end of this period, E_{cell} was measured. The MFC external resistance was then varied from high to low values in 20 minute intervals to allow the potential to stabilise, with E_{cell} recorded at the end of each interval. For some of the polarisation curves, cathode and anode potentials were also recorded simultaneously to E_{cell} with REs placed into both of the anode and cathode chambers.

Electrode impedance spectroscopy (EIS) can be used to separate the different overpotential losses in an MFC; ohmic overpotentials, diffusion and charge transfer related electrode overpotentials [233]. In EIS, an AC potential with a small potential perturbation is applied between the electrodes, and the frequency varied, separating different electrode processes according to the time-scales over which they occur [233]. EIS spectra are often presented graphically as a Nyquist plot, with imaginary impedance plotted against real impedance.

EIS spectra can be obtained for the WE of electrochemical half-cells using a 3-electrode setup with an RE and CNE. The high-frequency intercept of the Nyquist plot gives R_{Ω} , where R_{Ω} is the ohmic resistance between the WE and RE, whilst the low-frequency intercept is the sum of both R_{ct} and R_{Ω} [233]. R_{Ω} is easily measured for any given half-cell, and the distance between the WE and RE reduced if this value is too high, so as to reduce the ohmic drop (IR_{Ω}). For electrochemical half-cells, EIS was used to measure the ohmic resistance between the WE and RE in order to ensure a low ohmic drop. The EIS spectra were recorded at the electrode OCP using 50 frequencies from 100,000 Hz to 0.1 Hz with a 10 mV AC voltage amplitude. As the EIS spectra were used to extract the ohmic resistance from the high-frequency intercept in the Nyquist plot, the frequency range used was validated by the presence of the intercept.

EIS spectra can also be obtained for full MFC systems by applying a potential across the anode and cathode electrodes using a 2-electrode setup. In the Nyquist plot of the EIS spectrum, the low-frequency intercept is equal to the MFC ohmic resistance, R_{Ω} [233], whilst different resistances and capacitances relating to anode and cathode polarisation, such as charge transfer resistances, can be determined by fitting the entire spectrum to an appropriate equivalent circuit model [237, 238]. Nyquist plots for MFCs are complex, however, R_{Ω} can be reliably extracted from the high-frequency intercept. In practice, EIS spectra for MFCs were recorded at the OCP for the MFC using a 2-electrode setup, with the anode as the CNE and the cathode as the WE. EIS spectra were recorded with 50 frequencies from 100,000 Hz to 0.1 Hz with a 10 mV AC voltage amplitude. From the EIS spectra, the value of R_{Ω} for the MFC was determined. The presence of a high-frequency intercept in the recorded Nyquist plots validated the EIS frequency range used in determining R_{Ω} for the MFC.

For certain MFCs, polarisation curves then EIS spectra were recorded. From the polarisation curves, R_{int} was determined from the gradient of E_{cell} in the linear region, whilst from the EIS spectra, R_{Ω} was determined from the high-frequency intercept of the Nyquist plot. Using Equation 3.14, $R_p^{an} + R_p^{cat}$ was calculated for a particular MFC system, giving a measure of the combined activity of the anode and cathode electrodes.

3.2 Microbiological Methods

3.2.1 Sampling

Carbon felt electrodes with biocathode biofilms were taken from the half-cells at the end of their operational periods, and various microbiological analyses were carried out. For biomass determination, the carbon felt electrode was subsampled after taking out of the half-cell by taking two 10 mm diameter electrode bore samples from the center (sample 1) and near the edge of the electrode (sample 2), in order to account for uneven biomass distribution across the electrode surface. For community analysis, the carbon felt electrodes, minus the subsamples taken for biomass determination, were placed into individual sterile 50 ml centrifuge tubes containing 50:50% H₂O:EtOH by volume, and stored at -4 °C before community analysis. For biofilm imaging, a single carbon felt electrode was imaged immediately after taking the electrode out of the half-cell, and was not used for any other analysis.

3.2.2 Biofilm imaging

To image the bacteria on an electrode, a nucleic acid stain (SYBR gold, Life Technologies, USA), was used to stain all live/dead bacterial cells. SYBR Gold binds to bacterial DNA, resulting in a DNA-dye complex which fluoresces when exposed to light, with absorption maxima with wavelengths of 300 and 495 nm, and an emission maximum of 537 nm [239]. To image a carbon felt electrode with a biofilm of bacteria, the electrode was placed into a solution containing a x100 dilution of SYBR Gold in 50 mM phosphate buffer, covered with foil, and incubated at room temperature for 30 minutes. The front and back of the electrode were then imaged using a gel documentation system (Biospectrum imaging system, Ultra-Violet Products (UVP) Ltd, Cambridge, UK) equipped with a UV transilluminator using an excitation wavelength of 365 nm and an exposure time of 1 minute and 29 seconds. In order to estimate biofilm thickness, vertical electrode cross-sections were prepared from the electrode using a scalpel and imaged at x 100 magnification using an epifluorescence microscope (Olympus BX40) equipped with a filter for the detection of green light (WU filter) and a UV source (Olympus U-RFL-T). Images were taken using an attached digital camera (Olym-

pus E-400), and distances in the images were calibrated by taking an additional image of a graticule slide at x 100 magnification (with 1 mm/0.01 divisions), which can be found in the Appendix, Figure A.1.

3.2.3 Biomass determination

For biomass determination, protein was used as a proxy for biomass, and the protein content of the electrode subsamples was determined by first extracting the protein using the following method. For an individual bore sample, 1 ml of a detergent-based cell membrane lysis reagent (CelLytic B, Sigma-Aldrich, UK) was added to the sample in a 2 ml centrifuge tube to disrupt the bacterial cell membranes, the contents were grinded with a clean stainless steel rod, then shaken for 15 minutes using a shaking incubator. The solution was then filtered using a 0.2 micron polyethylenesulfone (PES) filter into a sterile 2 ml centrifuge tube. A further 1 ml of lysis reagent was added to the old 2 ml centrifuge tube and the whole procedure repeated, with the new filtrate added to the old filtrate. The filtrates were stored at -4 °C before protein determination.

A bicinchoninic acid (BCA) assay kit (BCA protein assay kit, Merck, UK) coupled with a UV-Vis microplate reader (SPECTROstarNano, BMG LABTECH) was used for protein determination. In the BCA assay, the sample is added to an alkaline solution of CuSO_4 and bicinchoninic acid, and Cu^{2+} is reduced to Cu^+ by peptide bonds in the protein, with the amount of Cu^{2+} reduced proportional to the number of peptide bonds [240]. Cu^+ then chelates with bicinchoninic acid, forming a purple complex with an absorption peak of 562 nm, which is analysed by UV-Vis spectroscopy. Calibration of the UV-Vis spectrometer with known concentrations of bovine serum albumin (BSA) then allows calculation of the sample protein concentration. A standard curve was obtained using 0, 25, 125, 250, 500 and 1000 $\mu\text{g/ml}$ BSA dilutions from a 2 mg/ml BSA stock. The standard curve was fitted using a quadratic function, and is available in the Appendix (Figure A.2). All reactions were incubated at 60 °C for 15 minutes in the microplate reader before measurement.

3.2.4 Community analysis

The community of an individual working electrode was sequenced using ion semiconductor sequencing technology targeting the V4-V5 hypervariable region of the 16S rRNA gene of bacteria and archaea (481 base pairs).

DNA extraction was carried out on small pieces of electrode material cut from the original electrode, each weighing 0.25 g, using a DNA isolation kit (PowerSoil DNA isolation kit,

MO-BIO, USA). DNA extraction was also carried out on a reagent blank. The DNA in the DNA extract was quantified using a microvolume UV-Vis (Nanodrop 3300, Thermo Fisher Scientific, USA) spectrometer to check that a significant amount of DNA had been extracted from the sample.

Polymerase chain reaction (PCR) was carried out on the extracted DNA using a barcoded V4 forward primer and a non-barcoded V5 reverse primer. The barcoded V4 forward primer had the following structure; 5'-adaptor-barcode-spacer-primer-3', with a primer sequence of 5'-GTGNCAGCMGCCGCGGTAA-3' (where the barcode is unique to the sample). The V5 reverse primer had the following structure; 5'-trP1-primer-3', with a primer sequence of 5'-CCGYCAATTYMTTTRAGTTT-3'. The fixed PCR reagents were provided from a master mix solution (MegaMix Blue, Cambio, UK), containing Taq DNA polymerase, dNTPs, MgCl₂, reaction buffer, and an enzyme stabiliser. PCR tubes were prepared containing 23.5 µl of the master mix solution, 0.5 µl of barcoded V4 forward primer, 0.5 µl of non-barcoded reverse primer, and 0.5 µl of DNA extract, giving a total reaction volume of 25 µl. 30 cycles of PCR were carried out using an automated thermal cycler (Techne TC-512 Thermal Cycler, Bibby Scientific Ltd, Staffordshire, UK) with the following program;

1. Denaturation step - 94 °C for 30s
2. Annealing step - 56 °C for 30s
3. Extension step - 72 °C for 45s
4. Final extension step - 72 °C for 7 minutes

The purity and quantity of the PCR products was assessed by electrophoresis, using a 1.5 % (w/v) agarose gel plate. The 1.5 % (w/v) agarose gel plate was prepared by mixing 1.6 µl of ethidium bromide and 1.5 g of agarose per 100 ml of water. 5 µl of PCR product and 2 µl of a loading dye (0.25 % Bromophenol blue, 40 % (w/v) sucrose) were loaded into each sample well of the agarose gel plate. Wells at the edges of the plate were loaded with 2.5 µl of a molecular weight marker with 15 bands ranging from 50 to 2000 basepairs (HyperLadder II, Bionline, USA). The gel plate was run for 45 minutes at 100 V in 1 x Tris-acetate-EDTA buffer (2M Tris-Acetate, 0.05 M EDTA, pH 8.3), and images of the gel plate were obtained using a gel documentation system (Biospectrum imaging system, Ultra-Violet Products (UVP) Ltd, Cambridge, UK).

The resulting PCR amplicons were subject to two rounds of purification using AMPure XP (Beckman Coulter, USA) to remove primer dimers by addition of x1.1 by volume of a magnetic bead solution to the samples containing PCR amplicons. AMPure XP is a size-selection technique, and x1.1 by V addition of magnetic beads recovers fragments sizes in the range

from 300 to 2000 base pairs. The purity of the samples was checked again by electrophoresis using a 1.5 % agarose gel plate using the method described above, with a molecular weight marker with 8 bands ranging from 50 to 2000 basepairs (PCR marker, Sigma, UK).

For each PCR product sample, 2 μ l of the sample was added to 198 μ l of working reagent containing a DNA-binding fluorescent dye (Quant-iT PicoGreen dsDNA reagent, Life Technologies, USA), and analysed using a fluorometer (Qubit fluorometer, Life Technologies, USA). This allowed exact determination of the DNA concentration in each sample. The quantified DNA was then diluted and combined with 26 pM of DNA per sample to create a pooled amplicon library.

Emulsion PCR was then carried out on this pooled DNA sample (Ion OneTouch, Life Technologies, USA). In emulsion PCR, an aqueous solution containing the amplicon library, μ m-scale beads and PCR reagents is mixed with an emulsion oil, resulting in a suspension of oil-water droplets, each containing an individual bead, DNA strand and the PCR reagents [241, 242]. PCR then follows, the result of which is multiple clonal copies of the same single-stranded DNA sequence immobilised onto an individual bead.

The beads were then randomly deposited into an array of μ m-scale wells called a microchip, with a single bead per well [241]. The microchip was a 314 microchip which allows a maximum of 250,000 reads. The microchip was then loaded into an ion semiconductor sequencing machine (Ion Torrent PGM, Ion Torrent, USA). In the semiconductor sequencing technology, the clonal single-stranded DNA strands in each well are sequenced by washing the 314 microchip sequentially with individual dNTPs [243]. For an individual well, successful incorporation of a nucleotide base by the polymerase results in release of a H^+ , triggering an electrical signal from the ion-sensitive field effect transistor in the base of the well [243]. Therefore, all of the DNA strands in each of the wells on the chip are sequenced simultaneously. One major drawback of the method is that the signal intensity does not vary proportionally with the number of nucleotides for homopolymer sections, leading to sequencing errors [244].

The ion torrent sequencing data was processed using the program quantitative insights into molecular ecology (QIIME) [245]. The following scripts were used in the following order to process the multiplexed sequences;

1. `split_libraries.py`

- This script was applied to demultiplex the sequences in the fasta file according to their sample ID using a mapping file, to filter out reads below a certain quality threshold using a quality score file ($s = 20$), and to discard sequences below a certain length ($l = 200$).

2. pick_otus.py
 - Operational taxonomic units (OTUs) were clustered at the 0.97 similarity threshold, corresponding to species-level identification, using the uclust clustering method.
3. pick_rep_set.py
 - Representative sequences were defined for each of the OTUs identified from step 2, based on the most abundant sequences in each OTU.
4. assign_taxonomy.py
 - Taxonomy was assigned to the representative sequences identified in 3 using the green genes database.
5. make_otu_table.py
 - An OTU table was built based on the assigned taxonomy and number of times a particular OTU appeared in each sample.
6. align_seqs.py
 - The PyNast algorithm was used to align the representative sequences from 3 to a pre-aligned database of template sequences (from the green genes database).
7. filter_alignment.py
 - This script was applied to remove positions which were gaps and common to every sequence from the aligned sequences.
8. parallel_identify_chimeric_seqs.py
 - This script identified chimeric sequences in the aligned and filtered sequences using the ChimeraSlayer algorithm.
9. filter_otus_from_otu_table.py
 - This script removed chimeric sequences identified in 8, from the OTU table built in 5.
10. summarize_taxa_through_plots.py
 - Using the output from 9, the OTUs were plotted graphically.
11. filter_fasta.py
 - Using the output from 8, this script filtered out chimeric OTUs from the fasta file.

12. make_phylogeny.py

- Using the output from 11, this script was used to make the phylogenetic tree.

13. beta_diversity_through_plots.py

- Using the output from 12, the mapping file and the filtered fasta (output from 11), this batch script was used to determine beta diversity.
- The batch script first calls single_rarefaction.py, in order to rarefy the sequences in the OTU table to achieve an even sample heterogeneity, by randomly subsampling. The subsampling size was chosen as equal to the number of reads for the sample with the smallest total number of reads.
- The batch script then computed the beta diversity using weighted and unweighted UniFrac.
- The batch script then runs a principal coordinates (PCoA) analysis, using the beta diversity matrix.
- The batch script then produced Emperor PCoA plots, using PCoA analysis results, allowing for easy visualisation of the PCoA analysis results.

Beta diversity was calculated, which assesses the differences between microbial communities based on composition. A square matrix was produced, containing phylogenetic distance values between communities, which were calculated using the UniFrac metric for pairwise combinations of microbial communities [246]. The beta diversity matrix was then interpreted using PCoA.

3.3 Analytical Methods

3.3.1 Sampling

Aqueous samples from a BES were sampled by first filtering with a 0.2 micron PES filter to remove bacteria, then stored in centrifuge tubes at $-4\text{ }^{\circ}\text{C}$ for later analysis. For long-term storage of samples for total organic carbon (TOC) analysis, a temperature of $-20\text{ }^{\circ}\text{C}$ was used. For the measurement of dissolved oxygen (DO) and pH, the probes were inserted through a port in the top of the MFC or half-cell, into the electrolyte.

3.3.2 Dissolved oxygen concentration determination

This was determined for the electrolyte in a given MFC or half-cell using a calibrated DO meter (9500 bench DO₂ meter, Jenway, UK). The DO meter is based around the chronoamperometric detection of O₂ at a Pt electrode (Clark electrode).

3.3.3 Acetate concentration determination

For aqueous samples containing acetate, acetate concentrations were determined by measuring the TOC using a TOC analyser (5050A with an ASI-5000A auto sampler, Shimadzu, Japan), and calibrating with fresh media containing known concentrations of acetate. The TOC analyser determines the TOC of a sample by determining both the total carbon (TC) and the inorganic carbon (IC) in a sample [42];

$$\text{TOC} = \text{TC} - \text{IC} \quad (3.15)$$

In the TOC analyser, the sample is divided into two. One half is acidified with acid (25 % phosphoric acid), then sparged with purified air to remove all inorganic carbon as CO₂, which is measured using an infrared gas detector. This measures the IC in the sample. The other half is oxidised at high temperature in purified air at 680 °C over a Pt catalyst to convert all carbon to CO₂, which is measured using the infrared gas detector. This measures the TC. As both the TC and IC are known, the TOC can be calculated for the original sample. The TOC analyser was calibrated using series dilution of fresh, filter-sterilised medium. A calibration curve for the TOC analyser is included in the Appendix, Figure A.3, for bioanode medium (1 g/L sodium acetate, 50 mM phosphate buffer and nutrient solutions - see Subsection 3.5.1).

3.3.4 pH measurement

Sample pH was measured using a calibrated pH meter (Hanna instruments, HI 9025 micro-computer pH meter, UK).

3.3.5 Cation and anion concentration determination

The concentration of K⁺ and Na⁺ in an aqueous sample was determined by inductively coupled plasma atomic emission spectroscopy (ICP-AES), whereas the concentrations of F⁻, Cl⁻,

phosphate, sulphate and nitrate were determined by ion chromatography (IC).

For the determination of K^+ and Na^+ concentrations in an aqueous sample, an inductively-coupled plasma atomic emission spectrometer (ICP-AES) was used (Vista-MPX, Varian, USA). In the ICP-AES instrument, the aqueous sample is introduced into an argon plasma stream as an aerosol, causing collisions with charged species in the plasma. These collisions result in both ionisation and electronic excitation of atoms in the sample, and subsequent characteristic atomic light emission from each element in the sample [247]. The total light emission from the sample enters an optical chamber where it is broken down into individual wavelengths using a diffraction grating, and the light intensity from each wavelength of light is measured simultaneously using an array of charge coupled devices. A calibration using solutions containing known concentrations of the cationic ions of interest was carried out.

The concentration of select anions was measured using an ion chromatography system (ICS-1000 with an AS40 auto sampler, Dionex, USA) equipped with a carbonate-based anion exchange column (Ionpac AS14A, 4 x 250 mm) for the detection of F^- , Cl^- , Br^- , nitrate, phosphate and sulphate anions. In the anion exchange process, Coulombic attraction between anions in the analyte and the stationary phase, and subsequent displacement of these anions with the mobile phase containing carbonate anions, causes anions of the analyte to elute with different retention times, depending on the anion [248]. The anions are then detected and quantified using a conductivity cell positioned at the end of the column [248].

For the analysis of anions, the ICS was operated with a flow rate through the column of 1 ml/min using an eluent solution containing 8.0 mM Na_2CO_3 / 1.0 mM $NaHCO_3$ at fixed concentration, and the sample was loaded into a 25 μ l sample loop.

3.4 Materials Characterisation for Aerobic Biocathode Half-Cells

3.4.1 Setup

An experimental setup was developed in order to polarise a porous carbon felt electrode at a potential at which ORR occurs, whilst simultaneously polarising a Pt secondary sensing electrode (SSE) in the same chamber at a potential at which H_2O_2 is oxidised, therefore detecting the H_2O_2 product from the carbon felt. The 4-electrode setup used to detect peroxide from porous carbon felt is described in Figure 3.3. The porous carbon felt under investigation was either HNO_3 treated or untreated. All of the carbon felt electrodes used in the abiotic studies had an area of 60 x 20 mm. The carbon felt was purchased from VWR (Cat. No. 43200.RR, Alfa Aesar, UK) and had a strand density of 3.65 g/cm³ (20 °C) and thickness of

0.5 cm. All carbon felt electrodes were washed in acetone prior to use to remove oil residues left over from manufacture, and left to dry in air for approximately 12 hours. The SSE used to detect H_2O_2 in all of the studies was a small piece of platinised titanium mesh of 2 cm^2 geometric area, and the counter electrode was a larger piece of platinised titanium mesh of 35 cm^2 geometric area.

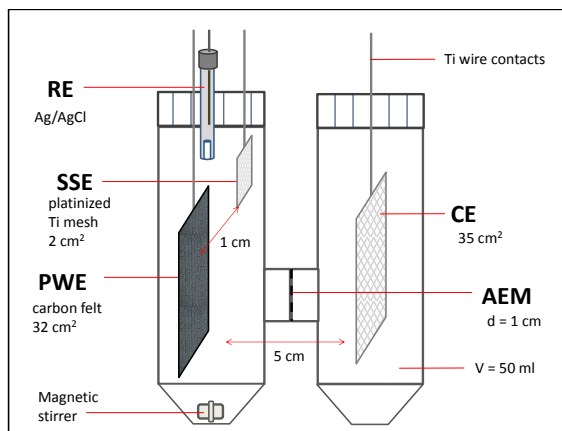


Figure 3.3: 4-electrode setup for the detection of H_2O_2 from porous CF electrodes, incorporating a primary working electrode (PWE) of the carbon felt material held at different CA potentials, a Pt secondary sensing electrode (SSE) held at $+0.6\text{ V}$, a reference electrode (RE) and a counter electrode (CNE).

HNO_3 treatment of the carbon felt was carried out using a method based on that used by Wang *et al.* and Scott *et al.* for the modification of carbon black supports [47, 190]. HNO_3 treatment of the carbon felt was carried out by placing the carbon felt electrode in a round-bottomed flask attached to a reflux condenser with 400 ml of concentrated HNO_3 (69% by weight, AnalaR Normapur, UK). The solution was then refluxed for 2 hours at $122\text{ }^\circ\text{C}$ until the colour of the gas in the reflux condenser went from dark brown to very light brown. The contents of the flask were then allowed to cool to room temperature before removing the HNO_3 and extracting the carbon felt. This carbon felt electrode was then washed repeatedly with deionised water until the filtrate had reached pH 6. The carbon felt electrode was then left to dry for approximately 12 hours before use.

The cell used to test the materials was constructed from two centrifuge tubes made from polypropylene, one forming the chamber for the two WEs, and the other centrifuge tube used for the CNE chamber. Each centrifuge tube was modified with a plastic flange made out of polypropylene, and glued into place using hot melt glue from a glue gun. These flanges allowed fixture of an AEM (Fumasep FAD, Fumatech, Germany) of 1 cm^2 geometric area between the two tubes, allowing the passage of anions between the two chambers, but not peroxide. The AEM functions to prevent the passage of peroxide, although a CEM would also have performed the same role in this system. One of the tubes contained the primary

working electrode (PWE) and SSE, as well as an RE (RRPEAGCL2 miniature Ag/AgCl RE, Pine Research Instrumentation, US). Both WEs were maintained in a fixed position relative to each other, and both were connected to titanium wire running out of the cell through ports drilled into the centrifuge tube cap. The separation between the PWE and SSE was small at 1 cm, so as to improve detection of peroxide at the SSE. As the potentials of the WEs are fixed separately using the potentiostat fitted with a bipotentiostat (4-electrode) module, the small separation between the two WEs has no impact on the potentials of the two electrodes. The platinum mesh CNE was fixed into position in the other chamber in the same way as the PWE and SSE. The experiments were performed in 50 mM pH 7.0 phosphate buffer, and this solution was stirred using a magnetic stirrer in order to improve the detection of H₂O₂ at the SSE.

3.4.2 Electrochemical characterisation

All electrochemical experiments were carried out using a potentiostat (Autolab PGSTAT302, Metrohm, UK) fitted with a bipotentiostat module. In the CA experiments, the SSE was polarised for 15 minutes at +0.6 V to get a stable background current, before simultaneous polarisation of both the PWE and SSE for 1 hour. When both electrodes were polarised simultaneously, the SSE was kept at +0.6 V, whereas the potential of the PSE was kept constant but varied depending on the experiment. The HNO₃-treated carbon felt was polarised at -1, -0.5, -0.1, -0.05, 0 and +0.05 V in separate experiments. The untreated carbon felt was polarised at -1, -0.5, -0.2 and -0.1 V in separate experiments. All CA experiments were conducted twice, the raw CA data smoothed using a Savitky-Golay filter, and the average taken.

3.5 Setup, Operation and Characterisation of Aerobic Biocathode Half-Cells

3.5.1 Setup

A potentiostatic method for the growth of aerobic biocathodes was developed in which the WE electrode potential was fixed at a potential at which it was assumed that the bacteria would be able to use the electrode as an electron source for autotrophic metabolism. All aerobic biocathodes were cultivated in poised-potential aerobic biocathode half-cells. The reactor design is depicted in 3.4. This is a 3-electrode setup with a WE, CNE and RE. The reactor chamber body was cylindrical with a 1 L volume and was made from polypropylene with ports for the WE, CNE, RE, sampling port and gas inlet/outlet. The WE and CNE faced each other with a 3 cm electrode spacing. The WE was a rectangular piece of carbon felt with an area of 12.16 cm² (1.9 x 6.4 cm) and a thickness of 0.5 cm (VWR Cat. No. 43200.RR,

Alfa Aesar, UK). The carbon felt was acetone washed beforehand and held between a polytetrafluoroethylene (PTFE) window, comprising a front and backing plate held together with nylon bolts, exposing only one side of the carbon felt to solution. The PTFE window is given in Figure 3.4c. A graphite plate was used to make contact between the carbon felt and the external circuit. The CNE was a two-sided, rectangular 12.16 cm^2 piece of Pt mesh attached to a Ti wire (24.32 cm^2), and the RE was an Ag/AgCl electrode (RE-5B, BASi, UK) housed within a polypropylene luggin capillary containing a 3 M NaCl agar salt bridge. The temperature for all half-cells was controlled at $30 \text{ }^\circ\text{C}$ by putting the half-cells into a dark incubator for their operational periods. The dark incubator was built in-house, and was a temperature regulated heating mat inside a polystyrene box.

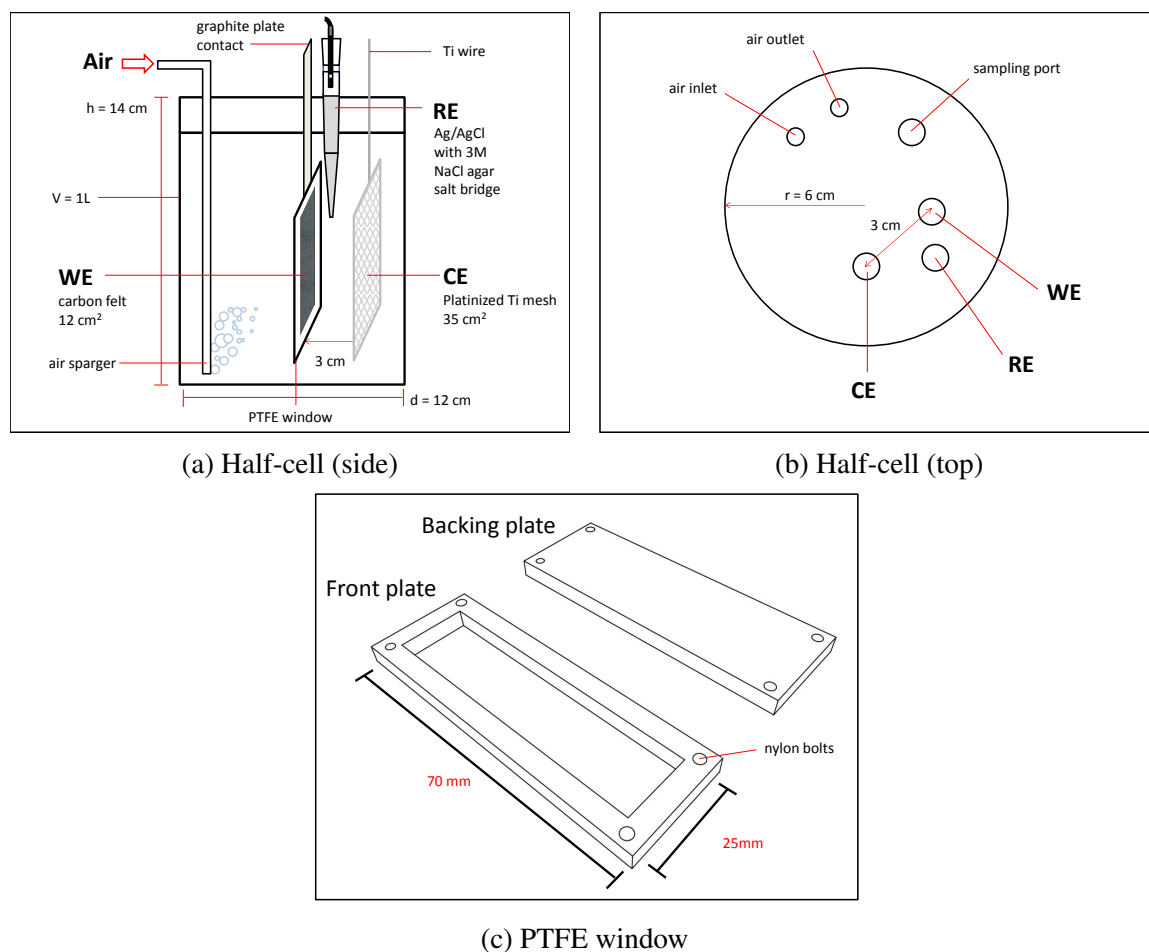


Figure 3.4: Setup diagrams showing side (a) and top (b) views of the half-cell. The PTFE window with front and backing plate used to hold the carbon felt WE is given in (c).

The biocathode medium used to cultivate the bacteria had a volume of 1 L and contained 50 mM of pH 5.8 phosphate buffer and nutrients for the bacteria. These nutrients were 10 ml/L of a macro nutrient solution, 1 ml/L of a metal nutrient solution, and 1 ml/L of a vitamin solution, as described by Heijne *et al.* [68, 166], with a few minor changes. Per litre, the macro nutrient solution contained 28 g of NH_4Cl , 10 g of $\text{MgSO}_4 \cdot 7 \text{H}_2\text{O}$ and 430

mg of CaCl_2 . Per litre, the metal nutrient solution contained 2 g of $\text{FeCl}_2 \cdot 4\text{H}_2\text{O}$, 1 g of $\text{CoCl}_2 \cdot 6\text{H}_2\text{O}$, 1 g of $\text{NiCl}_2 \cdot 6\text{H}_2\text{O}$, 500 mg of $\text{MnCl}_2 \cdot 4\text{H}_2\text{O}$, 105 mg of Na_2SeO_3 , 70 mg of $(\text{NH}_4)_6\text{Mo}_7\text{O}_{24} \cdot 4\text{H}_2\text{O}$, 50 mg of ZnCl_2 , 50 mg of H_3BO_3 , 40 mg of $\text{CuCl}_2 \cdot 2\text{H}_2\text{O}$ and 2 ml of conc. HCl. Per litre, the vitamin solution contained 1 g of pyridoxine.HCl, 500 mg of nicotinic acid, 250 mg of riboflavin, 250 mg of thiamine.HCl, 200 mg of biotin, 200 mg of folic acid and 10 mg of vitamin B12. All chemicals were purchased from Sigma Aldrich (UK).

3.5.2 Operation

I(A) was measured continuously for all half-cells. In some of the half-cells, the potential was applied using a potentiostat (Sycopel, UK), and I(A) measured manually at 1-2 day intervals. In the other half-cells, the potential was applied using a quad-potentiostat (Whistonbrook Technologies, UK) and I(A) was recorded every 15 minutes. In all of the half-cells, air was sparged into the half-cell chamber using an air pump and air sparger to maintain the DO at levels above 7.0 mg/L. The half-cell medium was topped up regularly with deionised water to compensate for water loss by evaporation, and the media replaced at regular 1-2 week intervals to compensate for potential nutrient depletion in the media over time (medium changes indicated on the CA graphs for each half-cell). RE drifts were measured regularly against a lab master and maintained at values of less than 5 mV. During operation, the pH was measured at the beginning and end of a batch cycle to ensure it did not increase by any more than 0.5 pH units during the batch cycle. Additionally, the ohmic resistance between the WE and RE for each half-cell was determined periodically by EIS, and was maintained at values less than 5Ω across all half-cells.

3.5.3 Electrochemical characterisation

CV and LSV for the half-cells were recorded at different points using a potentiostat (Autolab PGSTAT302, Metrohm, UK). LSV were recorded by sweeping the potential from +0.5 to -0.2 V at $\nu = 1 \text{ mV/s}$, whilst CV were recorded over the same potential range at $\nu = 5 \text{ mV/s}$, starting from the electrode OCP. For the CV, the last scan of 4 was taken as the stabilised CV response and was the scan reported.

Non-turnover CV at different scan rates were recorded for some of the half-cells in the absence of O_2 . Firstly, O_2 was removed from the half-cells by sparging with N_2 and polarising the WE at the normal half-cell operating poised-potential for one hour and until the reduction current was $> -100 \mu\text{A}$, before applying an N_2 blanket on the solution surface, which was

then maintained throughout the experiment. CV were then recorded at different scan rates between 1 and 100 mV/s, with two CV per scan rate and the second scan taken as the stabilised CV response and reported. The peak heights were then extracted from the CV.

CV in the presence of azide were carried out at the end of the operational period for some of the half-cells. This was achieved by adding 1 ml/L of a 2% NaN₃ stock solution to the electrolyte with stirring for 1 minute using a magnetic stirrer bar, before taking the CV. The CV were recorded in the same way as described above.

In order to detect diffusive redox active species, electrolyte samples and electrode bore samples were taken from some of the reactors at the end of their operational periods. Bore samples were prepared by grinding a piece of the carbon felt electrode with a stainless steel rod in 1 ml of 1M phosphate buffer before shaking for 15 minutes. Electrolyte and bore samples were filtered using 0.2 micron polyethersulfone (PES) membrane filters to remove bacteria, and used as the electrolyte in a special 1 ml volume half-cell designed for use with screen-printed electrodes (half-cell designed by Dr Eileen Yu, Newcastle University, UK). The screen printed electrodes have a carbon WE with a 4 mm diameter. 1 ml liquid samples were tested by CV using a screen-printed carbon electrode (DRP-110, DropSens, UK), using the same parameters as for CV in the aerobic biocathode half-cell.

3.5.4 Calculation of coulombic efficiency

For select aerobic biocathodes, the number of electrons transferred from the electrode to the TEA for the bacteria (O₂), or coulombic efficiency, was calculated and termed $C_E(O_2)$ (%). $C_E(O_2)$ was calculated at different points during the operational period for the half-cell by determining the charge passed and O₂ consumed during a small interval of operation using an external half-cell. The WE from the half-cell was transferred to the experimental setup depicted in Figure 3.5, and the WE polarised using a potentiostat (Autolab PGSTAT302, Metrohm, UK) at the half-cell operating poised-potential over a set time period of 7 hours. The current was measured continuously over the time period, whilst the DO was measured at the beginning and end of the experiment using a DO probe inserted into the WE chamber of the half-cell. The WE chamber was sealed during the experiment and the rate of O₂ mass transfer to the electrode was kept constant by stirring continuously at a fixed rate using a magnetic stirrer bar. From these measurements, $C_E(O_2)$ (%) was calculated using the following equation;

$$C_E(O_2) = \frac{M_s \int_0^t I dt}{F b_{es} \nu_{Cat} \Delta C} \quad (3.16)$$

Where M_s is the molecular mass of oxygen (16 g/mol), $\int_0^t I dt$ is the integrated current over the set interval (t = 0-7 hours), F is the Faraday constant, b_{es} and is the number of electrons transferred to the TEA (4 for bacterial ORR), ν_{Cat} is the volume of the WE chamber (285 ml), and $\Delta c = c_t - c_0$ is the change in DO concentration over the time interval (t = 0-7 hours).

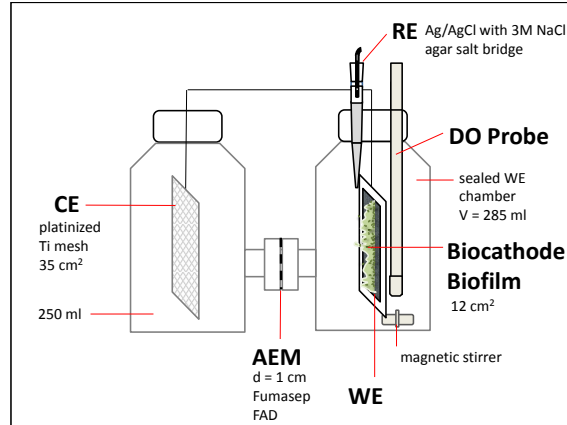


Figure 3.5: Experimental setup for determining $C_E(O_2)$. The WE with biocathode is sealed into the right hand chamber with the DO probe and RE, and separated from the CNE with a membrane.

3.5.5 Oxygen mass transfer experiment

To better understand the effect of O_2 mass transport on the aerobic biocathode biofilm, the current and DO were measured simultaneously over a small period of operation for a select half-cell, whilst changing the air flow rate of the attached air pump. During this experiment, the WE was polarised using a quad potentiostat (Whistonbrook Technologies, UK) at the operating poised-potential potential for the half-cell (-0.1 V), and the current measured continuously at 1 minute intervals with data logging software. Simultaneously, the flow rate of a pump attached to the half-cell was changed every 30 minutes from 0 to 1.4 LPM in 0.2 LPM intervals using an air flow meter, and the electrolyte DO concentration was measured using a DO probe inserted into the half-cell electrolyte.

3.5.6 Microbiological characterisation

Protein determination, community analysis and biofilm imaging were carried out on the WEs of select half-cells at the end of their operating periods using the procedures outlined in Section 3.2.

3.6 Membrane Characterisation for Microbial Fuel Cells

3.6.1 Overview

Three membranes of different types, a cation exchange membrane (CEM), an anion exchange membrane (AEM) and a batter separator (BS), were characterised abiotically to determine their principal ionic charge carriers, their ohmic resistances, and their diffusion coefficients for O₂ and acetate. This was carried out using the setups described in Figure 3.6. Comparison between the setups shows that they were not identical to each other, but these were different experimental tests requiring different methodology to measure different membrane properties. Air sparging, which affects the mass transfer of acetate, was not included in the membrane experiment examining acetate diffusion (c), as this would have promoted growth of aerobic bacteria consuming acetate. The CEM was Nafion-117 (Sigma, UK), the AEM was Fumasep FAD (Fumatech, Germany), and the BS was RhinoHide (Entek, UK). Hydrated membrane thicknesses were determined using a digital vernier caliper (RS, UK).

3.6.2 Determination of membrane principal charge carriers

The 2-electrode cell setup depicted in Figure 3.6a was used to analyse the three different membranes in terms of principal charge carriers. A fixed 2 mA current was passed between the two Pt electrodes using galvanostatic polarisation over a 92.00 hour period for the first run, and a 76.15 hour period for the second run. This allowed a precise charge of 662 and 548 C to be passed over the respective time intervals. Additionally, in the first run, a membrane diameter of 1 cm was used, whilst in the second run, a membrane diameter of 4 cm was used. Therefore, the second run was the same as the first but for an increased time interval and membrane area, and represented an improvement in cell design and procedure. The electrolyte was the same in both chambers and contained 1 g/L of sodium acetate, 50 mM pH 7.0 phosphate buffer, and nutrients (see Subsection 3.5.1 for nutrients). The electrolyte composition used for this experiment is given in Table 3.1. The concentration of all ions with a significant concentration in the electrolyte (> 5 mM) was determined in the starting electrolyte and in each chamber at the end of the time interval using the analytical methods described in section 3.3.5 (ICS dilution factor = 80, ICP dilution factor = 200), and the pHs were also measured. Electrolyte samples were filtered and stored at -4 °C before analysis.

From the ionic concentration data, a concentration change for an individual ion, Δc_{ion} , was calculated for both WE and CNE chambers at the end of the time interval. From Δc_{ion} , the change in charge attributed to the movement across the membrane of an individual ion,

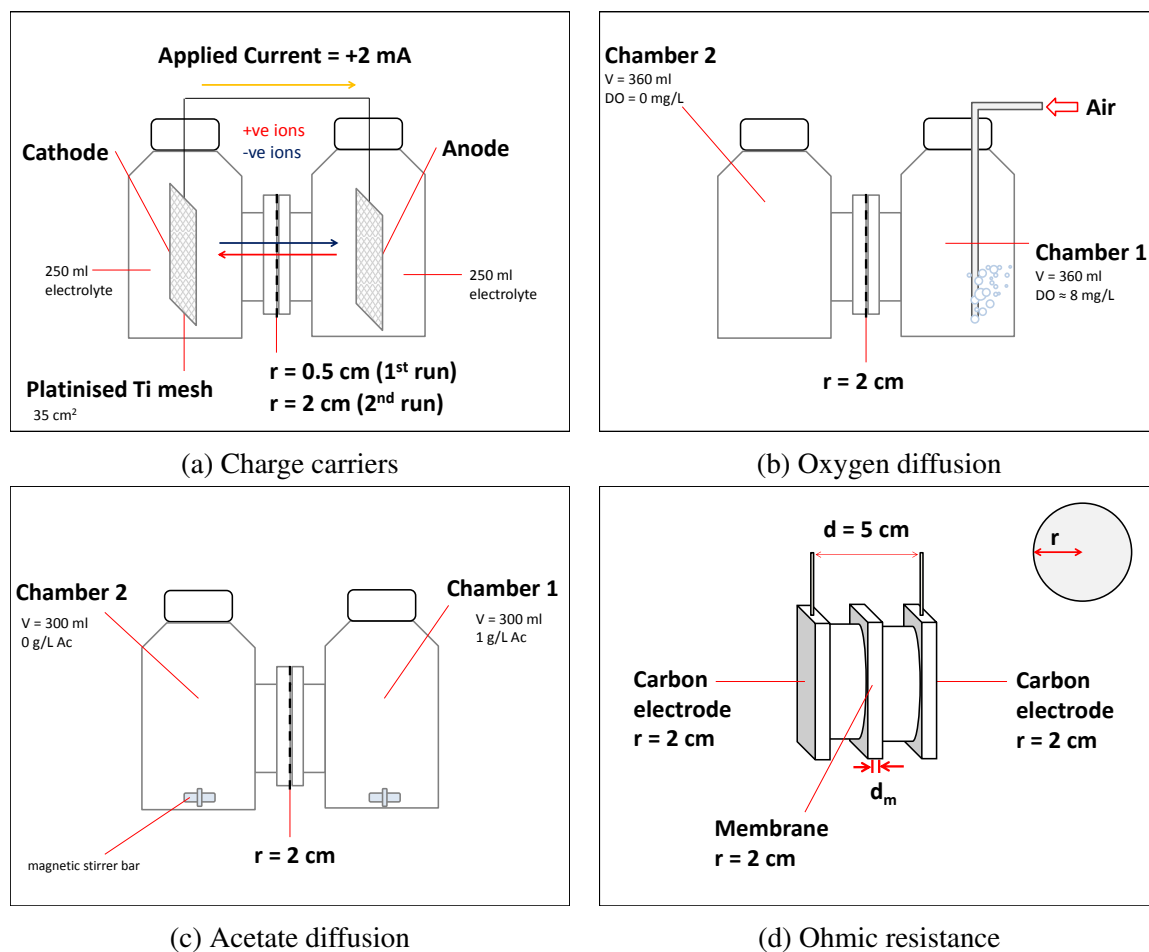


Figure 3.6: Setup diagrams for membrane experiments

Ion	[Ion]/mM
Cl^-	5.37
HPO_4^{2-}	28.84
H_2PO_4^-	21.15
SO_4^{2-}	0.41
K^+	78.83
NH_4^+	5.23
Mg^{2+}	0.41
Ca^{2+}	0.04
Ac^-	12.19
Na^+	12.19
pH	7.00

Table 3.1: Composition of electrolyte consisting of 50 mM pH 7.0 phosphate buffer, 1 g/L of sodium acetate, and nutrients (nutrients are described in Subsection 3.5.1). Ions with a lower concentration than 0.04 mM are not included. Ac^- is the acetate anion.

$Q_{ion}(\%)$, was calculated as a percentage of the overall charge passed, Q_{tot} , using the following equation;

$$Q_{ion}(\%) = \frac{\Delta c_{ion} z_{ion}}{Q_{tot}} \times 100 \quad (3.17)$$

Where z_{ion} is the charge for an individual ion. Two values of $Q_{ion}(\%)$ for the phosphate anion were calculated, giving an interval, as phosphate can adopt either the HPO_4^{2-} or H_2PO_4^- forms when passing through the membrane (between pH 5 to 9), which have 2- and 1- charges respectively. Phosphate is only present as PO_4^{3-} above pH 10, so calculations were not carried out based on $z_{ion} = 3-$.

3.6.3 Determination of membrane diffusion coefficients for acetate and oxygen

Oxygen diffusion coefficients for the different membranes were determined experimentally using the H-cell setup described in Figure 3.6b. The oxygen diffusion coefficient for a given membrane can be calculated by first considering Fick's first law of diffusion, which relates the flux of a chemical species to the concentration gradient;

$$J = -D \frac{dc}{dx} \quad (3.18)$$

Where J is the diffusion flux ($\text{kg s}^{-1} \text{m}^{-2}$), c is the concentration (kg m^{-3}), x is the distance (m) and D is the diffusion coefficient ($\text{m}^2 \text{s}^{-1}$). Equation 3.18 can be rewritten for the case of a membrane separating two chambers with equal volume (chambers 1 and 2), as depicted in Figure 3.6b;

$$J = -D_{O_2} \frac{c_1 - c_2}{L} \quad (3.19)$$

Where D_{O_2} is the diffusion coefficient for O_2 and L is the membrane thickness. The diffusion flux from chamber 1 to 2 is the change in mass, m , in chamber 2 with time per unit area, and can also be written as;

$$\begin{aligned} J &= -\frac{dm_2}{dt} \frac{1}{A} \\ J &= -V \frac{dc_2}{dt} \frac{1}{A} \end{aligned} \quad (3.20)$$

Where A is the membrane area and V is the chamber volume. Equations 3.19 and 3.20 can be equated, and c_1 substituted for $c_{1,0}$, the initial DO concentration in chamber 1, as the DO in chamber 1 is kept constant throughout the experiment through continual air sparging. The resultant expression is solved to give D_{O_2} for the membrane [196];

$$V \frac{dc_2}{dt} \frac{1}{A} = D_{O_2} \frac{c_{1,0} - c_2}{L} \quad (3.21)$$

$$D_{O_2} dt = \frac{VL}{A} \frac{1}{c_{1,0} - c_2} dc_2$$

$$D_{O_2} \times t = \frac{VL}{A} \times -\ln [c_{1,0} - c_2]_{c_{2,0}}^{c_{2,t}}$$

$$D_{O_2} = -\frac{VL}{At} (\ln(c_{1,0} - c_{2,t}) - \ln(c_{1,0} - c_{2,0}))$$

$$D_{O_2} = -\frac{VL}{At} \ln \left[\frac{c_{1,0} - c_{2,t}}{c_{1,0} - c_{2,0}} \right] \quad (3.22)$$

Where $c_{2,0}$ and $c_{2,t}$ are the initial and final concentrations of O_2 in chamber 2 respectively. Experimentally, chamber 2 was deaerated with N_2 , the DO measured, then sealed for 3 days before measuring the DO again. Chamber 1 was sparged continuously from an aeration pump to maintain a constant DO concentration, and the DO in chamber 1 was measured at the beginning and end of the run to check that it had not varied. Two runs were recorded for all 3 membranes. DI water with 1 ml/L of a 2% NaN_3 stock solution added was used in both chambers.

Acetate diffusion coefficients for the different membranes were determined experimentally using the H-cell setup described in Figure 3.6c. A similar equation to Equation 3.21 can also be written for the case of acetate diffusion through a membrane;

$$V \frac{dc_2}{dt} \frac{1}{A} = D_{Ac} \frac{c_1 - c_2}{L} \quad (3.23)$$

Where D_{Ac} is the diffusion coefficient for acetate. In the case of acetate, $c_1 = c_{1,0} - c_2$, as the system is closed and the mass of acetate in the system is therefore conserved. This expression can be substituted into Equation 3.23, and the resultant expression solved to give D_{Ac} [196];

$$V \frac{dc_2}{dt} \frac{1}{A} = D_{Ac} \frac{c_{1,0} - 2c_2}{L} \quad (3.24)$$

$$D_{Ac} dt = \frac{VL}{A} \frac{1}{c_{1,0} - 2c_2} dc_2$$

$$D_{Ac} \times t = \frac{VL}{A} \times -\frac{1}{2} \ln [c_{1,0} - 2c_2]_{c_{2,0}}^{c_{2,t}}$$

$$D_{Ac} = -\frac{VL}{2At} (\ln(c_{1,0} - 2c_{2,t}) - \ln(c_{1,0} - 2c_{2,0}))$$

$$D_{Ac} = -\frac{VL}{2At} \ln \left[\frac{c_{1,0} - c_{2,t}}{c_{1,0} - 2c_{2,0}} \right] \quad (3.25)$$

As the initial concentration of acetate in chamber 2 ($c_{2,0}$) is zero, Equation 3.25 can be rewritten;

$$D_{Ac} = -\frac{VL}{2At} \ln \left[\frac{c_{1,0} - c_{2,t}}{c_{1,0}} \right] \quad (3.26)$$

Experimentally, chamber 1 was filled with deionised water containing 1 g/L of sodium acetate and 1 ml/L of a 2% NaN_3 stock solution, and chamber 2 was filled with deionised water and 1 ml/L of a 2% NaN_3 stock solution. The azide stock solution was used to suppress potential bacterial growth. By taking samples and measuring the acetate concentration in each chamber at the beginning and at the end of the run, D_{Ac} was calculated for each of the 3 membranes. A second run was performed for the BS with additional samples taken at 1 and 2 days to check that there was no variation of D_{Ac} with time, and to act as a repeat for run 1 for the BS. The solutions in both chamber were stirred with magnetic stirrer bars.

Mass transfer coefficients, k , were calculated for the different membranes from diffusion coefficients using the following equation [196];

$$k = \frac{D}{L} \quad (3.27)$$

3.6.4 Determination of membrane ohmic resistance

Membrane resistances, area resistances, resistivities and conductivities were determined using the cell setup depicted in Figure 3.6d, using anode media as the electrolyte (50 mM pH 7.0 phosphate buffer, with 1g/L of sodium acetate and nutrients). The cell was made out of perspex and used two carbon cloth electrodes connected to Ti wires, with the membrane inbetween. The electrodes and membrane were of equal area. Experimentally, the ohmic

resistance of the cell was measured by EIS at the cell OCP, with and without a membrane, and the corresponding resistivities calculated [249];

$$\rho = R \frac{A}{d} \quad (3.28)$$

Where ρ is the resistivity of the cell, A is the cross-sectional area of the cell, and d is the electrode spacing. The membrane area resistance, $R_m(\text{area})$, is then given by [249];

$$R_m(\text{area}) = \rho_{m,s}(d_m + d) - \rho_s d \quad (3.29)$$

Where $\rho_{s,m}$ and ρ_s are the resistances with and without the membrane, and d_m is the membrane thickness. The membrane resistance, R_m , resistivity, ρ_m and conductivity, κ_m , were calculated using the following equations [250];

$$R_m(\text{area}) = R_m A_m \quad (3.30)$$

$$\rho_m = R_m \frac{A_m}{d_m} \quad (3.31)$$

$$\kappa_m = \frac{1}{\rho_m} \quad (3.32)$$

Where A_m is the membrane cross-sectional area.

3.7 Setup, Operation and Characterisation of Microbial Fuel Cells

3.7.1 Setup and operation

MFC configurations used in this thesis are given in Figure 3.7, and a general setup with parameters common to all of the MFC configurations is presented in Figure 3.7a. The MFC configurations given in Figures 3.7b and 3.7c were used to study the effect of light on MFC performance, the MFC configuration given in Figure 3.7d was used to study the effect of external resistance on the performance of MFCs with an aerobic biocathode, whilst the MFC configuration given in Figure 3.7e was used to study the effect of membrane-type on MFCs with an aerobic biocathode.

All MFC configurations were based on a basic H-cell configuration. This is not, however, the most optimised cell architecture, as it is well-known to suffer from high internal resistance

[22], which limits overall cell performance. This is principally due to a large anode-cathode electrode spacing and small membrane area. A much more optimised cell geometry would have a small anode-cathode electrode spacing, and a membrane of equal area to the anode and cathode. The reason why it was chosen in this thesis was that the focus of much of the work was on the development of an optimised aerobic biocathode in isolation from the rest of the MFC, and therefore there was not enough time toward the end of the thesis to develop a fully optimised MFC system. Because of this, the H-cell architecture was chosen, being both simple to use, easy to construct, and already available. For the same reasons, the MFC system was operated as a batch and not a flow system, as the batch system is less time-consuming and technically demanding to setup and operate. However, it is recognised that a flow system is preferable to a batch system, given that it more accurately approximates the running conditions in a real wastewater treatment plant, for instance. Any MFC system would be continuously supplied with substrate at the anode, in order for power generation to be continuous.

For all MFCs in this thesis, the anode medium contained 1 g/L of sodium acetate, 50 mM pH 7.0 phosphate buffer, and nutrients (see Subsection 3.5.1 for nutrients). The MFC configurations given in Figures 3.7b and 3.7c used 50 mM pH 7.0 phosphate buffer with nutrients as the catholyte, whilst the MFC configurations given in Figures 3.7d and 3.7e used 50 mM pH 5.8 phosphate buffer with nutrients (see Subsection 3.5.1 for nutrients).

To study the effect of light on MFC performance, the MFC configurations given in Figures 3.7b and 3.7c were used. The first was used to study the effect of light on already operational MFCs, whilst the second cell design was used to study the effect of light from the point of inoculation. The MFC configuration given in Figure 3.7b had a 1 cm diameter AEM separating the anode and cathode chambers (Fumasep FTAM-A, Fumatech, Germany). The anode chamber had a total volume of 300 ml and contained the anode electrode, which was a 1 cm thick rectangular 2.5 by 4.0 cm piece of carbon felt with an area of 33 cm². This anode electrode was connected to the external circuit by a 316 stainless steel rod current collector, which was sealed into the top of the cell using a rubber bung. Additionally, a port was made through the top of the anode chamber for sampling and sealed with a rubber bung. The cathode chamber had a total volume of 250 ml and contained the cathode electrode, which was a 2.5 by 7.0 cm (35 cm²) piece of platinised titanium mesh (acid washed prior to use) connected to a stainless steel wire current collector fed through a rubber bung at the top of the cathode chamber. The cathode chamber had a gas inlet port and a gas outlet port. A silicone tube connected to a plastic gas sparger was fed through the gas inlet port into the chamber to provide aeration to the cathode electrode. The anode and cathode electrodes were connected using crocodile clips and a 1 k Ω external resistance.

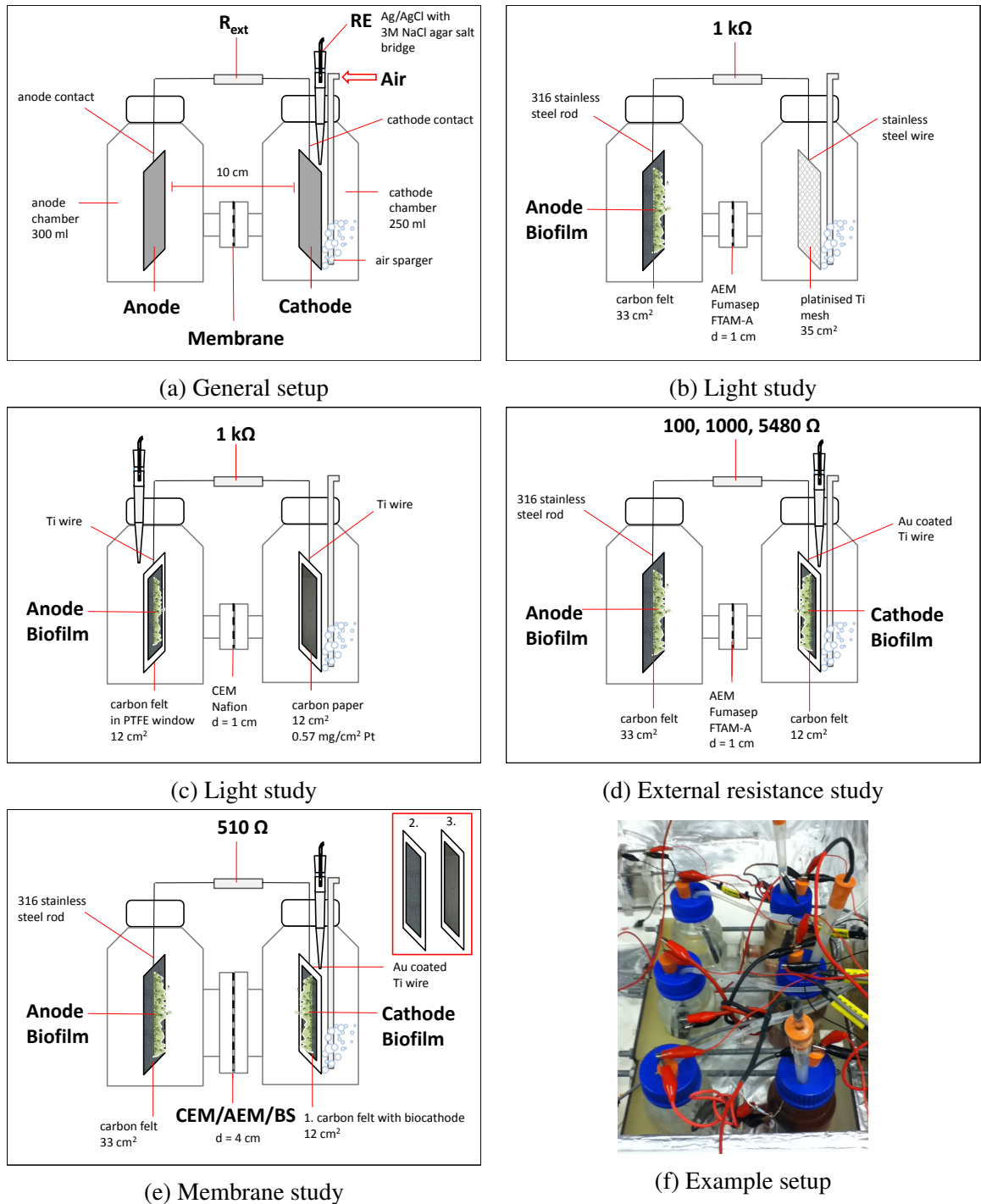


Figure 3.7: MFC setups used in this thesis. A general setup is given in (a) with setup details common to all of the studies. Setups (b) and (c) were used to study the effect of light on MFC performance. Setup (d) was used to study the effect of external resistance. Setup (e) was used to study the effect of membrane-type on MFC performance. Additionally setup (e) was also used to study the effect of O_2 mass transport on MFC performance with a biocathode, and to compare MFC performance using; a carbon felt electrode with a biocathode (1.), a plain carbon felt electrode with no biocathode (2.), and a carbon paper cathode with a Pt loading of 0.57 mg/cm^2 (3.).

The MFC configuration given in Figure 3.7c was also used to further study the effect of light on MFC performance. This was essentially the same H-cell configuration as described above in Figure 3.7b, apart from a few differences with the membrane, anode electrode and cathode electrode; The membrane separating the anode and cathode was a 1 cm diameter CEM (Nafion-117, Sigma-Aldrich, UK), the anode electrode was carbon felt with an area of 12.16 cm² held in a PTFE cassette with a Ti wire current collector, and the cathode electrode was constructed from a 12.16 cm² carbon paper Gas Diffusion Layer (GDL) (Freudenberg Fuel Cell Component Technologies, H2315 I2 C6) with a Pt loading of 0.57 mg/cm² held in a PTFE cassette with a Ti wire current collector. Additionally, the anode chamber was fitted with an RE through a hole in the top of the anode chamber which also doubled as the sampling port. The Pt carbon paper cathode electrode was prepared using the following method; A Pt ink was prepared by ultrasonically 5 zirconium balls with 2-3ml of EtOH, 108.58uL of Nafion solution (10% by weight of binder) and 50 mg of Pt-KJB for 30 minutes in an ice bath, then the homogeneous ink was applied by brushing evenly on the surface of the carbon paper. The Pt carbon paper electrodes had an area of 12.16 cm², and were held in PTFE cassettes, with a titanium wire as the current collector. The anode and cathode were connected with a 1 k Ω external resistance.

The MFC configurations given in Figures 3.7b and 3.7c which were used to study the effect of light, were an evolution of a basic cell architecture and were the first experiments in this thesis. Differences between these cell designs, which were the use or otherwise of a PTFE window at the anode, the use of either a platinised Ti mesh or Pt deposited on carbon at the cathode, and the use of either a CEM or AEM as the membrane separator, were the result of development in cell design over time. The differences were not thought to effect the outcome of the experiments, which were focused on light exposure of the bioanode, but the cell designs were not repeats of one another in the strictest sense. Findings from the experiments using these cell designs were compared.

The MFC configuration given in Figure 3.7d was used to study the effect of external resistance of MFCs with an aerobic biocathode. The bioanodes were pre-enriched on carbon felt from the previous MFC light study, whilst the aerobic biocathodes were pre-enriched on carbon felt at a poised potential of -0.1 V using aerobic biocathode half-cells. The membrane was an AEM with d = 1 cm (Fumasep FTAM-A, Fumatech, Germany), and an RE was inserted into the cathode chamber in order to continuously measure the cathode potential. The values chosen for the investigation on external resistance were 100, 1000 and 5480 Ω . These values were chosen so as to have a broad range of resistance values, typical of external resistance studies in the literature (REFs). In particular, low and high external resistance values were important, in order to cover the extreme cases. In the literature, most studies have had their lowest values in the region between 10-100 Ω and their highest between 5000-10000 Ω , and

the lowest and highest values used in this study fall within these intervals.

For assessing oxygen mass transport and comparing biocathode performance with a Pt carbon paper cathode and a plain carbon electrode, the MFC configuration given in Figure 3.7e was used. The Pt carbon paper electrode had a loading of 0.57 mg/cm^2 , whilst the plain carbon electrode was a piece of carbon felt which had not been enriched for an aerobic biocathode. For the Pt carbon paper electrode, a Pt loading of 0.57 mg/cm^2 was used as this was in the range between 0.5 and 1.0 mg/cm^2 , which are Pt loadings commonly used in the literature for MFCs.

The MFC configuration given in Figure 3.7e was used to study the effect of membrane-type on the performance of MFCs with an aerobic biocathode. The bioanodes and aerobic biocathodes were pre-enriched from the previous MFC external resistance study. The MFC configuration was identical to that used previously, but near the beginning of the experimental period, the AEM used in all three cells with $d = 1 \text{ cm}$ (Fumasep FAD, Fumatech, Germany) was replaced for a fresh AEM with an increased diameter of 4 cm . The membrane replacement corresponded to a 16-fold increase in membrane area for this study. When the $d = 4 \text{ cm}$ membranes were replaced as part of the study, the membranes were a CEM (Nafion-117, Sigma-Aldrich, UK), an AEM (Fumasep FAD, Fumatech, Germany), and a BS (RhinoHide, Entek, UK).

3.7.2 Electrochemical characterisation

For the different studies, CV/LSV were recorded for the different anode and cathode electrodes using a potentiostat (Autolab, PGSTAT302, Metrohm, UK) and a 3-electrode setup with a CNE and RE. For the MFC configurations in Figures 3.7b and 3.7c, anode CV/LSV were recorded insitu using the chemical cathode as the counter electrode, whilst cathode LSV were recorded at the end of the study by removing the cathodes to an identical H-cell and using a piece of platinised mesh as the CNE (35 cm^2). For the MFC configurations in Figures 3.7d and 3.7e, bioanode CV/LSV were recorded insitu by replacing the biocathode with a piece of platinised mesh, and using this as the CNE. Biocathode LSV/CV for these configurations were recorded by removing the biocathodes to an identical H-cell and using a piece of platinised mesh as the CNE. LSV curves for bioanodes were recorded by sweeping the WE potential from -0.8 to $+0.1 \text{ V}$ at $\nu = 1 \text{ mV/s}$, whilst LSV for biocathodes and chemical cathodes were recorded in the same way, but this time the potential was swept from $+0.5$ to -0.2 V .

MFC Polarisation curves and EIS spectra were recorded for the MFCs as described in Section 3.1.5. For the MFC configurations given in Figures 3.7b and 3.7c, anode and cathode poten-

tials were not recorded during the polarisation curves. For the MFC configurations given in 3.7d and 3.7e, anode and cathode potentials were recorded during the polarisation curves, and EIS spectra were taken directly afterwards.

3.7.3 Calculation of coulombic efficiency

The coulombic efficiency, C_E , for an acetate-fed batch MFC is the fraction of electrons in the acetate substrate which are transferred to the anode electrode and used in electricity generation. C_E can be calculated using the following equation [22];

$$C_E = \frac{M_s \int_0^t I dt}{F b_{es} \nu_{An} \Delta c} \quad (3.33)$$

Where C_E is the coulombic efficiency (%), M_s is the mass of the anode substrate (82.03 g/mol for anhydrous sodium acetate), $\int_0^t I dt$ is the integrated current over the batch cycle, F is the Faraday constant, b_{es} is the number of electrons (8 for complete oxidation of acetate), ν_{An} is the volume of the anode chamber (300 ml for the H-cell MFCs of Figure 3.7), and $\Delta c = c_t - c_0$ is the change in acetate concentration from the beginning of the batch cycle.

3.7.4 Membrane characterisation

Assessment of principal charge carriers for the MFC systems was carried out for a single batch cycle using the same experimental methodology as described in Section 3.6.2. This time, the charge passed in the system was calculated from the integral of the current over time from the measured MFC cell voltage.

Chapter 4. A Novel 4-Electrode Method for the Electrochemical Investigation of Porous Carbon Felt Material as a Biocathode Support

4.1 Introduction

Rotating ring Disk Electrode (RRDE) experiments are ideal for the assessment of carbon powders and carbon-supported catalysts that can be made into inks and immobilised onto glassy carbon disk electrodes, but this experiment cannot be used to characterise porous carbon felts, brushes or cloths, which may have unique surface chemistry. These unique surface properties arise because of the different ways in which porous carbon materials are manufactured. For example, porous carbon felt, which can be manufactured by carbonising viscose rayon or polyacrylonitrile (PAN) felts, is likely to have a different surface chemistry to a graphite plate. Given the different potential-dependent n_{e^-} numbers for different carbon powders and carbon-supported catalysts, it is unsurprising that it can be difficult to predict at which potential on a given porous carbon electrode H_2O_2 is generated. This information is important for determining the minimum potential at which it is possible to cultivate aerobic biocathode biofilms in poised-potential half-cells.

Therefore, a novel 4-electrode method was developed to detect the peroxide produced from porous carbon felt. It is entirely novel and is reported here for the first time. In this system, the carbon felt electrode, or primary working electrode (PWE), was polarised in the presence of a Pt secondary sensing electrode (SSE), which was itself polarised at a potential at which H_2O_2 is oxidised. This allowed for the determination of the potential at which peroxide is first produced in sufficient quantities so as to cause an oxidation current at the SSE. A detectable current at the SSE indicates the presence of peroxide in solution, which is assumed to inhibit biofilm growth and development. In order to validate the experimental method, comparison of two different carbon felts with different surface chemistry was carried out. Untreated carbon felt was compared with the same carbon felt which had undergone treatment with nitric acid, HNO_3 , in order to alter its surface chemistry. HNO_3 treatment has been shown

to enhance the ORR catalysis performance of carbon materials [251], and was predicted to increase the potential at which peroxide is initially formed on the carbon felt.

Only one porous carbon material, carbon felt, was investigated in this study. This was due to the fact that the novel 4-electrode method employed here for the first time was developed from first principals. Therefore, a considerable amount of time was spent in method development. However, in principal, this method should also be applicable to the study of other porous carbon materials in the future.

4.2 Experimental

A 4-electrode setup was used to determine the minimum applied potential for formation of peroxide on a HNO_3 -treated carbon felt and untreated carbon felt. Details of both the method for HNO_3 surface treatment and the 4-electrode setup can be found in materials and methods. Briefly, the 4-electrode setup used porous carbon felt as the primary working electrode (PWE) and a Pt secondary sensing electrode (SSE), as described in materials and methods. The PWE and SSE were separated by a 1 cm gap and were connected as working electrode one and two respectively of a potentiostat (Autolab PGSTAT302, Metrohm, UK) fitted with a bipotentiostat module. In this mode of operation, the potentiostat fixes the potentials of the working electrodes separately, and allows them to share the same CNE and RE. Experiments were performed using the following PWE potentials;

1. -1, -0.5, -0.1, -0.05, 0, +0.05 V for HNO_3 -treated carbon felt
2. -1, -0.5, -0.2, -0.1 V for untreated carbon felt

These potentials covered a significant range of potentials, and were investigated so as to bracket the point at which peroxide was detected on the SSE in order to save time. This was because each individual experiment (potential) took 150 minutes to investigate in total with duplication. However, given more time, a more systematic range of potentials using small set intervals would have been preferable.

In all of the experiments, the SSE potential was fixed at +0.6 V, a potential in the mass transport region for oxidation of peroxide on platinum electrodes [252], and therefore a potential at which maximal current from peroxide oxidation is produced given any specific concentration of peroxide. As the redox potential of the SSE is fixed, any oxidation current is almost certainly due to peroxide oxidation, as no other chemical species are known to be produced in a system containing only carbon and phosphate species. However, a positive control in which peroxide is added to the system externally from a chemical source would have been useful in assessing the effectiveness of the sensor and unequivocally confirming the process.

Given more time, this important control would have been included in order to calibrate the sensor, and certainly should be included as part of future sensor development.

4.3 Results and Discussion

4.3.1 Potentials for the formation of peroxide on HNO_3 -treated and untreated carbon felts

In the CA experiments, the SSE was polarised at +0.6 V for 15 minutes, before simultaneous polarisation of both the PWE and the SSE, with the PWE polarised at different potentials depending on the experiment. The CA curves for the SSE and PWE for HNO_3 -treated carbon felt and untreated carbon felt are given in Figures 4.1 and 4.2. Initial polarisation of the SSE produced a rapidly decaying capacitive current, tending towards a low background oxidation current. An increase in this oxidation current was then observed for the SSE when the PWE was also polarised, due to the oxidation of peroxide, that either increased then plateaued over the hour-long simultaneous WE polarisations, or increased then peaked, before decreasing, depending on the potential of the PWE. Therefore, the SSE acted as a sensor for the detection of peroxide in solution, given off by the PWE.

In the current-time profile of the PWE for both materials, seen in Figures 4.1a and 4.2a, the reduction current initially decreases rapidly due to capacitive discharge, then plateaus to a limiting reduction current. At more negative potentials, the observed CA reduction current continues to decrease after the initial capacitive discharge for the entire experimental period. The H_2O_2 product is produced in solution, but its decomposition is catalysed by the carbon electrode [253], and spontaneously in solution [254, 255]. The following equation and 1st order rate equation are found for catalysis by carbon and for spontaneous decomposition [253–255];



$$-\frac{d[\text{H}_2\text{O}_2]}{dt} \rightleftharpoons k[\text{H}_2\text{O}_2] \quad (4.2)$$

Where $[\text{H}_2\text{O}_2]$ is the concentration of hydrogen peroxide, t is the time in seconds, and k is the 1st order rate constant for the decomposition of hydrogen peroxide. The implications of the 1st order rate equation are that the rate of removal of peroxide increases as the concentration of peroxide increases in solution. In the experiments, the amount of carbon (catalyst) for the decomposition of peroxide is constant, which means that the 1st order rate is also constant for the system. As peroxide is both simultaneously produced and removed in the system,

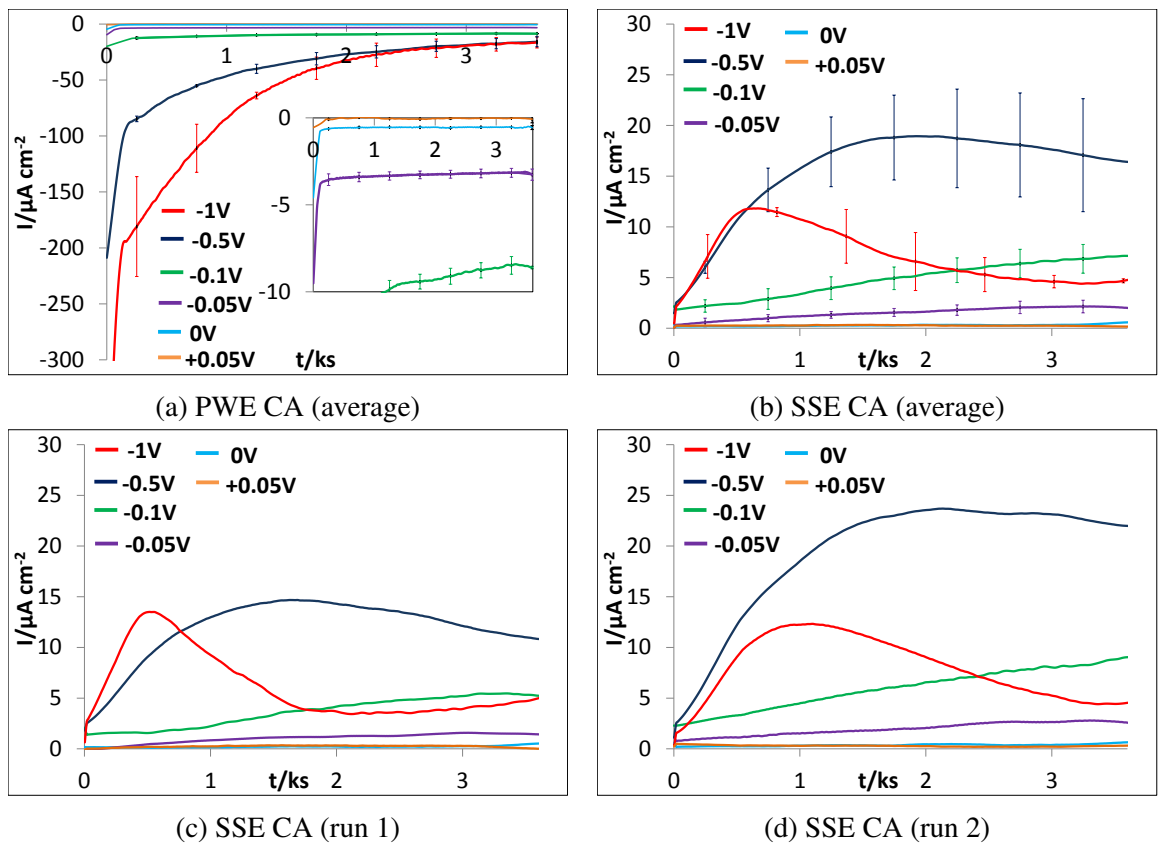


Figure 4.1: The average PWE and SSE current against time (two runs) for the HNO₃-treated carbon felt. The experiments were run for 1 hour, and the time-axis is in kilo seconds (ks). (a) and (b) show the average PWE and SSE currents against time, whilst (c) and (d) show the SSE currents against time for runs 1 and 2. Error bars are equal to the difference from the mean.

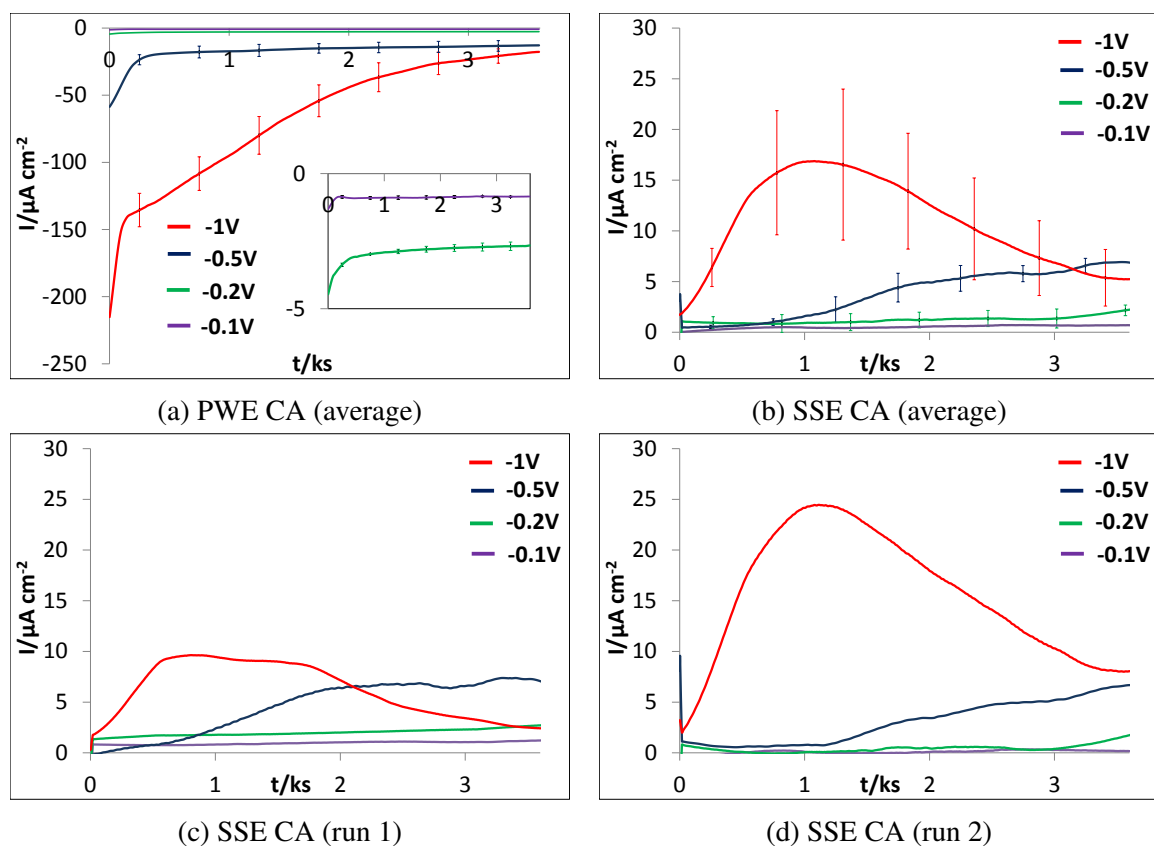


Figure 4.2: The average PWE and SSE current against time (two runs) for the untreated carbon felt. The experiments were run for 1 hour, and the time-axis is in kilo seconds (ks). (a) and (b) show the average PWE and SSE currents against time, whilst (c) and (d) show the SSE currents against time for runs 1 and 2. Error bars are equal to the difference from the mean.

the concentration of peroxide in solution plateaus and reaches a maximum value with time. The SSE is polarised at +0.6 V where the oxidation current due to peroxide oxidation is mass transport limited on platinum [252]. Therefore, at this potential for the SSE, the current observed at the SSE is proportional to the concentration of peroxide present in solution. The maximum oxidation current at which the SSE eventually plateaued at was dependent on the potential applied at the PWE; the more negative the potential, the higher the maximum oxidation current reached on the SSE. This behaviour was observed for all of the SSE CA experiments for both the HNO₃-treated and untreated carbon felts, apart from where the PWE was polarised at -0.5 and -1 V in the case of HNO₃-treated carbon felt, and -1 V for the untreated carbon felt. In these cases, the peak is caused by the falling rate of production of peroxide from the PWE as the experiment proceeds, combined with the decomposition of peroxide in solution.

From examination of the SSE data for both materials, it is possible to see at which potentials on the PWE that the oxidation current on the SSE increases above background levels. The potential of the PWE at which this first occurs is the potential at which peroxide is first formed at the electrode in sufficient quantity to be detected electrochemically. This point can be considered as the minimum potential for polarisation of the PWE for growth of an aerobic biocathode biofilm. The minimum potential, E_{min} , on the PWE at which an oxidation current is observed for the SSE above the background current for HNO₃-treated and untreated carbon felts is summarised in Table 4.1, along with the potentials used at the PWE for both materials.

Carbon felt	PWE potentials V vs. Ag/AgCl	E_{min} for an oxidation current at the SSE V vs. Ag/AgCl
HNO ₃ -treated	-1, -0.5, -0.1, -0.05, 0, +0.05	-0.05
untreated	-1, -0.5, -0.2, -0.1	-0.2

Table 4.1: Results summary for the 4-electrode electrochemical tests. The PWE potentials used and the minimum potential (E_{min}) at which an oxidation current is first detected at the SSE are listed for both the HNO₃-treated and untreated carbon felts.

An interesting comparison can be made between the two different porous electrode materials; the potential at which peroxide is first detected is -0.05 V for the HNO₃-treated carbon felt, and -0.2 V for the untreated carbon felt. On further examination of the SSE CA data for the two materials (Figures 4.1b and 4.2b for the average SSE current), the most negative potential on the PWE which yields no increase in SSE oxidation current is 0 V for the HNO₃-treated carbon felt, and -0.1 V for the untreated carbon felt. This is consistent with the improved catalysis and ORR onset potential on treatment of the carbon felt with HNO₃. Therefore, HNO₃ surface treatment enhances the abiotic catalysis of the carbon felt, but increases the

potential at which peroxide is first formed on the electrode.

Considering that the bacterial TEA is $4e^-$ ORR with an $E^{0'}$ equal to 0.60 V (pH 7.0, $pO_2 = 0.2$), the useable potential window over which growth of aerobic biocathodes using poised-potentials can be attempted is reduced on treatment of the carbon felt with HNO_3 . For HNO_3 -treated carbon felt, potentials between 0 and 0.60 V (600 mV potential window) can be applied to the carbon felt, whilst for untreated carbon felt, this potential window is from -0.1 to 0.60 V (700 mV potential window).

4.3.2 Mathematical model describing the solution peroxide concentration with time

A simple descriptive model of the current observed at the SSE was developed. Key to this model was the assumption that the current observed at the PWE was due entirely to the $2e^-$ ORR pathway, although this is not usually the case, as for most carbon materials, the average electron numbers, n_{e^-} , are both higher than 2.0, and potential-dependent. For example, Watson et. al obtained n_{e^-} values from RRDE experiments of approximately 2.3 for glassy carbon, and 2.5 for carbon black [46], which both varied to some degree with potential. With this assumption, the current at the PWE is approximated as equal to the number of mols of peroxide produced according to [232];

$$\text{Rate (mol/s)} = \frac{dN}{dt} = \frac{i}{nF} \quad (4.3)$$

Where i is the current, F is the Faraday constant, and $n = 2$ for $2e^-$ ORR. Therefore, the rate of production of peroxide in the system from the PWE at any point in time is known and is given the value r . This value varies with time, and is calculated directly from the PWE current and fed into the model. Additionally, the non-electrochemical decomposition of peroxide to O_2 and water catalysed at the PWE and occurring in the bulk solution is well-known to occur by 1st order kinetics [253–255]. By considering the rate of production at the PWE, r , which is known, and the rate of decomposition of peroxide, it is possible to write an equation for the concentration of peroxide in solution at time t ;

$$\text{Rate of production of peroxide at PWE} = r \quad (4.4)$$

$$\text{Rate of decomposition of peroxide} = k[H_2O_2] \quad (4.5)$$

$$\text{Net rate of production} = \frac{d[H_2O_2]}{dt} = r - k[H_2O_2] \quad (4.6)$$

$$[H_2O_2] = \frac{r}{k}(1 - e^{-kt}) \quad (4.7)$$

Where r is the rate of production of peroxide from the PWE which is known, k is the 1st order rate constant for the decomposition of peroxide, t is the time in seconds, and $[\text{H}_2\text{O}_2]$ is the concentration of peroxide in solution. The derivation of Equation 4.7 from Equation 4.6 is included in the Appendix (Equation A.1). Across all experiments, k is constant, but r is approximated as being proportional to the observed current at the PWE (Equation 4.3). Therefore, both r and t are variables which are introduced into Equation 4.7 in order to predict the peroxide concentration in solution with time. Values of k for HNO_3 -treated and untreated activated carbons were taken from the literature and were used for the HNO_3 -treated carbon felt and untreated carbon felt. These values were 0.007 and 0.019 min^{-1} respectively [253]. For the two carbon felt materials, modelling of $[\text{H}_2\text{O}_2]$ in solution with time yields the curves shown in Figure 4.3. It is observed that when the PWE is polarised at potentials more negative than -0.1 V , the current takes time to plateau, leading to a decreasing value of r , and therefore to a peak in the current observed at the SSE for both carbon felt materials. For the simulation, $[\text{H}_2\text{O}_2]_{\text{max}}$ is given by $\frac{r}{k}$, which is the point at which the SSE current plateaus.

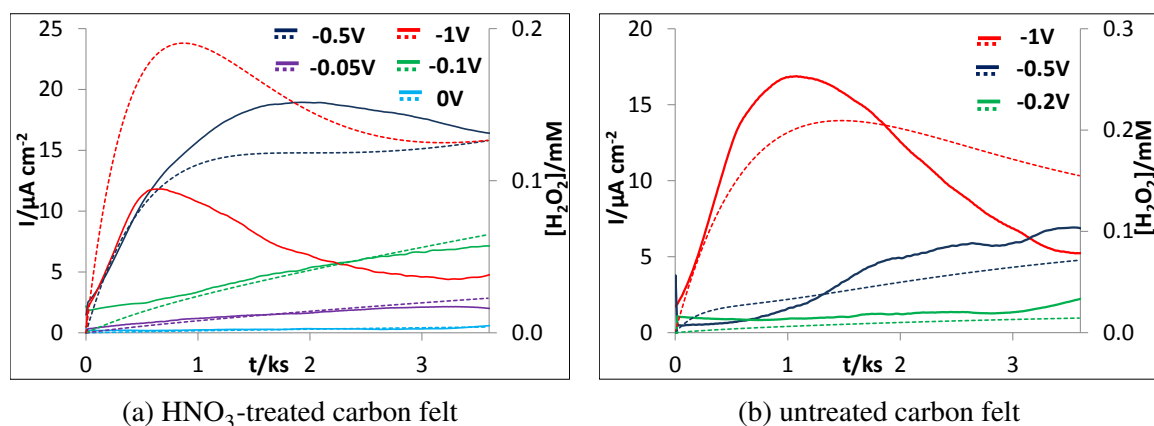
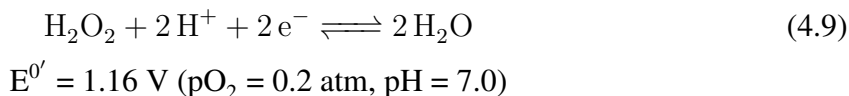


Figure 4.3: The SSE current (solid lines) and the modeled solution H_2O_2 concentration (dashed lines) against time for HNO_3 -treated carbon felt (a) and untreated carbon felt (b). On each graph, the left hand axis is the SSE current against time, whilst the right hand axis is the modeled H_2O_2 concentration against time. The curves are labeled according to the PWE potential.

For normal carbon felt, the modeled solution $[\text{H}_2\text{O}_2]$ and the SSE current agree reasonably well. However, a comparison of the current observed at the SSE for HNO_3 -treated carbon felt and the modeled solution $[\text{H}_2\text{O}_2]$ gives reasonable agreement apart from when the PWE is polarised at -0.5 and -1 V . At these potentials, the differences between the model and the experiment are likely due to competing processes at the PWE, such as the further reduction of peroxide to H_2O , the reduction of H^+ to H_2 , or potential-dependent changes in the ratio of $4e^-$ to $2e^-$ ORR pathways (given by the n_{e^-} number from RRDE experiments). For example, $4e^-$ reduction of O_2 to water might be increasingly favoured for the HNO_3 -treated carbon felt as the potential becomes more negative. The further reduction of peroxide to water and the re-

duction of H^+ to H_2 are processes which are described by the following equations [59];



Additionally, it is important to consider that detection at the SSE is affected by how fast H_2O_2 is transported from the PWE, and the timescale of this process in relation to H_2O_2 decomposition. A good fraction of the H_2O_2 molecules decompose before they reach the detector, which explains why the signal response at the SSE is lower than at the PWE. Detection for this experiment could be improved by improving H_2O_2 mass transport.

4.4 Conclusions

The results obtained from this experiment demonstrate the usefulness of this novel 4-electrode technique for assessing different porous carbon materials for the minimum potential at which they produce a detectable level of H_2O_2 . In this work, a minimum potential at which peroxide is produced by two different carbon felts in sufficient quantity to be detected electrochemically has been determined. This potential is hypothesised to be the minimum safe potential at which the aerobic biocathode community can be grown without the possibility of suffering from the adverse affects of peroxide formation on the carbon electrode support. Given that the potential of the TEA for the aerobic biocathode is 0.6 V (pH 7.0, $pO_2 = 0.2$ atm), a potential window over which the bacteria can be grown using a potentiostatically-poised carbon electrode is inferred. For the two carbon felt electrodes, these potential windows are;

1. 0 to +0.60 V for HNO_3 -treated carbon felt
2. -0.10 to +0.60 V for untreated carbon felt

Considering the findings from this work, the cultivation of aerobic biocathodes can be carried out at -0.1 V on untreated carbon felt, so as to maximise the energy level difference between the electrode and the bacterial TEA, and therefore the energy that is potentially available to

the bacteria for growth and metabolism.

The novel 4-electrode technique described here may also be of use for the characterisation of porous carbon materials for use as bioanode supports.

Chapter 5. Aerobic Biocathodes with a High Onset Potential for the Oxygen Reduction Reaction of +0.4 V vs. Ag/AgCl are Dominated by Unidentified Gammaproteobacteria

5.1 Introduction

In the literature, there is no common consensus as to which bacteria carry out ORR catalysis, how they do it, or even why they do it [72], and little is currently understood about the mechanisms of electron transfer in aerobic biocathodes in general [124]. The term electrotroph, where it has been used, denotes bacteria which gain energy for metabolism and growth by taking up electrons from the cathode¹. Given the benefits of aerobic biocathodes as completely free and sustainable ORR catalysts for MFCs, fundamental investigations into this important class of electroactive biofilm are required. In particular, the community composition of oxygen reducing biocathodes with an onset potential of +0.4 V has been determined only once, using a method of clone libraries built from a biofilm on the cathode of a sediment MFC [75]. The authors identified *Pseudomonas* species as the dominant bacteria in the community, but this study lacked a non-polarised control, and therefore the bacteria involved in ORR catalysis were not identified. Community analysis of these biofilms coupled with detailed electrochemical investigations are therefore key in attempts to identify how ORR catalysis is carried out and which bacteria are involved. Community analysis coupled with electrochemical investigation is an important combination given that aerobic biocathodes with different E_{ORR} are likely to involve different electroactive bacteria, and use different electron transfer mechanisms.

Poised-potential experiments on aerobic biocathodes with an E_{ORR} of +0.4 V have so far focused on modeling the response to varying applied potential and O_2 mass transfer condi-

¹The term electrotroph is used to describe the ability by bacteria to take up electrons from an insoluble cathode electrode and use these for metabolism and growth. The bacteria are, of course, evolved to uptake electrons from insoluble electron donors in the environment, possibly from minerals, or as part of a bio-corrosion process.

tions over short time periods [84, 85]. However, growth of aerobic biocathodes with an E_{ORR} of +0.4 V at different poised-potentials has not yet been investigated. In this long-term experiment, the cathode potential is changed, which is hypothesised to have an effect on the community composition, as well as selecting for different ET pathways. When the cathode potential is changed, the cathode bacteria may make use of different cytochromes for electron uptake, with different mid-point potentials. This could be a strategy to maximise their metabolic energy gain when using the electrode as their electron donor. Additionally, for any given ET pathway, the kinetics of the enzyme responsible for ET will change with the applied potential. This makes changing the poised-potential a powerful tool in investigating electron transfer mechanisms and bacterial communities in aerobic biocathode biofilms.

In the current work, the effect of applied potential on aerobic biocathode biofilms catalysing the ORR with an E_{ORR} of +0.4 V was studied using half-cells poised at -0.1 and +0.2 V. The electrochemical performance of these half-cells was then assessed to determine differences between applied potential, and as part of this performance assessment, half-cell response to changing O_2/pH conditions was also investigated. Next, a combination of turnover/non-turnover CV, and CV in the presence of azide were used in order to link features of the CV to physiological and mechanistic processes occurring at the electrode surface. Finally, the microbial communities of the aerobic biocathode biofilms at different applied potential were determined and the bacteria likely responsible for ORR catalysis identified. This study represents the first community analysis of aerobic biocathodes with a high onset potential for the ORR of +0.4 V vs Ag/AgCl.

5.2 Experimental

All aerobic biocathodes discussed in this chapter were grown in poised-potential half-cells and were setup and operated in exactly the same way. All half-cells used biocathode medium. Details of setup, operation and the biocathode medium used can be found in materials and methods. Briefly, the biocathode media was a minimal media containing pH 5.8 phosphate buffer at 50 mM buffer concentration. A pH of 5.8 was used in order to increase the reduction potential for O_2 , and therefore the bacterial energy gain from the electrode, whilst also maintaining the buffer capacity of the media. Additionally, the temperature of all half-cells was controlled at 30 °C. As described in materials and methods, the half-cells were operated in batch mode, with media changes at regular 1-2 week intervals to compensate for potential depletion of trace nutrients over time, indicated on the CA graphs for each half-cell. The half-cells were also topped up with deionised water to compensate for water loss through evaporation. The half-cells were operated as batch systems, although continuous flow systems would have been preferable in order to be closer to the how the real-world systems

would operate. This choice of batch operating condition was due to a need to simplify the system and save time, as continuous flow systems are more complicated and time-consuming to operate than batch systems.

The aerobic biocathode half-cells were classified according to three different operational parameters. These were the poised-potential used, the way the reactor was inoculated, and the operation time. The poised-potentials used were either -0.1 and +0.2 V, whilst the inoculum used was either 10% by volume of activated sludge in the case of a primary inoculum, or 100 % by volume of the effluent from an existing half-cell with an aerobic biocathode, in the case of a secondary inoculum. The activated sludge was obtained from Tudhoe wastewater treatment plant in the North East of England. Activated sludge was decided as the inoculum for the half-cells as it had previously been used successfully to generate aerobic biocathodes with an onset potential for ORR of +0.4 V [84, 85], and it is known to be a diverse source of bacteria [256]. It is important to note that the secondary inoculated half-cells did not use exactly the same inoculum each time (i.e. effluent from the same half-cell), unless indicated otherwise. This variable was very difficult to control for, as many of the reactors were not operated in parallel. Even when reactors are inoculated from wastewater, as is the case in much of the MFC literature, this wastewater will not have exactly the same composition each time. An ability to operate more reactors in parallel, and using homogenised inocula split equally across all reactors, would help in reducing these uncertainties, but this was not done for the majority of the half-cells in this study.

In this study, three different treatments were investigated using 3 duplicate² half-cells; primary inoculated half-cells at -0.1 V poised-potential (A and B), secondary inoculated half-cells at -0.1 V poised potential (E and F), and secondary inoculated half-cells at +0.2 V poised-potential (I and J). These 6 half-cells allowed a comparison between the inoculum at -0.1 V poised-potential, and between poised-potentials for secondary inoculum half-cells. Due to difficulties in inoculating successfully from activated sludge in order to get a biocathode biofilm, only one primary inoculated treatment was considered in this study (half-cells A and B). Additional secondary inoculated half-cells were setup in order to image the biocathode biofilm (half-cell C at -0.1 V), to investigate oxygen mass transfer to the biocathode biofilm (half-cell D at -0.1 V), to determine the biocathode coulombic efficiency through time (half-cells G and H at -0.1 V), and to assess the effect of peroxide formation on aerobic biocathode growth (half-cells K at -0.1 V and L at -0.2 V). With respect to the assessment of the effect of peroxide formation on aerobic biocathode growth, half-cells K and L were inoculated at the same time using the same effluent and operated for 20 days. In addition to

²*Triplication of the half-cells would have been preferable, but to have both triplication, and the depth of electrochemical analysis reported in this thesis, would not have been feasible, due to constraints in the time and resources required in setting up and operating multiple parallel potentiostat-poised reactors over long experimental periods.*

these half-cells, various control (CONT) half-cells were setup. These were;

1. Non-inoculated half-cell operated for 11 days at -0.1 V poised potential (CONT - no inoculum).
2. Non-inoculated half-cell operated for 4 days at -0.1 V poised potential using biocathode medium with x 10 the normal concentration of trace metals to control for potential metal reduction on carbon felt (CONT - x 10 [metals]).
3. Non-inoculated half-cell³ used to obtain CV of the nutrient solutions used to make the biocathode medium; macro nutrient, metals and vitamin solution at x500, x1000 and x1000 times their normal concentration respectively (CONT - nutrient solns).
4. Non-inoculated half-cell used to obtain CV of normal biocathode medium, with and without the addition of 1 ml/L of 2% NaN₃ stock solution (CONT - azide).
5. Two non-polarised secondary inoculated half-cells operated for 28 days in order to develop non-electroactive communities and serve as community analysis and biomass controls (CONT - community).

A summary of all of the half-cells used in the study, along with their operational parameters, is presented in an experimental matrix table, Table 5.1. The operational parameters give the differences between half-cells. In particular, there were some differences between the operation times of the duplicate half-cells. For example, the primary inoculated half-cells poised at -0.1 V, A and B, were operated for a much longer period of time than the secondary inoculated half-cells poised at -0.1 and +0.2 V, half-cells E, F, I and J. This introduces the variable of biofilm age, as the biofilm dynamics may change over time, although the systems may all reach an equilibrium after a certain length of time. This was not an ideal experimental design, and was a consequence of later difficulties in simultaneous management of multiple half-cell systems. However, the differences in operation time amongst half-cells E, F, I and J, were smaller (17 % maximum percentage difference). This would hopefully mean that effects associated with aging of these complex, dynamic biofilms, were minimised when comparing half-cells E, F, I and J with one another.

Table 5.1 also gives the various analyses carried out on each of the half-cells in this study. Individual analyses are described in detail in materials and methods. LSV and CV at the beginning and end of the operational periods for all of the half-cells and the non-inoculated controls were carried out. CV in the presence of air/N₂/azide, biomass and community analysis were all determined for primary inoculated half-cells at -0.1 V (A and B), secondary inoculated half-cells at -0.1 V (E and F), and secondary inoculated half-cells at +0.2 V (I

³using a modified 25 ml volume design given in materials and methods.

Half-cell	Operational parameters				Analyses								
	E_{poised} V	Inoc.	Op. time days	CA	CV Air	CV N ₂	CV Azide	LSV Air	CE	DO	Imaging	Biomass	Community
A	-0.1	prim.	266	✓	✓	✓	✓	✓				✓	✓
B	-0.1	prim.	266	✓	✓	✓	✓	✓				✓	✓
C	-0.1	secon.	47	✓	✓					✓			
D	-0.1	secon.	78	✓	✓					✓			
E	-0.1	secon.	115	✓	✓	✓	✓	✓				✓	✓
F	-0.1	secon.	110	✓	✓	✓	✓	✓				✓	✓
G	-0.1	secon.	96	✓	✓	✓	✓	✓					
H	-0.1	secon.	96	✓	✓	✓	✓	✓					
I	0.2	secon.	97	✓	✓	✓	✓	✓				✓	✓
J	0.2	secon.	97	✓	✓	✓	✓	✓				✓	✓
K	-0.1	secon.*	20	✓	✓	✓	✓	✓					
L	-0.2	secon.*	20	✓	✓	✓	✓	✓					
CONT - no inoculum	-0.1	none	11	✓	✓			✓					
CONT - x10 [micro]	-0.1	none	4	✓	✓								
CONT - nutrient soIns**	none	none	na	na	✓								
CONT - azide	none	none	na	na	✓			✓					
CONT - community	none	secon.	28	na								✓	✓
CONT - community	none	secon.	28	na								✓	✓

Table 5.1: Experimental matrix of operational parameters and analyses for all half-cells in the study. The half-cells are labeled A-L, with control half-cells (CONT) given as a second grouping at the bottom of the table. The analyses are chronoamperometry (CA), cyclic voltammetry (CV) in air/N₂/azide, linear sweep voltammetry (LSV) in air, coulombic efficiency (CE), dissolved oxygen (DO), imaging, biomass determination and community analysis. *Inoculated at the same time using the same effluent. **The three different nutrient solutions used to make the biocathode media.

and J). Community and biomass were also determined for the two non-polarised half-cells (CONT - community). The imaging analysis (half-cell C), O₂ mass transport investigation (half-cell D), and coulombic efficiency analysis (half-cells G, H, I and J), carried out on select half-cells is also shown in Table 5.1.

Additionally to the analyses indicated in Table 5.1, the effect of solution pH on the two primary inoculated half-cells poised at -0.1 V (half-cells A and B) was investigated by LSV over a 5 day period. This was achieved by replacing the biocathode medium in the half-cells at 2-3 day intervals with the biocathode medium containing different phosphate buffer ratios. The procedure was as follows;

1. The pH was measured at 132 days and the LSV taken.
2. The half-cell media were then changed for pH 7.2 media, the cells were operated for 2 days, then the pH and LSV taken again at 134 days.
3. The half-cell media were changed again for pH 8.4 media, the cells were operated for a further 3 days, then the pH and LSV taken again at 137 days.
4. The media were then exchanged for pH 6.2 media, the pH levels measured, and the LSV were taken again within the space of 15 minutes from the last set of LSV.

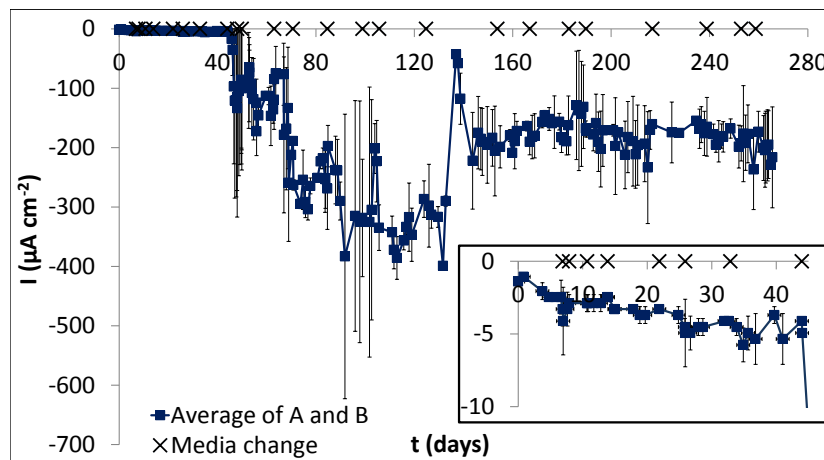
The medium exchanges were carried out by completely emptying the contents of the half-cell, and then filling it with new media. All compounds used in the medium were highly soluble, therefore there was no carry-over of residual compounds between tests.

5.3 Results and Discussion

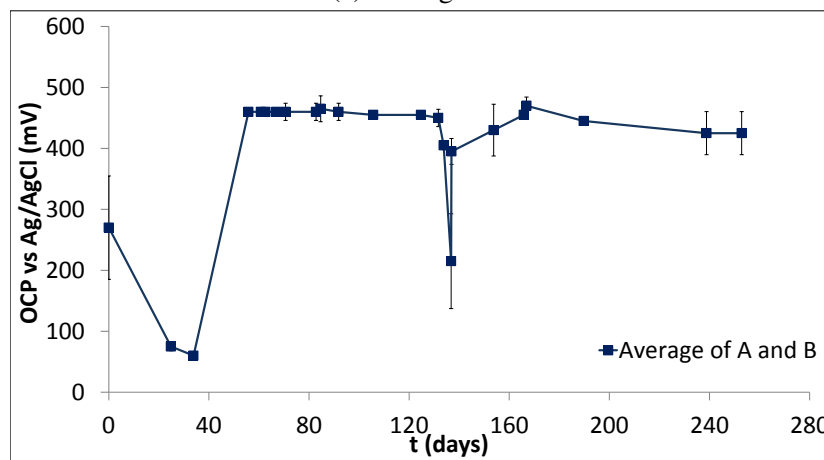
5.3.1 Development of aerobic biocathodes

The aerobic biocathodes were initially cultivated from activated sludge at -0.1 V poised-potential in duplicate half-cells A and B. The average CA current and OCP over time for these two half-cells during their entire operation period is given in Figure 5.1. From 0 to 50 days, the average CA reduction current was less than 5 $\mu\text{A}/\text{cm}^2$ (inset of Figure 5.1a). At 50 days, the reduction current increased from 5 to at least 200 $\mu\text{A}/\text{cm}^2$. During the initial cultivation period of 0 to 50 days, the reduction current increased by a small amount from 1 to 5 $\mu\text{A}/\text{cm}^2$. At 50 days, the OCP increased from less than 100 to 460 mV, and maintained values greater than 400 mV during the rest of the operational period (Figure 5.1b). Therefore, the significant increase in OCP coincided with the sudden large increase in CA reduction current at 50 days in both half-cells. From 50 days until the end of the operational period,

the reduction current averaged approximately $200 \mu\text{A}/\text{cm}^2$. One further point to make is that at approximately 130 days in both half-cells A and B, an experiment looking at the effect of solution pH on aerobic biocathode performance was carried out (see the experimental section of this chapter), hence the sudden large drop in CA reduction current. The results of this experiment will be discussed later in more depth.



(a) Average CA



(b) Average OCP against time

Figure 5.1: Average CA and OCP against time for primary inoculated half-cells poised at -0.1 V (A and B) over their 266 day period of operation. Error bars are one standard deviation.

Throughout their operational period, the primary inoculated half-cells operated at -0.1 V poised potential (A and B) were characterised electrochemically by CV. The CV spectra are presented in Figure 5.2 and 5.3.

The CV spectra for half-cell B exhibited the same trends as those for A. CV graphs at 26 and 34 days of Figure 5.2 show how the biocathode in half-cell A developed within the first 50 days, when the CA current was negligible. Comparing these CV spectra to the one at 0 days, the difference between the forward and reverse scans of the CV over the entire potential range increased by at least an order of magnitude. These changes in the CV spectra must be due to

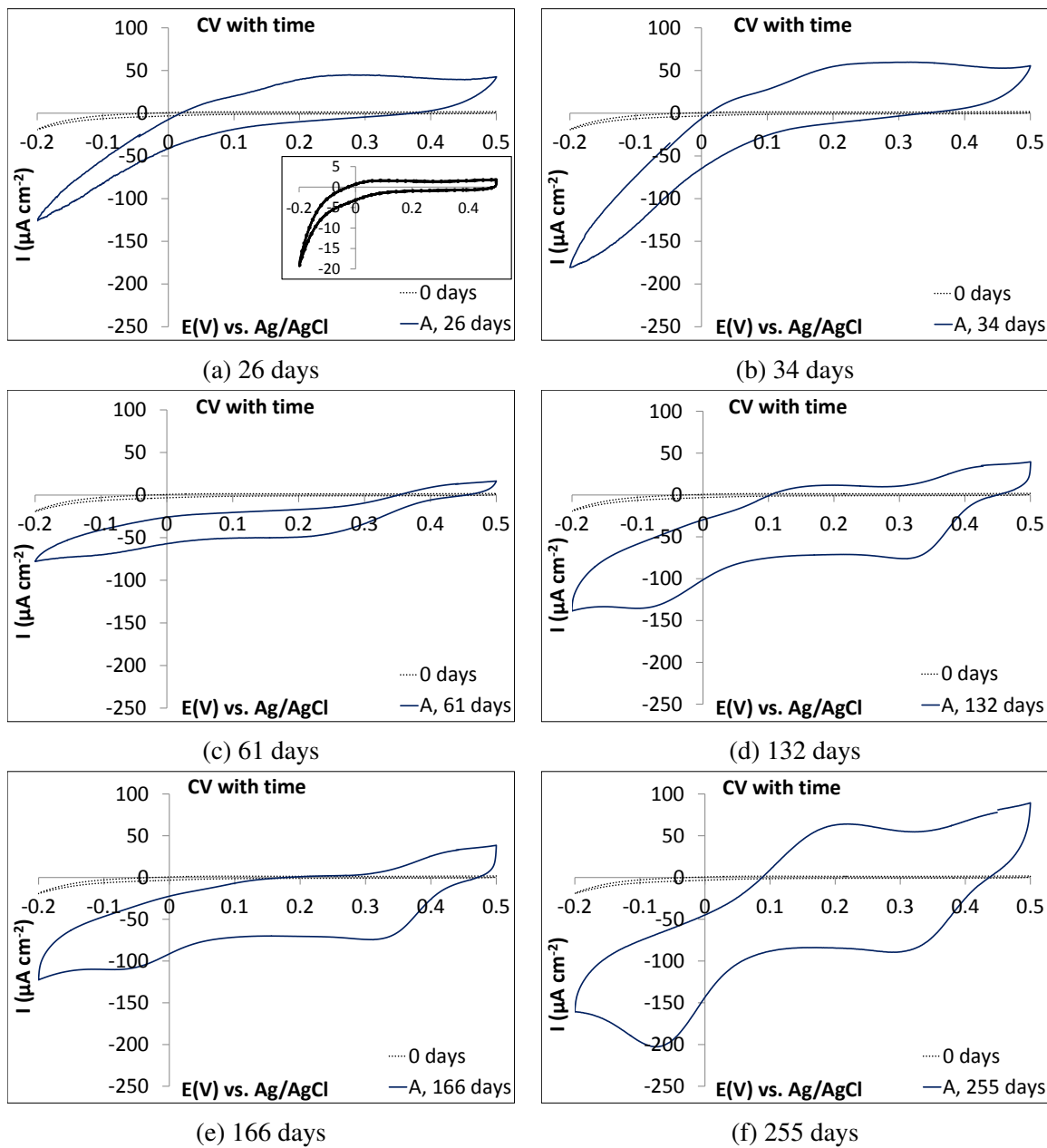


Figure 5.2: CV ($\nu = 5 \text{ mV/s}$) for a primary inoculated half-cell (A) taken at 26, 34, 61, 132, 166 and 255 days of operation (in air).

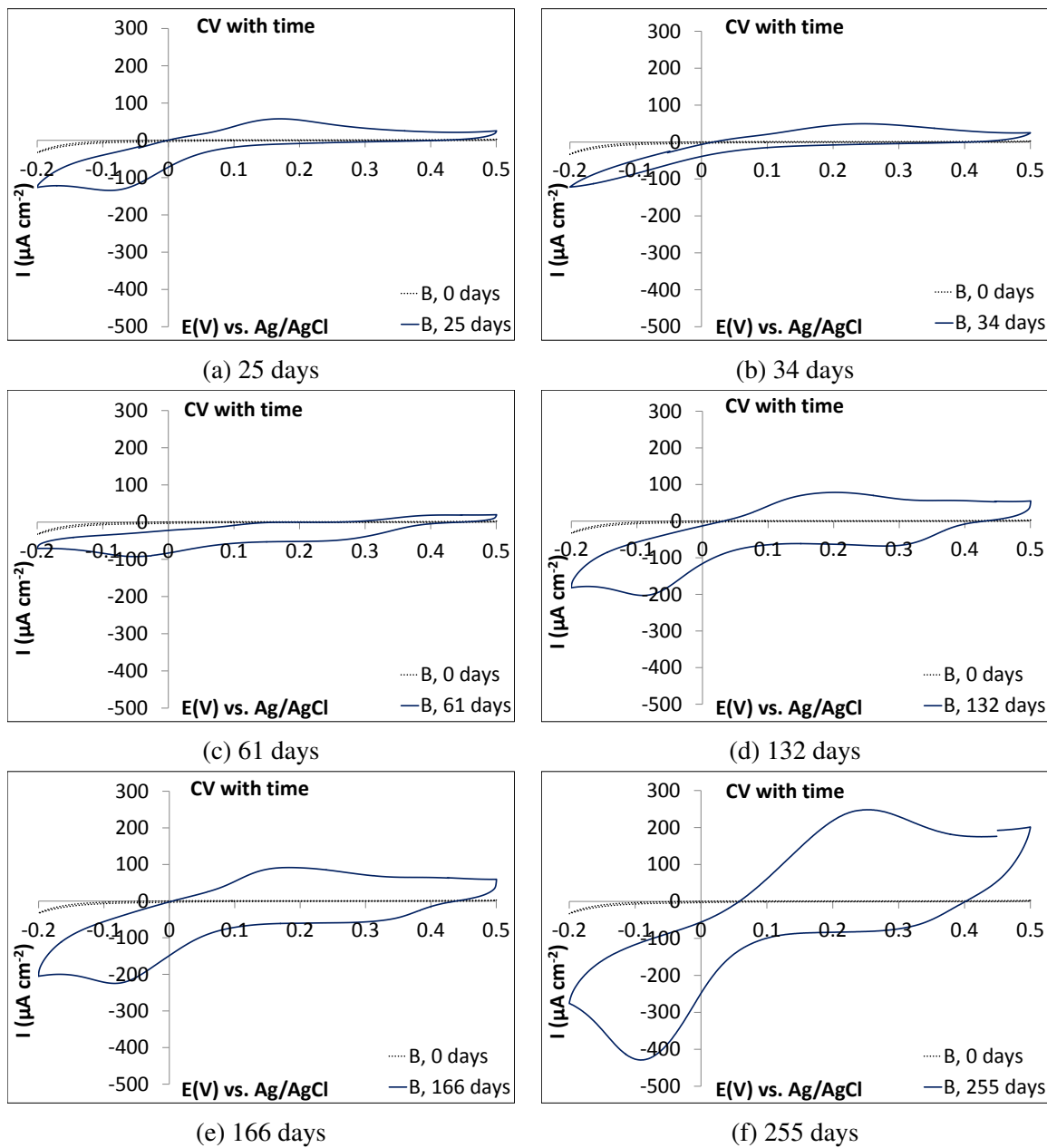


Figure 5.3: CV ($\nu = 5 \text{ mV/s}$) for a primary inoculated half-cell (B) taken at 25, 34, 61, 132, 166 and 255 days of operation (in air).

an increase in electrode capacitance, as the CA reduction current was negligible during the first 50 days of operation ($<5 \mu\text{A}/\text{cm}^2$). This capacitance increase is likely associated with biofilm formation, although one that is not significantly enriched in electrotroths, given the negligible CA current. At 50 days, the CA reduction current suddenly increases, which must be due to a sudden increase in activity of the biofilm toward ORR catalysis. Although the CV for both half-cells A and B exhibited changes before 50 days, these changes must have been associated with an increase in electrode capacitance, which can produce apparent increases in oxidation and reduction currents on the electrode as the electrode potential is scanned, but which are not faradaic currents i.e. not associated with electrochemical reactions. This increase in electrode capacitance is associated with biofilm formation, although it not presently clear what the exact mechanism is. EIS has been used in the literature to monitor the development of biofilms, and changes in capacitance over time do occur [257,258]. Interestingly, an inverse relationship has been observed previously between biofilm thickness and capacitance for a non-electroactive biofilm, as determined by EIS [257]. This would be an interesting avenue to explore as part of a future investigation using complimentary microbiological analysis techniques.

At 61 days in Figures 5.2 and 5.3, after a considerable increase in CA reduction current for both half-cells, there was a clear change in the CV spectra. This change is the appearance of an ORR wave with an onset potential of 400 mV, which is considerably more positive than the abiotic ORR wave at $t = 0$ days with an onset potential of approximately -100 mV. This considerable increase in the ORR onset potential occurs at the same time as a large increase in the CA reduction current and OCP (Figure 5.1), and this new ORR wave plateaus at approximately $50 \mu\text{A}/\text{cm}^2$ reduction current. It must be stressed that this change in the CV spectrum was not an activity decline. The activity on the electrode increased, as is apparent in the change in CA reduction current at 50 days, and it was accompanied by changes in electrode capacitance. As a proxy for electrode capacitance, in all CV spectra shown in both Figures 5.2 and 5.3, the difference in current between the forward and reverse scans in a non-faradaic region of the CV spectra (e.g. at +0.5 V), changes over time. For example, for half-cell A (Figure 5.2), this difference is fairly constant at 26 and 34 days, drops at 61 days (with a sudden increase in CA reduction current), and continues to increase over the rest of the cell operational period (from 132 to 255 days). This could be due to changes in biofilm thickness over time [257].

The high onset potential of +0.4 V for ORR has been observed previously in the literature, and is believed to be due to the activity of aerobic, electrothrophic bacteria [84]. These bacteria are believed to be lithotrophs, which gain energy for metabolism and growth by using electrons derived from the electrode, using the energy to fix CO_2 , and catalysing the ORR at the same time. The high onset potential of the catalytic wave implies that the bacteria use

an outer-membrane cytochrome with a mid-point potential exceeding +0.4 V. For the two half-cells poised at -0.1 V, the average measured OCP after enrichment was 453 ± 14 mV (excluding the OCP measurements taken between 132 to 137 days, where the pH was deliberately varied), so it is likely that the mid-point potential of the outer-membrane cytochrome used by the electrotrophs is close to this value. The highest redox potential measured so far for an outer-membrane cytochrome is 350 mV (pH 4.8) for *cyc2*, which oxidises Fe^{2+} to Fe^{3+} in the iron oxidising/ O_2 -reducing super-complex of *Acidithiobacillus ferrooxidans* [60]. The onset potential for the biologically catalysed ORR wave in the CV spectra for half-cell A is approximately 0.4 V, so these bacteria have outer-membrane cytochromes with redox potentials comparable to *cyc2* of *Acidithiobacillus ferrooxidans*.

Figures 5.2 and 5.3 also show subsequent CV taken for both half-cells A and B at points much later in the operational period. From 132 to 255 days, an oxidation peak at +0.2 V, and a reduction peak at -0.1 V, convoluted with the ORR wave beginning to appear and increasing in magnitude; the reduction current peak increases from 150 to 200 $\mu\text{A}/\text{cm}^2$, whilst the oxidation current peak increases from less than 10 to 60 $\mu\text{A}/\text{cm}^2$. These peaks will be discussed later in the context of the electron transfer mechanism.

Non-inoculated control half-cells were used to identify any potential electrochemical behavior not associated with bacteria. Therefore, an identical non-inoculated control half-cell polarised at -0.1 V (CONT - no inoculum) was operated for 11 days. The CA data over the operational period for this half-cell, as well as the CV data at the beginning and end of the operation period, are presented in Figures 5.4a and 5.4b, respectively. The CA reduction current remained below 3 $\mu\text{A}/\text{cm}^2$ (Figure 5.4a), consistent with abiotic reduction of O_2 on carbon felt, whilst the CV (Figure 5.4b) were identical, exhibiting only the reduction current associated with abiotic ORR on carbon felt. Therefore, the non-inoculated media could not generate the same electrochemical behavior as observed in Figures 5.1a, 5.2 and 5.3 for the primary inoculated half-cells poised at -0.1 V (half-cells A and B). This half-cell was operated for 11 days before termination, and was not run for as long as many of the other inoculated half-cells. This was due to constraints on time and resources, and this half-cell would ideally have been operated for a longer period of time (e.g. 266 days). This half-cell shows that, in the absence of inoculum/bacteria, polarisation of the WE for a significant time period, does not cause a change the appearance of the CV.

The results of CV on the nutrient solutions used to make the biocathode medium using a 25 ml abiotic half-cell is presented in Figure 5.4e. The vitamin and macro nutrient solutions at x500 and x1000 their normal concentrations in the biocathode medium exhibited the same abiotic ORR feature as for 50 mM pH 5.8 phosphate buffer, and no additional electrochemical features. The vitamin solution did not exhibit the reversible oxidation and reduction peak

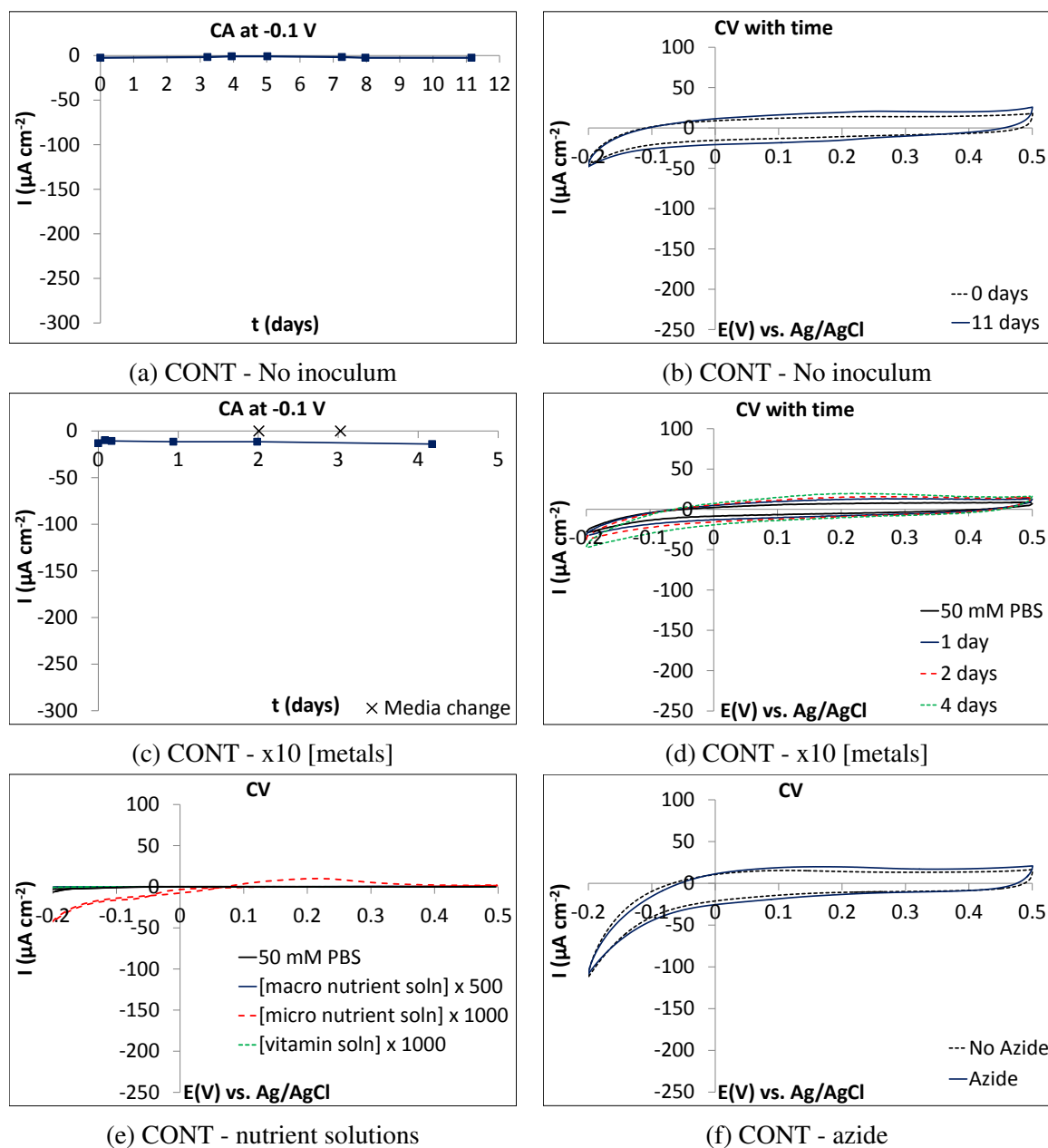


Figure 5.4: Control data for the half-cell study. Graphs (a) and (b) are the CA and CV ($\nu = 5$ mV/s) data respectively for a non-inoculated abiotic control half-cell poised at -0.1 V using normal biocathode medium. Graphs (c) and (d) are the CA and CV ($\nu = 5$ mV/s) data for a half-cell poised at -0.1 V using normal biocathode medium with micro nutrients at x 10 the normal concentration. Graph (e) contains the CV ($\nu = 5$ mV/s) data for the nutrient solutions used to make the biocathode medium; macro, metals and vitamin solutions at x 500, x 1000 and x 1000 times the normal concentration in the biocathode medium. Graph (f) contains the CV ($\nu = 5$ mV/s) data for normal biocathode medium with/without the addition of 1 ml/L of a 2% NaN_3 stock solution.

of riboflavin, which occurs at -0.42 V (pH 7.0) on graphite electrodes [135], outside of the range of the CV. The micro nutrient solution, however, containing Fe, Cu and Co species in high concentrations, amongst other metal ions, exhibited a small oxidation feature, centered at approximately +0.2 V and a reduction wave with an onset potential of +0.1 V. These electrochemical features could be due to deposition and dissolution of Cu, which has a reduction potential of 0.136 V vs Ag/AgCl [259].

To test whether any of the trace metal ions present in the biocathode medium deposit onto the surface of the carbon felt over time in sufficient concentration to cause an electrochemical response, a non-inoculated control half-cell was polarised for 4 days at -0.1 V with biocathode medium containing x 10 the normal concentration of metal ions. For this control half-cell, the medium was changed twice during the course of operation at 1-2 day intervals to allow for sequential metal reduction from the solution onto the carbon electrode. The CA and CV data for this control half-cell are presented in Figures 5.4c and 5.4d, respectively. The CA exhibited a small average background reduction current of 10 $\mu\text{A}/\text{cm}^2$, whilst the CV exhibited only abiotic ORR and no significant change over time. This implies that the trace metal ions do not cause an electrochemical response at the concentrations used.

To test whether the addition of 1 ml/L of an azide stock solution (2% NaN_3) had any electrochemical effect, CV were recorded for a non-inoculated half-cell with biocathode medium, with and without the addition the azide. This result is presented in Figure 5.4f. The CV with and without the azide addition were the same, exhibiting only abiotic ORR, therefore the addition of the azide had no electrochemical effect. This control was necessary for later experiments.

The effect of peroxide formation on aerobic biocathode growth was assessed by setting up two secondary inoculated half-cells (K and L) at the same time, using the same half-cell effluent. One was polarised at -0.1 V (K), whilst the other was polarised at -0.2 V (L). The CA current over a period of 20 days and CV taken at 0 and 7 days for these two half-cells are presented in Figure 5.5. Figure 5.5a gives the CA data, showing an increase in reduction current in the half-cell poised at -0.1 V from background levels of 5 $\mu\text{A}/\text{cm}^2$ to values ranging between 100 and 200 $\mu\text{A}/\text{cm}^2$. This is consistent with the formation of an aerobic biocathode biofilm. The half-cell poised at -0.2 V, however, exhibited only a small CA reduction current of 50 $\mu\text{A}/\text{cm}^2$ at 0 days, and this quickly dropped away over the first 5 days to values close to 0 $\mu\text{A}/\text{cm}^2$. This indicates that an aerobic biocathode did not develop for the half-cell polarised at -0.2 V. Operating at least duplicate reactors for both treatments would have been highly desirable in order to assess the statistical significance of the recorded data, but this was not possible due to constraints on time and resources i.e. the time-consuming and resource-intensive process of setting up and operating multiple 1 L biological reactors in

parallel, and the time required in repeating experimental runs in the case of technical failures. This particular experiment was therefore only descriptive, although it did show an interesting trend.

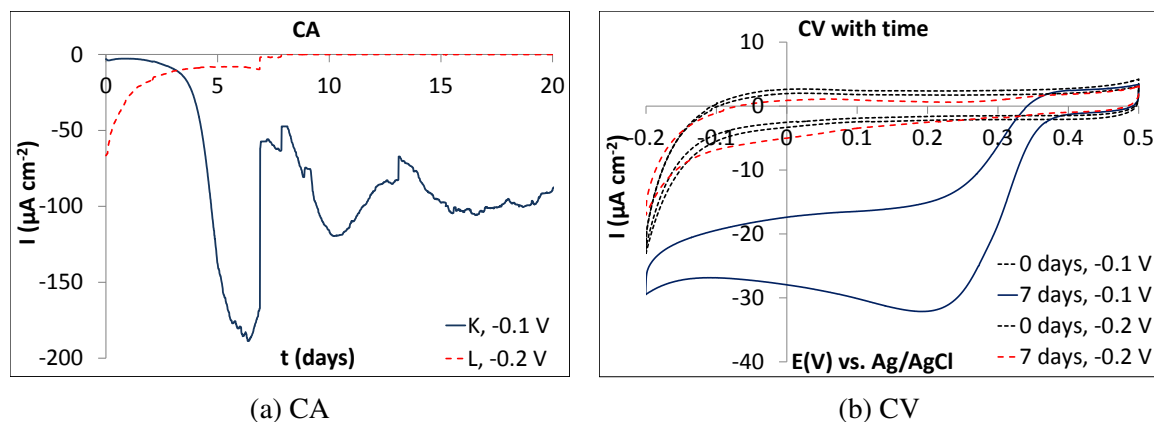


Figure 5.5: CA and CV ($\nu = 5 \text{ mV/s}$) data for two secondary inoculated half-cells (K and L), one polarised at -0.1 V , the other at -0.2 V , over 20 days of operation. The CV ($\nu = 5 \text{ mV/s}$) are recorded on both half-cells at 0 and 7 days of operation.

The CV curves for the two half-cells are presented in Figure 5.5b, and are consistent with aerobic biocathode formation in the half-cell polarised at -0.1 V , and a lack of aerobic biocathode formation in the half-cell poised at -0.2 V . This is because the half-cell polarised at -0.1 V has a biologically catalysed ORR wave with an onset potential of $+0.4 \text{ V}$, whereas the half-cell polarised at -0.2 V exhibits only abiotic ORR on carbon. The difference between these two half-cells was likely due to peroxide formation on the carbon felt surface, which was shown in Chapter 4 to occur at -0.2 V , but not at -0.1 V poised potential. Any peroxide formed on the surface of carbon felt electrodes forms reactive oxygen species, such as superoxide, which cause oxidative stress and cell damage [260]. Biofilms, electroactive or otherwise, will be damaged and potentially sterilised through continued exposure to reactive oxygen intermediates generated from peroxide. One further interesting trend to take note of, is the large drop in CA reduction current at 7 days for half-cell K (Figure 5.5a). As this is the point at which the CV were recorded, it is possible that the large drop in CA reduction current could be associated damage to the biofilm due to electrode polarisation. This is an interesting observation, but one that would need to be verified experimentally with multiple parallel reactors coupled to statistical analysis as part of future work.

Understanding where the aerobic biocathode biofilm occurs and how this relates to the dimensions of the carbon support is essential in development of the aerobic biocathode. With this in mind, a secondary inoculated half-cell polarised at -0.1 V (half-cell C) was operated for 47 days, before the electrode was imaged in order to determine biofilm thickness and location. CA and LSV data for this half-cell showing aerobic biocathode formation can be

found in the appendix (Figures A.4c and A.7c respectively), and fluorescence images taken of the electrode surface are presented in Figures 5.6 and 5.7.

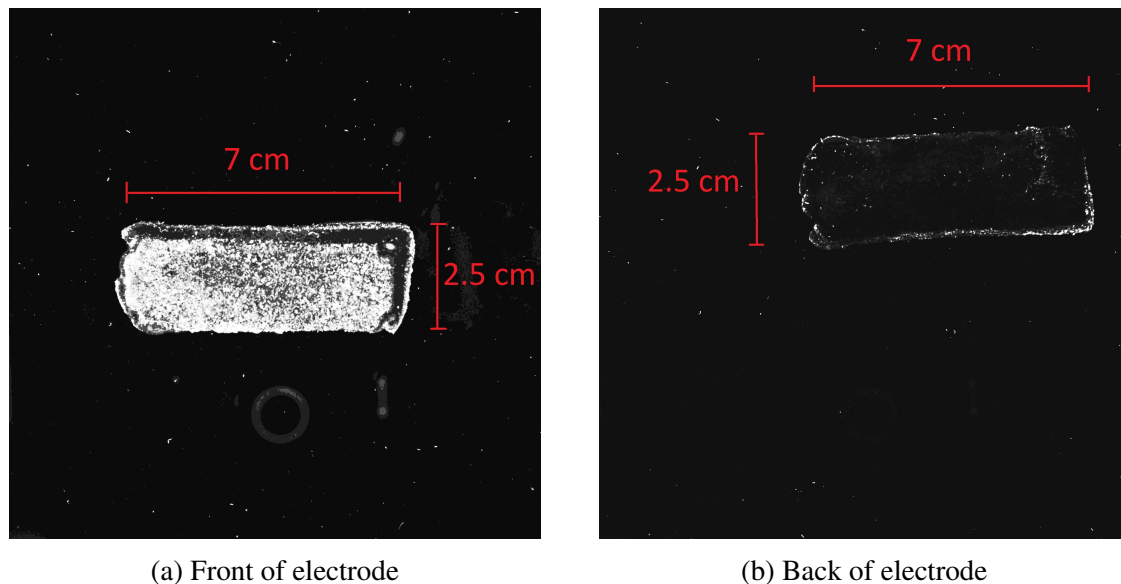
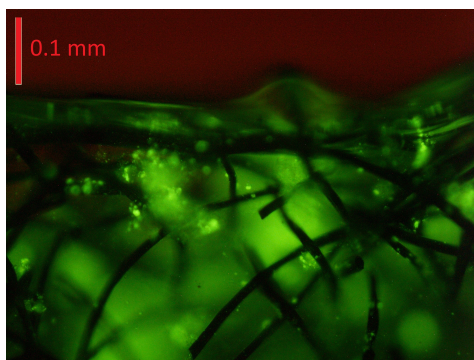
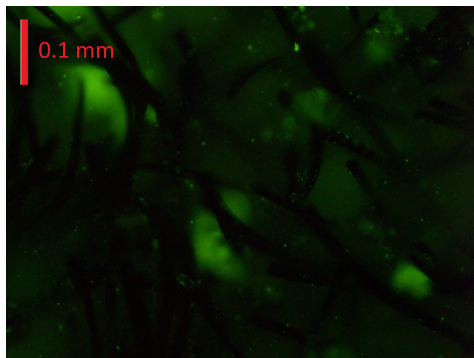


Figure 5.6: Gel documentation system images of the front (a) and back (b) of the carbon felt working electrode used in a secondary inoculated half-cell poised at -0.1 V (half-cell C), using an excitation wavelength of 365 nm and an exposure time of 1 min and 29 seconds. Fluorescence is shown in white. The contrast between white and black has been enhanced using InfranView 3.97.

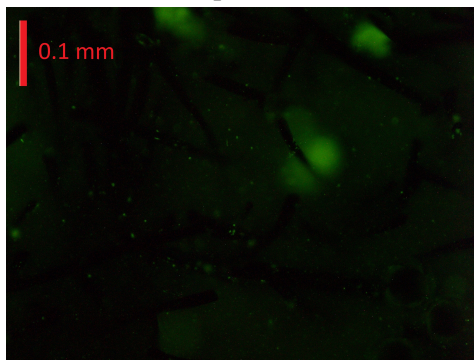
At the end of the operational period (47 days), the carbon felt WE was taken from the half-cell (half-cell C), and stained with SYBR Gold nucleic acid stain before imaging. The gel documentation system images of the front and back of the WE without magnification are presented in Figure 5.6. The image of the front of the electrode shown in picture Figure 5.6a is white where fluorescent emission was detected, whereas the image taken of the back of the electrode shown in Figure 5.6b is white at the edge only and black otherwise. The back of the electrode was not exposed to the process electrolyte, as it was the side pressed up against the PTFE backing plate, whereas the front of the electrode was exposed to the process electrolyte. This indicates that biomass does not penetrate all the way through to the back of the 0.5 cm carbon felt WE, despite its porous structure. This has important implications with respect to electrode materials for aerobic biocathodes, indicating that porous structures, like carbon felt, do not maximise biofilm coverage in their internal surfaces. This finding was further investigated by taking higher resolution images of the biofilm. Epifluorescence images of an electrode cross-section are presented in Figure 5.7. The frame height was calculated as 0.55 mm using the scale bar. These images were consecutive frames starting from the carbon felt surface (Figure 5.7a), going further into the porous carbon felt electrode (Figures 5.7b to 5.7d), and show a diminishing gradient of fluorescence emission intensity. No fluorescence is observed in the image shown in Figure 5.7d. This implies that the biofilm penetrates into



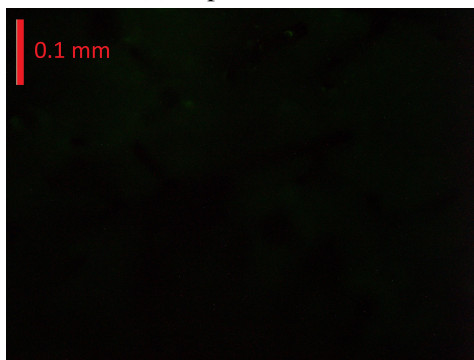
(a) Top



(b) Top - 1 frame



(c) Top - 2 frames



(d) Top - 3 frames

Figure 5.7: Epifluorescence microscope images of a cross-section of the carbon felt working electrode of a secondary inoculated half-cell poised at -0.1 V (half-cell C). The images are ordered as consecutive frames starting from the electrode surface (a) and going into the cross-section, in the order of (a), (b), (c) then (d). The images are taken at $\times 100$ magnification and a scale bar is included on all 4 images.

the carbon felt by no more than two to three frames, corresponding to a penetration depth of 1.0 to 1.5 mm into the electrode. This represents penetration into the electrode by the biofilm of approximately 20-30 % of the carbon felt electrode thickness (5 mm).

It is clear from the above analysis that the biocathode biofilm largely resides near the surface of the carbon felt electrode, and does not penetrate into the interior of the carbon felt electrode. This is despite the fact that carbon felt is a porous structure. Carbon felt strands are clearly visible in Figure 5.7a, and the 2D space between consecutive strands varies in the order of 100 μm . Most known bacteria vary in size between 0.5 and 5.0 μm in length [43], so porous electrode materials, such as carbon felt, should be able to incorporate bacteria throughout their entire structure. This limited biofilm penetration depth may be associated with O_2 depletion in the interior due to O_2 consumption by the biofilm at the electrode surface. Given this analysis, the dimensions of the carbon support could be optimised to improve O_2 mass transfer. For example, a carbon brush electrode could be used instead of carbon felt, as these electrodes give the highest performing MFC anodes due to a high surface area and a structure that allows efficient mass transfer to the biofilm [14, 168]. Alternatively, the amount of carbon felt electrode used could be reduced on the basis that most of the biomass occupies only 20-30 % of the electrode structure, therefore lowering cost.

As discussed in the literature review of this thesis, planar carbon electrodes with no porosity, such as graphite plate, do not exhibit good performance as bioanode electrode materials. This is likely due to their lack of porosity. In the case of carbon felt, a smaller fraction of the internal surfaces are occupied than are unoccupied. This indicates that some level of porosity is important for the electrode material, but that much of the electrode surface area can be wasted if the electrode is 3D and too thick. Materials such as carbon cloth, carbon veil and carbon fiber fabric, are likely to be good choices for biocathode electrode materials, as they are not thick 3D structures like carbon felt, but possess some level of porosity. These factors together optimise biofilm thickness, without wasting electrode material. As discussed in the literature review of this thesis, carbon felt is too expensive for MFC applications, and now it can be seen in this experiment, that it has narrow activity, due to the low activity of the material substrata.

5.3.2 Electrochemical performance of aerobic biocathodes grown at -0.1 and +0.2 V poised-potential

The electrochemical performance of all half-cells in the study was assessed by LSV, and by taking the average CA current over the operational period for the half-cell. The average CA current for all of the half-cells is given in Table 5.2, and the raw CA data can be found in Figures A.4, A.5, and A.6 of the Appendix. LSV were taken at the beginning and end of

the half-cell operational periods for all of the half-cells, and have been summarised by taking the LSV reduction current at +0.2 V, and the onset potential for ORR, at the beginning and end of the operational period, for the half-cell. These summarised LSV data are presented in Table 5.3, and the raw LSV data for all half-cells can be found in Figures A.7, A.8, and A.9 of the Appendix. Select LSV of replicate half-cells spanning the three different treatments (-0.1 V primary inoc., -0.1 V secondary inoc., +0.2 V secondary inoc.) are shown in Figure 5.8.

Considering just the CA reduction current data presented in Table 5.2, the uninoculated control half-cell (CONT - no inoculum) exhibited an average CA reduction current of $1 \pm 0 \mu\text{A}/\text{cm}^2$, and the secondary inoculum half-cell poised at -0.2 V (half-cell L) exhibited an average reduction current of $6 \pm 22 \mu\text{A}/\text{cm}^2$. All other half-cells with an aerobic biocathode exhibited average reduction currents between 104 and 254 $\mu\text{A}/\text{cm}^2$. For each half-cell with an aerobic biocathode, there was considerable variation in the average CA reduction current, giving high values for the standard deviations. Comparing the mean of the average CA reduction currents using an analysis of variance across the three different treatments, -0.1 V primary inoc., -0.1 V secondary inoc. and +0.2 V secondary inoc. (excluding half-cells K and L, which were operated for only 20 days), no statistically significant difference was found between the treatments (p-value = 0.18). In particular, poised-potential did not appear to affect the average CA reduction current.

Looking at the start up periods presented in Table 5.2, for all half-cells which developed an aerobic biocathode, there was a distinct difference between the two primary inoculated half-cells polarised at -0.1 V (A and B), and all the other secondary inoculated half-cells polarised at -0.1 and +0.2 V. The primary inoculated half-cells (A and B) had start-up periods of 56 days and 47 days, as compared to 3-10 days for the secondary inoculated half-cells (C-K). Therefore, inoculation using the effluent from existing half-cells reduced the start-up period by over a month. This is believed to be due to an effluent enriched in electrothrophic bacteria, which is not the case with activated sludge, where the electrothrophic bacteria are presumably in much lower concentrations.

Further inspection of Table 5.2 shows that there was a distinct change in the OCP across all half-cells when comparing the OCP at start-up, to the OCP at the end of the half-cell operation period. For those half-cells which developed a biocathode (average CA reduction currents between 104 and 254 $\mu\text{A}/\text{cm}^2$, well above the background levels for the control half-cells), the OCP increased from an average of $255 \pm 98 \text{ mV}$ to an average of $448 \pm 28 \text{ mV}$ across all cells (p-value = 0.00004 for a two sample T-test assuming unequal variances). The average increase in OCP of 193 mV was accompanied by a thirding of the standard deviation. This is believed to be due to the fact that the OCP is more sensitive to contaminants and impurities

Half-cell	Operational parameters				CA	OCP	
	E_{poised} V	Inoc.	Op. time days	Ac. time days		I(ave.) $\mu\text{A}/\text{cm}^2$	Start mV
A	-0.1	prim.	266	56	-195 ± 95	330	450
B	-0.1	prim.	266	47	-212 ± 64	210	400
C	-0.1	secon.	47	5	-162 ± 74	280	440
D	-0.1	secon.	78	9	-254 ± 94	230	450
E	-0.1	secon.	115	3	-208 ± 42	220	400
F	-0.1	secon.	110	5	-155 ± 56	400	470
G	-0.1	secon.	96	10	-176 ± 84	280	460
H	-0.1	secon.	96	7	-134 ± 69	240	465
I	+0.2	secon.	97	9	-129 ± 37	110	474
J	+0.2	secon.	97	7	-130 ± 66	110	487
K	-0.1	secon.	20	5	-104 ± 42	400	430
L	-0.2	secon.	20	na	-6 ± 22	320	390
CONT - no inoculum	-0.1	none	11	na	-1 ± 0	210	-10

Table 5.2: CA and OCP data summary; average current after the acclimatisation period, average I, calculated from the CA for each half-cell, and the OCP for each half-cell at the start and end of the operation period. The acclimatisation period for each half-cell is also given (Ac. time). Operational parameters for each half-cell have been included; poised potential (E_{poised}), type of inoculation (primary or secondary), and the operation time.

Half-cell	Operational parameters			LSV at 0 days		LSV at end	
	E_{poised} V	Inoc.	Op. time days	E_{ORR} V	I at +0.2 V $\mu\text{A}/\text{cm}^2$	E_{ORR} V	I at +0.2 V $\mu\text{A}/\text{cm}^2$
A	-0.1	prim.	266	-100	0	430	-50
B	-0.1	prim.	266	-100	0	420	-45
C	-0.1	secon.	47	-100	0	410	-24
D	-0.1	secon.	78	-100	0	400	-17
E	-0.1	secon.	115	50	-1	410	-46
F	-0.1	secon.	110	0	0	430	-14
G	-0.1	secon.	96	50	-3	450	-34
H	-0.1	secon.	96	0	-2	440	-38
I	+0.2	secon.	97	-100	0	450	-47
J	+0.2	secon.	97	-100	0	450	-45
K	-0.1	secon.	20	0	0	400	-25
L	-0.2	secon.	20	-50	0	-100	-2
CONT - no inoculum	-0.1	none	11	0	-2	0	-3

Table 5.3: LSV ($\nu = 1$ mV/s) data summary; current, I , at +0.2 V, and the onset potential for ORR, E_{ORR} , for each half-cell in the study, at $t = 0$ days and at the end of the half-cell operation period. Operational parameters for each half-cell have been included; poised potential (E_{poised}), type of inoculation (primary or secondary), and the operation time.

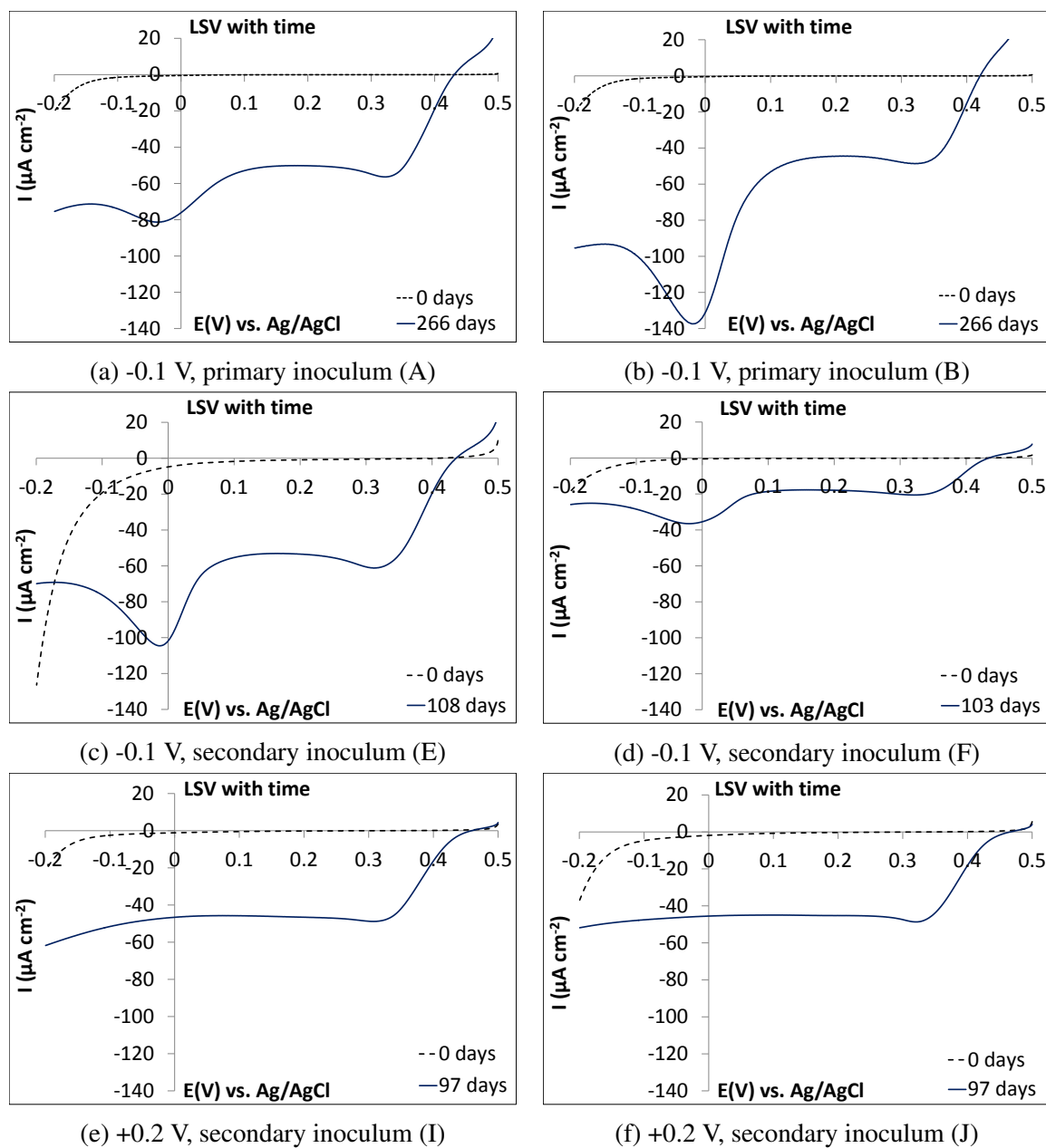


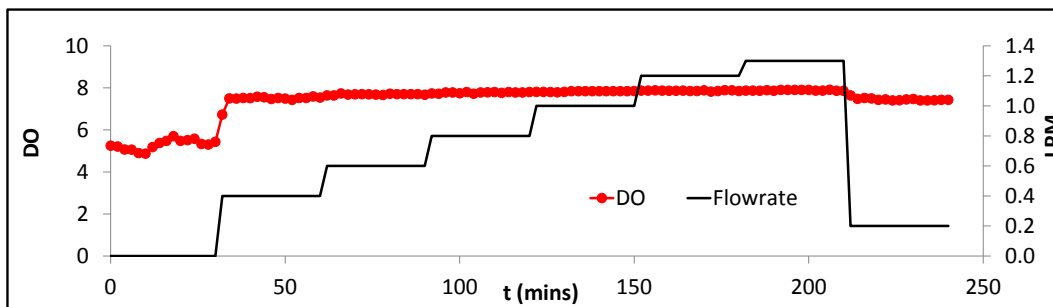
Figure 5.8: LSV ($\nu = 1 \text{ mV/s}$) spectra for duplicate half-cells covering the three different treatments; -0.1 primary inoculum ((a) and (b)), -0.1 V secondary inoculum ((b) and (c)) and +0.2 secondary inoculum ((d) and (e)). For each half-cell, the LSV at $t = 0$ days and at the end of the half-cell operation period are presented.

on the surface of the carbon felt at inoculation when there is no biofilm, but as the aerobic biocathode biofilms develop, the OCP becomes much more tightly defined as a small set of electrochemical reactions begin to dominate on the surface of the electrode.

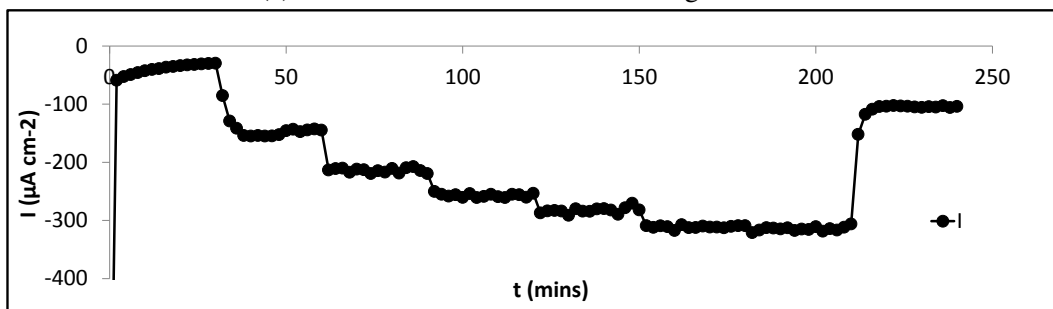
The LSV data for all half-cells is summarised in Table 5.3, which gives the onset potential for ORR and the reduction current at +0.2 V in the LSV for each half-cell, at 0 days and at the end of the operation period. Across all half-cells with an aerobic biocathode, the reduction current at +0.2 V, in the mass transfer region of the LSV curve, increased from 0.6 ± 1.0 to $35 \pm 13 \mu\text{A}/\text{cm}^2$ (p-value = 5.4×10^{-6}), whilst the onset potential for ORR increased in a positive direction from -45 ± 65 to $426 \pm 20 \mu\text{A}/\text{cm}^2$ (p-value = 2.7×10^{-11}). These trends can be seen clearly in Figure 5.8, across all three treatments. For the inoculated half-cell poised at -0.2 and the uninoculated control half-cell poised at -0.1 V, the LSV reduction current remained less than $2 \mu\text{A}/\text{cm}^2$ at the beginning and end of the experiments, and there was no increase in the onset potential for ORR. In terms of the I_R values at +0.2 V in Table 5.3 for the three different treatments (-0.1 V primary inoc., -0.1 V secondary inoc., +0.2 V secondary inoc.), analysis of variance indicated no statistically significant difference between the treatments (p-value = 0.09). However, the LSV for the half-cells with primary and secondary inoculum grown at -0.1 V poised potential shown in Figure 5.8, all exhibited two reduction waves (half-cells A, B, E and F), whilst the half-cells grown at +0.2 V exhibited only one reduction wave (half-cells I and J). This implies that for the half-cells grown at -0.1 V, there is an additional electrochemical process occurring which does not occur for the half-cells grown at +0.2 V. This is discussed in more detail in Section 5.3.3.

Due to an inability to distinguish electrochemical performance levels between the 3 different treatments based on CA and LSV data, an additional assessment was made on the response of a single half-cell (D, -0.1 V, secondary inoc.) to changing O_2 concentration. Half-cell D was a different half-cell to the others, but was subjected to exactly the same processes as the other half-cells. Mass transport of O_2 to the aerobic biocathode biofilm was investigated by varying the flow rate of air from the air pump used to sparge the electrolyte, and recording the DO in the electrolyte and the CA current at the poised potential used for the half-cell (-0.1 V). The results from this experiment are presented in Figure 5.9. For the first 25 minutes of the experiment with no air sparging, the reduction current was less than $50 \mu\text{A}/\text{cm}^2$ and the DO was between 5.0 - 5.5 mg/L. This is consistent with the LSV mass transfer limited currents found for all of the half-cells with an aerobic biocathode, which were between 14 and $50 \mu\text{A}/\text{cm}^2$ at a potential of +0.2 V in the LSV graph, and which are recorded without active aeration. As the air was switched on with a flow rate of 0.4 LPM, this resulted in an instantaneous increase in both the DO and reduction current to 7.5 mg/L and $180 \mu\text{A}/\text{cm}^2$ respectively. The DO and reduction current then further increase as the sparge rate was increased in 0.2 LPM increments, reaching limiting values of 8.0 mg/L and $300 \mu\text{A}/\text{cm}^2$ respectively. The

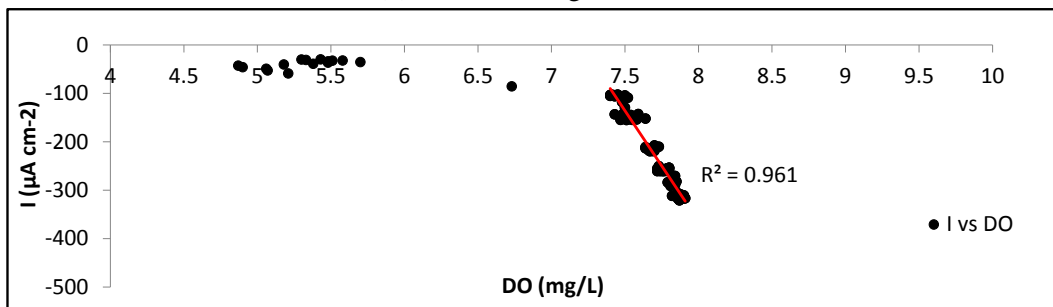
large variation in reduction current between 180 and 300 $\mu\text{A}/\text{cm}^2$ when the electrolyte was sparged probably accounts for the high standard deviations for the average CA currents observed for the half-cells with an aerobic biocathode, which ranged from between 37 to 95 $\mu\text{A}/\text{cm}^2$, as shown in Table 5.2. Examination of Figure 5.9b shows a clear saturation effect, with a plateau observed in the reduction current as the flow rate was further increased beyond 0.8 LPM. This would indicate that at a reduction current of 300 $\mu\text{A}/\text{cm}^2$, the maximum rate of oxygen reduction by cytochrome oxidase occurred, as further increasing the flow rate did not increase the reduction current.



(a) DO concentration and flow rate against time



(b) CA current against time



(c) CA current versus DO concentration

Figure 5.9: Variation of current with changing electrolyte DO concentration for a secondary inoculated half-cell poised at -0.1 V (D) . Graph (a) is a plot of DO concentration and flow rate against time, where the flow rate from the air pump sparging the electrolyte was changed in 0.4 LPM increments. Graph (b) is a plot of current versus time for the half-cell over the same time period. Graph (c) is a plot of current versus DO concentration taken by combining the data from (b) and (c).

Examination of Figure 5.9c shows that between 7.5 and 8.0 mg/L DO concentration, a large

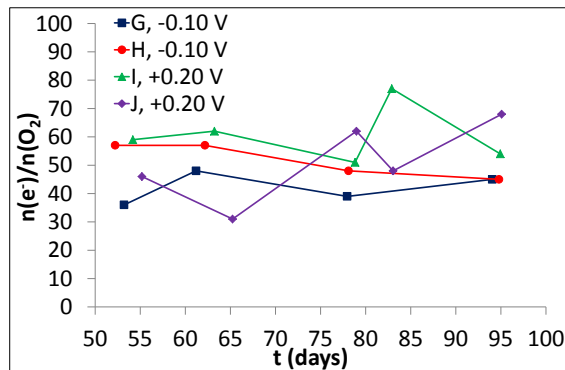
linear increase ($R^2 = 0.961$) in the reduction current was observed of a magnitude of approximately $200 \mu\text{A}/\text{cm}^2$, which did not plateau. This result demonstrates how the aerobic biocathode is limited by the mass transfer of O_2 , requiring constant aeration in order to achieve reduction currents greater than $180 \mu\text{A}/\text{cm}^2$. For the half-cells with an aerobic biocathode, this result accounts for differences between the LSV mass transfer limited reduction currents in the absence of aeration (14 to $50 \mu\text{A}/\text{cm}^2$ at +0.2 V in the LSV graph), and the higher average CA currents under conditions of constant aeration (104 and $254 \mu\text{A}/\text{cm}^2$).

The abrupt change between aeration and no aeration is a consequence of the low solubility of O_2 in water (8.0 mg/L at 25°C as compared to e.g. 1000 mg/L for sodium acetate in the electrolyte for a bioanode), and signifies the importance of active aeration of the electrolyte in order to improve O_2 mass transfer to the biofilm and maintain high reduction currents. Active aeration adds a significant cost to the MFC system. This result is in agreement with the work by Heijne *et al.*, who found that mass transfer of O_2 limits the performance of aerobic biocathodes catalysing the ORR [84]. However, the use of O_2 is attractive for MFCs given its high reduction potential ($E^{0'} = 0.60 \text{ V}$ at $\text{pH } 7.0$, $\text{pO}_2 = 0.2$) and availability in the environment, and active aeration can be substituted with passive aeration, by growing the aerobic biocathodes on gas diffusion electrodes for example. Gas diffusion electrodes for aerobic biocathodes in MFCs have shown some early promise [81], though this type of electrode has problems with scale-up, due to the increased pressure on the GDE as the reactor size increases.

As previously indicated, there were no systematic trends in the O_2 mass transfer limited reduction currents in the LSV for the aerobic biocathodes across the three different treatments (-0.1 V primary inoc., -0.1 V secondary inoc. and $+0.2 \text{ V}$ secondary inoc.). This is likely a result of the poised potentials studied. As both -0.1 and $+0.2 \text{ V}$ poised potentials are in the mass transfer region for O_2 , the reduction current is therefore impacted significantly by variations in O_2 mass transfer with sparging using an air pump. This leads to large standard deviations in the average CA currents over time. If poised-potentials in the potential region between 0.35 and 0.45 V had been used, these may have given different results, as this is the kinetic region of the biocathode LSV curve, which would have subjected the aerobic biocathodes to kinetic and not mass transfer limitations. For example, Xia *et al.* operated three aerobic biocathode half-cells which had an onset potential for ORR of approximately 250 mV at -144 , 16 and 156 mV poised-potential, obtaining average CA reduction currents of $3.39 \pm 0.89 \text{ mA}$, $3.53 \pm 0.97 \text{ mA}$ and 2.32 ± 0.46 , respectively [88]. The CA current was lowest for the half-cell operated at 156 mV , a potential in the kinetic region of the resultant CV. Additionally, from the errors in the average CA current, it can be seen that greater variability was observed in the average CA current for the half-cells operated at -144 and 16 mV poised-potential, both poised potentials which lie in the O_2 mass transfer region of the resultant CV.

The aerobic biocathode coulombic efficiency was determined for a selection of aerobic biocathodes to compare the % of current going into metabolism, versus biomass/parasitic processes. By determining the charge passed and O₂ consumed by the aerobic biocathode over a 7 hour period, the coulombic efficiency was calculated, providing a comparison between the number of electrons used for metabolism (the charge passed/electrons deposited onto the TEA for the electrotrophs, O₂), to the theoretical number of electrons which could have been used for metabolism based on the quantity of O₂ consumed in the half-cell.

The coulombic efficiency (%) of secondary inoculated half-cells grown at -0.1 and +0.2 V (G, H, I and J) was determined through time over a 50 day period toward the end of the half-cell operational period. These data are presented in Figure 5.10. Half-cells G and H poised at -0.1 V had values of 42 ± 5 and 52 ± 6 % respectively, whereas half-cells I and J poised at +0.2 V had values of 61 ± 10 and 51 ± 15. An analysis of variance showed that differences between the four data sets (four half-cells) were not statistically significant (p-value = 0.10). However, the average coulombic efficiency for all four half-cells, regardless of poised-potential, was 52 ± 11, indicating that approximately 50 % of the O₂ was consumed for ATP generating reactions (assuming direct ORR catalysis). The remaining 50 % of the O₂ was used either for biomass production by the electrotrophs, or lost in parasitic processes, such as ammonia oxidation by AOB, or respiration by predatory microorganisms e.g. protozoa.



(a)

Figure 5.10: O₂ coulombic efficiency at different points through time for secondary inoculated half-cells poised at -0.1 V (G and H) and +0.2 V (I and J).

Ammonia oxidation coupled with oxygen reduction is a viable metabolic pathway due to the significant quantity of NH₄⁺Cl⁻ present in the process electrolyte, which is required as a macro nutrient for the growth of bacteria. However, ammonia oxidation does not usually occur at values less than pH 7.0 [261], and the process electrolyte was buffered to pH 5.8, therefore it was unlikely to be a viable alternative metabolism for the bacteria. Du *et al.* recently reported that a coupling of metabolic pathways occurs between nitrifiers and cathodic bacteria in aerobic biocathodes [92]. However, given the lower pH used in this study, it

is unlikely to be the case here. Further investigations looking at improving the biocathode coulombic efficiency might examine the effect of pH to see if this induces community shifts and alters aerobic biocathode performance.

To examine the effect of solution pH on the aerobic biocathode performance, LSV were recorded for the two primary inoculated half-cells grown at -0.1 V poised potential (half-cells A and B) as the pH was increased from 6.1/6.2 to 7.3 to 8.5/8.6 in 2-3 day intervals. The LSV results for the two half-cells are presented in Figure 5.11, and Figure 5.11f gives the average solution pH and media changes for the two half-cells over time.

The LSV presented in Figures 5.11a and 5.11b show that increasing the solution pH on both half-cells caused the biocathode performance to decrease; the biologically catalysed onset potential for ORR became more negative, whilst the mass transfer limited reduction current decreased. This result is in agreement with the recent work by Strik *et al.*, who found that the optimal pH for oxygen reducing biocathodes is pH 5.0 [80]. For both half-cells (A and B), as the pH was increased from 6.1/6.2 to 7.3 to 8.5/8.6 in 2-3 day intervals, the average mass transfer limited reduction currents decreased from 42 ± 9 to 41 ± 4 to $10 \pm 5 \mu\text{Acm}^2$, whilst the ORR onset potentials decreased from 400 to 380 to 300 mV. These results therefore show a drop in electrochemical performance as the pH increases. The largest drop in performance occurred when the pH was increased from 7.3 to 8.5/8.6. An LSV in media buffered to 6.3 was recorded immediately after the LSV in media buffered at pH 8.5/8.6 for both cells, resulting in an instantaneous increase in both the mass transfer limited reduction current and ORR onset potential from 10 ± 5 to $22 \pm 4 \mu\text{Acm}^2$ and 0.30 to 0.40 V, respectively. These results are presented in Figures 5.11c and 5.11d.

The changes observed in the mass transfer limited reduction currents are related to either mass transport of H^+ and/or loss of bacteria catalysing the ORR reaction; as the solution pH is increased, the concentration of H^+ decreases which can create a H^+ mass transport limitation for the biofilm, but additionally, as the catalyst is biological, it may reduce the surface cell density of electrotophs if the pH is not optimal, particularly at the highest pH of 8.5/8.6. However, with regard to the latter, this would not explain the instantaneous increase in ORR mass transfer limited reduction current when the solution pH was decreased rapidly from 8.5/8.6 to 6.3 (shown in Figures 5.11c and 5.11d), as the surface cell density is unlikely to change significantly over a short time-scale of no more than 15 minutes. However, the mass transfer limited current did not return to its previous value of 42 ± 9 at the start of the experiment, which suggests some reduction in the surface density of electrotophs due to the high pH. The negative change in onset potential and OCP for the biologically catalysed ORR on increasing solution pH is associated with the thermodynamic potential of the overall reaction being catalysed at the electrode;

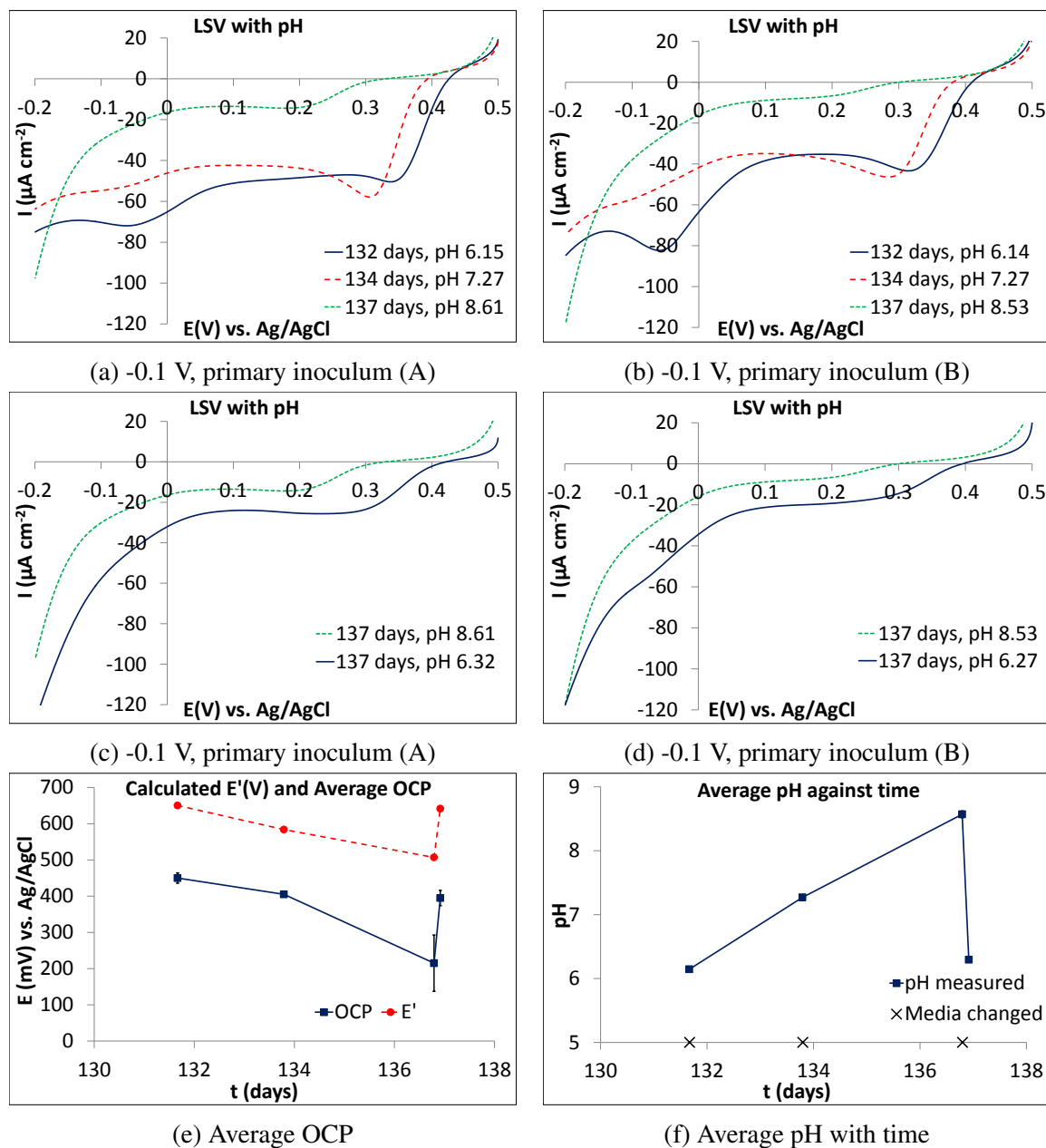


Figure 5.11: Performance of primary inoculated half-cells grown at -0.1 V poised potential (A and B) with changing solution pH. LSV curves taken at 2-3 day intervals at pH 6.1/6.2, 7.3 and 8.5/8.6 are presented in graphs (a) and (c) for both half-cells. LSV curves at pH 6.3 taken immediately after the LSV at pH 8.5/8.6 are presented in (b) and (d). The variation of average OCP and pH for both half-cells at 132, 134 and 137 days is presented in graphs (c) and (d) respectively. Media changes are indicated on graph (f).



Shifts in the OCP for each biocathode can be predicted from the Nernst equation (Chapter 3, Equation 3.2), which calculates the equilibrium potential for the ORR. Figure 5.11e gives the calculated equilibrium potential ($p\text{O}_2 = 0.2$) and the experimentally determined average OCP measurements at each pH, and shows how the two correlate. This shows that as the pH increases, the ORR reaction catalysed by the bacteria becomes less thermodynamically favourable.

5.3.3 The mechanism of electron transfer in aerobic biocathodes grown at -0.1 and +0.2 V poised-potential

In order to gain more insight into the mechanism of electron transfer occurring at the electrode surface, CV were recorded in the presence and absence of O_2 at the end of the experimental period for duplicate primary inoculated half-cells polarised at -0.1 V (A and B), secondary inoculated half-cells polarised at -0.1 V (E and F), and secondary inoculated half-cells polarised at +0.2 V (I and J). These spectra are presented in Figure 5.12. In the spectra for all half-cells, the reduction wave with $E_{\text{onset}} = +0.4$ V is removed by sparging under N_2 . Further comparison of the CV show how the half-cells polarised at -0.1 V still possess an oxidation peak at +0.2 V and a reduction peak at -0.1 V in their spectra, which form a reversible redox couple with an $E_{1/2}$ of +0.1 V. It must be noted that there were differences in the size of this reversible redox couple between half-cells A, B, E and F, shown in Figure 5.12. The differences in the size of this peak may be associated with the different ages of some of the reactors. For example, half-cells A and B had approximately double the operational period of half-cells E and F. Additionally, as the reactors were operated for such a long period, the communities may have diverged to some extent due to small variations in oxygen flow over long time periods. These differences in peak height could be associated with biofilm thickness/activity, as peak height size correlates with the difference in current between the forward and reverse sweeps of the CVs at +0.5 V, a proxy for electrode capacitance. It can also be seen from the CV through time for half-cells A and B, presented in Figures 5.2 and 5.3, that the current difference at +0.5 V increased. Assuming a DET mechanism, a possible explanation is that as the biofilms age, the electroactive bacteria become further enriched, and the density of cytochromes at the electrode surface increases, increasing the electrode capacitance. This would be analogous to the situation for biofilms of *Geobacter*, where a change in anode potential causes the oxidation/reduction of c-type cytochromes situated at the electrode surface, with the charge associated with these peaks termed pseudocapacitance [262].

In the absence of O_2 , the reversible redox peak must be associated with processes occurring at the electrode surface. As this reversible redox peak does not appear in the non-inoculated control polarised at -0.1 V (Figures 5.4b and 5.4d), it must be associated with activity of the biofilm, and is likely a bacterially produced electron mediator or reversible cytochrome interacting with the electrode surface, both of which would give a reversible peak. An ET component with a mid-point potential of +0.1 V is intermittent between an electrode potential of -0.1 V and the potential of O_2 of +0.67 V (pH 5.8, $pO_2 = 0.2$), allowing it to participate in an electron transfer chain between the two. As an electron mediator or cytochrome, it would exist in its reduced form at -0.1. Biocathodes polarised at +0.2 V do not exhibit an electron transfer component at +0.1 V in their non-turnover CV, which fits with the fact that it is not thermodynamically possible for such a component to participate in an electron transport chain between an electrode polarised at +0.2 V and O_2 with a potential of +0.67 V (pH 5.8, $pO_2 = 0.2$). For aerobic biocathodes poised at -0.1 V, the presence of an O_2 reduction wave at +0.4 V, and an electron transfer component with an $E_{1/2}$ of +0.1 V suggests the presence of two distinct mechanisms of electron transfer. A single O_2 reduction wave for aerobic biocathodes poised at +0.2 V suggests only one mechanism of electron transfer at this poised-potential.

To see whether this reversible redox couple with $E_{1/2}$ of +0.1 V present in the absence of O_2 for half-cells polarised at -0.1 V was surface absorbed or diffusive, CV were recorded in the absence of O_2 at different scan rates for a half-cell F, from $\nu = 1$ -100 mV/s. From these CV, the oxidation and reduction peak heights were plotted against ν and $\sqrt{\nu}$. This peak analysis for half-cell F is presented in Figure 5.13.

Peak analysis of both the oxidation and reduction peaks shows linearity in the plots of peak height versus $\sqrt{\nu}$ up to approximately 50 mV/s, as shown in Figures 5.13d and 5.13f. After this point, increasing ν causes any observed linearity to rapidly break down. This is likely due to an increasing contribution of non-faradaic capacitive currents as ν is increased. A linear trend in the peak height versus $\sqrt{\nu}$ usually implies that the reversible peak is diffusive, and is not confined to the surface of the electrode, as in the case of an electron shuttle (MET). However, there are other models which may also explain this behavior. For example, the current thinking for the bioanode bacterium *Geobacter sulfurreducens* is that it is able to use a network/chain of c-type cytochromes to shuttle electrons to the electrode surface [129]. Such a network may produce a diffusive-like peak response in the CV.

Given the evidence supporting a diffusive mechanism of ET, CV analysis of electrolyte and biofilm samples was performed in order to try and detect any potential diffusive redox shuttles, using special half-cells with carbon screen printed electrodes and small electrolyte volumes. These small, 1 ml volume, half-cells were entirely different to the large, 1 L volume,

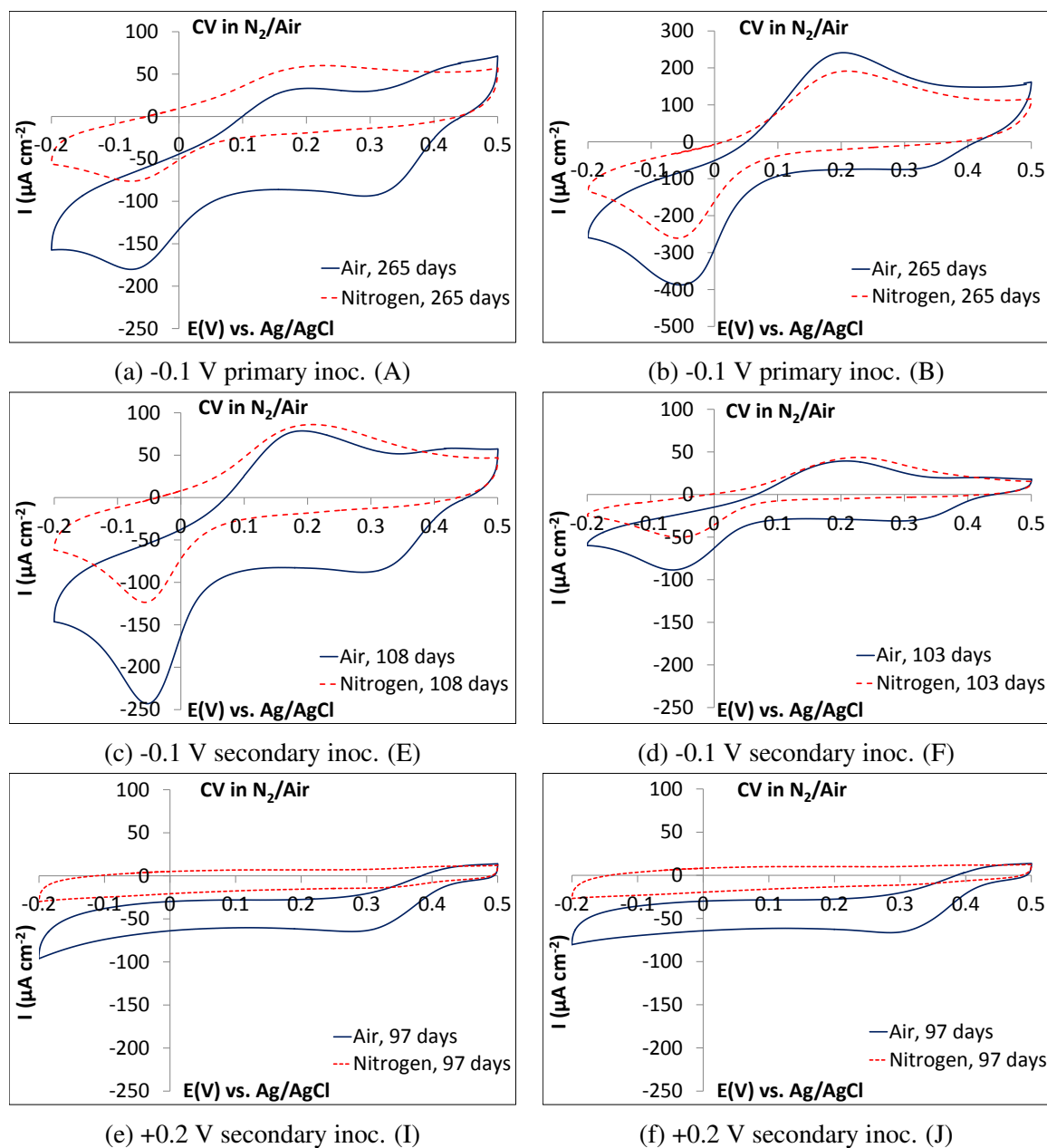


Figure 5.12: CV ($\nu = 5 \text{ mV/s}$) spectra recorded in the presence and absence of O_2 for primary (A and B) and secondary (E and F) inoculated half-cells poised at -0.1 V , and secondary inoculated half-cells poised at $+0.2 \text{ V}$ (I and J)

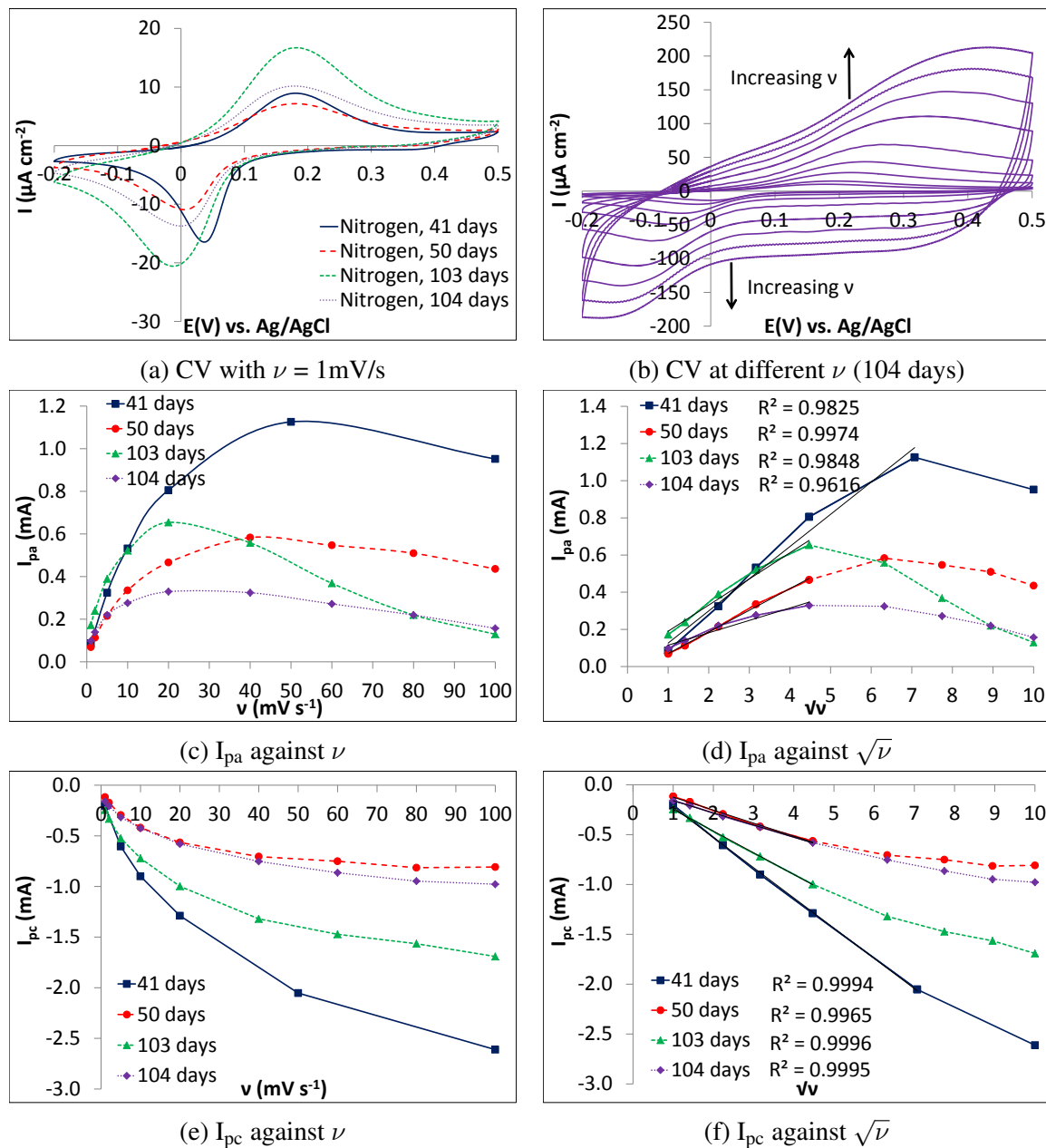


Figure 5.13: Peak analysis of the reversible redox couple with $E_{1/2} = +100\text{ mV}$ in the absence of oxygen for a secondary inoculated half-cell poised at -0.1 V (F) at 41, 50, 103 and 104 days with $\nu = 1\text{-}100\text{ mV/s}$. Graph (a) shows the reversible redox peak at $\nu = 1\text{ mV/s}$ on all occasions that the peak analysis was undertaken. Graph (b) shows the variation of the peak height with increasing ν at 104 days. Graphs (c) and (d) show the oxidation peak heights plotted against ν and $\sqrt{\nu}$, whilst graphs (e) and (f) show the reduction peak heights plotted against ν and $\sqrt{\nu}$.

half-cells used to cultivate the aerobic biocathodes (see materials and methods). CV on filtered samples of the electrolyte and carbon electrode bore samples taken from the primary (A and B) and secondary (E and F) inoculated half-cells polarised at -0.1 V are presented in Figure 5.14. The electrolyte and bore samples were filtered to remove bacteria, and the bore samples were prepared by vortexing a 1 cm diameter piece of the electrode and re-suspending in 1 ml of 1 M phosphate buffer.

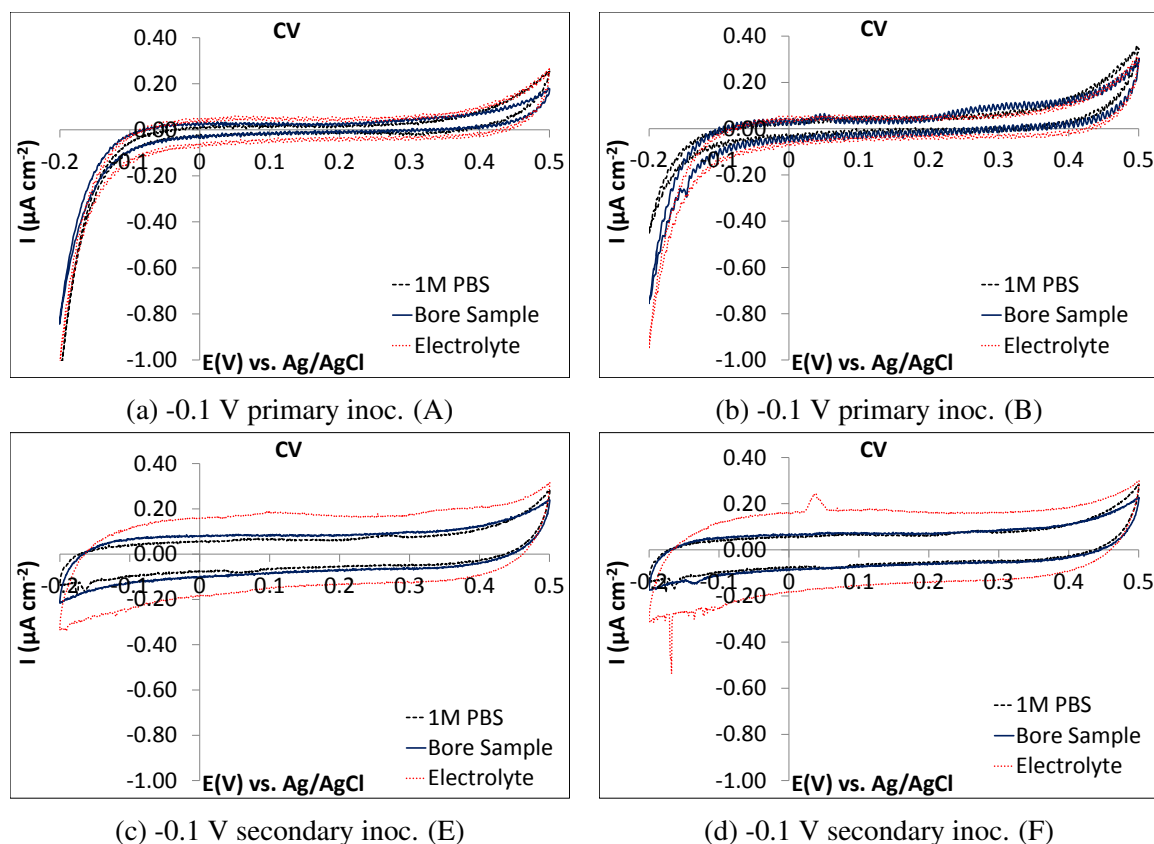


Figure 5.14: CV at $\nu = 5\text{mV/s}$ for electrolyte and bore samples taken from primary (A and B) and secondary (E and F) inoculated half-cells poised at -0.1 V at the end of their operational periods.

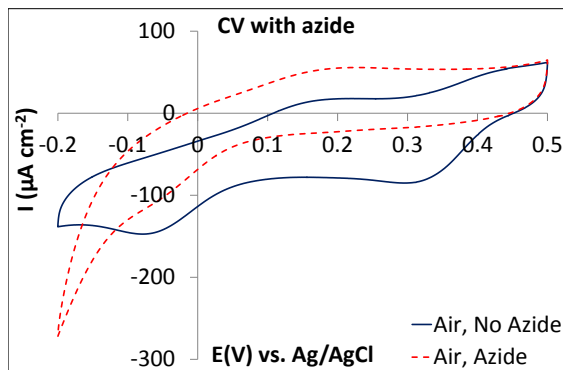
In the CV for the samples from all four half-cells, ORR occurs at -0.1 V, but this is the only feature observed in all of the CV. The electrolyte and bore sample spectra are identical to the 1M phosphate buffer controls, and do not show a redox peak at +0.1 V. This would suggest that if the diffusive redox peak present for the half-cells polarised at -0.1 V (Figure 5.12) is an electron shuttle, then it must not be present at sufficiently high concentrations to be detected, or it may be lost to absorption onto the filters used to remove bacteria. If there is no mediator in the biofilms, then coupled with the diffusive peak response, this would be consistent with a mechanism involving a network/chain of cytochromes which relay electrons from the electrode to the bacteria.

Features of the ORR current in the CV may be associated with ATP-producing, energy-

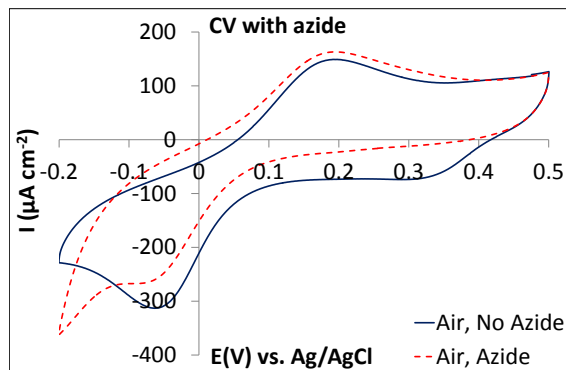
conserving reactions in the bacteria, or simply indirect catalysis by secreted metabolites. To link the ORR current observed in the CV to an electron transport chain and energy generation for the bacteria, azide inhibition was used. The bacterial electron transport chain in aerobes involves reduction of O_2 to water by electrons providing proton motive force which is used to generate ATP. This reaction is catalysed by cytochrome c oxidase, which accepts electrons from cytochrome c, and consists of two heme-containing cytochromes and two copper-containing centers [263, 264]. Sodium azide binds reversibly to the heme-containing cytochromes within cytochrome c oxidase [265], and therefore inhibits the enzyme and stops ATP generation occurring within the bacterial cell. Additionally, it is known to specifically inhibit Gram negative bacteria, so it has long been used as a means of distinguishing between Gram positive and Gram negative bacteria [265–267]. If biologically catalysed ORR by aerobic biocathodes is linked with ATP generation for the bacteria, then the current in CA and CV measurements should decrease considerably. This would imply that the bacteria use electrons derived from the electrode to reduce oxygen as part of an electron transport chain, generating ATP in the process.

The electrochemical response to the addition of azide for the half-cells polarised at -0.1 V (A and B), and half-cells polarised at $+0.2$ V (I and J) at the end of their operational periods is shown in Figure 5.15. All four half-cells, possess the biologically catalysed ORR wave with $E_{\text{ORR}} = +0.4$ V, in the presence of O_2 . When sodium azide is added to the half-cells and the solutions mixed, this biologically catalysed ORR wave is removed from the CV spectra. This proves that this biologically catalysed ORR wave is linked directly to bacterial ATP generation. In all 4 half-cells, the appearance of the abiotic ORR wave with the addition of azide is believed to be due to inhibition of the aerobic biocathode bacteria, allowing greater mass transfer of O_2 to the carbon surface.

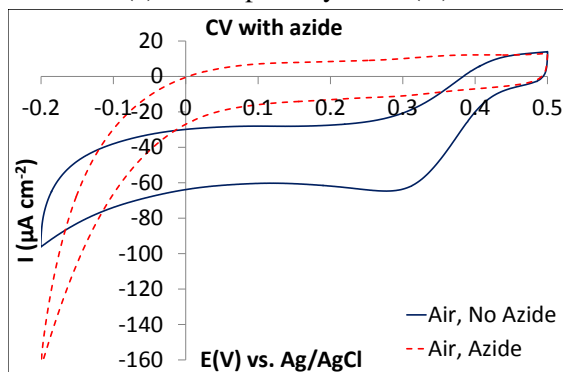
The electrochemical characterisation by CV of aerobic biocathode biofilms grown at -0.1 and $+0.2$ V poised-potential gives insight into the mechanisms of ET at the electrode surface. Turnover CV (CV recorded when substrate, O_2 , is present) show that both biocathodes possess an ORR wave with an onset potential of $+0.4$ V. However, the non-turnover CV (CV recorded when substrate, O_2 , is not present) show differences; no redox peaks are observed in the CV spectra for biocathodes poised at $+0.2$ V, whilst a reversible redox couple with an $E_{1/2}$ of $+0.1$ is observed for biocathodes polarised at -0.1 V. For biocathodes grown at -0.1 V, this suggests an additional pathway for ET not available at $+0.2$ V poised potential. Researchers have previously suggested that *Shewanella oneidensis* MR-1 uses MET at more negative poised-potentials, and switches to a DET mechanism as the potential is increased [268, 269], so shifts in ET mechanism are not unprecedented. The additional pathway reported here may involve a diffusive component, such as an electron mediator, although a chain/network of cytochromes may also give a diffusive-like peak response [129].



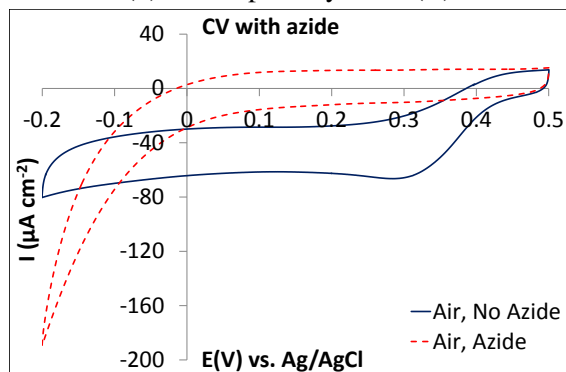
(a) -0.1 V primary inoc. (A)



(b) -0.1 V primary inoc. (B)



(c) +0.2 V secondary inoc. (I)



(d) +0.2 V secondary inoc. (J)

Figure 5.15: CV ($\nu = 5 \text{ mV/s}$) in the presence and absence of azide for primary inoculated half-cells polarised at -0.1 V (A and B), and secondary inoculated half-cells polarised at +0.2 V (I and J).

Given that no reversible redox peaks are detected at +0.4 V in the non-turnover CV, which is the potential of E_{onset} for the catalytic wave, this suggests that the mode of ET involving the catalytic wave at +0.4 V must be by some currently unidentified DET mechanism. Aerobic biocathodes grown at a poised-potential of -0.1 V then possess an additional ET pathway involving a reversible redox peak with an $E_{1/2} = +0.1$ V, not available to the bacteria at +0.2 V poised-potential. If this additional pathway is MET, an electron shuttle with a mid-point potential of +0.1 V could mediate electron transfer between the bacteria and the electrode polarised at -0.1 V. This may confer a competitive advantage for the bacteria as the kinetics of mediated-enzyme electrocatalysts improve as the potential difference between the enzyme (outer-membrane cytochrome) and the formal potential of the mediator increases due to an increased electron transfer driving force according to;

$$\Delta E_{\text{T}} = E_{0'enz} - E_{0'm} \quad (5.2)$$

Where $E_{0'enz}$ is the formal redox potential of the enzyme and $E_{0'm}$ is the formal redox potential of the mediator [270]. As the redox potential of the mediator is shifted further from the redox potential of the active site, the rate of enzyme-mediator electron transfer rate increases exponentially due to the increased driving force [271]. This would give the aerobic biocathode microbes an effective means of maximising the electron transfer rate between the electrode polarised at -0.1 V, by utilising a mediator with a mid-point potential which is close to the electrode poised-potential.

If the redox couple at +0.1 V is acting as an electron shuttle, it could be one of many different potential chemical species. Trace riboflavin is present in the biocathode medium but has a mid-point potential of -0.42 V on carbon electrodes at pH 7 [135], so could not be used to mediate electron transfer for these biofilms. However, flavin derivatives of riboflavin will have different mid-point potentials, and it is possible that the bacteria are therefore able to derive a suitable electron shuttle. As already discussed, quinones are known to be secreted by bacteria, but these compounds have also been shown to be used for MET in bacteria. In particular, Freguia *et al.* found that *Acinetobacter calcoaceticus*, a Gram negative bacterium from the Gammaproteobacteria, uses pyrroloquinoline quinone (PQQ) as a diffusive mediator to catalyse the ORR [123]. The use of mediators for electron transport has been widely reported for *Shewanella oneidensis* MR-1. This versatile species is reported to be able to utilise flavins [272], phenazines [134] and humic acids [132] to interact with outer-membrane decaheme cytochromes to facilitate electron transport to solid-phase electron acceptors.

Alternative explanations for the appearance of the peak with $E_{1/2} = +0.1$ V are that it is an enzyme or metabolite secreted metabolite which catalyses abiotic ORR, but which is other-

wise not involved in the electron transport chain of the electrothrophic bacteria. Freguia *et al.* discuss this as a possibility for quinones and heme-containing groups, which are known to be secreted by bacteria [123]. Quinones can catalyse the reduction of oxygen at cathode surfaces by auto-oxidising O_2 to O_2^- , which is then subsequently electrochemically reduced to H_2O_2 [123,273]. Heme-containing groups and free cytochromes may result from cell lysis on the cathode surface, [123], and catalase has also been reported to catalyse the ORR on glassy carbon electrodes [274]. However, these alternative indirect mechanisms would not account for the fact that the peak with $E_{1/2} = +0.1$ V is not present in the biocathodes polarised at +0.2 V poised-potential.

All biocathodes grown in this study possessed a biologically catalysed ORR wave with an onset potential of +0.4 V which is very likely to be coupled to ATP generation for the bacteria, given the electrochemical response to azide inhibition. Given the evidence for different ET pathways for the bacteria, these can be analysed in terms of the potential energy gain for the bacteria. If the component with an $E_{1/2}$ of +0.1 V is involved in electron transfer to the biofilm, analysis of the difference in potential between this and the formal potential for 4 electron ORR of +0.67 V (pH 5.8, $pO_2 = 0.2$) gives a potential difference of 0.57 V. All aerobic biocathodes in this study have an ORR wave with an onset potential of +0.40 V and an average OCP of +0.43 V. The difference between this and the formal potential for 4 electron ORR is +0.24 V. These potential energy differences can be equated to a Gibbs free energy changes according to the following equation [43];

$$\Delta G^{0'} = -nF\Delta E^{0'} \quad (5.3)$$

Where $\Delta E^{0'} = E_{electron\ acceptor}^{0'} - E_{electron\ donor}^{0'}$, $n = 4$ and $F = 96.48$ kJ/mol. If $\Delta E^{0'} = 0.24$ V, the $\Delta G^{0'}$ is -93 kJ/mol, whilst if $\Delta E^{0'} = 0.57$ V, the $\Delta G^{0'}$ value increases to -220 kJ/mol. The energy used to convert 1 mol of ATP to ADP is -30.5 kJ/mol [43], therefore 3 or 7 molecules of ATP can be generated by biocathode bacteria utilising 4 electrons at the electrode as part of an electron transport chain. This analysis shows how the electrode potential may be important in selecting for more efficient ET pathways to increase ATP yield for the bacteria, and how the bacteria may adapt their ET pathways to a different cathode potential. Non-turnover CV have previously been used to assess different poised-potentials in *Geobacter sulfurreducens* biofilms [140]. In this study, the authors found that the appearance of different redox peaks was dependent on the applied potential, which suggested that the bacteria were able to regulate their use of different ET pathways dependent on the applied potential. This may also be the case for aerobic biocathodes too, but further investigations on mixed communities and isolates are required first before these ET pathways can be fully understood.

5.3.4 Bacterial community analysis of aerobic biocathode biofilms grown at -0.1 and +0.2 V poised-potential

The quantity of biomass and community composition was determined for primary inoculated half-cells poised at -0.1 V (A and B), secondary inoculated half-cells poised at -0.1 V (E and F), secondary inoculated half-cells poised at +0.2 V (I and J), and two unpolarised control electrodes (CONT - community). The biomass data are presented in Table 5.4.

Half-cell	Operational parameters			Biomass		
	E_{poised} V	Inoc.	Op. time days	Centre $\mu\text{g}/\text{cm}^2$	Edge $\mu\text{g}/\text{cm}^2$	Average $\mu\text{g}/\text{cm}^2$
A	-0.1	prim.	266	106	115	111
B	-0.1	prim.	266	165	267	216
C	-0.1	secon.	47	-	-	-
D	-0.1	secon.	78	-	-	-
E	-0.1	secon.	115	42	62	52
F	-0.1	secon.	110	76	160	118
G	-0.1	secon.	96	-	-	-
H	-0.1	secon.	96	-	-	-
I	0.2	secon.	97	59	52	56
J	0.2	secon.	97	43	40	42
K	-0.1	secon.	20	-	-	-
L	-0.2	secon.	20	-	-	-
CONT - community	none	secon.	28	42	67	55
CONT - community	none	secon.	28	46	49	48

Table 5.4: Biomass data for the polarised/unpolarised half-cell communities. Operational parameters are also given.

Examination of the biomass data presented in Table 5.4 reveals a distinct trend with respect to the location of sampling. For the majority of the half-cells, the concentration at the edge is greater than that at the center. This is likely a geometric effect associated with an increased number of directions from which O_2 can diffuse to the biofilm near the edges in comparison to the center of the electrode, and it is likely that the current distribution is greatest near the edges than at the center. Therefore, variation in the distribution of biomass across individual electrodes was large, and there was no significant difference between the primary inoculated half-cells at -0.1 V (A and B), the secondary inoculated half-cells at -0.1 V (E and F), the secondary inoculated half-cells at +0.2 V (I and J), and the unpolarised control electrodes (CONT - community). In particular, biomass determination did not show a significant difference between polarised and non-polarised electrodes.

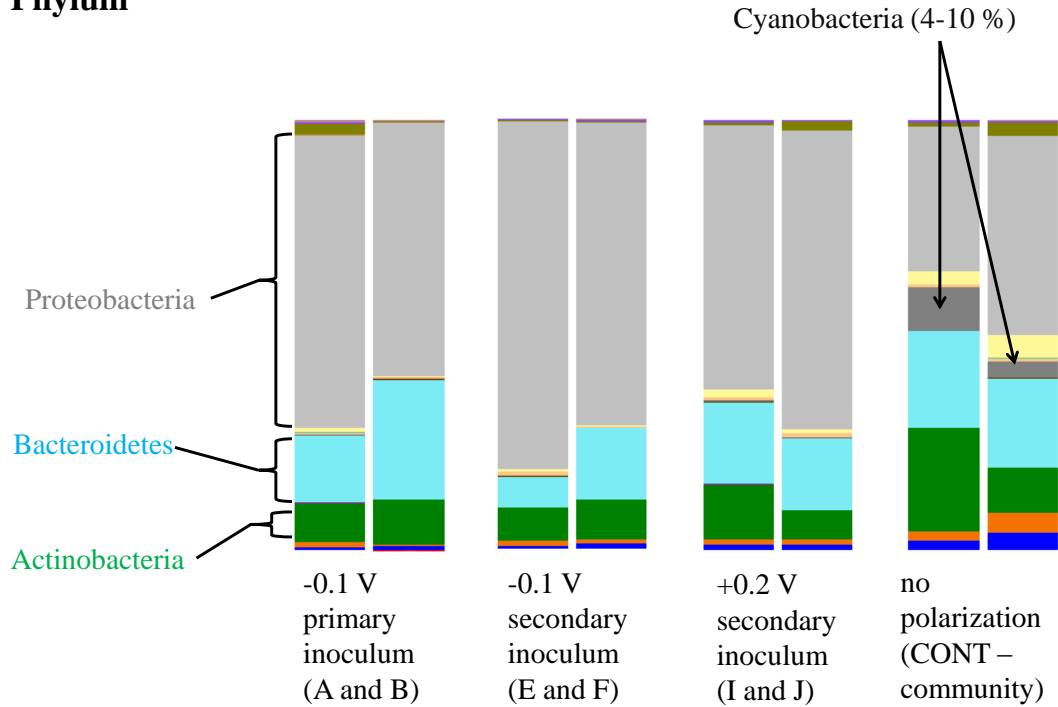
The aerobic biocathode communities were analysed on the working electrodes of the primary

inoculated half-cells at -0.1 V (A and B), the secondary inoculated half-cells at -0.1 V (E and F), the secondary inoculated half-cells at +0.2 V (I and J), and the unpolarised control electrodes (CONT - community). Sequences recovered from these different communities were clustered into operational taxonomic units (OTUs), and the number of sequences belonging to different taxonomic groups as a % of the total number of sequences for a given community were determined. The taxonomic groups were ranked according to phylum, class, order, family and genus, and these data are presented in stacked bar charts given in Figures 5.16, 5.17 and 5.18. The size of a section in an individual bar chart represents the total number of sequences, as a %, with a given taxonomic assignment for that community.

At the phylum level, all electrodes had differing proportions of *Proteobacteria*, *Bacteroidetes* and *Actinobacteria*. On all electrodes, the majority of sequences were *Proteobacteria*. The two control electrodes were the only electrodes to possess any *Cyanobacteria* (4-10 % of sequences). At the class level, the first major difference between the unpolarised electrode and the polarised electrodes was observed. The polarised electrodes possessed 43-65 % *Gammaproteobacteria*, whilst the unpolarised electrodes had between 3-11 %. The three other major classes of bacteria present on all 8 electrodes were the *Alphaproteobacteria*, *Saprospirae* and *Actinobacteria*. At the order level, the *Gammaproteobacteria* on the polarised electrodes could be further subdivided into unidentified *Gammaproteobacteria*, accounting for 23-44 %, and *Xanthomonadales* accounting for 6-20 % of the sequences. For the unpolarised electrodes, unidentified *Gammaproteobacteria* accounted for less than 1 % of the sequences, whilst 2-9 % were also identified as being *Xanthomonadales*. The other three significant contributors to the communities were *Rhizobiales*, *Saprospirales* and *Actinomycetes*. At the family level, the *Xanthomonadales* were further identified as *Xanthomonadaceae*, accounting for 6-20 % of the communities on the polarised electrodes, and 2-7 % on the unpolarised electrodes. The presence of *Xanthomonadaceae* in aerobic biocathodes has been observed previously, so these bacteria may have some involvement in ORR catalysis [76, 78, 106].

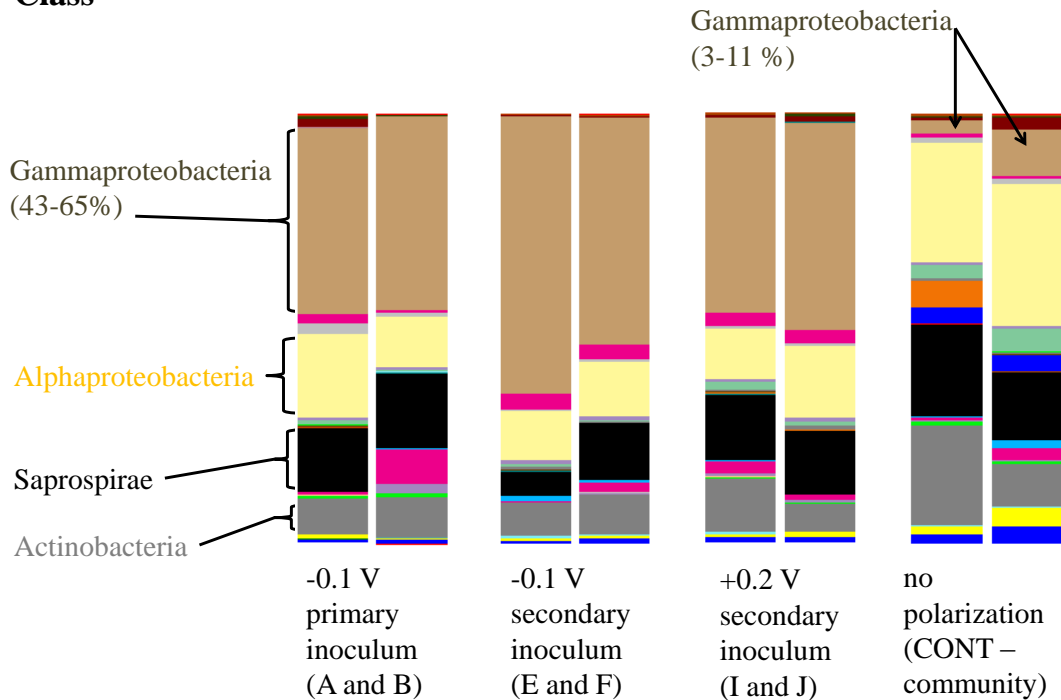
The highest level of identification was at the genus level, shown in Figure 5.18. At this level, it can be seen clearly that the polarised electrodes were dominated by sequences assigned as unidentified *Gammaproteobacteria*, which accounted for 23.3-44.3 % of their total sequences, whereas for the unpolarised electrodes, only 0.5-0.7 % of their total sequences were assigned as unidentified *Gammaproteobacteria*. These bacteria are likely to play an important part in the biologically catalysed ORR observed for the polarised electrodes in this study. Additionally, these sequences were identified as belonging to the *Gammaproteobacteria*, which are inhibited by azide as they are Gram-negative [265–267]. This is consistent with the earlier finding in this study that the ORR catalytic wave with E_{onset} of +0.4 V was removed with the addition of azide.

Phylum



(a)

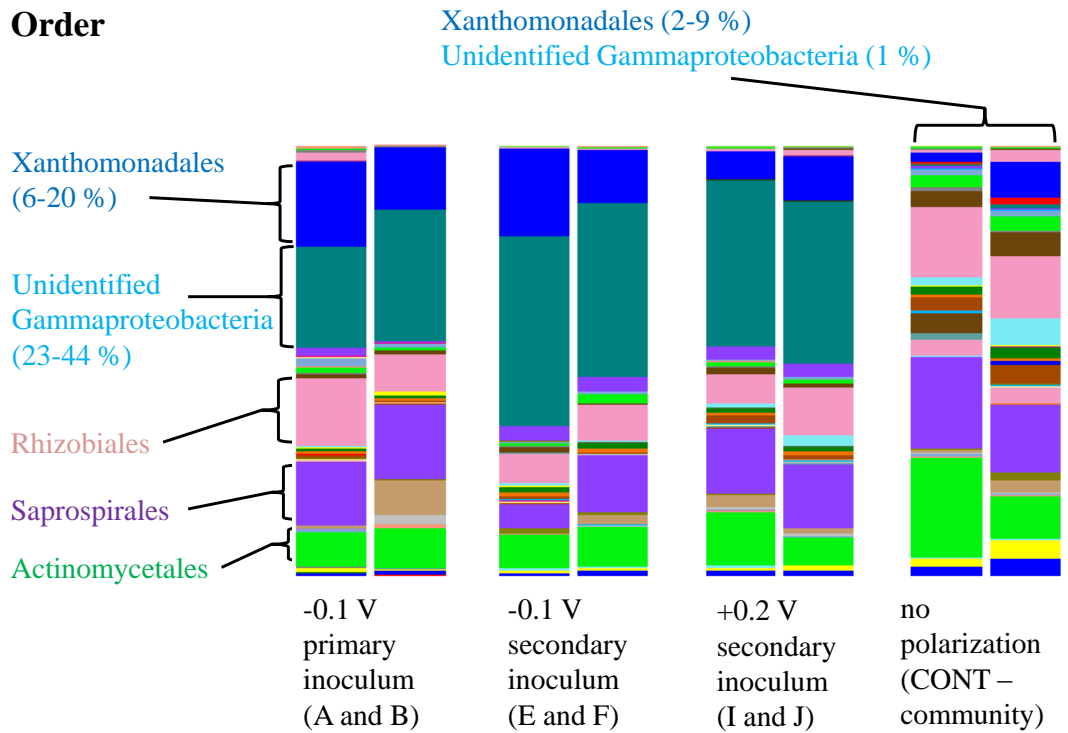
Class



(b)

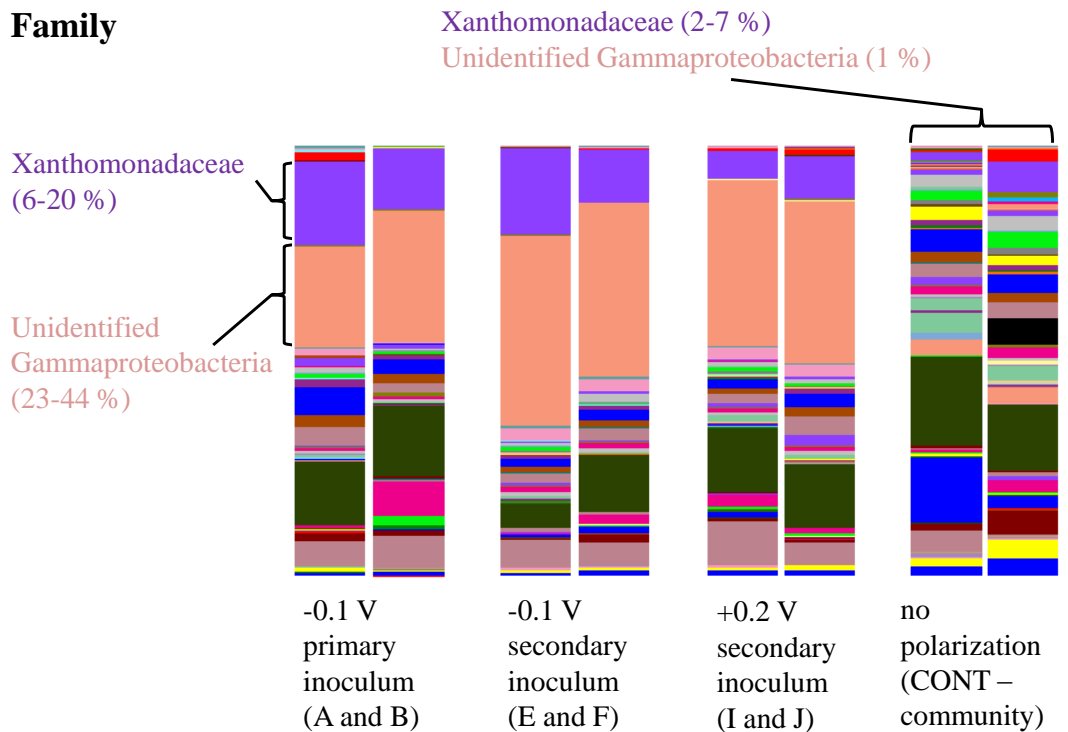
Figure 5.16: Stacked-bar chart giving the total number of sequences (%) for a particular taxon, classified according to phylum and class for the polarised/unpolarised half-cell communities.

Order



(a)

Family



(b)

Figure 5.17: Stacked-bar chart giving the total number of sequences (%) for a particular taxon, classified according to order and family for the polarised/unpolarised half-cell communities.

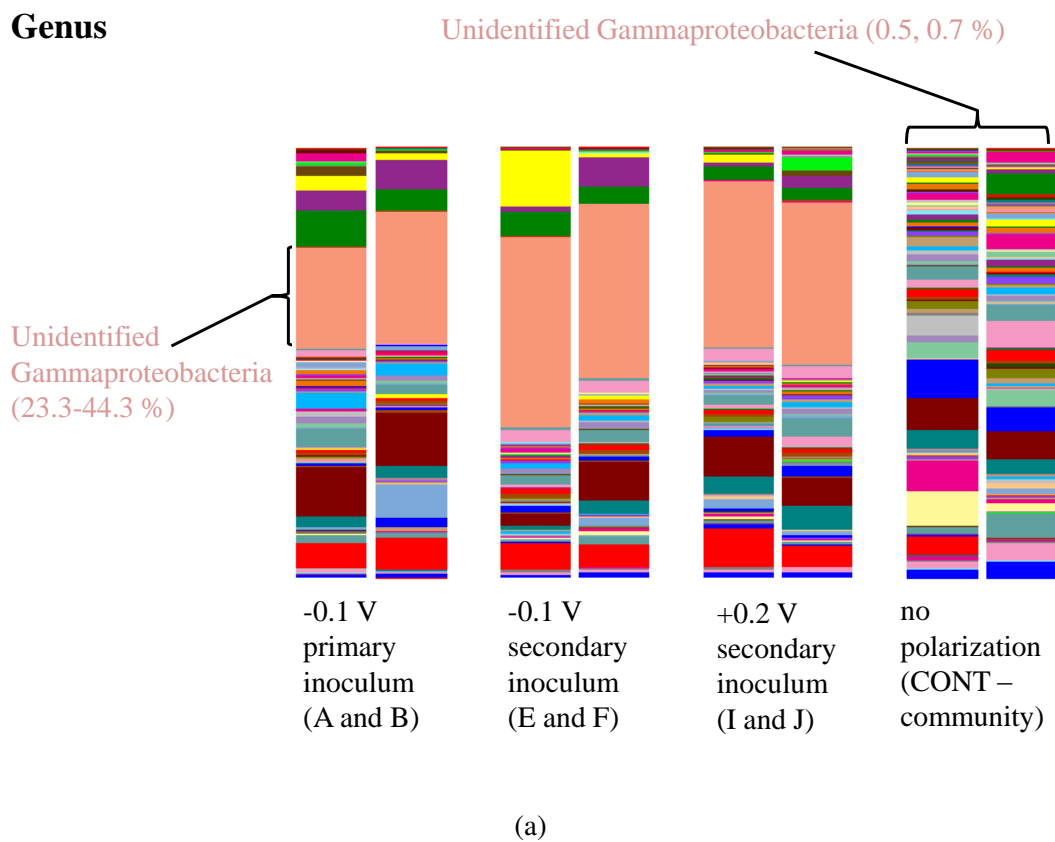


Figure 5.18: Stacked-bar chart giving the total number of sequences (%) for a particular taxon, classified according to genus for the polarised/unpolarised half-cell communities.

Of the sequences assigned as uncultured *Gammaproteobacteria* across all polarised communities, 56 % belonged to a single species-level OTU, 9 % belonging to the next largest, and 6 % to the next etc. The results from a BLAST search of the GenBank database revealed that the OTU containing 56 % of the sequences was 97 % similar to a clone assigned as *Alkalilimnicola* recovered at 3 % abundance from a poised-potential biocathode biofilm cultivated in a study from China [88]. For this biocathode, the E_{onset} for ORR was approximately +0.25 V for the biocathode, indicating a less efficient oxygen reduction catalysis, and this may have been associated with the low abundance, although it was not present in all of the biocathodes in that study, some of which exhibited higher currents. The OTU with 56 % of the uncultured *Gammaproteobacteria* was also 96 % similar to 3 unidentified *Gammaproteobacteria* clones isolated from bacterial communities in steel waste [275], and also 96 % similar to the dominant DGGE band of an aerobic biocathode grown on carbon felt with an E_{onset} for ORR of +0.35 V recovered from a freshwater sediment MFC *Schamphelaire2010*.

Principal coordinates analysis plots of weighted UniFrac beta diversity analysis of the different communities are presented in Figure 5.19. For the weighted beta diversity, 95 % of the total diversity could be explained by the first 4 axes from the principal coordinates analysis, with 65 % explained by the first axis, 15 % explained by the second, 8 % by the third and 7 % by the fourth. For graph 5.19a, which explains 70 % of the observed variation, the polarised half-cells cluster away from the non-polarised controls, and the half-cells polarised at +0.2 V form a subcluster. This result shows that polarised and non-polarised communities are distinct from one another. For graph 5.19b, which explains a further 15 % of the variation, the poised-potential half-cells remain clustered together, and the half-cells polarised at +0.2 V remain as a subcluster. For the weighted beta diversity, electrode polarisation had a very strong effect on the clustering of communities, with distinct clusters for polarised and unpolarised electrodes. Additionally, there was some subclustering of primary versus secondary inocula. Clusters based on poised-potential did not appear to form.

Principal coordinates analysis plots of unweighted UniFrac beta diversity of the different communities are also presented in Figure 5.19. For the unweighted analysis, 66 % of the variation is explained by the first 4 axes. For graph 5.19c, which explains 39 % of the observed variation, the communities cluster according to treatment. In particular, there was a big division between polarised and non-polarised electrodes along the primary axis, which accounted for 24 % of the variation. Primary and secondary inoculated polarised half-cells tended to cluster away from one another. For graph 5.19d, representing the next 27 % of variation, the secondary inoculated half-cells tended to cluster together according to poised-potential. When abundance of each OTU is not considered in unweighted beta diversity, underlying patterns appeared to exist, with half-cells clustering according to inoculum and poised-potential. Therefore, the poised-potential, inoculum-type, and whether the electrode

was polarised or not, appeared to matter in terms of which bacteria were present in the community.

5.4 Conclusions

The duplicate primary inoculated half-cells polarised at -0.1 V (half-cell A and B) took an average of 52 ± 6 days to enrich from activated sludge, and a large increase in CA reduction current from background reduction currents of less than $5 \mu\text{Acm}^2$ to values of 195 ± 95 and $212 \pm 64 \mu\text{Acm}^2$ was observed for A and B respectively. This was accompanied by the appearance of an ORR wave with an onset potential of +0.4 V in the CV spectra. The large increases in CA reduction current and E_{ORR} in the CV are believed to be due to the establishment of a biofilm of electrotrophic bacteria on the electrode which catalyse the ORR. A negligible CA current and CV lacking an ORR wave with an onset potential of +0.4 V were observed for a non-inoculated control half-cell. Polarisation of a secondary inoculated half-cell at -0.2 V did not form an aerobic biocathode, given that the CA reduction current was negligible and the CV was the same as for abiotic ORR on carbon felt. This is believed to be due to the formation of peroxide from the carbon support, which is detectable at a potential of -0.2 V. Given the presence of an O_2 reduction wave at +0.4 V, this sets a range for aerobic biocathode growth between -0.2 and +0.4 V poised potential. Imaging of a secondary inoculated half-cell polarised at -0.1 V, shows that the aerobic biocathode biofilm resides on the front face of the carbon felt, and is estimated to be no thicker than 1.0-1.5 mm, or 20-30 % of the electrode thickness (5 mm).

Comparison of the CA currents for duplicate primary inoculated half-cells poised at -0.1 V, secondary inoculated half-cells poised at -0.1 V and secondary inoculated half-cells poised at +0.2 V shows large variations in the CA reduction current and no discernible systematic trends between poised-potential. These variations are believed to be due to variations in O_2 mass transfer over time, which were shown to significantly impact the CA reduction current for a secondary inoculated half-cell poised at -0.1 V. Over a DO range from 7.5 to 8.0 mg/L, reduction currents range from 180 to $300 \mu\text{Acm}^2$, whilst in the absence of any aeration when the DO concentration was between 5.0 to 5.5 mg/L, the reduction current was found to be less than $50 \mu\text{Acm}^2$. Variations in O_2 mass transfer are likely to be the root cause of the large variations in average CA reduction currents and LSV mass transfer limited reduction currents for the primary inoculated half-cells at -0.1 V, secondary inoculated half-cells at -0.1 V and secondary inoculated half-cells at +0.2 V. These variations dominate over any differences in applied potential when the applied potential is in the O_2 mass transfer region of the LSV/CV.

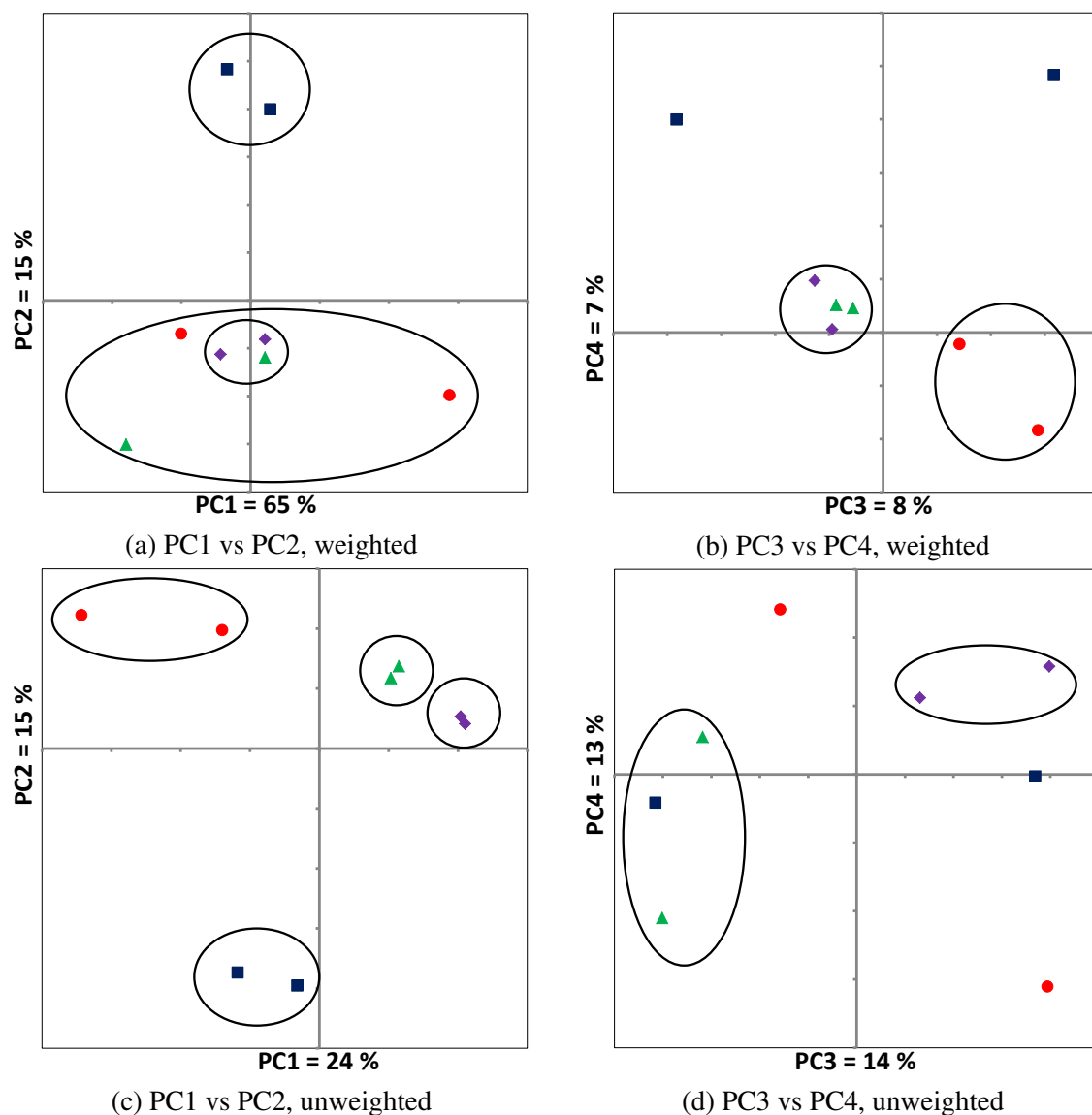


Figure 5.19: Principal coordinates analysis for weighted ((a) and (b)) and unweighted ((c) and (d)) beta diversity (UniFrac) for the 4 different treatments; non-polarised controls (blue squares), primary inoculated half-cells polarised at -0.1 V (red circles), secondary inoculated half-cells polarised at -0.1 V (green triangles), and secondary inoculated half-cells polarised at +0.2 V (purple diamonds). Graphs (a) and (b) show the first 4 axes representing 95 % of the variation for the weighted beta diversity, whilst graphs (c) and (d) show the first 4 axes representing 66 % of the variation for the unweighted beta diversity.

In addition to the O₂ mass transport limitation, the aerobic biocathode was also strongly affected by solution pH. As the solution pH is increased systematically from pH 6.2 to 8.6, the OCP, onset potential for ORR and the mass transfer limited reduction current all decrease significantly. The decrease in OCP and the onset potential for ORR can be rationalised in terms of the Nernst equilibrium, whilst the change in mass transfer limited current could be associated with a reduction in bacteria cell density or H⁺ mass transfer limitations into the biofilm.

Investigations of mechanisms using non-turnover CV at -0.1 and +0.2 V show the appearance of a unique redox peak ($E_{1/2} = +0.1$ V) for those biocathodes poised -0.1 V, and non-turn over CV with no discernible peaks or features for those biocathodes poised at +0.2 V. Biocathodes polarised at both -0.1 and +0.2 V both have a characteristic ORR wave with an onset potential of +0.4 V. These data are interpreted as an additional mechanism of ET in the biocathodes poised at -0.1 V, which is not present for aerobic biocathodes poised at +0.2 V. This shift in ET mechanism may be associated with increased energy gain from the electrode for the bacteria. The addition of azide removed the biologically catalysed ORR wave with E_{onset} of +0.4 V in all biocathodes, implying that this biologically catalysed wave is linked directly with ATP generation for the bacteria, and that the bacteria use electrons from the electrode directly for energy metabolism. A simple thermodynamic analysis shows that the biocathode bacteria can gain between 3 to 7 mols of ATP for every 4 e⁻ from the poised-potential cathode, dependent on whether they are able to utilise the additional energy available from the electrode poised at -0.1 V in comparison to +0.2 V. Coulombic efficiencies for four of the biocathode biofilms (half-cells G, H, I and J), were 52 ± 11 . Given the low pH, meaning that nitrification is not likely significant, this would indicate that a significant fraction of the electrons likely go aerobic biocathode biomass production.

Community analysis of polarised versus non-polarised biofilms shows that uncultured *Gammaproteobacteria* dominated the polarised electrodes at 23.3-44.3 % sequence abundance, but were present at only 0.5-0.7 % sequence abundance on the unpolarised control electrodes. This represents the most in-depth identification of the bacteria responsible for ORR catalysis in aerobic biocathode communities with an E_{onset} of +0.4 V. These bacteria were 96 % similar to the dominant DGGE band (assigned as *Proteobacteria*) of an aerobic biocathode grown on carbon felt with an E_{onset} for ORR of +0.35 V recovered from a freshwater sediment MFC [83], and they were 96 % similar to 3 unidentified *Gammaproteobacteria* clones isolated from bacterial communities in steel waste [275]. The latter is an indicator that the uncultured *Gammaproteobacteria* which are likely responsible for ORR catalysis in the aerobic biocathodes developed in this study, perform this catalysis as part of metal bio-corrosion processes in the natural environment.

These bacteria dominate on electrodes at both -0.1 and +0.2 poised-potential, and in both primary and secondary inoculated half-cells. Principal coordinates analysis of the beta diversity data shows that the communities cluster strongly according to whether the electrode was polarised or not. Additional clustering was also observed for treatment, indicating differences between poised-potential and inoculum.

Chapter 6. The Effect of Light on the Performance of Acetate-fed Microbial Fuel Cells

6.1 Introduction

At the heart of the MFC technology are the ARB at the bioanode which transfer electrons to the surface of the solid electrode. Electrogenic biofilms must compete with other anaerobic metabolisms, dependent on the substrates and electron acceptors available, and other growth conditions, such as temperature and available light. If light promotes anode respiration at the bioanode, or other anaerobic metabolisms not associated with power generation, then this will affect overall MFC performance. A variable, such as light, which may significantly affect bioanode performance, will therefore also significantly affect aerobic biocathode MFC performance with both a bioanode and biocathode. Light is an important variable to understand in MFC operation, as the degree of exposure of the anolyte to light can be easily controlled by modifying the design of the system.

Two studies in the literature have found an enhancement in the performance of mixed-community acetate-fed MFCs on exposure to light [152, 153]. Both studies suggested that this enhancement was due to the presence of anode respiring anoxygenic purple non-sulphur (PNS) bacteria [152, 153]. However, it is well-known that anoxygenic PNS bacteria are able to utilise light for the conversion of acetate into H_2 for energy/biomass under anaerobic conditions [154, 155]. This form of metabolism would therefore be competitive with anode respiration. Additionally, as carbon has no activity for H_2 oxidation [156], PNS using this metabolic pathway cannot contribute to overall power generation. Therefore, the presence of PNS bacteria at the anode may result in a lowering of MFC performance.

By monitoring the performance of acetate-fed batch MFCs in the presence and absence of an external light source, it is possible to build up a picture of the effect of light on bioanode performance. This information can be later used to make decisions regarding the operation of aerobic biocathode MFCs with both a bioanode and biocathode. Therefore, the purpose of this study was to gauge the effect of light on the MFC with just a bioanode, and to therefore

control this as a variable in later studies when the same MFC architecture, the H-cell, was operated with both a bioanode and biocathode.

6.2 Experimental

H-cell MFCs were operated in the presence and absence of an external light source, and characterised electrochemically at different points. To have a direct comparison with the work by Xing *et al.* and Cao *et al.* [152, 153], the experiments in this chapter used the same H-cell architecture with a similar anode volume (300 ml), the same substrate (acetate), a similar anode inoculum (domestic wastewater), and light source (incandescent light bulb). The H-cells used in this investigation were very similar to the H-cells used in later chapters, as illustrated in Figure 3.7, Chapter 3. Therefore, the results from this investigation can be used to make decisions regarding operation of the MFCs with aerobic biocathodes used in later chapters.

The H-cell architecture was chosen for this investigation, as this was the same cell architecture used to couple a pre-enriched bioanode to a pre-enriched biocathode in later chapters. The H-cell architecture is an available and established cell architecture, but suffers from high internal resistance as it is not an optimised cell geometry. Unfortunately, this means that the true MFC performance for the optimised system is not known (which would be important for scale-up), and studying other system variables becomes more difficult as the cell ohmic resistance becomes system-limiting. This cell architecture was chosen for the different MFC studies due to time constraints, as much effort went into developing an optimised aerobic biocathode. An optimised cell architecture would be the next stage of development for this MFC system, in order to examine feasibility of the system for scale-up. Additionally, the MFC system was run in batch mode at both anode and cathode, and not as a continuous flow system. This was due to a need to simplify the system and save time, as continuous flow systems are more complicated and time-consuming to operate than batch systems, and much effort had already gone into developing an optimised aerobic biocathode. Despite this, batch systems do provide insight into the factors which would affect the real-world continuous flow system.

Two studies were conducted to assess the impact of light on acetate-fed batch MFCs. The light exposure conditions for the MFCs in each of these studies is presented in Figure 6.1. In the first study, the impact of light on operational acetate-fed MFCs cultivated in the darkness was assessed (triplicate cells), whilst in the second study, the impact of light from the point of inoculation was assessed using a light and a dark cell (non-replicated cells). Limitations on experimental apparatus and time meant that it was not possible to operate triplicate (requiring

6 H-cell MFCs) or duplicate (requiring 4 H-cell MFCs) for the second study, and therefore data was recorded for only singlet MFCs.

Table 6.1: 1st and 2nd light studies with light exposure conditions for each of the MFCs

1st study (178 days)			
Time interval (days)	Cell A	Cell B	Cell C
0 to 20	Dark	Dark	Dark
20 to 59	Light	Light	Light
59 to end	Dark	Dark	Dark
2nd study (74 days)			
Time interval (days)	Light cell	Dark cell	
0 to 74	Light	Dark	

For the first study, three identical H-cell MFCs were setup, operated and characterised electrochemically, as described in Section 3.7 of Chapter 3. They were operated for 178 days. On startup, the anolytes were inoculated with 50 % by volume of domestic influent from a wastewater treatment plant (Tudhoe, UK), and the anode chambers covered in foil to eliminate light. From the beginning of the second cycle, at 20 days, the anodes were illuminated by positioning a 40 W lamp fitted with an incandescent light bulb next to the experiment and removing the foil. At 59 days, the beginning of the 4th cycle, the anode chambers were covered with foil again, and the lab light removed from the system in order to eliminate light from the experiments. All three MFCs were operated at room temperature and pressure. Coulombic efficiencies were calculated for all 3 cells by assuming complete acetate depletion at the end of a batch cycle [22].

For the second study, two identical H-cell MFCs were setup, operated and characterised electrochemically, as described in Section 3.7, Chapter 3. They were operated for 74 days. On startup, the anolytes were inoculated with 50 % by volume of domestic influent from a wastewater treatment plant (Tudhoe, UK). One of the MFCs was kept in the dark in a polystyrene box (dark cell), whilst the other was exposed to light from a 40 W lamp fitted with an incandescent light bulb (light cell). Both MFCs were operated at room temperature and pressure. Coulombic efficiencies were calculated by determining the acetate concentration at the end of a batch cycle.

For both the first and second studies, the temperature was not controlled or measured, which is important in order to rule out heat dissipation from the light bulb. This is a flaw in the experimental design, but could be corrected as part of future work.

6.3 Results and Discussion

6.3.1 *Electrochemical characterisation of three identical MFCs exposed to alternating light and dark conditions*

The cell voltage data of the 3 identical MFCs (MFCA, MFCB and MFCC) are given in Figure 6.1. Initial enrichment in the dark took between 10 and 15 days from domestic influent, and the first cycle for all 3 MFCs ended at 20 days. From the start of the second batch cycle, the MFCs were exposed to light from a lab light. During the 2nd cycle, the cell voltage was relatively stable and averaged approximately 100 mV for all 3 MFCs. Additionally, the 2nd batch cycle length varied between the 3 MFCs, in the order MFCA = 21 days, MFCB = 29 days and MFCC = 35 days. The differences in the 2nd batch cycle times were likely due to variation in proximity from the light source between the triplicate MFCs. The distances could have been made the same for all three MFCs by situating the light source above the MFCs arranged in a triangle formation, instead of positioning the light source on the desk adjacent to the MFCs. The 3rd batch cycle was a maintenance batch cycle, in order to allow all three MFCs to be fed together from the start of the 4th batch cycle, as the triplicate MFCs had run out of media at different times to one another at the end of their 2nd batch cycles (note that the 3rd batch cycle is not marked on Figure 6.1). From the start of the 4th batch cycle, the MFCs were exposed to dark conditions, and the average cell voltage increased considerably, as indicated in 6.1. The length of the 4th batch cycle for all 3 MFCs was at least 88 days, representing a large cycle length increase from the 2nd batch cycle.

Coulombic efficiencies for the triplicate acetate-fed batch MFC H-cells, MFCA, MFCB and MFCC, for their 2nd and 4th batch cycles are given in Table 6.2. From light conditions (batch cycle 2) to dark conditions (batch cycle 4), both the CE values and the cycle lengths increased across the triplicate H-cells. For the 2nd batch cycle, the CE values were 5.6-11.6 %, whereas for the 4th batch cycle, the CE values were 34.1-53.7 %, representing at least a 3-fold increase in the average % CE for the triplicate MFCs. For the 2nd batch cycle, the cycle lengths were 21-35 days, whereas for the 4th batch cycle, the cycle lengths were 88-119 days, representing an approximate 3 to 4-fold increase in the average cycle length for the triplicate MFCs. Variation in 4th batch cycle length may have been due to divergence between the MFC communities as the biofilms aged. For the 2nd batch cycle, there was a trend in the observed cycle length and CE values for the triplicate MFCs, with MFCC > MFCB > MFCA (35 > 29 > 21 days 2nd batch cycle length and 11.6 > 9.5 > 5.6 % CE values) which may have been due to variation in proximity from the light source (variation in light intensity).

Photos of the triplicate MFCs were taken at the beginning of the 2nd batch cycle at 20 days, and toward the end of the 2nd batch cycle at 40 days, and are presented in Figure 6.2. In both

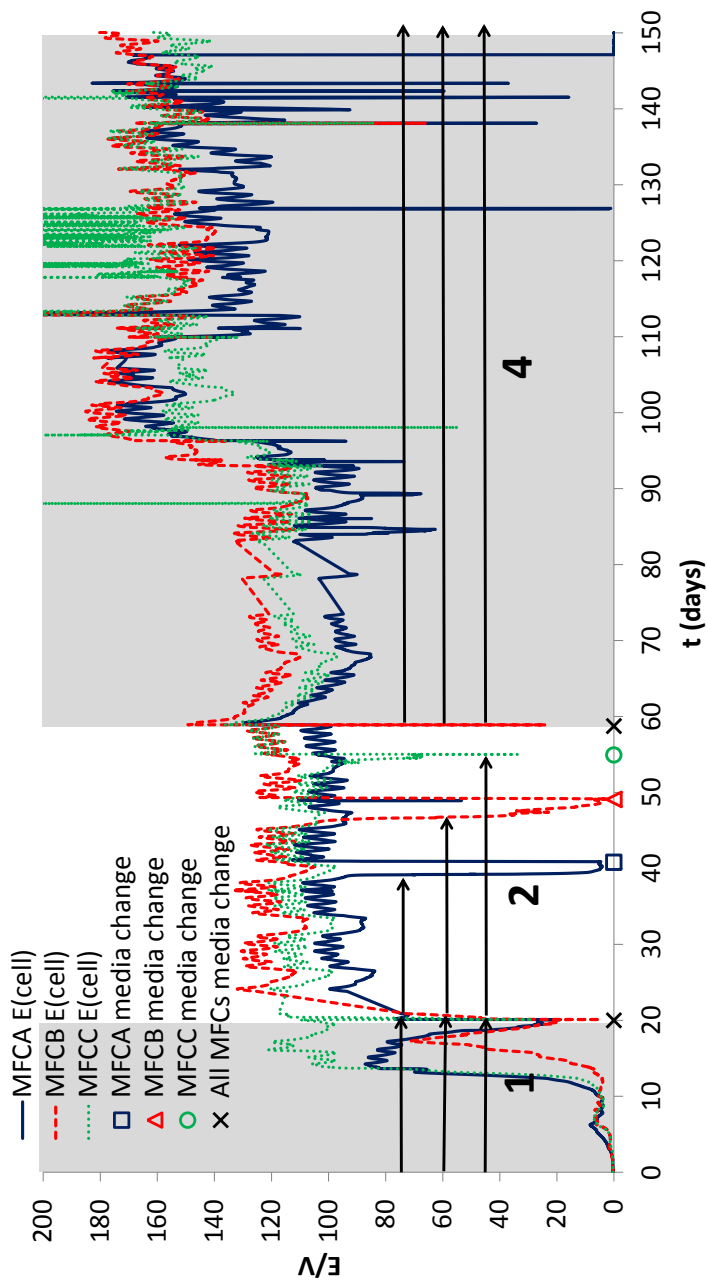


Figure 6.1: $E(\text{cell})/\text{mV}$ for $t = 0-150$ days for triplicate acetate-fed batch MFC H-cells, MFCA (solid line), MFCB (dashed line) and MFCC (dotted line). Media changes are indicated as symbols along the time axis for MFCA (square), MFCB (triangle), MFCC(circle) and for when the media was changed on all of the MFCs simultaneously (crosses). Batch cycle lengths and numbers are indicated on the graph with arrows. The shaded area indicates the period when the MFCs were kept in the dark, the light area indicates the period when all three MFCs were exposed to the lab light.

Cycle No.	MFCA			MFCB			MFCC		
	Cycle		CE %	Cycle		CE %	Cycle		CE %
	Interval days	Length days		Interval days	Length days		Interval days	Length days	
2	20-41	21	5.6	20-49	29	9.5	20-55	35	11.6
4	59-147	88	34.1	59-178	119	53.7	59-168	109	48.3

Table 6.2: Coulombic efficiencies of triplicate acetate-fed batch MFC H-cells (MFCA, MFCB and MFCC) for their 2nd and 4th batch cycles

photos, MFCA has been highlighted. What is observed is that the anolyte of the triplicate MFCs takes on a red color throughout the electrolyte, which is most apparent for MFCA. This change in color indicates the formation of planktonic cell mass which may have been the cause of the low CE values and shorter cycle times when comparing the 2nd batch cycle in the light to the 4th batch cycle in the dark for the triplicate MFCs. It is important to emphasise that differences in batch cycle lengths between the 2nd and 4th batch cycles for the triplicate MFCs were due to light exposure during the 2nd batch cycle, which depleted substrate at a faster rate because of proliferation of substrate-consuming bacteria in the anolyte which were not present during the 4th batch cycle. The observation of acetate-utilising planktonic cell mass in the triplicate MFCs during exposure to light is consistent with the shorter batch cycle lengths and CE values during the second batch cycle. This is because the planktonic cell mass must be utilising acetate without contributing to power generation.

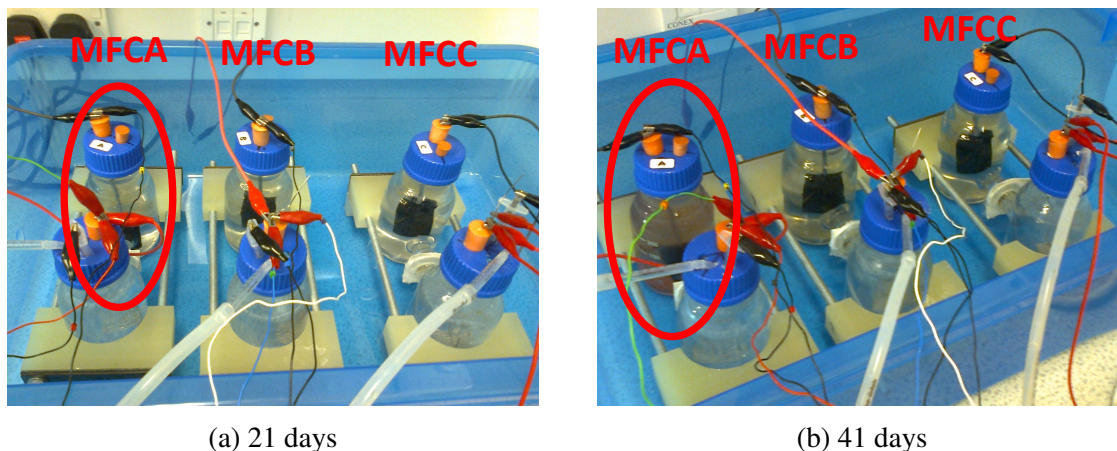


Figure 6.2: Photos of triplicate acetate-fed batch MFC H-cells (MFCA, MFCB and MFCC) during the 2nd batch cycle at 21 (a) and 41 (b) days of operation. MFCA has been highlighted with a red circle in both photos.

In addition to the lack of temperature control during this experiment, another possible source of error was that the biofilms may not have reached maturity at the end of their 1st batch cycle. Therefore, to further support the finding that light negatively impacts acetate-fed batch MFC

performance, a further, 2nd investigation was carried out to assess the impact of light from the point of inoculation. In this separate investigation, two identical acetate-fed batch MFCs were setup, with one exposed to light conditions, and the other exposed to dark conditions, from the point of inoculation ($t = 0$ days). The results from this study are discussed in the next section.

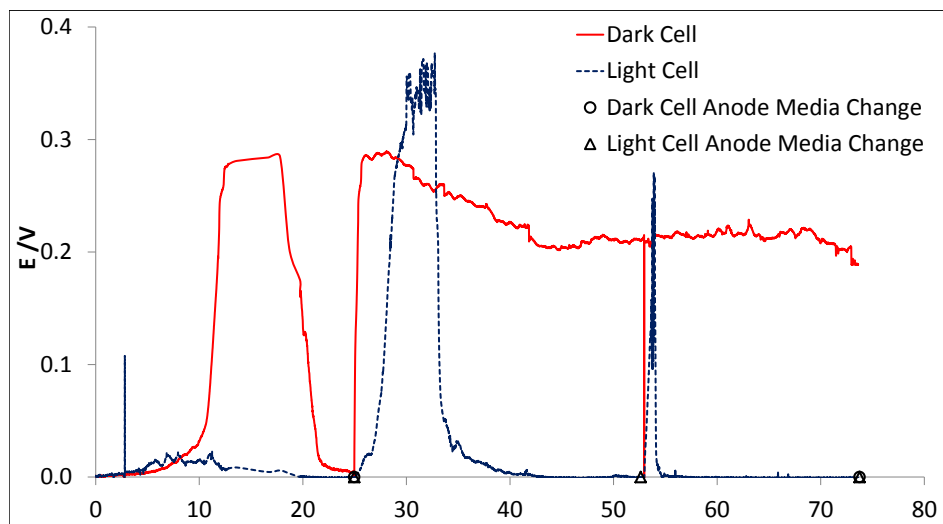
6.3.2 Electrochemical characterisation of an MFC kept in the dark and an identical MFC kept in the light

The cell voltage and anode potential data for two new acetate-fed batch MFC H-cells, one kept in the dark (dark cell), and one kept in the light (light cell), are presented in Figure 6.3a. In these graphs, the points at which the anode media were changed on both cells are indicated. For the dark cell, cycling in the cell voltage occurred normally as expected for an acetate-fed batch MFC system. For the first batch cycle, the cell voltage increased to 300 mV, plateaued, then decayed to less than 5 mV at the end of the cycle. For the second batch cycle, the cell voltage immediately increased back to 300 mV, then maintained average values between 200 and 300 mV over a 49 day period, before the cell was terminated at 76 days. The anolyte of the dark cell did not change color over the course of the operational period.

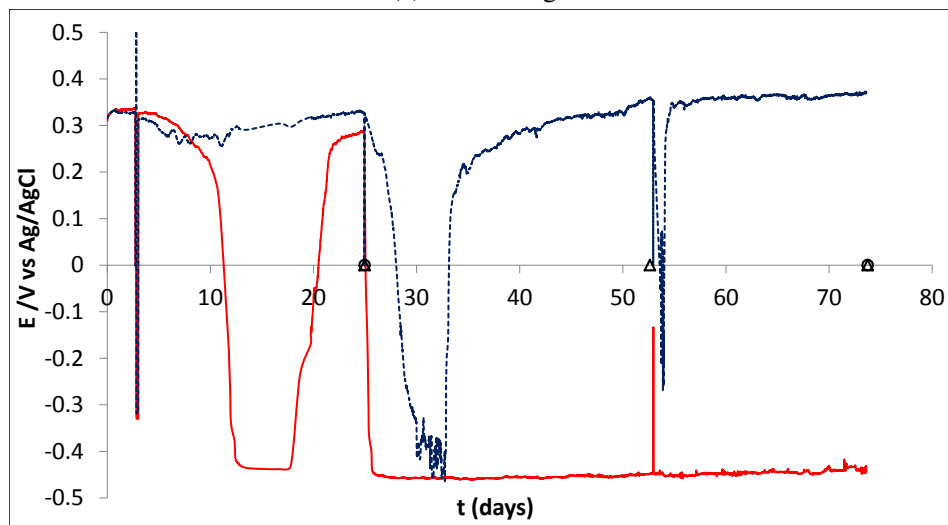
For the 1st batch cycle of the light cell, the cell voltage increased to a value of no more than 20 mV, before decaying to values less than 5 mV at the end of the cycle. At the beginning of the second batch cycle, the light cell exhibited a sudden increase in cell voltage to 350 mV, which lasted no more than 10 days, before decaying back to less than 5 mV for most of the second batch cycle. At the beginning of the third batch cycle, another voltage spike was observed of similar magnitude to that observed previously, but with a shorter duration of approximately 3 days, before the cell voltage again decayed back to less than 5 mV for most of the third batch cycle.

Batch cycles times were not the same for the light and the dark cell. This was caused by the different conditions for the two MFCs. The cell voltage decreased much more rapidly in the light cell due to light exposure, whilst the cell voltage did not do this for the dark cell. Figure 6.3a shows this difference. For the 1st batch cycle, the cell voltage decreases to zero in both MFCs before the media are changed, whilst during the 2nd batch cycle, the cell voltage decreases rapidly for the light cell, but is constant for the dark cell until the end of the experiment (74 days). This demonstrates how dynamic the system is, and how operation as a batch system is more difficult because the cells are not synchronised with each other.

Examination of the anode potential data for the light and dark cells presented in Figure 6.3b shows that the anode potential was the inverse of the cell voltage data for both cells, implying



(a) Cell voltage



(b) Anode potential

Figure 6.3: Cell voltage (a) and anode potentials (b) for two acetate-fed batch MFC H-cells, one kept in the dark (solid lines), one kept in the light (dashed lines). Anode media changes are indicated for the dark cell (circles) and the light cell (triangles).

that the cell voltage was controlled by the anode potential. Throughout most of the operational period for the dark cell, the anode potential was consistently low at -500 mV, whilst for the light cell, the anode potential was consistently high at +300 mV.

The CE values for the dark and light cells are presented in Table 6.3. The CE values for the dark cell were greater than those of the light cell. For the first cycle, the dark cell exhibited a CE value of 9 %, which was ten fold higher than that seen for the light cell which had a CE value of <1 %. The media were then changed in both MFCs for 3 g/L of sodium acetate. The CE value for the dark cell was then 40 % at the end of the second cycle, whilst the CE values for the 2nd and 3rd cycle for the light cell were both < 3 %.

Cycle No.	Dark Cell				Light Cell			
	Length days	[Ac] start mg/L	[Ac] end mg/L	CE %	Length days	[Ac] start mg/L	[Ac] end mg/L	CE %
1	25	1000	91	8.9	25	1000	166	0.6
2	49	3000	2092	39.0	28	3000	274	2.1
3	na	na	na	na	21	1000	101	0.4

Table 6.3: Coulombic efficiency values of different batch cycles for two acetate-fed batch MFC H-cells, one kept in the dark and one kept in the light.

These CE values strongly suggest depletion of acetate by processes occurring in the light cell which were not occurring in the dark cell. The second batch cycle length for the dark cell was 49 days at a minimum, as the cell was terminated at 49 days into the second batch cycle. At the point of termination, the concentration of acetate was 2092 mg/L, which was 2/3 of the original starting acetate concentration of 3 g/L. In contrast, the second batch cycle length for the light cell was 28 days. When the acetate concentration was measured at the end of the 2nd batch cycle for this cell, this was low at 274 mg/L, down from 3 g/L.

The polarisation curves, cathode LSV and anode LSV were taken for both the light and the dark cells at the end of their operational periods, and are shown in Figure 6.4. In Figure 6.4c, the peak power density normalised to anode surface area for the light cell was 1.4 $\mu\text{W}/\text{cm}^2$, whilst the peak power density for the dark cell was 4.2 $\mu\text{W}/\text{cm}^2$. Therefore, the dark cell had a peak power density which was 3-fold larger than that for the light cell.

Further electrochemical characterisation on individual electrodes was carried out on both cells at the end of their operational periods, which is shown in Figures 6.4a and 6.4b. The LSVs of the Pt-loaded carbon paper cathodes for both the light and dark cell overlap and have the same performance over the potential window, with a peak in the LSV reduction current observed at -240 $\mu\text{A}/\text{cm}^2$ for the dark cell cathode, and -256 $\mu\text{A}/\text{cm}^2$ for the light cell cathode, both at approximately +0.1 V peak position. These values are similar, implying

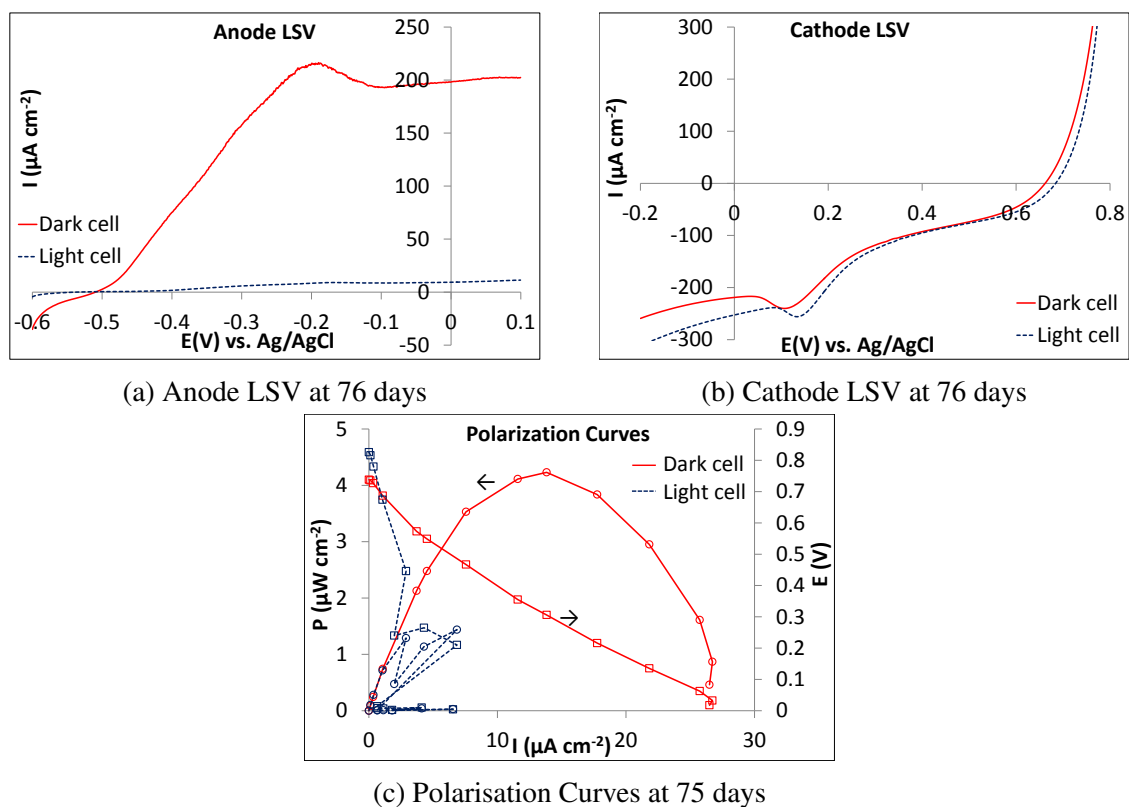


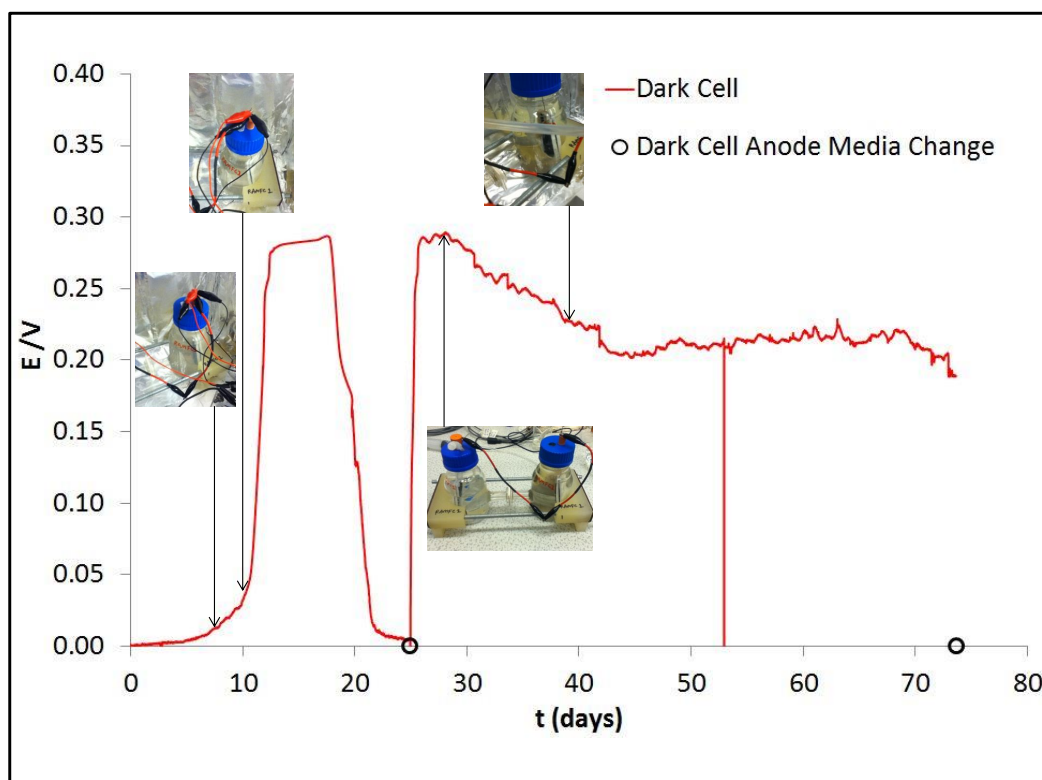
Figure 6.4: Anode LSV (a) and cathode LSV (b) and polarisation curves (c), for two acetate-fed batch MFC H-cells, one kept in the dark (solid lines) and one kept in the light (dashed lines).

similar cathode electrochemical activity at the end of the experimental period, and that any changes in overall MFC performance were not due to different cathode performances. In contrast to this, LSV on the light and dark cell bioanodes show clear differences in behaviour. For the dark cell bioanode, the peak bioanode current density was $216 \mu\text{A}/\text{cm}^2$, with a peak position of approximately $+0.2 \text{ V}$, whilst for the light cell, the peak bioanode current density was $11 \mu\text{A}/\text{cm}^2$. This corresponds to a 20-fold increase in peak bioanode current for the dark cell as compared to the light cell, implying significantly higher bioanode electrochemical activity for the dark cell as compared to the light cell.

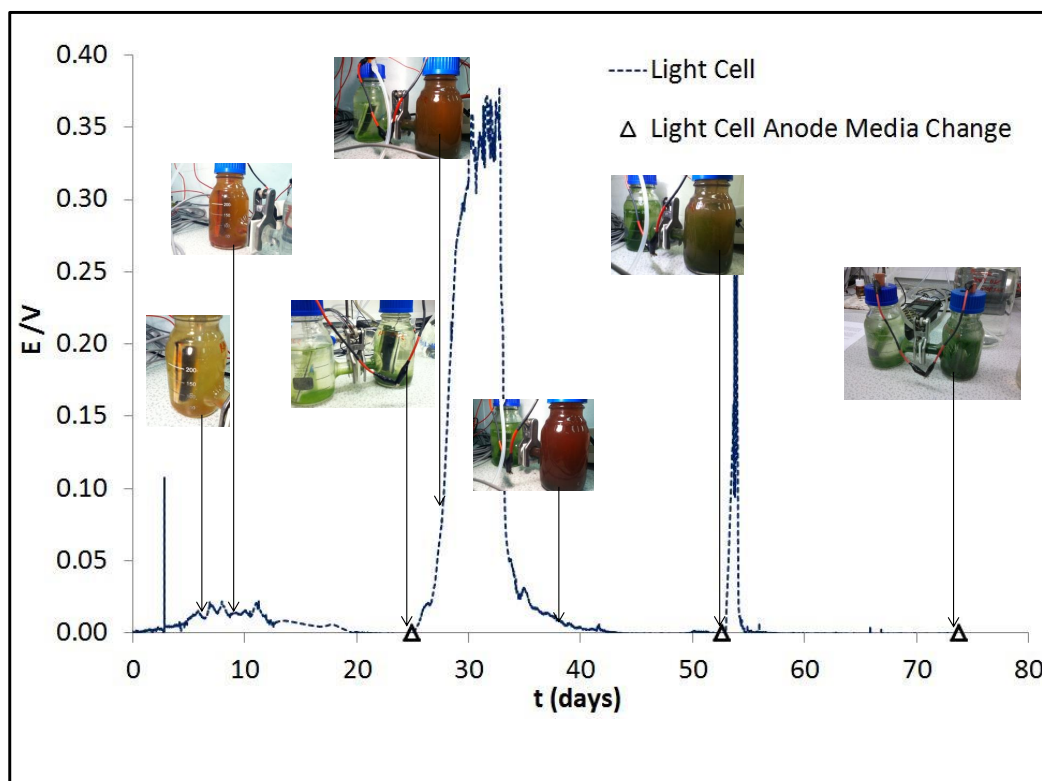
Combining the findings from the polarisation curves, cathode LSV and bioanode LSV for the dark and light cells, it is clear that the 3-fold higher peak power density for the dark cell in comparison to the light cell was caused by a 20-fold higher peak bioanode LSV current density for the dark cell as compared to the light cell, and not a change in cathode performance. Additionally, the dark cell had longer batch cycle times, higher coulombic efficiencies, and significantly higher cell voltage over most of the 76 day operational period.

Photos were taken of the dark and light cells at different points during their batch cycles, as shown in Figure 6.5a for the dark cell, and Figure 6.5b for the light cell. From Figure 6.5a, it can be seen clearly that the dark cell anolyte had no colour and did not change over the operational period, whilst from Figure 6.5b, the light cell anolyte had either a green or red colouring, which varied over the operational period. For the 2nd batch cycle of the light cell, the photos show that the anolyte took on a strong red colouration at the beginning of the batch cycle (27 and 39 days), and then a green colouration toward the end of the batch cycle (53 days). Additionally, the dissolved oxygen concentration of the dark and light cell anolytes were measured at the end of the cell operational periods, and were found to be 0 mg/L in both cases, indicating anaerobic conditions, and ruling out formation of oxygen producing algae at the anode in the case of the light cell. In the light cell, a pressure build-up was observed at 40 days which was not present in the dark cell, with anolyte seeping up through the rubber bung sealing the reactor, indicating the production of a gas with low solubility. The head space of the anolyte chambers of the MFCs was not analysed by gas chromatography, as this would have required a specialised collection vessel to have been attached to the anode chamber to collect the gas, which was not included as part of the experimental setup. When the experiment was designed, it was not known that an insoluble gas was going to be produced in the head space of the anode chamber. A gas collection vessel would be an important addition for future experiments.

It is likely that the significantly lower bioanode electrode performance for the light cell is linked to the proliferation of planktonic red/green cell mass at the anode electrode which is not present at the anode electrode of the dark cell. In this case, the gas with low solubility



(a) Dark cell



(b) Light cell

Figure 6.5: Cell voltage data with accompanying photos taken at different points during operation of two acetate-fed batch MFC H-cells, one kept in the dark (a), one kept in the light (b). Anode media changes are indicated for the dark cell (circles) and the light cell (triangles).

at the anode of the light cell may have been H₂, produced by planktonic PNS bacteria (red biomass) from the conversion of acetate using light [154]. The presence of green cell mass towards the end of the second batch cycle may then be explained as follows; as acetate is depleted by PNS bacteria and converted to H₂, green sulphur bacteria utilise the available H₂ and light and become dominant. Similar community shifts in phototrophic bacteria can be observed in the lab in a Winogradsky column [43].

This result is in disagreement with earlier work by Xing *et al.* and Cao *et al.* [152, 153]. In these papers, the authors suggest that light enhances the performance of acetate-fed batch MFCs inoculated from domestic influent, and identify PNS bacteria in the mixed community as the reason for this improvement in MFC performance.

For all MFCs in both studies, the temperature was not controlled or measured, which is important in order to rule out a heating effect from the light bulb. However, all MFCs were operated in a lab at room temperature (25 °C), and a warming effect from the incandescent light bulb on the cells exposed to light would likely have the effect of improving MFC performance, as MFC performance is optimal at temperatures above room temperature, between 32-35 °C [276, 277]. Assuming that heat dissipation from the light bulb did not cause an increase in anolyte temperature by more than 10 °C, then any heating effect would likely improve MFC performance, not significantly decrease performance, as observed in the two studies described here.

6.4 Conclusions

The acetate-utilising MFCs exposed to light in the studies discussed in this chapter show considerable reductions in performance in terms of cell voltage, anode potential, peak power density and coulombic efficiency in comparison to acetate-utilising MFCs not exposed to light. For the light/dark cell study, electrochemical characterisation revealed that the 3-fold lower peak power density for the light cell in comparison to the dark cell was due to a lower performing bioanode. Additionally, significantly lower coulombic efficiencies were observed for the dark cell as compared to the light cell. Photos of the light and dark cells show apparent proliferation of red/green planktonic cell mass in the anolyte of the light cell not present in the anolyte of the dark cell. This phototrophic biomass is likely the root cause of the lower performance of the light cell as compared to the dark cell. The performance data, CE data, and physical appearance of the MFCs therefore point to the conclusion that planktonic phototrophic cell mass competes with the ARB for available acetate substrate.

The formation of competing planktonic phototrophic organisms using both acetate and light for metabolism limits MFC performance and should be avoided by keeping MFCs away from

sources of light. From this study assessing the impact of light on the performance of acetate-fed batch MFCs, it is clear that acetate-fed batch MFC systems utilising an aerobic biocathode should not be exposed to external light sources. A light study on the MFC was included in this thesis, as it was found that light had a large negative effect on MFC performance. Variable exposure to light would have introduced an important hidden variable in aerobic biocathode MFC operation, making it more difficult to study the biocathode in the full MFC system.

Chapter 7. The Effect of External Resistance and Oxygen Mass Transfer on the Performance of Aerobic Biocathode Microbial Fuel Cells

7.1 Introduction

If aerobic biocathodes are to be used as a substitute for chemical cathodes, then their performance needs to be assessed in full MFC systems under different conditions. It is important to assess full MFC systems utilising biocathodes over time to determine system stability, performance criteria such as current, power, voltage and coulombic efficiency, as well as to identify important factors in order to understand and further improve the system. In the aerobic biocathode MFC, changing pH and external resistance may effect the performances of both bioanode and biocathode, which then impact MFC performance, and variation in cell ohmic resistance may also indicate changes occurring in the system due to changing electrolyte composition. Additionally, O₂ mass transport to the biocathode is predicted to play an important role in MFC performance, as indicated in half-cell studies with high-performing aerobic biocathodes [84, 85]. As the goal in an MFC is to minimise internal resistance, all of these factors must be considered together to further improve performance.

External resistance is known to have an effect on the performance of conventional MFCs [157–162]. For example, Rismani *et al.* compared performance of cellulose-fed MFCs at different resistances, and found that the MFCs at lower resistance out-performed those at higher resistance due to a shift in community composition in the MFCs away from fermentation toward anode respiration [162]. For external resistance studies on conventional acetate-fed batch MFCs [157–159], lower R_{ext} values tend to favour higher coulombic efficiencies, higher peak power, and better bioanode performance. This is likely due to a higher growth rate for the ARB when R_{ext} is lower, therefore increasing the density of ARB and the fraction of substrate which they use in comparison to parasitic processes.

For aerobic biocathode MFCs, it is anticipated that changing R_{ext} will exert an effect on both the bioanode and biocathode biofilms. Operation over higher R_{ext} should cause decreases in

coulombic efficiency, bioanode performance, and biocathode performance. This is because the current is reduced, which means a lower growth rate for both the bioanode and biocathode biofilms, and makes the electroactive bacteria at both electrodes less competitive with competing metabolic pathways, such as methanogenesis at the anode, and nitrification at the cathode. The effect of external resistance on an MFC with biological catalysts at both the anode and cathode has not previously been reported.

A further point of investigation is the effect of oxygen mass transport to the biocathode biofilm, which as seen in Chapter 5, has the potential to limit biocathode performance, and therefore MFC performance, and may be an important factor in the feasibility of this type of system for energy production. Finally, a comparison of the performance of the aerobic biocathode against that of a Pt cathode (a benchmark chemical catalyst) within the MFC will be useful in determining whether the aerobic biocathode is a realistic substitute for a chemical cathode in an MFC system. An additional comparison with an unmodified carbon cathode will illustrate the improvement in MFC performance due solely to the aerobic biocathode biofilm.

O₂ reducing biocathodes were incorporated into full MFC systems, and system response to different external loads was examined over a 63 day operational period. The effect of O₂ mass transfer at the cathode was then examined. Finally, MFC system performance with a carbon cathode, a Pt cathode, and an aerobic biocathode, all of equal geometric area, was assessed in order to evaluate the effect of the aerobic biocathode biofilm on MFC performance.

7.2 Experimental

The three MFC H-cells with bioanodes used in Chapter 6, were maintained and used again for this line of work. The H-cell architecture was chosen for this investigation, as it is an established and available cell architecture, but suffers from high internal resistance, and the MFCs were operated in batch mode at both the anode and cathode, in order to simplify MFC operation. An optimised cell geometry, and continuous flow at both bioanode and biocathode, would have been preferable for reasons already discussed, but were not adopted due to time constraints, as much effort had gone into developing an optimised aerobic biocathode biofilm. Limitations on experimental apparatus, limitations on the number of pre-enriched bioanodes/biocathodes, the time which experiments took to complete, the dynamic nature of the biological systems, and the labour in maintaining/analysing the reactors, also meant that it was not possible to operate duplicate or triplicate MFCs in parallel (9 or 6 MFCs, respectively), and therefore data was recorded for singlet MFCs only (3 MFCs). Replication is preferable for biological systems, so that the data is statistically significant, but was not

possible in this study, due to the constraints discussed above.

All three MFCs were maintained at room temperature and pressure, and the bioanodes were assessed by LSV at the beginning of the study (0 days) to confirm identical performance. Three half-cell pre-enriched aerobic biocathodes grown at -0.1 V were used as the biocathodes for this study, as described in materials and methods. The cathode medium was buffered to pH 5.8, whilst the anode medium was buffered to pH 7.0, and contained 1 g/L of sodium acetate, as described in materials and methods.

For the external resistance study, the three cells were operated at different resistances; 100 Ω , 1000 Ω and 5480 Ω to examine the effect of external resistance on MFC performance over a 63 day operational period. These resistances were chosen on the basis of covering a broad range in external resistance. Resistances of 100, 1000 and 10000 Ω have been found previously to give peak current densities with an order of magnitude difference for conventional MFC H-cells [161]. When the cell voltage dropped to zero in one of the cells, the media were changed on all 3 cells. The acetate concentration was determined on the spent anolyte medium by total organic carbon (TOC) analysis in order to calculate the coulombic efficiency for that batch cycle. Catholyte pH measurements were taken at regular 1-2 day intervals, and anolyte pH measurements were taken at the beginning and end of different batch cycles. MFC polarisation curves and EIS were recorded as described in materials and methods, and EIS were recorded directly after taking the polarisation curve. Polarisation resistances were calculated as described in materials and methods. Bioanode LSV and biocathode LSV were recorded as described in materials and methods. Replication in the electrochemical measurements through time was carried out for the three singlet MFC H-cells.

After the external resistance study, an experiment was performed on the MFC previously operated at 100 Ω external resistance, at peak power for this cell ($R_{ext} = 510 \Omega$, at 518 days of continuous operation for this cell. This was the resistor giving peak power for this MFC, connected at all idle times.) to assess the effect of O_2 mass transfer on aerobic biocathode MFC performance. In this experiment, the rate of O_2 mass transfer to the aerobic biocathode was varied over a period of 100 minutes, by changing the flow rate of air into the catholyte chamber by adjusting a connected flow rate valve. During this period, the cell voltage and cathode potential were measured continuously at 10 second intervals, and the catholyte DO measured continuously at 30 second intervals, using a calibrated DO probe inserted into the catholyte. This test was carried out on an operational aerobic biocathode MFC, and not replicated with the same aerobic biocathode MFC, or using another aerobic biocathode MFC, due to the time taken to perform the test.

After the external resistance study, an experiment was performed on the MFC previously operated at 5480 Ω external resistance, at peak power for this cell ($R_{ext} = 510 \Omega$, at 624-626 days

of continuous operation for this cell. This was the resistor giving peak power for this MFC, connected at all idle times.), in order to compare performance of the MFC with a biocathode, Pt cathode (0.57 mg/cm^2 Pt loading) and a carbon cathode, all with the same geometric area. Both the anolyte and catholyte were buffered to pH 7.0 using fresh bioanode and biocathode media before recording the polarisation curves. This test was carried out on an operational aerobic biocathode MFC, and not replicated with the same aerobic biocathode MFC, or using another aerobic biocathode MFC, due to the time taken to perform the test.

Within 12 hours of the end of the MFC polarisation curve, the biocathode electrode was transferred into a fresh biocathode medium in an external, H-cell fitted with a Pt mesh CE (35 cm^2). Potential step voltammetry was then carried out from +0.5 to -0.2 V at 0.1 V intervals of ten minutes each, in the presence of air sparging ($\text{DO} > 7.5 \text{ mg/L}$). Potential step voltammetry runs under the same conditions were also carried out using the Pt cathode and the carbon cathode.

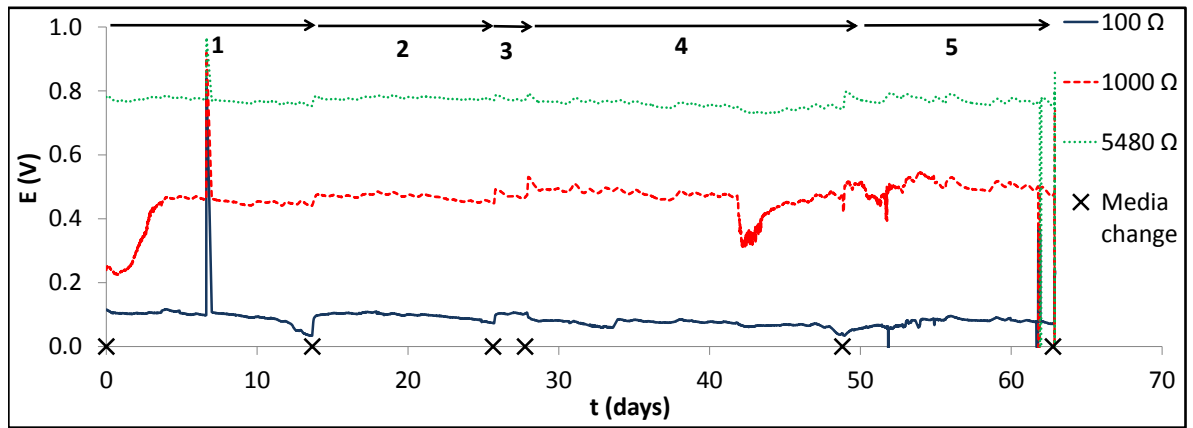
7.3 Results and Discussion

7.3.1 *The effect of external resistance*

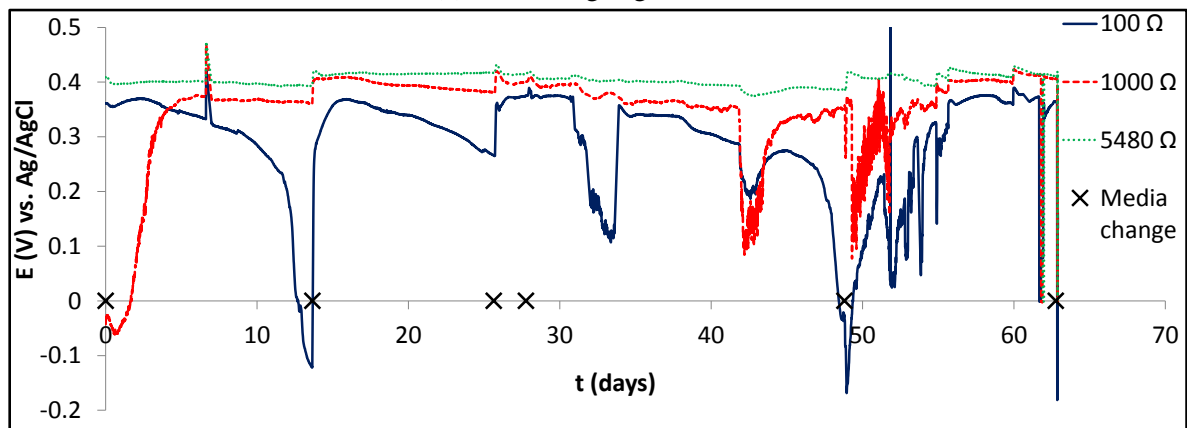
The cell voltage, cathode potential and pH over the experimental period with the acetate-fed batch biocathode MFCs over different resistances are given in Figure 7.1. The cell voltage for the 100Ω cell averaged 80 mV ($66 \mu\text{A/cm}^2$), the 1000Ω cell averaged 460 mV ($38 \mu\text{A/cm}^2$) whilst the 5480Ω cell averaged 770 mV ($12 \mu\text{A/cm}^2$). Therefore, the observed currents for the three MFCs, 100Ω , 1000Ω and 5480Ω , varied in the ratio 5.5:3.2:1.0, respectively.

The same order was also observed in the magnitude of cathode and anode pH changes for the first batch cycle of the three cells, 100Ω , 1000Ω and 5480Ω ; the cathode pH increases were 2.58 pH units, 0.98 pH units and 0.53 pH units respectively, whilst the anode pH decreases were 1.12 pH units, 0.48 pH units and 0.16 pH units respectively. Therefore, the lowest resistance 100Ω cell with the highest current had the highest pH increase at the cathode and pH decrease at the anode, whilst the highest resistance 5480Ω cell with the lowest current had the smallest pH increase at the cathode and pH decrease at the anode, and shows that the extent of pH splitting in the dual chamber MFC increases as the current flowing through the MFC increases. This pattern of pH splitting repeated itself for each new cycle. pH splitting is a result of the transfer of ions in the electrolyte other than H^+ and OH^- through the membrane, and is a process which is accelerated as the ionic flow through the membrane increases.

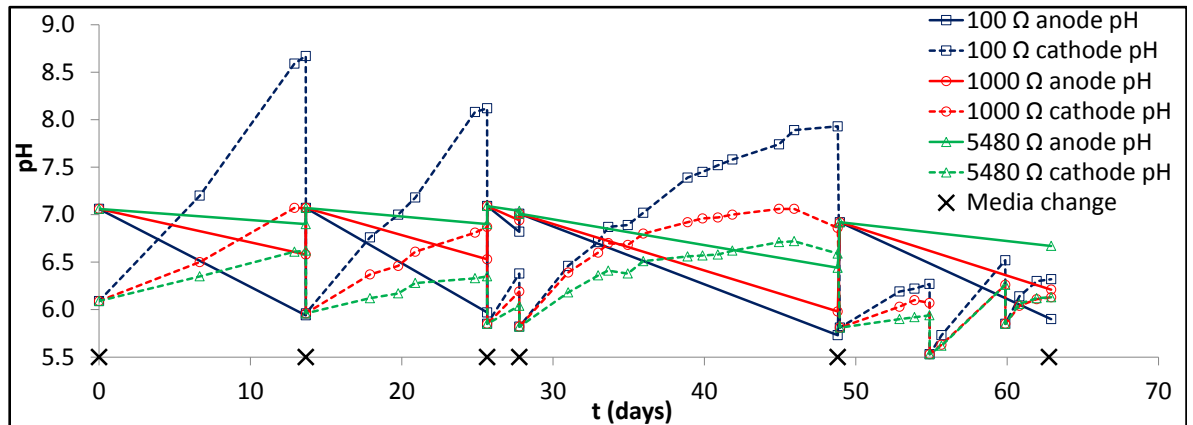
The increased pH splitting at higher current is likely associated with the marked drop in cathode potential from 409 to -121 mV during the first batch cycle for the MFC at 100Ω . A



(a) Cell voltage against time



(b) Cathode potential against time



(c) Cathode and anode pH against time

Figure 7.1: Cell voltage against time (a), cathode potential against time (b), and cathode and anode pH against time (c), for the three cells at 100 Ω , 1000 Ω and 5480 Ω , for $t = 0$ -63 days of cell operation. For the cell voltage (a) and cathode potential (b) graphs, 100 Ω = solid line, 1000 Ω = dashed line and 5480 Ω = dotted line. For the pH graph (c), anode pH = solid lines, cathode pH = dashed lines, 100 Ω = square, 1000 Ω = circle and 5480 Ω = triangle. Media changes are indicated on graphs (a) to (c) (crosses), and batch cycle numbers with cycle lengths are indicated in graph (a).

significant increase in pH splitting at higher current likely causes changes in MFC ohmic resistance and a reduction in both biocathode and bioanode performance. Significant increases in pH were shown to degrade aerobic biocathode performance in Chapter 5, and a decreasing anode pH is also predicted to cause bioanode performance losses.

For batch cycles 4 and 5 for the 3 cells, the coulombic efficiency values are presented in Table 7.1. These values varied depending on the MFC external resistance. The average CE for the cell at 100 Ω was 60 ± 7 %, the average CE for the cell at 1000 Ω was 7 ± 0 %, and the average CE for the cell at 5480 Ω was 3 ± 0 %, giving a ratio of 20:2.3:1, respectively. This ratio of CE values is of the same order as the MFC current, which is dependent on the rate of oxidation of acetate by the anode biofilm.

Cycle No.	Cycle Length Days	Cell at 100 Ω	Cell at 1000 Ω	Cell at 5480 Ω
		CE %	CE %	CE %
4	21	54.6	6.6	2.8
5	14	64.7	7.1	3.4
Average		60 ± 7	7 ± 0	3 ± 0

Table 7.1: Coulombic efficiencies for cycles 4 and 5 for all three cells at 100 Ω , 1000 Ω , and 5480 Ω . The average of both cycles has been calculated with the standard deviation.

If the rate of oxidation of acetate by the anode biofilm is altered by changing the external resistance, then this will change the coulombic efficiency as competing processes occurring within the MFC anolyte which are not dependent on the external resistance are likely to occur at similar rates across all three cells. These competing processes may be antagonistic metabolisms at the anode, such as methanogenesis and heterotrophic metabolism fed by membrane O_2 cross-over from the cathode. When the external resistance is high, these processes use proportionally more of the acetate leading to lower MFC coulombic efficiencies. These CE results are in agreement with the work previously reported by Ren *et al.* using normal acetate-fed batch MFCs [158]. The authors of this study determined CE values for MFC batch cells with $R_{ext} = 10, 50, 265, 1000$ and 5000Ω , finding values of 45.0, 42.5, 28.2, 10.8 and 6.1 % respectively.

Polarisation curves followed by EIS spectra were recorded for all 3 MFCs at 7, 27, 32 and 61 days. The polarisation curve data are presented in Figures 7.2, 7.3 and 7.4 for the same polarisation curves, whilst the corresponding EIS spectra are presented in Figure 7.5. The polarisation power and cell voltage are shown in Figure 7.2, and show that over the operational period, the peak powers of the three cells varied between 16 and 21 $\mu\text{W}/\text{cm}^2$ (normalised to cathode electrode area). The order of peak powers varied between the 3 cells depending

on the time the polarisation curve was taken. The order was $100 \Omega > 1000 \Omega > 5480 \Omega$ at 7 days, $100 \Omega > 1000 \Omega > 5480 \Omega$ at 27 days, $1000 \Omega > 5480 \Omega > 100 \Omega$ at 32 days and $1000 \Omega > 5480 \Omega > 100 \Omega$ at 61 days. Therefore, there was no constant trend in MFC peak power when comparing the 3 cells. As the peak power in the MFC depends on many factors, further investigation was carried out, and is discussed below. Apart from the power, the voltage for each cell dropped at a fairly constant rate from approximately 1 V at OCP to values less than 100 mV at low resistance, corresponding to a 900 mV voltage loss. This implies a high R_{int} .

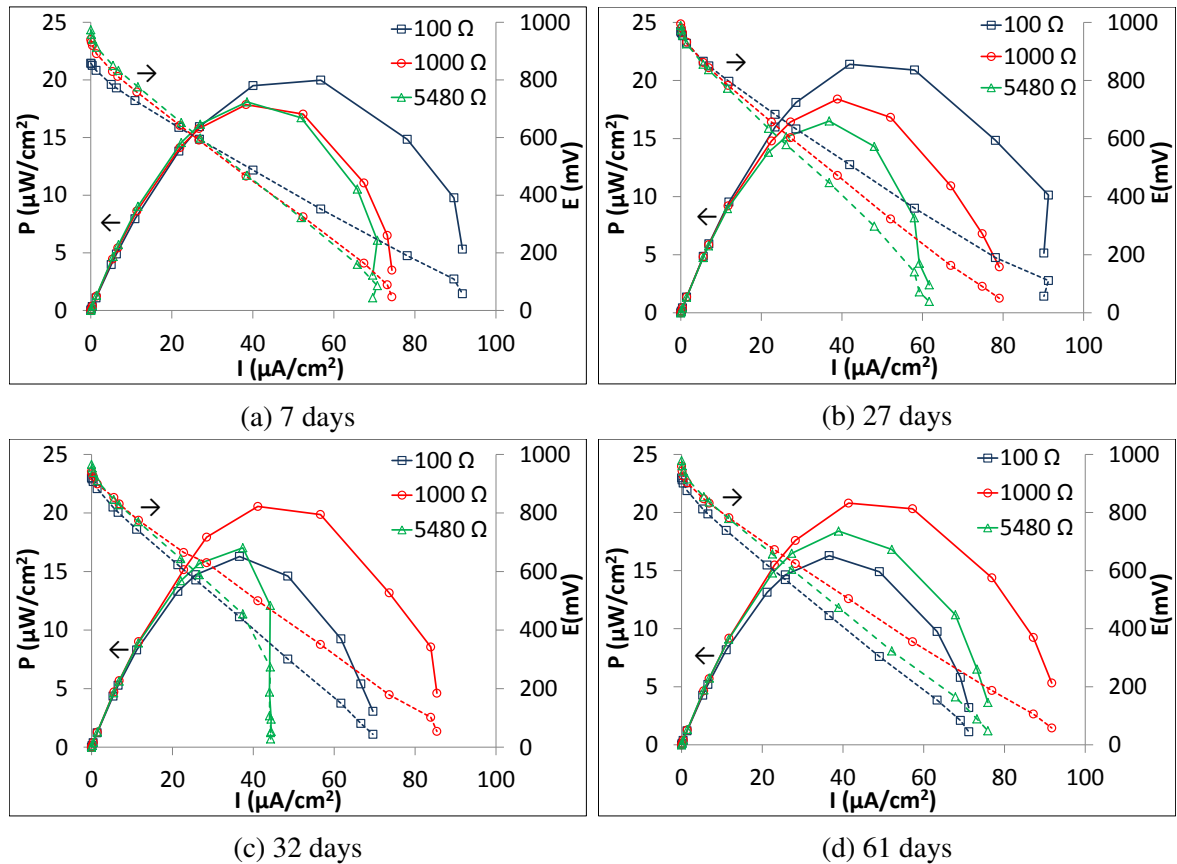


Figure 7.2: Polarisation curves taken for all 3 cells at (a) 7, (b) 27, (c) 32 and (d) 61 days of operation. Dashed lines represent cell voltages and solid lines represent power. Both Curves are given at each time for each of the 3 cells at 100Ω (square), 1000Ω (circle) and 5480Ω (triangle).

The cathode and anode potential data for the same polarisation curves discussed above are presented in Figure 7.3. Across all 3 cells, the anode potential increased by no more than 10 mV from the anode OCP of -500 to -490 mV, whereas the cathode potential decreased by no more than 50 mV from the cathode OCP of 450 to 400 mV, with the exception of the cell at 5480Ω at 27 and 32 days, where the cathode potential dropped abruptly at the end of the curve to 200 mV at 27 days, and 0 mV at 32 days. This is in contrast to the 900 mV drop in cell voltage observed for the 3 cells. Therefore, both the cathode and anode potential

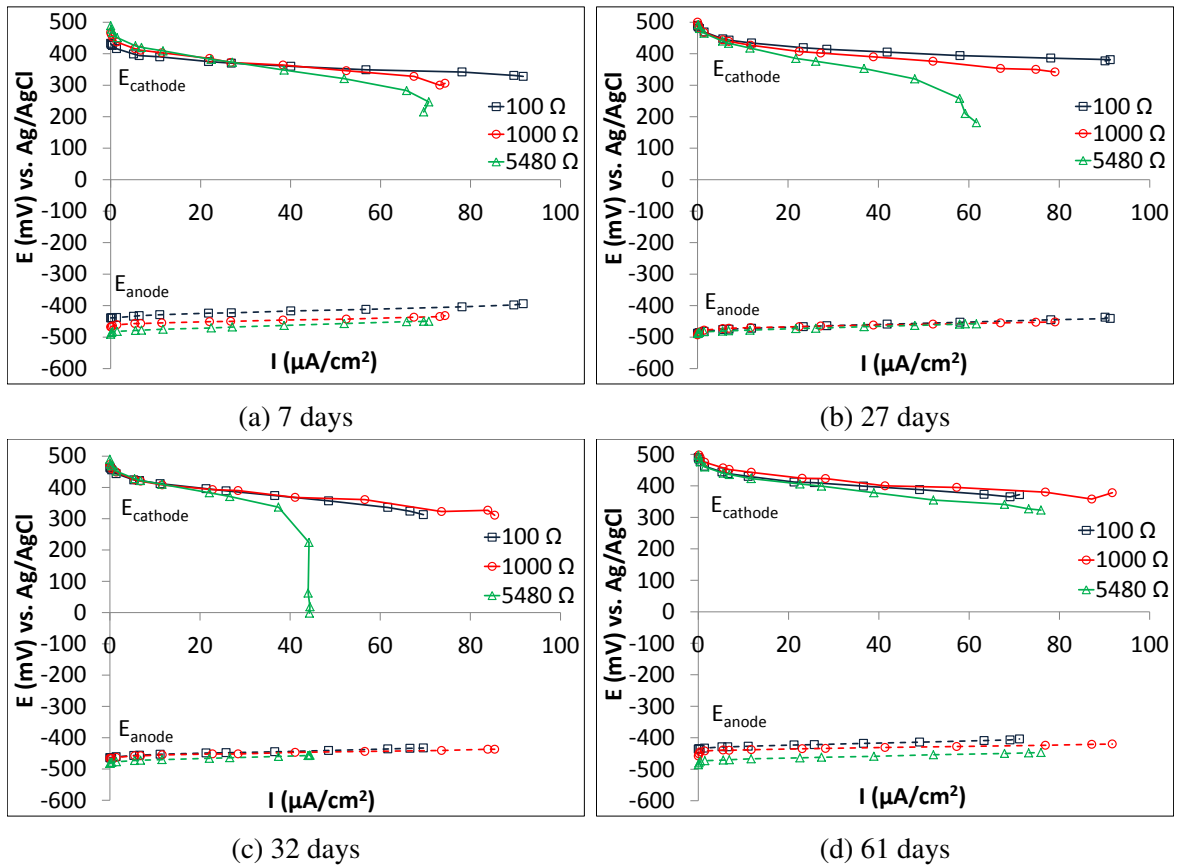


Figure 7.3: Cathode and anode potentials during the polarisation curves taken for all 3 cells at (a) 7, (b) 27, (c) 32 and (d) 61 days of operation. Solid lines represent cathode potentials and dashed lines represent anode potentials. Both curves are given at each time for each of the 3 cells at 100 Ω (square), 1000 Ω (circle) and 5480 Ω (triangle).

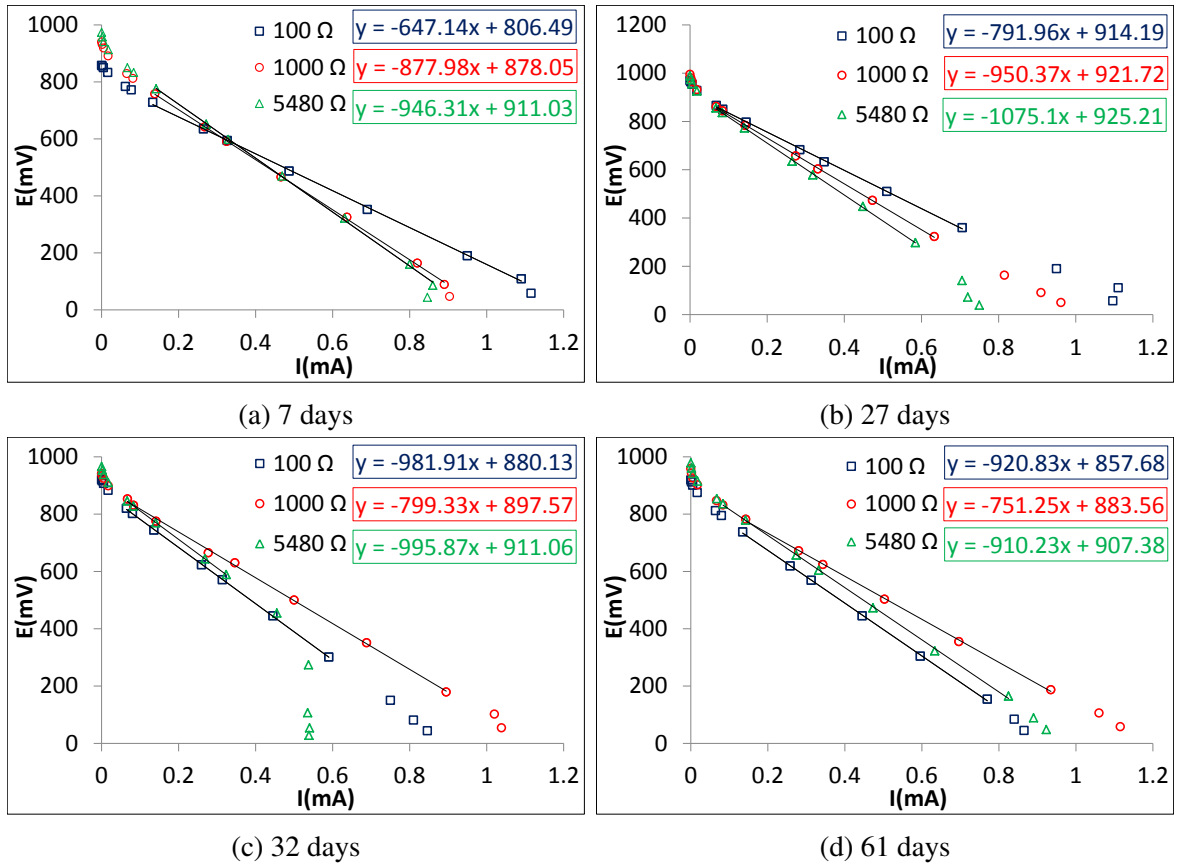


Figure 7.4: Linear best fits of the linear region of the cell voltage from the polarisation curves taken for all 3 cells at (a) 7, (b) 27, (c) 32 and (d) 61 days of operation. The best fits are given at each time for each of the 3 cells at 100 Ω (square), 1000 Ω (circle) and 5480 Ω (triangle).

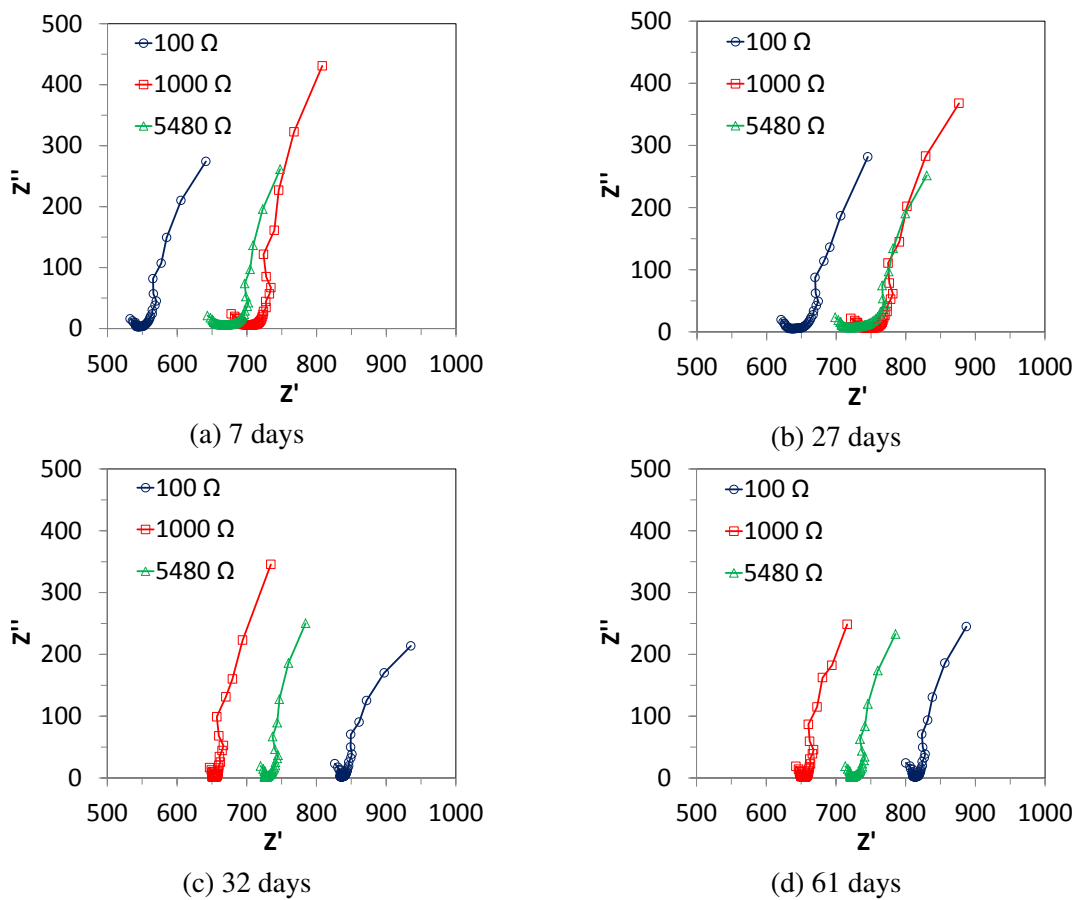


Figure 7.5: EIS taken for all 3 cells at (a) 7, (b) 27, (c) 32 and (d) 61 days of operation (immediately after the polarisation curves). The EIS are given at each time for each of the 3 cells at 100 Ω (square), 1000 Ω (circle) and 5480 Ω (triangle).

exhibited much smaller changes than for the cell voltage.

Internal resistances were calculated by fitting a linear trend line to the linear region of the cell voltage curves from the cell polarisation curves presented in Figure 7.2. These lines of best fit are presented in Figure 7.4. The internal resistances varied between 647-1075 Ω across all of the cells, and comparison of the internal resistance across the three cells gave an order of values mirroring the order of the corresponding peak powers. EIS spectra recorded directly after the polarisation curves are presented in Figure 7.5. Ohmic resistances determined from the high-frequency intercepts of the EIS spectra varied between 540-835 Ω across all cells. For the cell at 100 Ω , R_{Ω} varied between 514 and 815 Ω (301 Ω range), for the cell at 1000 Ω , R_{Ω} varied between 650 and 753 Ω (103 Ω range), whilst for the cell at 5480 Ω , R_{Ω} varied between 650 and 725 Ω (75 Ω range). These ranges, which mirror the trend in currents and pH splitting for the cells discussed previously, are likely due to a more rapidly changing electrolyte composition at higher current, as ions other than H^+ and OH^- , which cause the pH splitting, are transported across the membrane.

The internal resistances, ohmic resistances and calculated MFC polarisation resistances have been collected in Table 7.2. The ratio of R_{Ω}/R_{int} (%) for all of the cells on all occasions ranged from between 65-88 %. Therefore, the ohmic resistance accounts for at least 65 % of the internal resistance, which is very high. This result is in agreement with the observations made previously from Figures 7.2 and 7.3 that the cell voltage drops at much higher rates than either the anode or cathode potentials during the polarisation curve. Further improvements to the cell architecture in this system would lower the ohmic resistance and increase the power output. For example, by increasing the membrane area and reducing the electrode spacing. It is well-known that the H-cell MFC architecture suffers from high ohmic resistance [22].

The calculated polarisation resistances were averaged for each of the cells, and the standard deviation calculated; for the cell at 100 Ω , $R_p = 127 \pm 23$, for the cell at 1000 Ω , $R_p = 159 \pm 44$ and for the cell at 5480 Ω , $R_p = 282 \pm 78$. Therefore, within the degree of certainty, the cell at 5480 Ω had a higher R_p than both cells at lower resistance. The order of R_p between the cells at 100 Ω and 1000 Ω could not be distinguished, within the degree of certainty. A higher polarisation resistance indicates a lower combined bioanode and biocathode catalytic activity, which is the case for the cell at 5480 Ω . This combined catalytic activity can be thought of as the sum of the gradients of the cathode and anode potentials in the linear region of the polarisation curves in Figure 7.3, and is therefore a measure of the electrode kinetics and/or density of electroactive bacteria on the electrodes.

This result takes into account variations in the ohmic resistance of the cells over time, and is likely associated with current in the MFC, as the order of current and therefore rate of

Time days	Cell at 100 Ω						Cell at 1000 Ω						Cell at 5480 Ω							
	R_{int}	R_{Ω}	R_p	R_{Ω}/R_{int}	Power	R_{int}	R_{Ω}	R_p	R_{Ω}/R_{int}	Power	R_{int}	R_{Ω}	R_p	R_{Ω}/R_{int}	Power	R_{int}	R_{Ω}	R_p	R_{Ω}/R_{int}	Power
	Ω	Ω	Ω	%	$\mu\text{W}/\text{cm}^2$	Ω	Ω	Ω	%	$\mu\text{W}/\text{cm}^2$	Ω	Ω	Ω	%	$\mu\text{W}/\text{cm}^2$	Ω	Ω	Ω	%	$\mu\text{W}/\text{cm}^2$
7	647	540	107	83	20.0	878	690	188	79	17.9	946	650	296	69	18.1	946	650	296	69	18.1
27	792	645	147	81	21.4	950	753	197	79	18.4	1075	700	375	65	16.5	1075	700	375	65	16.5
32	982	835	147	85	16.3	799	650	149	81	20.6	996	725	271	73	17.0	996	725	271	73	17.0
61	921	815	106	88	16.3	751	650	101	87	20.8	910	725	185	80	18.4	910	725	185	80	18.4
Average	836	709	127	85	18.5	845	686	159	81	19.4	982	700	282	72	17.5	982	700	282	72	17.5
SD	149	141	23	3	2.6	88	49	44	4	1.5	71	35	78	6	0.9	71	35	78	6	0.9

Table 7.2: Summary of peak power densities and internal resistances determined from the polarisation curve data given in Figures 7.2 and 7.4, and the ohmic resistances determined from the EIS given in Figure 7.5, for all 3 cells at 100 Ω , 1000 Ω , and 5480 Ω external resistance, at 7, 27, 32 and 61 days of operation. Corresponding polarisation resistances (R_p) and ratios of ohmic resistance to internal resistance (R_{Ω}/R_{int}) have been calculated. Average values and standard deviations (SD) have also been calculated.

acetate substrate utilisation by the ARB at the anode was $100 \Omega > 1000 \Omega > 5480 \Omega$. A lower current means a lower growth rate for the bacteria at both electrodes, which could result in a drop in the biofilm activity at both electrodes, and increased polarisation resistance for the MFC. Lower growth rates of ARB and electrotrophic bacteria also changes the community dynamics between fixed rate parasitic processes and the electroactive bacteria, as indicated by the CE values determined for batch cycles 4 and 5. The lower growth rates for the biofilms in the cell at 5480Ω , gave this cell the highest average polarisation resistance, in comparison to the cells at lower external resistance. Operating the MFC system at 100Ω gives a significantly higher coulombic efficiency, but the power over time is lower than at 1000Ω . Depending on whether power or a high rate of substrate utilisation are required, this MFC system should be operated at 1000 or 100Ω , respectively i.e. equal to or less than the determined peak power.

The biocathodes and bioanodes were assessed by LSV at 0 days and at 34 days. These LSV spectra are presented in Figure 7.6. Just considering the biocathode LSV first, the onset potentials were $+0.4$ V for the three biocathodes at 0 days, but there was a large variation in the biocathode O_2 mass transfer limited current between cells; at 5480Ω it was $-70 \mu A/cm^2$, at 1000Ω it was $-30 \mu A/cm^2$, whilst at 100Ω it was $-20 \mu A/cm^2$. After operation in the MFC for 34 days, the biocathode onset potentials were the same at $+0.4$ V, and the O_2 mass transfer limited currents were the same at $-20 \mu A/cm^2$. This indicates that biocathode performance was greater in the poised-potential system, from where the biocathodes originated at 0 days, than in the MFCs at 34 days. Additionally, at 34 days, the biocathode performance was much more homogenous than at 0 days, particularly in terms of O_2 mass transfer limiting current. These differences are likely due to differences in cathode potential. In the poised-potential system, the applied cathode potential was in the O_2 mass transfer region (-0.1 V), therefore, the biocathodes were limited by variable O_2 mass transfer conditions. For the MFCs over different external resistances, the cathode potentials were typically between 300 and 400 mV, which are values in the kinetic region of the LSV where the biocathodes are limited by electrochemical kinetics. An important observation is that the gradient in the kinetic region between 300 and 400 mV in the biocathode LSV is less for the cell at 5480Ω than for the other two cells, which indicates worse kinetics/surface coverage of biocathode bacteria for the biocathode in this cell as compared to the other two cells.

Just considering the anode LSV, the onset potential for acetate oxidation remained the same in all LSV spectra, at -450 mV. At 0 days, all three bioanodes had a peak current of $100 \mu A/cm^2$ at -0.3 V peak potential, whereas at 34 days, the bioanode peak current varied between cells; at 5480Ω it was $110 \mu A/cm^2$, at 1000Ω it was $125 \mu A/cm^2$, whilst at 100Ω it was $150 \mu A/cm^2$. Therefore, the worst performing bioanode was the one in the MFC at 5480Ω , outperformed by the other two bioanodes in the MFCs at 1000Ω and 100Ω . For the

biocathodes, the smallest gradient was observed in the kinetic region between 300 to 400 mV in the cell at 5480 Ω . Both biocathode and bioanode performance appeared to be worse in the cell at 5480 Ω . These changes are in agreement with the high average polarisation resistance determined previously for the cell at 5480 Ω in comparison to the other two cells.

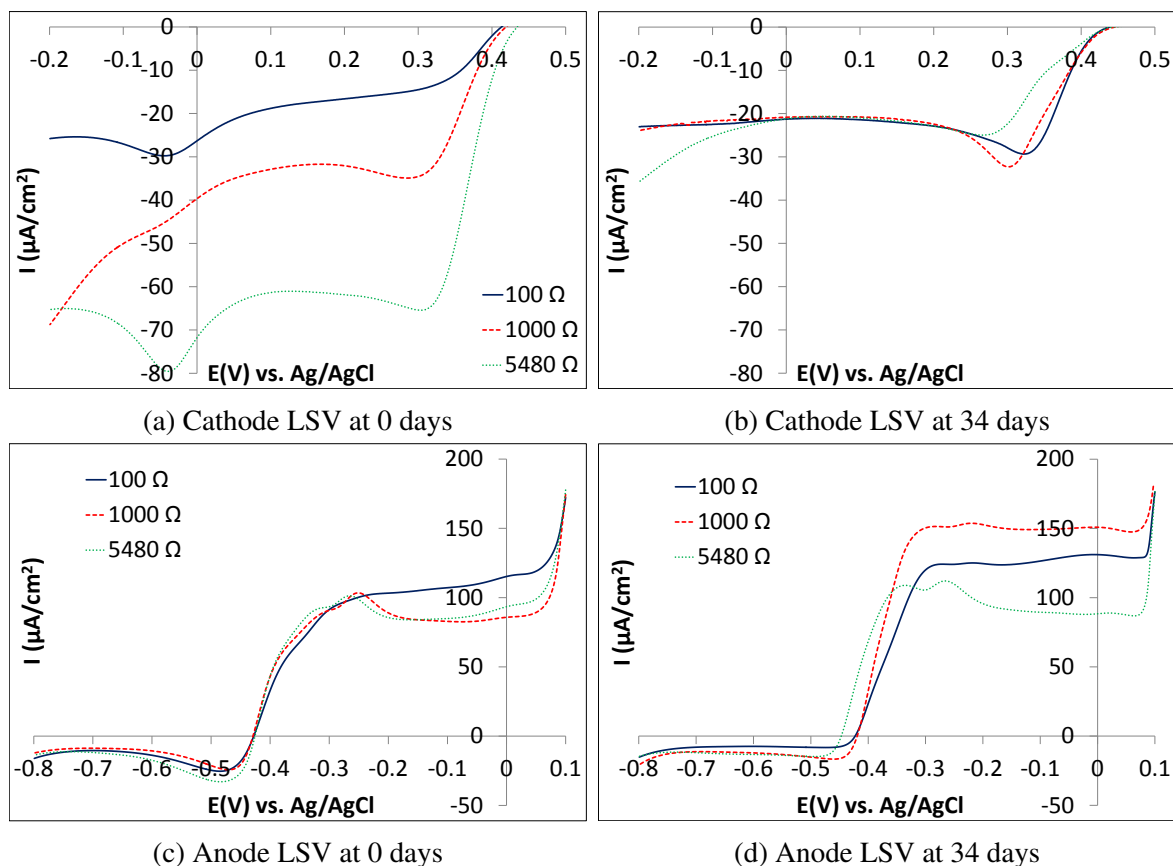


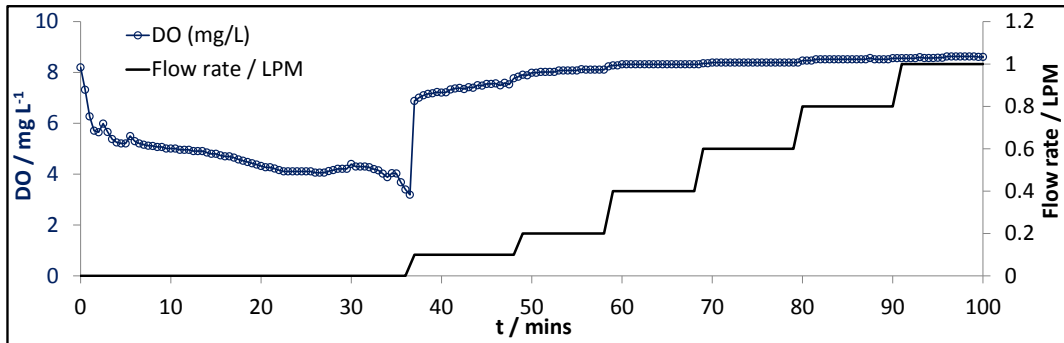
Figure 7.6: Anode and cathode LSV for all 3 cells at 0 and 34 days of operation; cell at 100 Ω (solid lines), cell at 1000 Ω (dashed lines) and cell at 5480 Ω (dotted lines).

7.3.2 The effect of oxygen mass transport

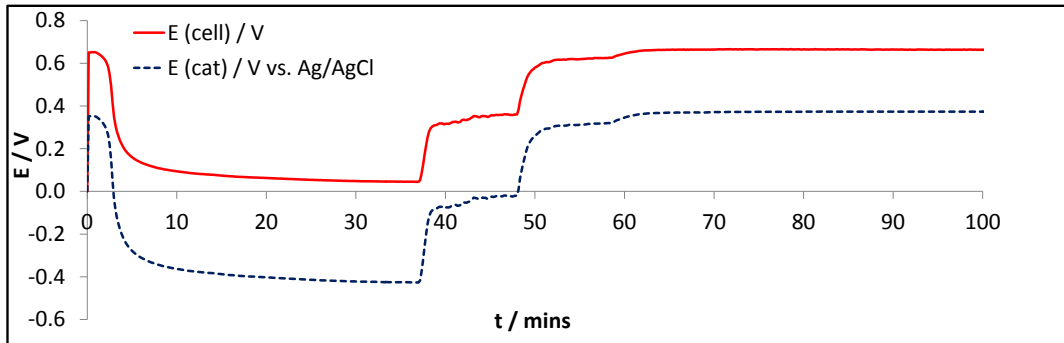
The rate of air sparging to the biocathode MFC previously operated at 100 Ω (at 518 days of continuous operation) was varied from 0 to 1 LPM using a flow valve and the cathode potential, cell voltage and dissolved oxygen (DO) measured with time. This experiment was performed using a 510 Ω external resistor (corresponding to the external resistance at peak power for this cell at 518 days), and the data is given in Figure 7.7. During the experiment, the cell voltage, cathode potential and DO all varied proportionally to each other as the air sparge rate was changed, indicating that the catholyte DO controlled the cathode potential which in-turn controlled the cell voltage. The catholyte was sparging before the beginning of the experiment (normal MFC operation), so during the first 30 minutes of the experiment

whilst the catholyte was not sparged, the cathode potential dropped rapidly from 400 to -400 mV, and the cell voltage dropped rapidly from 650 to 50 mV. The rate of sparging to the catholyte was then increased from 0 to 0.1 LPM, which accounted for a large increase in DO from 4-7 mg/L, the cathode potential increased from -400 to -100 mV, and the cell voltage increased from 50 to 350 mV. The DO, cathode potential and cell voltage then continued to increase as the sparge rate was increased from 0.1 to 1.0 LPM, reaching maximum values of 8.5 mg/L in DO, 400 mV in cathode potential and 650 mV in cell voltage. An increase in flow rate from 0.0 to 0.4 LPM accounts for most of the DO increase and therefore cathode potential and cell voltage increase. Figure 7.7c gives the relationship between catholyte DO and cell voltage clearly. At DO levels below 5.0 mg/L in the non-sparged solution, the cell voltage was less than 100 mV, whereas at DO levels of 8.5 mg/L the cell voltage was 650 mV.

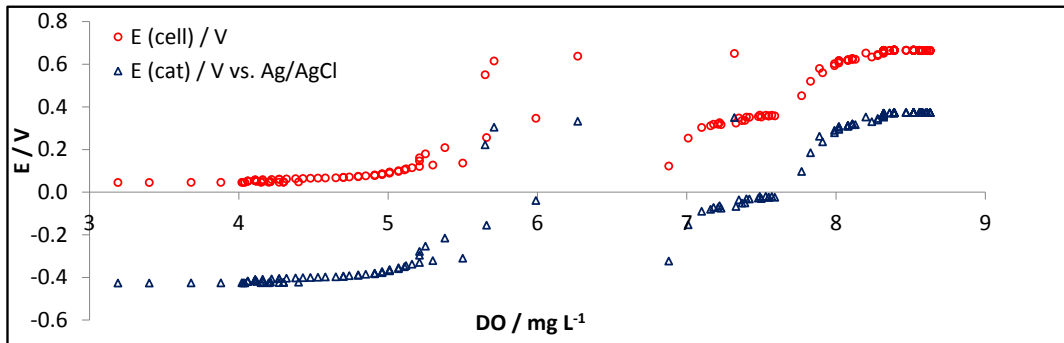
This result demonstrates the importance of continuous aeration to the MFC using an aerobic biocathode, as the cathode potential and therefore cell voltage are effected to a large extent by the catholyte DO level, which is controlled by the mass transfer of oxygen to the aerobic biocathode. Improvements in oxygen mass transfer to the aerobic biocathode by increasing the oxygen sparging rate and therefore the degree in which the solution/air contact is increased improve the MFC voltage and performance. For catalysis to occur in the biocathode, oxygen must reach the biocathode bacteria in the biofilm and permeate through the membrane of individual cells to reach the site of oxygen reduction. When oxygen mass transfer is improved by sparging the electrolyte, performance increases considerably for the biocathode, indicating that cell performance is strongly affected by the mass transport of oxygen to the site of ORR within the bacteria. Heijne *et al.* [84, 85] identify mass transfer as the dominant factor controlling the performance of aerobic biocathodes grown at poised potential, and this experiment further highlights the importance of oxygen mass transfer to the aerobic biocathode. However, aeration comes at an energy cost, which means that this particular system is likely to cost far more energy through aeration than it produces in electrical power, due to the electrical consumption of the aeration pump. Further improvements to this MFC system could be made by considering alternatives to active aeration, such as passive aeration using a GDE, in which the biocathode is immobilised on the solution-facing side, and oxygen is allowed to permeate through the electrode from the air-exposed side [81, 91]. Alternatively to GDEs, a catholyte flow past the cathode, which has been used for the biocathode of a sediment MFC [83], the tubular system developed by Rabaey *et al.* in which catholyte was dripped over the external face of the MFC [77], and the submersible MFCs developed by Ieropoulos *et al.* [278], might be good options. For system scale-up, flow systems would be easier to increase in size, whilst systems using GDEs would be better suited to stacking.



(a) Cathode dissolved oxygen concentration and flow rate against time



(b) Cell voltage and cathode potential against time



(c) Cell voltage and cathode potential against cathode dissolved oxygen concentration

Figure 7.7: Cathode dissolved oxygen concentration against time (a), cell voltage and cathode potential against time (b), and cell voltage and cathode potential against cathode dissolved oxygen concentration (c), for the cell previously operated at 100Ω , operated at peak power with $R_{ext} = 510 \Omega$ (The measurements were taken at 518 days of continuous operation for this cell).

7.3.3 Comparison of biocathode performance with a Pt cathode and an unmodified carbon electrode

The performance of an aerobic biocathode, Pt cathode and carbon cathode was compared by potential step voltammetry under conditions of constant aeration and catholyte buffered to neutral pH, and this data is presented in Figure 7.8. For the biocathode potential step voltammetry experiment, the onset potential for ORR was between 0.3 and 0.4 V, whilst the mass transfer limited current was $-120 \mu\text{A}/\text{cm}^2$. Between -0.1 and -0.2 V, the reduction current further increased from -120 to $-210 \mu\text{A}/\text{cm}^2$, which is attributed to abiotic oxygen reduction on carbon. For the Pt cathode potential step voltammetry experiment, the onset potential for ORR was between 0.2 and 0.3 V, whilst the mass transfer limited current was $-300 \mu\text{A}/\text{cm}^2$. For the carbon cathode potential step experiment, the onset potential was -0.1 V, whilst the mass transfer limited current was not reached, but the highest reduction current was $-10 \mu\text{A}/\text{cm}^2$.

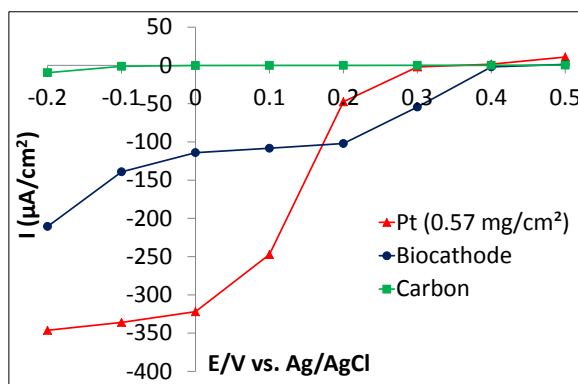


Figure 7.8: Potential step voltammetry on a biocathode grown at a poised-potential of -0.1 V, a Pt cathode and a carbon cathode. The potential-step voltammograms were taken under conditions of continuous sparging with air from an air pump, and using biocathode medium buffered to pH 7. The steady-state current was taken at 10 minutes at each potential.

Both the biocathode and Pt cathode had significantly more positive onset potentials for the ORR (seen in Figure 7.8) than the unmodified carbon cathode, and much higher mass transfer limited reduction currents. The onset potential for ORR was more positive by at least 0.4 V for the biocathode versus the unmodified carbon cathode. The mass transfer limited reduction current between -0.1 and 0.5 V for the biocathode versus the plain carbon cathode was 120 times greater. This represents a significant improvement in catalysis on modification of the plain carbon felt material with aerobic biocathode bacteria.

The onset potential for ORR for the biocathode was at least 0.1 V higher than for the Pt cathode, but the mass transfer limited reduction current for the biocathode was 2.5 times smaller than that for the Pt cathode. The 100 mV more positive ORR onset potential for the biocathode indicates that the biological catalyst has a smaller over-potential for the ORR than the Pt

cathode. However, the lower mass transfer limited reduction current for the biological catalyst indicates that O₂ mass transfer to the site of ORR catalysis within the biocathode occurs at a lower rate and/or the surface density of bacteria is lower than for Pt. The higher onset potential indicates how the catalysts responsible for the ORR in the biocathode bacteria are more efficient than for Pt, but the surface density of bacteria or possible limitations associated with O₂ mass transport into the biocathode biofilm/bacterial cells may limit performance in aerobic biocathodes in comparison to Pt electrodes.

Performance of an operational MFC with either a biocathode, Pt cathode or carbon cathode was compared with both the anolyte and catholyte buffered to pH 7.0, using a 510 Ω external resistance, and using the cell previously operated at 5480 Ω external resistance (at 624-626 days of continuous operation). Performance was assessed using polarisation curves, and these data are presented in Figure 7.9. The MFC had a peak power of 62 μW/cm² when operated with a biocathode, 70 μW/cm² when operated with a Pt cathode, and 7 μW/cm² when operated with a carbon cathode.

For all three tests, the onset potential for acetate oxidation at the anode was -0.5 V and the anode potential decreased linearly at a rate of -0.21 mV per μA/cm², indicating that the bioanode was constant between tests. Visual inspection of the cathode potential during the polarisation curves for all three tests shows that the gradient of the cathode potential in each test was significantly higher than the anode gradient. As all 3 experiments were conducted within 2 days of each other using the same cell and fresh media for each test, the MFC ohmic resistance was assumed to be constant between the three tests. As the anode potential and ohmic resistance were the same between the three tests, this indicates that the cathode electrode was the limiting electrode, and therefore that any difference in power was entirely due to differences in cathode performance. Further to this, the O₂ mass transfer limited currents (maximum MFC currents) at low resistance values were the same as those observed from the potential-step experiment for the biocathodes (apart from for carbon, where the cathode potential reached -0.3 V), which also shows that the cathodes were the limiting electrode in this system.

In this cell, the enrichment of carbon felt with aerobic biocathode bacteria increased the peak power density of the MFC by 9 times. The peak power density of the MFC when it had a biocathode was 89 % of the peak power density of the MFC when it had a Pt cathode with a loading of Pt at 0.57 mg/cm². These results indicate that for this system, enrichment of the carbon felt electrode with aerobic biocathode bacteria significantly improved MFC performance, and that this performance is comparable to Pt when the catholyte is actively aerated.

This system was actively aerated, whilst other methods of aeration include the use of GDEs

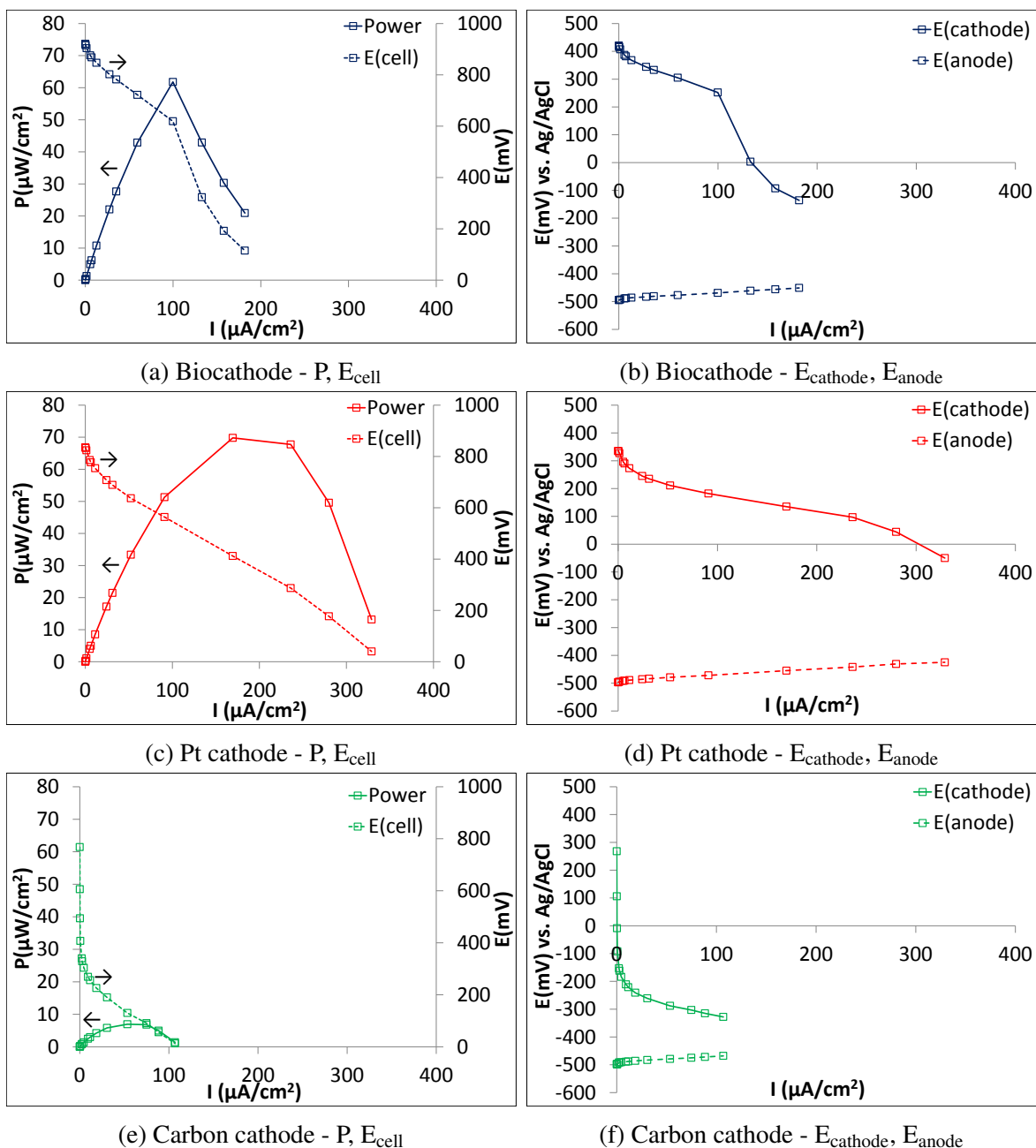


Figure 7.9: Polarisation curves taken for the cell previously operated at 5480Ω , at peak power density with $R_{ext} = 510 \Omega$ (the curves were taken at 624-626 days of continuous operation for this cell), using a biocathode grown at a poised potential of -0.1 V (a and b), a Pt cathode (c and d) and a carbon cathode (e and f). The power (solid lines) and cell voltage (dotted lines) are given in graphs (a), (c) and (e), whilst the corresponding cathode (solid line) and anode potentials (dashed lines) are given in graphs (b), (d) and (f).

as aerobic biocathode supports [81, 91]. As discussed in the literature review to this thesis, Xia *et al.* achieved a stable peak power of $55 \mu\text{W}/\text{cm}^2$ for a dual-chamber MFC with a high-performing aerobic biocathode on a GDE (E_{onset} for ORR of +0.4 V) [81]. This peak power performance was lower than that observed for the MFC H-cell system used here ($62 \mu\text{W}/\text{cm}^2$). However, this dual-chamber MFC had a spacing of 4 cm between the aerobic biocathode GDE and the AEM, and the anode was a carbon brush aligned horizontally in the anode chamber, both arrangements which were unlikely to have given an optimised cell geometry (although better than the 10 cm electrode spacing in the MFC H-cell used here). Additionally, the GDE was constructed using a method devised by Chen *et al.*, which was found to give an optimal rate of O_2 mass transfer for a conventional, membraneless single chamber air-cathode MFC [193], but is unlikely to be optimal for a dual-chamber aerobic biocathode MFC with a GDE. GDEs can be constructed using different methods [193–195], changing the rate of O_2 mass transfer in particular, a factor which could dramatically influence aerobic biocathode performance on a GDE. A GDE constructed for an aerobic biocathode should also include a significant element of porosity, to maximise biofilm size. A comparison of the high internal resistance H-cell MFC system discussed in this work, and the GDE system devised by Xia *et al.* [81], demonstrates how the performances of these systems could be improved by considering all of the important factors affecting overall MFC performance.

7.4 Conclusions

Changing the external resistance had the following effects on the performance of aerobic biocathode MFCs;

1. At 100Ω , the CE was $60 \pm 7 \%$, compared to $7 \pm 0 \%$ at 1000Ω and $3 \pm 0 \%$ at 5480Ω . Therefore, higher resistance resulted in lower CE values, which is thought to be due to a changing rate of acetate oxidation by the bioanode bacteria on changing the external resistance, in relation to a fixed rate of acetate utilisation by non-ARB, parasitic processes, and a fixed rate of O_2 mass transfer through the membrane.
2. The degree of pH splitting is greatest at lowest resistance, when the current is higher. This may cause degradation of the bioanode and biocathode, as well increases in the ohmic resistance, over longer batch cycles for cells operated at low resistance. Cathode potential decrease was apparent for the system operated at the lowest external resistance toward the end of a batch cycle, which could be associated with the rapidly increasing cathode pH.
3. The internal resistances for all of the MFCs were dominated by high ohmic resistances, accounting for at least 65% of the internal resistances of the MFCs. This was due to

the inefficient H-cell architecture.

4. The calculated polarisation resistances were 282 ± 78 for the cell at 5480Ω , 159 ± 44 for the cell at 1000Ω , and 127 ± 23 for the cell at 1000Ω . This result indicates a lowering of the combined activity of both the bioanode and biocathode in the cell at 5480Ω , probably due to reduced growth rates at both bioanode and biocathode, and therefore reduced ARB/electrotroph cell density.
5. LSV data suggest that the bioanode and biocathode in the cell at 5480Ω had lower performances than in the cells at 1000Ω and 100Ω , consistent with the lower calculated polarisation resistance for this cell.

Considering all of these findings together, it is clear that there are many competing processes in the MFC. At high resistances, the growth rates of the biofilms are reduced in relation to fixed rate processes competing for substrate, resulting in low CEs and reduced bioanode/biocathode performances. At low resistances, higher CEs and better bioanode/biocathode performances result due to higher growth rates and substrate consumption in comparison to fixed rate processes, but the system decays at a more rapid rate as evidenced by the increased rate of pH splitting. In the latter case, this may cause degradation of the biocathode and bioanode biofilm performances over longer batch cycles, due to a mixture of thermodynamic limitations and bacterial cell losses. Batch decay like this, could be solved by operating a continuous flow system, whereby the media is continuously replenished, although pH splitting effects might occur if there is high enough hydraulic retention time and rate of substrate degradation by the ARB.

MFC performance is heavily influenced by the rate of sparging to the catholyte when operated at peak power. An increase in the DO of the catholyte from 3.2 to 6.9 mg/L resulted in an increase in cell voltage from 45 to 300 mV, and a further increase from 7.5 to 8.0 mg/L resulted in a cell voltage increase from 360 to 600 mV. Cell voltage, and therefore power, in the fully biological MFC is limited to a large extent by the mass transfer of oxygen to the biocathode, which means that a significant energy investment must be made to aerate the catholyte and maintain fuel cell performance. This large change in cathode potential on aeration is associated with mass transfer limitations of oxygen through the biofilm/bacterial cell membranes to the site of ORR catalysis. An improvement in this system would be to explore methods of passive aeration, so as to avoid the need for energy intensive aeration. In particular, GDEs may be the best supports for aerobic biocathodes [81,91], if the intention is to scale-up as a stacked MFC system. Passive systems of aeration are also of interest, as have been adopted by Rabaey *et al.* using a tubular MFC configuration [77].

Replacing the unmodified carbon cathode with the biocathode in the full MFC system gave a 9-fold increase in peak power density performance, from 7 $\mu\text{W}/\text{cm}^2$ to 62 $\mu\text{W}/\text{cm}^2$. The MFC with a Pt cathode (0.57 mg/cm^2 Pt loading) had a peak power density of 70 $\mu\text{W}/\text{cm}^2$. Therefore, 89 % of the peak power density performance of the MFC was retained on going from Pt to the biocathode, implying that the biocathode is a good substitute for Pt in this type of MFC system with active aeration. The onset potential for ORR for the biocathode was at least 100 mV higher than for the Pt cathode. This indicates that the enzymes at the surface of the electrode responsible for the ORR catalysis are comparable to Pt.

Chapter 8. The Effect of the Membrane on the Performance of Aerobic Biocathode Microbial Fuel Cells

8.1 Introduction

In conventional MFCs, the membrane separates the anode from the cathode, preventing O₂ crossover from cathode to anode, and substrate cross-over from anode to cathode, both of which affect MFC performance. Additionally, pH splitting between the anode and cathode chambers, where the anode pH decreases and the cathode pH increases due to the transfer of ions other than H⁺/OH⁻ [279], causes performance losses at both bioanode and cathode catalysts, and degradation of the bioanode. Membranes also have resistance, which contributes to the MFC internal resistance, and the costs between membranes can be very different. All of these factors must be considered when choosing an appropriate membrane for the MFC system.

In the literature, many different types of membranes have been used in conventional MFCs, broadly falling into three different categories; cation exchange membranes (CEMs), anion exchange membranes (AEMs) and non-ion selective membranes [280]. These membranes are typically taken from other fuel cell technologies and installed into MFCs, and are not designed for use in MFCs. AEMs were originally developed for alkaline fuel cells, whilst Nafion is an example of a CEM which was originally developed for use in polymer electrolyte fuel cells. In terms of principal charge carriers over these different membranes in the phosphate buffered electrolyte usually used in MFCs, it has been found that CEMs, such as Nafion, transport H⁺/OH⁻ and K⁺/Na⁺ species, whilst AEMs have been found to transport OH⁻/H⁺ and phosphate species [196, 198–200]. Therefore, membranes may be more or less selective for different ions, and this affects the degree of pH splitting caused by the membrane. The ionic charge carriers across non-ion selective membranes have not yet been assessed in this way for MFCs, and a comparison between CEMs/AEMs is useful in determining whether the special functionality of CEMs/AEMs is important for MFC performance.

Ion selective CEMs and AEMs have been investigated in depth for MFCs [196, 198–200],

yet the same cannot be said for non-ion selective membranes. Non-ion selective separators cover a wide-range of materials, such as salt bridges [205–209], fabrics [210–212], polymers [143, 213–215], glasses [211, 216] and ceramics [39, 41, 104, 143, 217–222, 224]. Salt bridges suffer from high ohmic resistance, many of the fabrics and polymers which have been tested have been found to degrade, and glasses are fragile. However, there has been much recent interest in ceramic separators [39, 143, 222, 224], which are cheap, do not degrade, and can function as both the cell walls and the separator material of the MFC. In this study, ceramic separators were not investigated, primarily due to time constraints, but a cheap, non-ion selective polymer battery separator was investigated. Future studies should investigate ceramic separators using the same in-depth experimental methodology used here, to see how they differ to conventional CEMs and AEMs, and also to low-cost battery separators.

For the aerobic biocathode MFC system, significant acetate flux into the cathode is predicted to degrade aerobic biocathode performance, due to competition of the autotrophic bacteria performing ORR catalysis with heterotrophic bacteria which use the acetate. For example, when the abiotic Pt catalyst cathode GDE of a membraneless, single chamber air-cathode MFC, was replaced with a pre-enriched aerobic biocathode GDE by Xia *et al.*, the peak cell voltage output for individual batch cycles was initially stable for a few days, before declining over a one week period [81]. As the enzymes at both anode and cathode catalyse specific reactions, mixed potential effects due to fuel cross-over, which can occur in e.g. PEM fuel cells due to the mixing of H₂ and O₂ at Pt electrodes, do not occur for MFCs. Instead, mixing of acetate and O₂ promotes competitive heterotrophic metabolisms not associated with the electrodes, which can also deplete the power output of the device. Therefore, the membrane used in an aerobic biocathode MFC must also have low organic substrate cross-over. Additionally, as the cathode catalyst is biological, increasing cathode pH due to pH splitting not only lowers performance, it can also potentially degrade the biocathode catalyst.

To date, there are no investigations looking at the effect of the membrane for MFCs with an aerobic biocathode. Therefore, the aim of this chapter was to investigate different membrane types to lower the cost and maintain the performance of the aerobic biocathode MFC system. To achieve this aim, membrane characterisation was carried out on three different types of commercially available membranes; a CEM (Nafion-117, Sigma, UK), an AEM (Fumasep FAD, Fumatech, Germany) and a non-ion selective battery separator (BS) (RhinoHide, Entek Ltd., UK). The cost of these membranes is presented in Table 8.1. The CEM and AEM membranes were chosen on the basis of being commonplace in MFCs from the literature, whilst the BS was chosen as a low cost alternative to CEMs/AEMs. The RhinoHide BS is conventionally used in lead-acid batteries for automotive applications. Although the RhinoHide BS was also developed for other purposes, it was hypothesised to possess many of the characteristics that would make it a suitable separator in MFCs, without any unnecessary

functionality, as is the case with CEMs/AEMs. A RhinoHide BS has been used previously in pilot-scale MEC studies [203,204], but has not yet been characterised as apart of an in-depth, comparative, electrochemical membrane characterisation experiment. Additionally, battery separators have not yet been tested in MFCs with an aerobic biocathode, to see how the properties of a battery separator might influence aerobic biocathode performance and the system as a whole.

These membranes were initially characterised abiotically in terms of principal charge carriers and in terms of their oxygen/acetate diffusion properties, using abiotic tests, as described in materials and methods. The membranes were then each installed into an aerobic biocathode MFC, previously operated for 40 days before membrane installation. The cells were then operated for a further 40 days. At the end of both operational periods, MFC performance was assessed. Therefore, the effect of membrane-type on aerobic biocathode MFC performance was assessed.

Membrane	Type	Cost (£ m ⁻²)
Nafion-117	CEM	1460
Fumasep FAD	AEM	411
RhinoHide	BS	1.5

Table 8.1: Cost of the CEM, AEM and BS used in this study

8.2 Experimental

The CEM, AEM and BS were all characterised abiotically in terms of membrane ohmic resistance, ionic charge carriers and for acetate/oxygen crossover. This characterisation was carried out as described in materials and methods. The membranes were then assessed in full acetate-fed aerobic biocathode MFCs.

Three acetate-fed batch aerobic biocathode MFCs (cells A, B and C) were setup as described in materials and methods, using the bioanode and biocathodes developed in Chapter 7. The MFCs were operated at the external resistance corresponding to their peak power densities, which was 510 Ω for all three cells. The bioanode medium contained 50 mM pH 7.0 phosphate buffer, 1 g/L of sodium acetate, and nutrients, as described in materials and methods. The biocathode medium contained 50 mM pH 5.8 phosphate buffer and nutrients, as described in materials and methods. The H-cell architecture was again chosen for the MFCs used in this investigation, and the MFCs were operated in batch mode at both the anode and cathode in order to simplify MFC operation. Additionally, singlet MFCs were operated without parallel replication. An optimised cell geometry, continuous flow at both bioanode

and biocathode, and replication, would have been preferable, for all of the reasons discussed previously. These deficiencies were due to limitations on experimental apparatus, the numbers of pre-enriched bioanodes/biocathodes available (and the time taken to generate them), the time which the experiments took to complete, and the labour/time involved in maintaining/analysing a large number of reactors.

For the first operational period, the three acetate-fed batch aerobic biocathode MFCs (cells A, B and C) were fitted with AEMs, and operated for 40 days and 5 batch cycles at peak power density. The AEMs were then changed for a CEM on cell A, a new AEM on cell B, and a BS on cell C. After membrane replacement, all three MFCs were run for a second operational period at peak power density, lasting 40 days and 5 batch cycles. This information is summarised in Table 8.2. For both operational periods, the coulombic efficiency was determined at the end of the first batch cycle by analysing anode effluent samples by TOC. At the end of both operational periods, the MFCs were assessed by polarisation curves then EIS, and individual bioanode and biocathode electrodes were assessed by LSV, using the methodology described in materials and methods.

	Cell A	Cell B	Cell C
1st 40 days of operation	AEM	AEM	AEM
	membrane change		
2nd 40 days of operation	CEM	new AEM	BS

Table 8.2: The two different periods of operation for the three acetate-fed batch aerobic biocathode MFCs. For the second period of operation, the three MFCs used different membrane types.

During the first batch cycle of the second operational period, the concentration of all significant ions other than H^+/OH^- were measured in both the bioanode and biocathode chamber effluents, using the same methodology as for the abiotic membrane characterisation tests for ionic charge carriers, described in materials and methods.

8.3 Results and Discussion

8.3.1 Principal charge carriers and oxygen/acetate diffusion coefficients for a CEM, AEM and a BS

Membrane resistance, area resistance, resistivity and conductivity were determined for the three membranes in pH 7.0 anode medium (50 mM pH 7.0, phosphate buffer, 1 g/L sodium acetate, nutrients), using the setup described in materials and methods. These values have been compiled in Tables 8.3 and 8.4 for the three membranes. The raw EIS spectra are

available in the Appendix, Figure A.10. The BS had the highest membrane resistance of 5.1 Ω , whilst the CEM and AEM membranes had resistances of approximately 2/3 of this, at 3.5 and 3.6 Ω , respectively. These values corresponded to the membrane resistance of a 4 cm diameter circular piece, the same membrane area as used later in the MFC studies. In terms of membrane area resistances, the BS had a value of 64 $\Omega \text{ cm}^2$, whilst both the CEM and AEM membranes had similar values of 44 and 45 $\Omega \text{ cm}^2$ respectively. The CEM membrane had approximately half the resistivity, and therefore double the conductivity, of the AEM and BS.

From the cell resistance values given in Table 8.3 without the membranes, the electrolyte resistivity of the anode medium can be calculated as approximately 112 $\Omega \text{ cm}$. All three membranes had much higher resistivity than this, of 2193, 4750 and 3902 $\Omega \text{ cm}$, for the CEM, AEM and BS, respectively. This relates to the selectivity of the membranes for different ions. The greater molar ionic conductivity and concentration of cationic species in the process electrolyte may be part of the reason. Examination of the electrolyte composition, given in Chapter 3, Table 3.1, shows that $[\text{K}^+] = 79 \text{ mM}$, in comparison to 50 mM for phosphate, and the conductivities at 298 K can be contrasted, where K^+ has a limiting molar ionic conductivity of 74 $\text{S cm}^2 \text{ per mol}$, and the values are 57/32 $\text{S cm}^2 \text{ per mol}$ for $\text{HPO}_4^{2-}/\text{H}_2\text{PO}_4^-$ [281]. Additionally, at neutral pH, $[\text{H}^+] = [\text{OH}^-]$, yet the limiting molar ionic conductivities are 350 and 199 $\text{S cm}^2 \text{ per mol}$ for H^+ and OH^- , respectively [281]. However, the actual ionic conduction across the membrane is dependent on the interaction of these mobile ions with the polymer network of positively/negatively charged groups which comprise the ion exchange membrane [201], therefore the situation is more complicated than this, although this is a useful comparison.

In terms of area resistance/resistivity, Harnisch *et al.* found values of 9.2 $\Omega \text{ cm}^2 / 503 \Omega \text{ cm}$ for Nafion 117 (CEM), and 12.4 $\Omega \text{ cm}^2 / 1378 \Omega \text{ cm}$ for Fumasep FAD (AEM), using a direct current method [201, 279]. Therefore, the values determined in this study were considerably higher. Given that 50 mM phosphate buffer was also used for the Harnisch measurements, the differences may have been due to the method used [249]. A similar H-cell type setup, with a high electrode spacing, small membrane area (4.16 cm^2) in relation to larger electrode areas (100 cm^2 Pt meshes), was used for this study [201].

For decreased membrane area, the membrane resistance increases. In Chapter 7, MFC ohmic resistances ranging from 540 to 835 Ω were determined for the acetate-fed batch MFCs over different external resistances, using the H-cell configuration given in Figure 3.7d, Chapter 3. This configuration had substantially higher resistance due to the decreased membrane area and cell cross-sectional area (long 1 cm diameter cell flanges) between the bioanode and biocathode electrodes. Given that the AEM membrane diameter was 1 cm for these

cells, a 1 cm diameter AEM is expected to contribute $45 \Omega \text{ cm}^2 / 0.79 \text{ cm}^2 = 57 \Omega$ to the MFC ohmic resistance. Therefore, most of the ohmic resistance determined for these H-cells came from the 1 cm diameter cross-sectional area of the long glass flanges between the electrodes. This demonstrates how important cell architecture is to the MFC. Increasing cell cross-sectional areas, membrane areas, and decreasing electrode spacings should increase the flux of O_2 /acetate, but these processes are counter-balanced by higher currents in the MFC, due to the lower ohmic resistance. Membrane resistance does contribute to MFC internal resistance, therefore a comparison of membrane resistances in the process electrolyte is important when making decisions regarding the membrane for the system.

Membrane	cell R_Ω (membrane) Ω	membrane resistance Ω
No mem.	44.4	n/a
CEM	47.7	3.5
AEM	47.9	3.6
BS	49.3	5.1

Table 8.3: Cell ohmic resistances as determined by EIS using the membrane ohmic resistance testing cell given in materials and methods. Ohmic resistances are given for the cell, without a membrane, for with a CEM, AEM and BS membrane, with anode medium as electrolyte (50 mM pH 7.0 phosphate buffer, 1 g/L sodium acetate, nutrients).

Membrane	thickness cm	Area Resistance $\Omega \text{ cm}^2$	Resistivity $\Omega \text{ cm}$	Conductivity $\mu\text{S/cm}$
CEM	0.200	44	2193	456
AEM	0.095	45	4750	211
BS	0.163	64	3902	256

Table 8.4: Calculated area resistance, resistivity and conductivity, for a CEM, AEM and BS in anode medium (50 mM pH 7.0 phosphate buffer, 1 g/L sodium acetate, nutrients), using the cell ohmic resistances determined in Table 8.3. Membrane thicknesses were determined for the hydrated form of the membrane.

In order to determine principal charge carriers through each of the three membranes, a fixed current was passed through each membrane between a WE and CNE, and the ionic composition of both the WE and CNE chambers was determined before and after the test, as described in materials and methods. This experiment was repeated twice, although with different parameters of run time and membrane size (runs 1 and 2). The values for run time and current (2 mA) were chosen so as to obtain an appreciable transfer of ions over the membrane, and therefore an appreciable difference in concentration of ions for analysis. The results from the first run with a membrane diameter of 1 cm, and a run time of 92 hours at 2 mA applied current, have been compiled in Table 8.5.

Ion	Start [WE] and [CNE] mM	CEM (End)			AEM (End)			BS (End)		
		[WE] mM	[CNE] mM	[WE] mM	[CNE] mM	[WE] mM	[CNE] mM	[WE] mM	[CNE] mM	
K ⁺	76.77	57.50	97.49	73.98	79.50	64.14	88.72			
Na ⁺	24.45	21.58	29.43	24.73	25.07	23.87	26.98			
F ⁻	5.01	4.87	4.88	6.45	4.49	5.61	4.33			
Cl ⁻	8.17	8.14	na	9.63	na	8.76	na			
Phosphate	60.65	67.14	57.07	71.63	52.04	65.20	57.48			
SO ₄ ²⁻	0.00	0.00	0.00	0.00	0.00	0.00	0.00			
pH	7.03	5.62	10.02	6.14	10.28	5.86	10.02			
z		$\Delta Q/Q_{\text{pass}}$ %	$\Delta Q/Q_{\text{pass}}$ %	$\Delta Q/Q_{\text{pass}}$ %	$\Delta Q/Q_{\text{pass}}$ %	$\Delta Q/Q_{\text{pass}}$ %	$\Delta Q/Q_{\text{pass}}$ %			
K ⁺	1	70	-75	10	-10	46	-44			
Na ⁺	1	10	-18	-1	-2	2	-9			
F ⁻	-1	-1	0	5	-2	2	-2			
Cl ⁻	-1	0	na	5	na	2	na			
H ₂ PO ₄ ⁻	-1	24	-13	40	-31	17	-12			
HPO ₄ ²⁻	-2	47	-26	80	-63	33	-23			
SO ₄ ²⁻	-2	0	0	0	0	0	0			
Total (H ₂ PO ₄ ⁻)		104	-107	60	-45	69	-67			
Total (HPO ₄ ²⁻)		127	-120	100	-77	86	-78			

Table 8.5: 1st run results for the abiotic electrolysis experiment using a H-cell with a 1cm diameter membrane and 3 different membrane types; CEM, AEM and BS. Ion concentrations at the start and end of the experiment and % changes in charge for each ion after passing 2mA of current for 92.00 hours (662C) are presented. ΔQ is the change in charge in coulombs for each ion assuming a specific ionic charge (z), and Q_{pass} is the charge passed in the external circuit, equal to 662C.

At the CNE (cathode), phosphate depleted in the solution, whilst K^+ accumulated, and the pH increased. At the WE (anode), phosphate accumulated, K^+ depleted, and the pH decreased. This occurred for all three membranes to varying extents. At the end of the first run, white crystal-like shards were observed in the CNE chambers for some of the cells, which were attached to the Pt mesh counter electrodes or present on the bottom of the CNE chambers. Because of this, the CNE chambers were carefully acidified with concentrated HCl in order to redissolve the precipitates, and hence, Cl^- was ignored in the measurements for the CNE chamber. For the first run, the potential between the WE and CNE at the end of the run, just before the cell was switched into OCP, was 4.95 V. Precipitate formation in the cathode chamber was thought to be due to increasing solution pH coupled with increasing cathode potential. More specifically, a change in the cathode reaction from reduction of oxygen, to reduction of a phosphate containing species, as oxygen reduction became less thermodynamically favourable, was thought to occur as the solution pH increased.

The results from the second run with a membrane diameter of 4 cm, and a run time of 76.15 hours, have been compiled in Table 8.6. In the second run, the membrane area was made larger using an otherwise identical cell setup to lower the ohmic resistance (ionic) of the cell, and less electrical charge was passed by reducing the run time at a fixed current of 2 mA current to 76.15 hours (548 C for the second run as compared to 662 C for the first run). For the second run, precipitate formation was avoided in the CNE chamber, and acidification of the CNE electrolyte was not required. Additionally, at the end of the second run, the potential between the WE and CNE just before the cell was switched into OCP was 2.00 V. In comparison to the first run, this is a reduction by more than half in the measured cell potential. However, the reduction in ohmic resistance is unlikely to have been critical in precipitate formation, as a reduction in cell ohmic resistance should not alter the applied cathode potential. The critical parameter is likely to have been the reduced time for the second run, resulting in a lower cathode pH. Comparison of Tables 8.5 and 8.6 shows how the average CNE pH was 10.11 ± 0.13 for the first run, and 7.63 ± 0.21 for the second run, across all three membranes.

The results from the second run were similar to the first, and the same trends in pH, K^+ and phosphate were observed. However, in retrospect, the second run should have been run as a strict repeat of the first one, with all parameters kept constant. The desire to further develop the method led to this outcome. Further development of the method described here would be interesting as a subject of future study. For both runs, the concentrations changes have been equated to a change in charge, also compiled in Tables 8.5 and 8.6, and the average over the two runs has been depicted graphically in Figure 8.1. Initial examination of Figure 8.1 shows how sulphate concentration increased slightly in both chambers across all three membranes. These changes were low with large associated errors, and no significance was attached to

them.

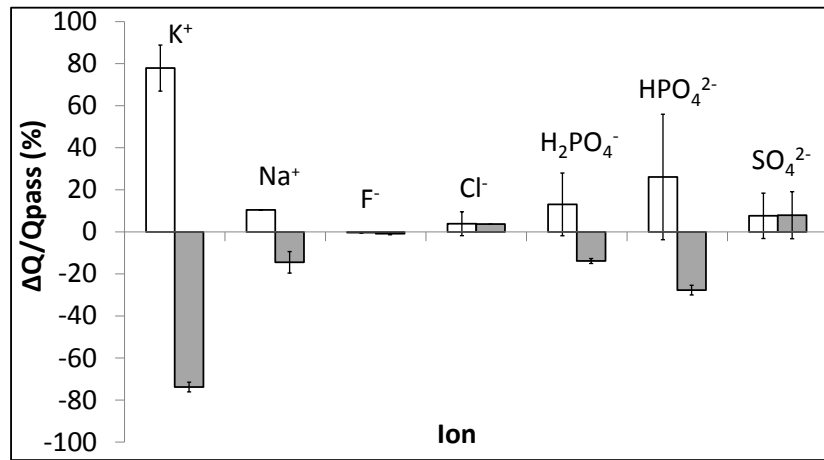
For the CEM, K^+ accounted for 70-75% of the charge in the 1st run, and 72-86% in the 2nd run. Na^+ accounted for 10-18% of the charge in the 1st run, and 10-11% in the 2nd run. Assuming $H_2PO_4^-$ was the principal form of phosphate transferred, phosphate accounted for 13-24% in the 1st run and 15-29% in the 2nd run. Assuming HPO_4^{2-} , phosphate accounted for 26-47% of the charge in the 1st run, and 29-57% during the second run. The form of phosphate transferred across the membrane is assumed to be HPO_4^{2-} in many of the papers in the literature [199, 200], yet at neutral pH, the monoanionic form of phosphate still accounts for 42% of the phosphate species present in solution, so it cannot be assumed that HPO_4^{2-} is the only charge carrier across the membrane. Across the two runs, the total charges were occasionally in slight excess, sometimes dependent on whether it was assumed that HPO_4^{2-} was the principal phosphate charge carrying species. These excesses could be due to unaccounted transfer of H^+/OH^- , which could not be measured. Across both runs, however, 70-86% of the charge could be accounted for by the transfer of K^+ . This explains why the pH splits for this membrane. Interestingly, there was some change in phosphate concentration, indicating the passage of this ion through the membrane, even though it is a CEM. The passage of phosphate indicates that the CEM membrane is not completely impermeable to the transfer of negative ions.

For the AEM, K^+ accounted for 10% of the charge in the 1st run, and 0-3% in the 2nd run. Assuming $H_2PO_4^-$ was the principal form of phosphate transferred, phosphate accounted for 31-40% in the 1st run and 29-42% in the 2nd run. Assuming HPO_4^{2-} , phosphate accounted for 63-80% of the charge in the 1st run, and 57-85% during the second run. Across the two runs, the totals were in deficit, and significantly in deficit when the monoanionic form of phosphate was assumed as the charge carrier. Regardless of the form of phosphate carrying the charge, phosphate was the most significant measured charge carrier for this membrane. The results, however, strongly suggest that H^+/OH^- was also an important charge carrier for the AEM, even when the dianionic form of phosphate was assumed. Transfer of K^+ was negligible for this membrane. Further investigation would be required in order to find out which form the phosphate is in as it transfers over the AEM.

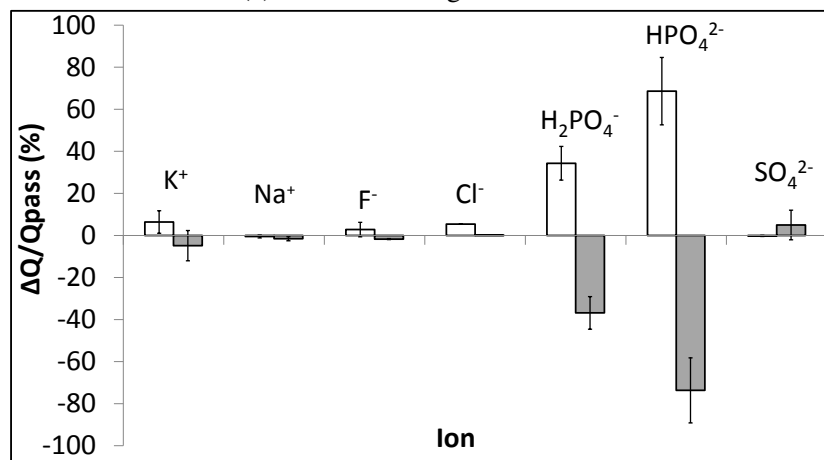
For the BS, K^+ accounted for 44-46% of the charge in the 1st run, and 45-58% in the 2nd run. Na^+ accounted for 2-9% of the charge in the 1st run, and 4-6% in the 2nd run. Assuming $H_2PO_4^-$ was the principal phosphate charge carrier, phosphate accounted for 12-17% in the 1st run and 7-23% in the 2nd run. Assuming HPO_4^{2-} , phosphate accounted for 23-33% of the charge in the 1st run, and 15-46% during the second run. Across the two runs, the totals were in deficit to a smaller degree than for the AEM. The primary charge carrier for the BS membrane was K^+ , accounting for approximately 50% of the transferred charge. However, this is

Ion	Start [WE] and [CNE] mM	CEM (End)		AEM (End)		BS (End)	
		[WE] mM	[CNE] mM	[WE] mM	[CNE] mM	[WE] mM	[CNE] mM
K ⁺	78.43	62.21	92.10	77.94	78.39	67.54	86.89
Na ⁺	11.62	9.65	13.68	11.63	11.79	10.41	12.30
F ⁻	2.80	2.77	2.57	2.87	2.50	2.80	2.50
Cl ⁻	6.44	7.93	7.14	7.47	6.45	7.63	6.01
Phosphate	52.51	52.98	49.73	57.94	44.50	53.89	48.15
SO ₄ ²⁻	0.81	2.26	2.31	0.77	1.75	2.48	1.56
pH	6.99	6.07	7.81	6.47	7.39	6.21	7.68
z		$\Delta Q/Q_{\text{pass}}$ %	$\Delta Q/Q_{\text{pass}}$ %	$\Delta Q/Q_{\text{pass}}$ %	$\Delta Q/Q_{\text{pass}}$ %	$\Delta Q/Q_{\text{pass}}$ %	$\Delta Q/Q_{\text{pass}}$ %
K ⁺	1	86	-72	3	0	58	-45
Na ⁺	1	10	-11	0	-1	6	-4
F ⁻	-1	0	-1	0	-2	0	-2
Cl ⁻	-1	8	4	5	0	6	-2
H ₂ PO ₄ ⁻	-1	2	-15	29	-42	7	-23
HPO ₄ ²⁻	-2	5	-29	57	-85	15	-46
SO ₄ ²⁻	-2	15	16	0	10	18	8
Total (H ₂ PO ₄ ⁻)		122	-79	37	-34	95	-67
Total (HPO ₄ ²⁻)		124	-94	65	-77	102	-90

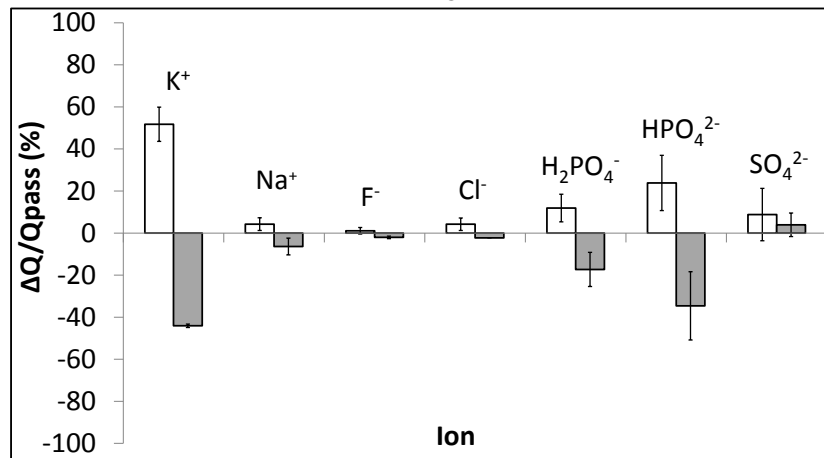
Table 8.6: 2nd run results for the abiotic electrolysis experiment using a H-cell with a 4 cm diameter membrane and 3 different membrane types; CEM, AEM and BS. Ion concentrations at the start and end of the experiment and % changes in charge for each ion after passing 2mA of current for 76.15 hours (548C) are presented. ΔQ is the change in charge in coulombs for each ion assuming a specific ionic charge (z), and Q_{pass} is the charge passed in the external circuit, equal to 548C.



(a) Cation exchange membrane



(b) Anion exchange membrane



(c) Battery separator

Figure 8.1: Average charge transfer across the CEM, AEM and BS across the 1st and 2nd runs of the ionic charge carriers experiment. ΔQ is the charge attributed to each measured ion assuming a specific ionic charge (z), whilst Q_{pass} is the charge passed in the external circuit of the cell. The ratio between the two is $\Delta Q/Q_{\text{pass}}$, expressed as a %. Empty bars are for charge changes at the WE, filled bars are for charge changes at the CNE. The error bars are equivalent to the differences from the mean.

less than for the CEM, indicating that phosphate and H^+/OH^- also contribute significantly. In this respect, the BS exhibits intermediate behaviour between the CEM and the AEM.

The analysis indicates that the primary charge carrier is K^+ for the CEM, whilst phosphate is prominent for the AEM and transfer of K^+ is negligible. For the BS, the primary charge carrying ion is K^+ , but phosphate and H^+/OH^- must also contribute significantly. The % charge over both runs has been averaged and depicted graphically in Figure 8.1, providing a clear illustration of the % charge transferred by each of the ions measured across each of the membranes in this experiment. Preferential transfer of ions other than H^+/OH^- tends to occur in buffered electrolytes at neutral pH due to differing concentrations of ionic species, despite the higher limiting ionic conductivities of protons and hydroxide in comparison to potassium and phosphate ions. In the pH 7.0 media used, $[\text{H}^+] = [\text{OH}^-] = 0.1 \mu\text{M}$, as compared to 50 mM in K^+ or phosphate ions. Therefore, K^+ and phosphate are both 0.5 million times greater in concentration than H^+/OH^- . This difference in concentration means that the principal charge carriers across cation and anion selective membranes during electrolysis are K^+ and phosphate, respectively, and not H^+/OH^- , and is the origin of the pH splitting, whereby H^+ accumulates at the anode and OH^- accumulates at the cathode. Interestingly, for the AEMs tested in the literature, H^+/OH^- was determined as the principal charge carrier, and transfer of phosphate was found to be negligible [200], or less than 25 % [199] of the transferred charge. However, the AEMs used in these studies were of slightly different types (Fumasep FAA and FAB, respectively, Fumatech, Germany).

For the three membranes, values were averaged across the CNE and WE chambers, and across the two experimental runs, giving one value for the membrane for each of the significant ionic charge carriers (e.g. K^+);

1. For the CEM, 76 ± 7 % of the charge was transported by K^+ , with the deficit being H^+/OH^- , and some phosphate transfer.
2. For the AEM, 36 ± 7 to 71 ± 13 % of the charge was transferred by phosphate ions, depending on the assumed charge, with the remainder being H^+/OH^- . No K^+ was transferred.
3. For the BS, 48 ± 6 % of the charge was transferred by K^+ , with the other half consisting of phosphate species and H^+/OH^- .

When comparing these findings to the membrane conductivities, shown in Table 8.4, the order of % transfer of K^+ mirrors the order in membrane conductivities, and the AEM, which had the lowest conductivity, had the highest % transfer of phosphate. Selectivity for K^+ ions therefore appears to result in a high membrane conductivity. Interestingly, in phosphate buffered electrolyte, the BS had a higher conductivity than the AEM, and transferred a higher

proportion of K^+ . Therefore, anion selectivity appeared to decrease membrane conductivity in this phosphate buffered electrolyte, in comparison to a non-ion selective membrane.

For the CEM, Nafion-117, Rozendal *et. al* found that 1/3 of the charge was transferred by K^+ , and 1/3 by Na^+ using phosphate buffered electrolyte, with a catholyte that was continuously dosed with NaOH to maintain neutral pH [199]. In this study, K^+ was been found to be far more important for charge transfer across Nafion-117, using conditions more frequently encountered in MFCs i.e. the catholyte is not dosed with NaOH. Additionally, AEMs which have been characterised in this way have been found to transfer higher proportions of OH^-/H^+ than phosphate species, with approximate percentages of 50 % [199] and 80 % [200] for OH^-/H^+ . This is in contrast to the finding here, where phosphate was found to be more significant for charge transfer.

Additionally to the charge transfer and ohmic resistance measurements, oxygen diffusion, D_{O_2} , and mass transfer coefficients, k_{O_2} , and acetate diffusion, D_{Ac} , and mass transfer coefficients, k_{Ac} , were calculated for the CEM, AEM and BS, using the methodology described in materials and methods. The results are presented in Tables 8.7 and 8.8. Both the acetate and oxygen diffusion experiments were run for 3 days, which was a greater time than for the charge carriers experiment. This time was chosen as it was found, experimentally, to give appreciable concentration differences between the two chambers in both the oxygen and acetate diffusion tests.

Membrane	Exp.	Chamber 1 DO		Chamber 2 DO		D_{O_2} 10 ⁻⁶ cm ² /s	k_{O_2} 10 ⁻⁴ cm/s
		Start mg/L	End mg/L	Start mg/L	End mg/L		
CEM	1	9.00	9.27	0.52	5.98	2.22	1.11
	2	9.24	9.80	0.08	6.53	2.53	1.27
	Ave.					2.37 ± 0.16	1.19 ± 0.08
AEM	1	8.76	9.00	0.19	6.60	1.27	1.34
	2	9.84	9.70	0.82	7.50	1.43	1.51
	Ave.					1.35 ± 0.08	1.42 ± 0.09
BS	1	9.02	9.03	0.03	5.83	1.87	1.14
	2	9.06	8.80	0.18	5.59	1.72	1.06
	Ave.					1.79 ± 0.08	1.10 ± 0.04

Table 8.7: CEM, AEM and BS diffusion, D_{O_2} , and mass transfer, k_{O_2} , coefficients for O_2 in 50 mM phosphate buffer solution. Concentration changes have been given in both chambers of the testing H-cell.

Oxygen diffusion and mass transfer coefficients for the CEM, AEM and BS were calculated from oxygen concentration changes between two different chambers separated by the membrane. The coefficients are given in Table 8.7. In terms of oxygen diffusion, all membranes

Membrane	Exp.	Chamber 1 [Ac]		Chamber 2 [Ac]		D_{Ac} 10 ⁻⁷ cm ² /s	k_{Ac} 10 ⁻⁵ cm/s
		Start mg/L	End mg/L	Start mg/L	End mg/L		
CEM	1	933.4	934.6	-1.6	-1.6	0.00	0.00
AEM	1	979.2	879.8	-1.6	-1.6	0.00	0.00
BS	1	935.6	733.4	-1.6	227.6	5.11	3.13
	2	993.6	945.4	-1.6	329.7	8.12	4.98
	Ave.					6.62 ± 1.51	4.06 ± 0.93

Table 8.8: CEM, AEM and BS diffusion, D_{Ac} , and mass transfer, k_{Ac} , coefficients for acetate in deionised water. Concentration changes have been given for both chambers of the testing H-cell.

exhibited some cross-over. These coefficients were in the order CEM > BS > AEM, with values $2.37 \pm 0.16 > 1.79 \pm 0.08 > 1.35 \pm 0.08 \times 10^{-6}$ cm²/s, and the O₂ diffusion coefficient determined for Nafion-117 (CEM) was in exact agreement with the value determined by Kim *et al.* of 2.4×10^{-6} cm²/s [196]. In terms of oxygen mass transfer coefficients, the membranes were in the order AEM > CEM > BS, with values $1.42 \pm 0.09 > 1.19 \pm 0.08 > 1.10 \pm 0.04 \times 10^{-4}$ cm/s. Therefore, the AEM had a significantly higher oxygen mass transfer coefficient than the other two membranes, so it is therefore predicted to have a significantly higher rate of O₂ flux from the cathode to anode when used in a full MFC. This is important, as increased O₂ flux to the anode is predicted to lower MFC coulombic efficiency and performance. The BS and CEM had significantly lower and equal O₂ mass transfer coefficients. All of the membranes allowed some O₂ mass transfer, which is due to the fact that O₂ is a small molecule and is able to diffuse through the membrane polymer structures. Considering just O₂ diffusion, CEM and AEM ion-selectivity is not predicted to confer any improvement on MFC coulombic efficiency or performance in comparison to the BS.

Acetate diffusion and mass transfer coefficients for the CEM, AEM and BS were calculated from acetate concentration changes between two different chambers separated by the membrane. The coefficients are given in Table 8.8. A change in acetate was not detected at all for the CEM and AEM, whereas acetate cross-over was considerable for the BS. For the BS, acetate was conserved in the first run ($733 + 228 = 961$ mg/L), but not for the second ($945 + 330 = 1275$ mg/L). This may have been due to an error in the chamber one reading for the second run, as the chamber two readings for both runs are not zero and are in good agreement with each other (279 ± 51 mg/L). For the BS, the diffusion coefficient for acetate was $6.62 \pm 1.51 \times 10^{-7}$ cm²/s and the mass transfer coefficient was $4.06 \pm 0.93 \times 10^{-5}$ cm/s. The fact that no acetate was detected going through the Ion Exchange Membranes (IEMs) is interesting, as acetate diffusion occurred through the Nafion-117 membrane and AEM (AMI-7001, mem-

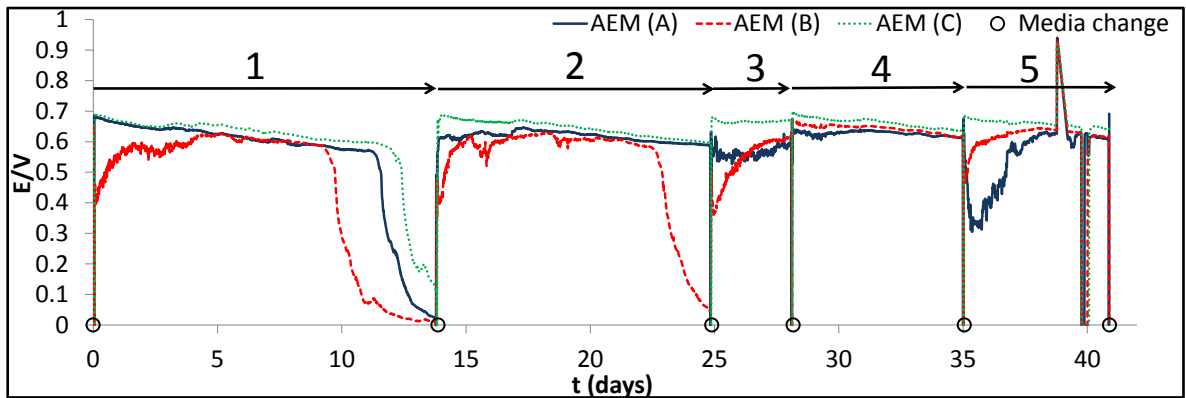
brane international, US) used in tests by Kim *et al.*, with diffusion coefficients of 0.82 and 2.6×10^{-9} cm²/s, respectively [196]. However, these values are still approximately 2 orders of magnitude lower than the diffusion coefficient reported for the BS in this study. In the case of the BS, the acetate diffusion coefficient was less than half the O₂ diffusion coefficient. However, in the aerobic biocathode MFC, acetate is typically in much higher concentration in the anode chamber (1000 mg/L) than O₂ is in the cathode chamber (8 mg/L). The situation may be different for a cell under load, as migration of negatively charged acetate occurs in the cathode to anode direction, but in the MFC system, acetate is only initially present in the anode chamber.

Acetate cross-over from the bioanode to biocathode in the MFC is predicted to have a detrimental effect on performance, primarily by lowering biocathode performance. This is predicted to be caused by heterotrophic growth in the biocathode chamber. Therefore, the BS is predicted to be the least suitable membrane for the MFC with an aerobic biocathode in terms of simple diffusion of acetate, although the situation may be different under load. It is unsurprising that the BS exhibits some acetate cross-over, as it has micro-channels of sufficient size to allow diffusion of larger molecules, such as acetate. For the ion-selective membranes, it may be that the pore size is much smaller, hindering the diffusion of acetate. Additionally, the CEM is not selective for negatively charged ions, such as acetate. These results indicate that the CEM and AEM do not allow acetate to cross-over in an MFC at the OCP. However, the situation may be different when the MFC is operated under a load, as acetate is a charged molecule. Measurements of acetate concentrations under load would have been more useful, in retrospect, particularly for the BS. This would be an interesting avenue to explore as part of future membrane characterisation work.

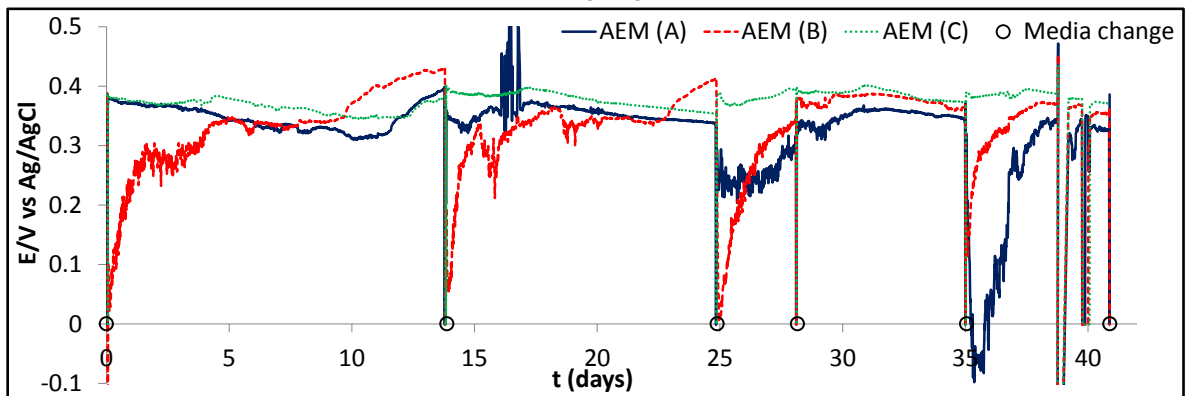
8.3.2 The effect of membrane-type on MFCs with an aerobic biocathode

The cell voltage, cathode potential and anode/cathode pH data for three acetate-fed batch aerobic biocathode MFCs (cells A, B and C) before membrane replacement operated with identical AEMs, were measured over 5 batch cycles and a 40 day operational period. These data are presented in Figure 8.2. The MFCs were operated over 510 Ω, a resistance previously determined as the resistance at peak power density. The same measurements were made for the 3 MFCs after membrane replacement with a CEM (cell A), an AEM (cell B) and a BS (cell C), over 5 batch cycles and a 40 day operational period. These data are presented in Figure 8.3.

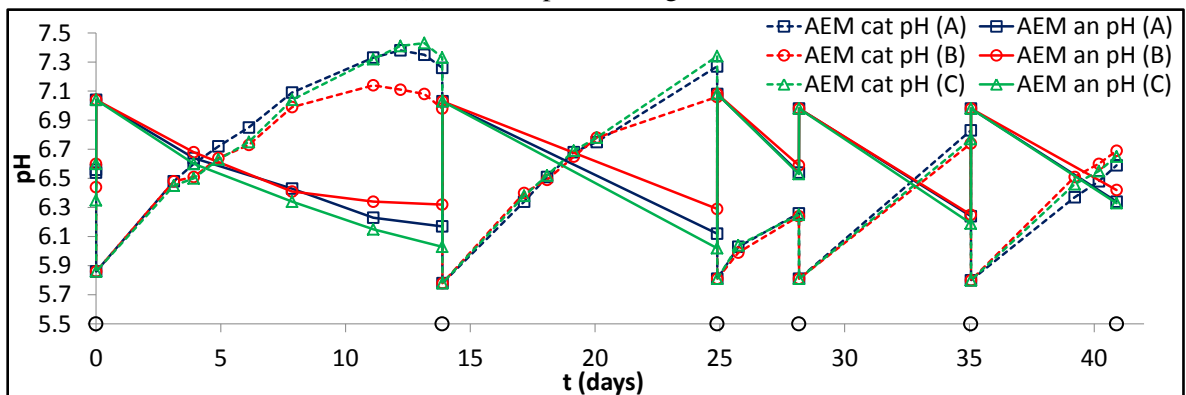
For the 1st period of operation before membrane replacement, with all cells having AEMs, the cell voltages were relatively constant, producing approximately 600 mV in cell voltage on



(a) Cell voltage against time

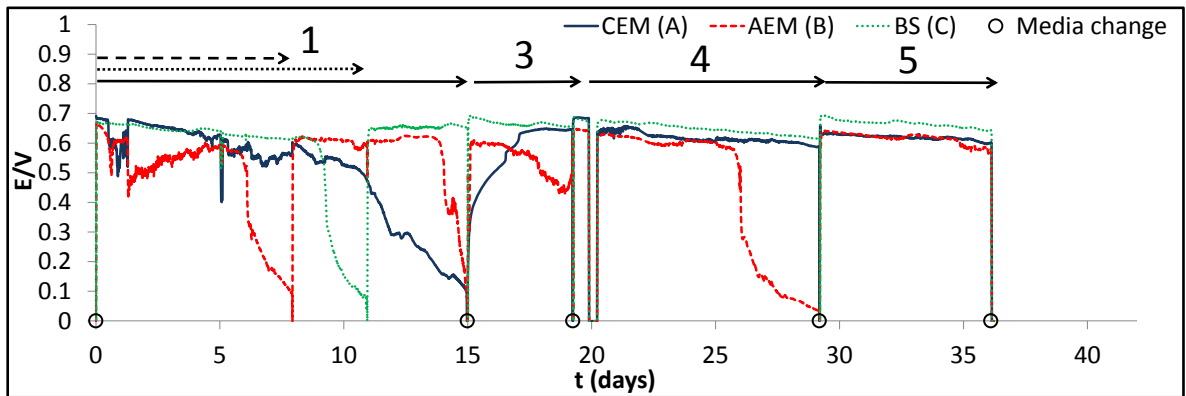


(b) Cathode potential against time

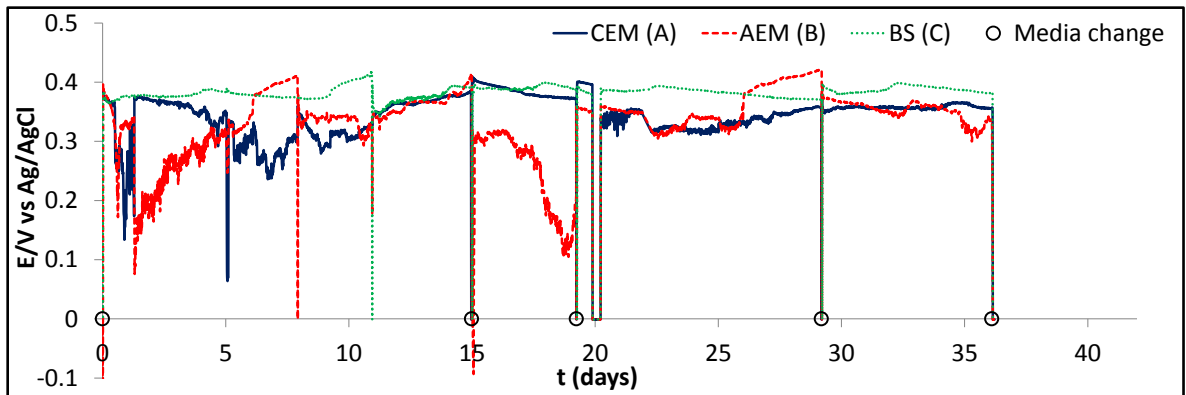


(c) Cathode and anode pH against time

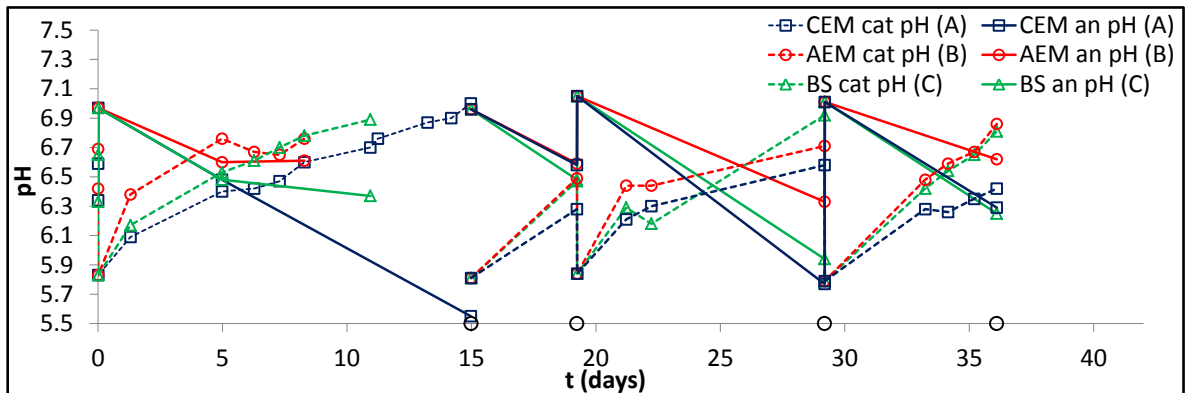
Figure 8.2: Cell voltage against time, cathode potential against time, and anode/cathode pH against time during the first operational period of 40 days for the three acetate-fed batch aerobic biocathode MFCs, fitted with AEMs (cells A-C). Media changes are given by circles along the time axes. Batch cycles are numbered.



(a) Cell voltage against time



(b) Cathode potential against time



(c) Cathode and anode pH against time

Figure 8.3: Cell voltage against time, cathode potential against time, and anode/cathode pH against time during the second operational period of 40 days for the three acetate-fed batch aerobic biocathode MFCs, fitted with different membranes; a CEM (cell A), a new AEM (cell B) and a BS (cell C). Media changes are given by circles along the time axes. Batch cycles are numbered.

average. This is shown in Figure 8.2. Batch cycle lengths were not kept constant, with latter batch cycles (3, 4 and 5) kept shorter to avoid significant pH splitting. This was not an ideal choice of operation, introducing experimental inconsistencies. Continuous flow operation would have been preferable, to avoid the need for batch operation, although continuous flow mode would have masked the pH splitting behaviour of the separators. Alternatively, MFCs could have been fed when the cell voltage reached zero, even though it can be seen from Figure 8.2 that these triplicate MFCs exhibit sufficient variation that the cells do not always deplete at the same time to be fed together (e.g. cell B during cycle 2). Equal batch cycle lengths, as determined by the operator, irrespective of MFC behaviour, may have been the best mode of operation for these MFCs.

The cathode potentials were between 300-400 mV for most of the batch cycles, with some deviation at the beginning of a batch cycle. For the second period of operation after membrane replacement, when the cells had a CEM (cell A), and AEM (cell B) and a BS (cell C), the cell voltages were fairly constant, and again averaged approximately 600 mV over the last two batch cycles (batch cycles 4 and 5). This is shown in Figure 8.3. Similarly, the cathode potentials during these last two cycles averaged between 300 and 400 mV, and were fairly constant. This indicates that in terms of cell voltage and cathode potential, there was not much difference between the CEM, AEM and BS membranes in the three cells.

For the first period of operation before membrane replacement, with all cells having AEMs, pH splitting was observed at both the anode and cathode. This is shown in Figure 8.2. Within each batch cycle, the biocathode potential and cell voltage decreased as the cycle progressed, and this was correlated with the splitting of pH.

For the second period of operation after membrane replacement, when the three cells with a CEM (cell A), an AEM (cell B) and a BS (cell C), pH splitting was again observed for each cell, and occurred to a similar extent. This is shown in Figure 8.3. This indicates that all three membranes split the pH due to transport of ions other than H^+/OH^- . This result agrees with the previous abiotic membrane tests.

For the first period of operation before membrane replacement (Figure 8.2), the coulombic efficiency values of batch cycle 1 with the 3 MFCs with identical AEMs were 48, 39 and 40 %, giving an average of 43 ± 5 %. For batch cycle 1 of the second period of operation after membrane replacement (Figure 8.3), the coulombic efficiencies were 46 % for the cell with the CEM (cell A), 26 % for the cell with the AEM (cell B), and 40 % for the cell with the BS (cell C). This corresponded to changes of -2, -13 and 0 % in the cell coulombic efficiencies on membrane replacement. Therefore, the only significant coulombic efficiency change was when the AEM was changed for a new AEM, which was perhaps due to the removal of the membrane biofouling. After membrane replacement, the lowest coulombic efficiency was

observed for the cell with the AEM, which may have been associated with the high O_2 mass transfer coefficient for this membrane in comparison to the other two. This cell also exhibited a shorter batch cycle length of 8 days. However, the lack of replicate MFCs meant that it was difficult to draw conclusions. Additionally, for the second period of operation, the batch cycle lengths were again inconsistent, like in the first period of operation, for the reasons discussed above. A better mode of operation would have been to maintain constant batch cycle lengths, irrespective of changes occurring in the cells (e.g. such as when the cell voltages reduced to zero, indicating complete substrate depletion), to ensure experimental consistency.

The coulombic efficiency of the cell with the BS did not change at all, which was not expected, as a high acetate cross-over from the anolyte to the catholyte was anticipated for the cell with the BS on the basis of high D_{Ac} and k_{Ac} values for the membrane, as shown in Table 8.8. However, acetate is negatively charged, and the ion should not be transported by migration from anode to cathode. Abiotic measurement of acetate concentration changes under load would be required to investigate this.

Polarisation curves, EIS and LSV were taken for all three cells at the end of the first 40 day operational period when all 3 cells had AEMs, and at the end of the second 40 day operational period when all 3 cells had different membranes. The polarisation curve, EIS and LSV data for the three cells at the end of these two operational periods is given in Figures 8.4, 8.5 and 8.6.

The polarisation curve data for all 3 cells taken before and after membrane replacement, presented in Figure 8.4, shows how the peak power density changed from 64 to 67 $\mu W cm^{-2}$, for the AEM to CEM cell (cell A), from 72 to 59 for the AEM to AEM cell (cell B), and from 92 to 80 for the AEM to BS cell (cell C). Therefore, the cell with the BS performed slightly better than the other two cells, with only a small measured reduction in performance. Considering the electrode potential data, also presented in Figure 8.4, it is clear that the limiting electrode was the biocathode, and that changes in the performance of this electrode mirrored changes in the peak power density performance. Significantly, the cell with the BS had a high-performing biocathode, and that this performance had not deteriorated significantly in comparison to the other two membranes, which was believed to be the case for the BS because of a possible significant transfer of acetate from the bioanode to the biocathode. However, the performance of the MFC with a BS may have been an event of singularity, without replicate reactors to confirm the results.

The EIS spectra were recorded immediately after the polarisation curves were taken before and after membrane replacement are presented in Figure 8.5. The absolute ohmic resistances varied between 122 and 153 Ω . These values were significantly smaller than the ohmic resistances reported in Chapter 7, Subsection 7.3.1, due to the significant increase in membrane

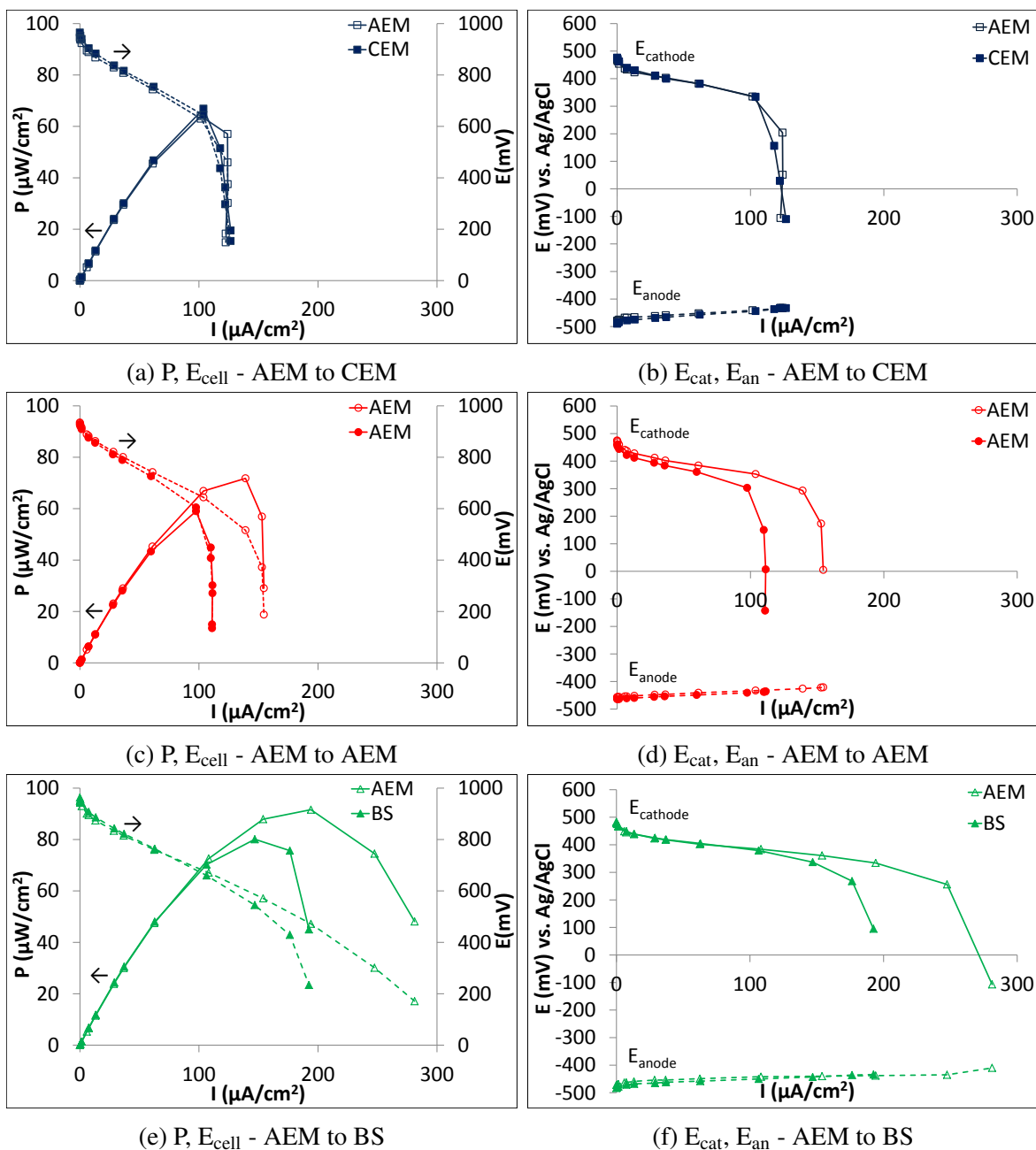
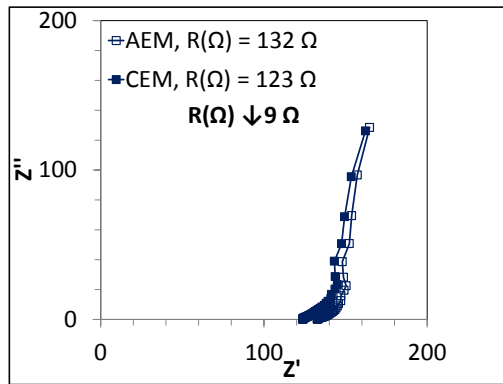
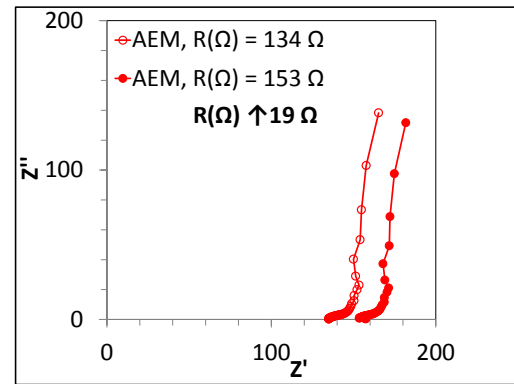


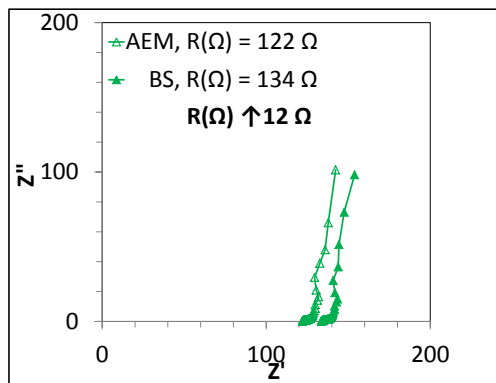
Figure 8.4: Polarisation curves with corresponding electrode potentials taken for the three aerobic biocathode MFCs at the end of the two operational periods; 1st 40 day operational period when the three cells had AEMs (cells A-C) (empty symbols), and the 2nd 40 day operational period when the cells had a CEM (cell A), a new AEM (cell B) and a BS (cell C) (filled symbols). Therefore, cell A is defined as AEM to CEM, cell B as AEM to AEM, and cell C as AEM to BS.



(a) EIS - AEM to CEM



(b) EIS - AEM to AEM



(c) EIS - AEM to BS

Figure 8.5: EIS taken for the three aerobic biocathode MFCs at the end of the two operational periods; 1st 40 day operational period when the three cells had AEMs (cells A-C) (empty symbols), and the 2nd 40 day operational period when the cells had a CEM (cell A), a new AEM (cell B) and a BS (cell C) (filled symbols). Therefore, cell A is defined as AEM to CEM, cell B as AEM to AEM, and cell C as AEM to BS.

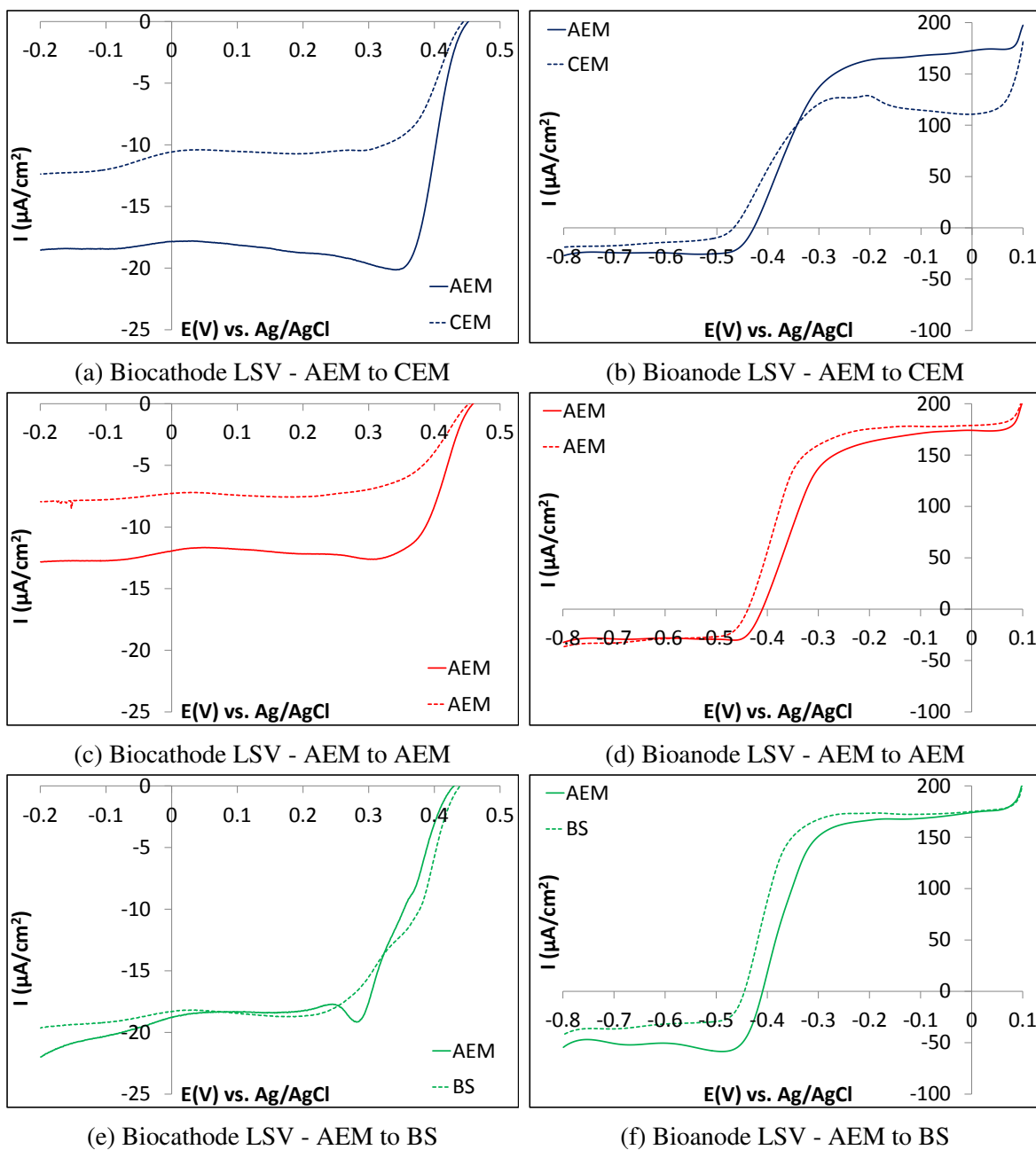


Figure 8.6: Biocathode and bioanode LSV taken for the three aerobic biocathode MFCs at the end of the two operational periods; 1st 40 day operational period when the three cells had AEMs (cells A-C) (solid lines), and the 2nd 40 day operational period when the cells had a CEM (cell A), a new AEM (cell B) and a BS (cell C) (dashed lines). Therefore, cell A is defined as AEM to CEM, cell B as AEM to AEM, and cell C as AEM to BS.

diameter on all 3 MFCs from 1 to 4 cm. This 16-fold increase in membrane area proportionally increased the MFC power outputs from approximately 20 to between 60 and 90 $\mu\text{W}/\text{cm}^2$ across all cells.

For the cell which had the AEM to CEM change, R_Ω decreased by 9 Ω , for the cell which had the AEM to new AEM change, R_Ω increased by 20 Ω , whilst for the cell which had the AEM to BS change, R_Ω increased by 12 Ω . The magnitude of the changes in cell ohmic resistance cannot be explained by differences in the type of membrane, as the membranes had ohmic resistances between 3 and 6 Ω , as determined by abiotic membrane characterisation (See Figure 8.4). Therefore, differences in membrane-type were negligible in comparison to changes in the electrolyte conductivity due to pH splitting. This demonstrates that the variation in ohmic resistance over time due to changing electrolyte composition is significant for the MFCs, and changes in electrolyte conductivity were reduced by recording the polarisation curve, EIS and LSV data 1-2 days after a media change, but they were not entirely eliminated. In terms of cell ohmic resistance, all MFC systems performed similarly, in the range between 122 and 153 Ω . The experimental methodology could be improved with respect to these measurements, in particular, by operating replicate reactors, and recording ohmic resistance measurements over time to understand how it varies. Additionally, an optimised cell architecture would have been useful so as to make the membrane a more significant contributor to cell ohmic resistance, versus the electrode spacing.

The LSV spectra taken after the polarisation curve and EIS spectra, at the end of both of the operational periods are presented in Figure 8.6. Comparison of the LSV spectra reveals some differences. For the cell with the AEM to CEM change, the biocathode LSV mass transfer limited current halved from -20 to -10 $\mu\text{A}/\text{cm}^2$, whilst the mass transfer limited current for the bioanode decreased from 175 to 125 $\mu\text{A}/\text{cm}^2$. For the cell with the AEM to new AEM change, the biocathode LSV mass transfer limited current decreased from -13 to -7 $\mu\text{A}/\text{cm}^2$, whilst the mass transfer limited current for the bioanode remained the same. The LSV for both the bioanode and biocathode of the cell with the AEM to BS change were the same before and after membrane incorporation.

Examination of the spectra shows that there was considerable variation in bioelectrode performance, particularly at the biocathode, in agreement with the MFC polarisation curves reported in Figure 8.4, which showed that the biocathode was the limiting electrode in all cases, and that the performance of this electrode varied, causing the changes in peak power. These LSV also indicate that the cell with the AEM to BS change did not suffer a large performance loss, which was predicted to occur as a consequence of significant acetate cross-over. However, acetate cross-over was not measured under load in the abiotic membrane tests, which means that there is uncertainty as to whether this occurs significantly for the BS in the

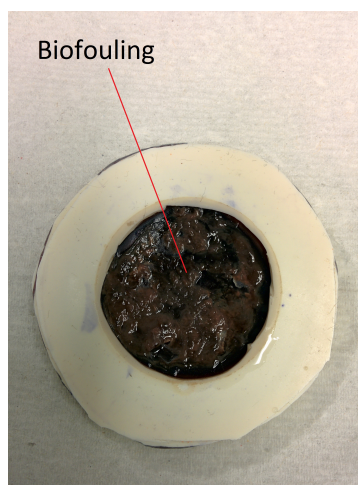
MFC.

Acetate transfer from the anode to the cathode was predicted to cause significant deterioration in biocathode performance for the cell where the AEM was changed to a BS, in comparison to the other membranes, as the other membranes exhibited no measurable acetate cross-over. However, this did not happen, and all 3 membrane MFC systems exhibited similar performances. For the BS, this may be because acetate is charged, and behaves differently under load, or that significant biofouling occurs at the membrane interface. Biofouling at the membrane interfaces was found to occur for all three of the membranes tested. Photos of thick biofouling for the AEM and BS are given as examples in Figure 8.7.

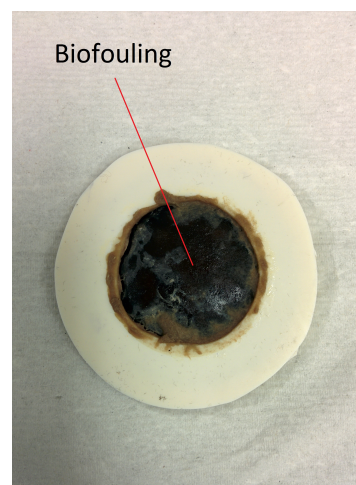
Biofouling is to be expected, given that O₂ crossover was observed for all three membranes, as shown in Table 8.7. Biofouling consumes acetate/O₂ at the membrane interface, regardless of membrane type, and is likely a big contributor to the reduced coulombic efficiency observed for these cells (43 ± 5 % before membrane replacement, when all 3 cells had AEMs) in comparison to those observed in some parts of the literature. For example, a coulombic efficiency of 75 % was observed for an acetate-fed tubular MFC system using ferricyanide as the catholyte [191]. Acetate concentration was measured for all of the MFCs catholytes during cycle 1 of the second operational period, but was found to be zero in all catholytes. This is because it is instantly consumed by the biofilm which develops at the catholyte-membrane interface. Membrane biofouling is a consequence of oxygen/acetate cross-over at the membrane/electrolyte interfaces (regions where acetate and oxygen mix).

Ionic concentrations were determined during the second operational period at the start and end of the first batch cycle, after changing the three membranes on the three cells to a CEM (cell A), AEM (cell B) and a BS (cell C). These data, as well as the calculated charges, are presented in Table 8.9. Additionally, a graph of the changes in charge at both the anode and cathode is given in Figure 8.8.

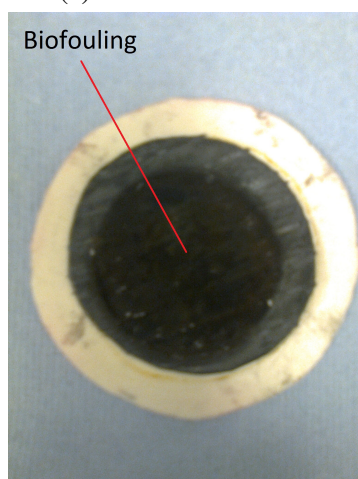
Initial examination of Table 8.9 shows how the charges were not very well conserved, having totals in excess of 100 % in some instances. This could be due to buffer imbalance between anode and cathode in the MFC, as the anode was buffered to pH 7.0, whilst the cathode was buffered to pH 5.8, therefore skewing the concentrations of K⁺, H⁺/OH⁻ and phosphate species, and creating diffusion gradients. In all of the results, phosphate accumulation at the anode was not balanced with depletion at the cathode, and skewed toward accumulation. This may have been due to diffusion of neutral H₂PO₄K / HPO₄K₂ / KOH between the two chambers, and might help to explain the net transfer of K⁺/Na⁺ from anode to cathode observed for the AEM, which was not observed at all in the abiotic test using equal buffer concentrations (Table 8.1). This additional effect may have caused error in the calculated charges. Therefore, a combination of migration and diffusion likely gave the results in Table



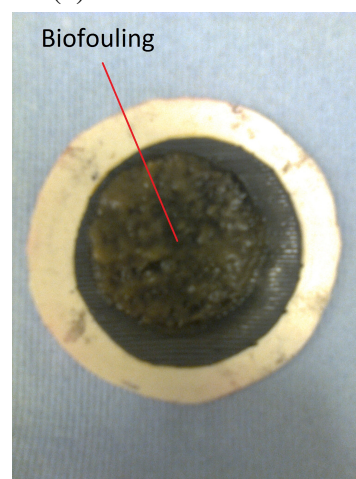
(a) AEM - anode side



(b) AEM - cathode side



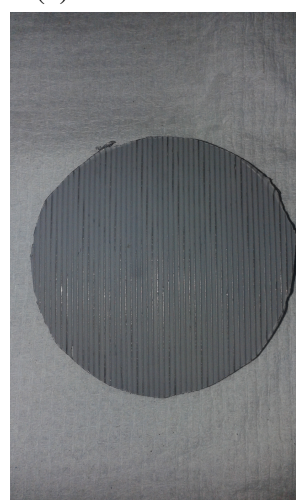
(c) BS - anode side



(d) BS - cathode side



(e) New AEM

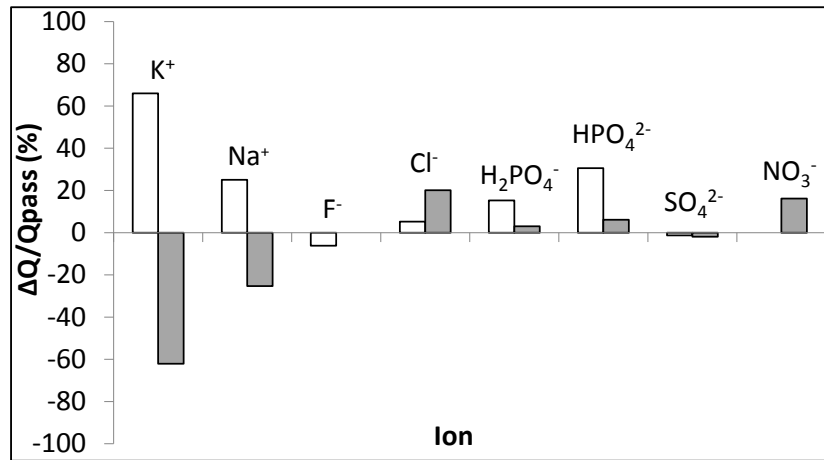


(f) New BS

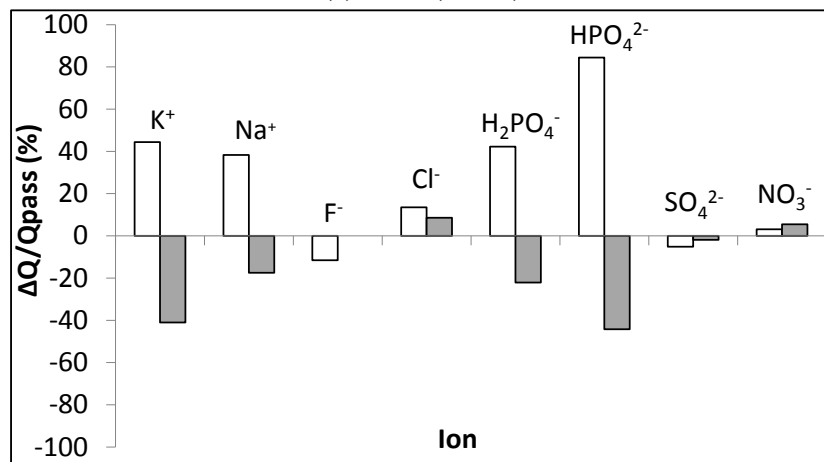
Figure 8.7: Images of biofouling on the AEM of cell A at the end of the 1st operational period on the anode-facing side (a) and cathode-facing side (b), and on the BS of cell C at the end of the 2nd operational period on the anode-facing side (c) and cathode-facing side (d). A fresh AEM (e) and BS (f) are presented for comparison.

Ion	Start		CEM (End)		AEM (End)		BS (End)	
	[AN] mM	[CAT] mM	[AN] mM	[CAT] mM	[AN] mM	[CAT] mM	[AN] mM	[CAT] mM
K ⁺	77.73	50.93	48.39	84.06	67.18	62.62	61.72	76.16
Na ⁺	18.22	0.30	7.08	13.80	9.13	5.28	7.12	8.57
F ⁻	2.74	0.00	0.00	0.00	0.00	0.00	0.00	0.00
Cl ⁻	5.58	5.87	7.90	16.61	8.78	8.31	9.39	9.78
Phosphate	48.61	51.94	55.40	53.57	58.63	45.64	58.35	54.30
SO ₄ ²⁻	1.38	1.45	1.09	0.94	0.77	1.18	1.14	1.22
NO ₃ ⁻	0.00	0.00	0.00	8.62	0.74	1.55	0.28	3.19
z	$\Delta Q/Q_{\text{pass}}$ %		$\Delta Q/Q_{\text{pass}}$ %		$\Delta Q/Q_{\text{pass}}$ %		$\Delta Q/Q_{\text{pass}}$ %	
K ⁺	1		66	-62	44	-41	44	-58
Na ⁺	1		25	-25	38	-17	30	-19
F ⁻	-1		-6	0	-12	0	-8	0
Cl ⁻	-1		5	20	13	9	10	9
H ₂ PO ₄ ⁻	-1		15	3	42	-22	27	5
HPO ₄ ²⁻	-2		31	6	84	-44	53	11
SO ₄ ²⁻	-2		-1	-2	-5	-2	-1	-1
NO ₃ ⁻	-1		0	16	3	5	1	7
Total (H ₂ PO ₄ ⁻)			104	-50	125	-69	103	-56
Total (HPO ₄ ²⁻)			119	-47	167	-91	130	-51

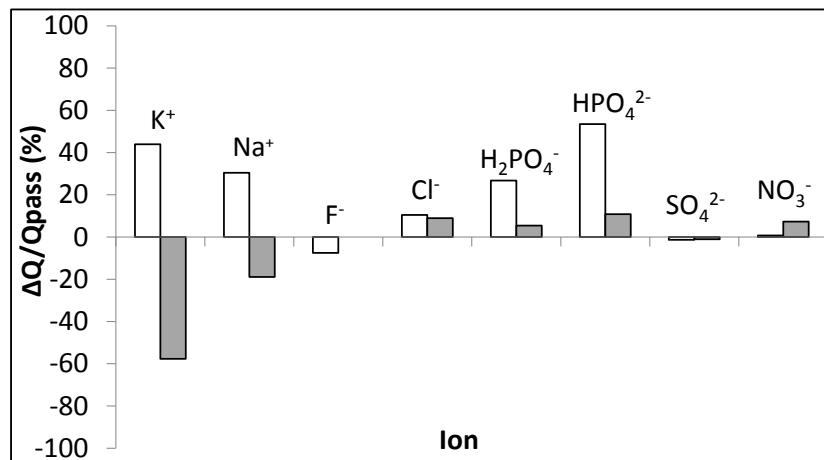
Table 8.9: Cathode and Anode ion concentrations in cells A (CEM), B (AEM) and C (BS) at the start and end of cycle 1 of the second operational period, and % changes in charge for each ion. ΔQ is the change in charge in coulombs for each ion assuming a specific ionic charge (z), and Q_{pass} is the charge passed in the external circuit for each MFC.



(a) CEM (cell A)



(b) AEM (cell B)



(c) BS (cell C)

Figure 8.8: % charge transfer at the anode and cathode for cell A (CEM), cell B (AEM) and cell C (BS) during batch cycle 1 of the second operational period. ΔQ is the charge attributed to each measured ion assuming a specific ionic charge (z), whilst Q_{pass} is the charge passed in the external circuit of the MFC. The ratio between the two is $\Delta Q/Q_{\text{pass}}$, expressed as a % . Empty bars are for charge changes at the anode, filled bars are for charge changes at the cathode.

8.9. Further examination of Table 8.9 shows that NO_3^- was detected in the catholytes at the end of the batch cycles, but not at the beginning. The reason for the presence of this ion is likely due to aerobic oxidation of NH_4^+ by nitrifying bacteria through a series of oxidations to NO_3^- (the ammonium present is from the macronutrient solution used to make the catholyte media). It was not considered in the charge balance, as it was not detected in significant concentration.

The summarised results given in Figure 8.8 show the same broad trends as observed for the abiotic membrane characterisation results, shown in Figure 8.1, despite the buffer imbalance in the MFC test. The changes for the cell with the CEM indicate that approximately 60 % of the charge was transferred by K^+ for this cell, whilst phosphate had the largest change in charge for the cell with the AEM, dependent on whether H_2PO_4^- or HPO_4^{2-} is assumed as the principal charge carrier. For the cell with the BS, an intermediate situation exists, though the combined total of K^+ and Na^+ is greater than that for phosphate, assuming either H_2PO_4^- or HPO_4^{2-} .

These findings agree broadly with the abiotic membrane characterisation, despite the likely occurrence of additional diffusive processes. Further experiments and/or models taking into account diffusive processes would likely improve the accuracy of the results. However, the general conclusion is that pH splitting is caused by the movement of phosphate and K^+ ions across the membrane in the MFC; the CEM transports K^+ over H^+/OH^- , the AEM transports phosphate over H^+/OH^- , and the BS transports K^+ /phosphate over H^+/OH^- . This is the origin of the pH splitting in this MFC system, and is a process which occurs regardless of membrane type.

8.4 Conclusions

Various properties of the membrane are predicted to have an impact on the performance of aerobic biocathode MFCs, such as pH splitting, oxygen/acetate cross-over and ohmic resistance. Abiotic membrane tests show that the reason for the pH splitting is due to the preferential transport of anions/cations other than H^+/OH^- . The results are summarised;

1. For the CEM, 76 ± 7 % of the charge was transported by K^+ , with the deficit being H^+/OH^- , and some phosphate transfer.
2. For the AEM, 36 ± 7 to 71 ± 13 % of the charge was transferred by phosphate ions, depending on the assumed charge, with the remainder being H^+/OH^- . No K^+ was transferred.

3. For the BS, $48 \pm 6\%$ of the charge was transferred by K^+ , with the other half consisting of phosphate species and H^+/OH^- .

The % of K^+ transferred over the membrane appeared to mirror membrane conductivities, with Nafion having the highest selectivity for H^+ and the highest membrane conductivity, and the AEM having the lowest selectivity for H^+ and the lowest conductivity. The pH splitting occurs regardless of membrane type; A CEM transports primarily K^+ , an AEM transports primarily phosphate species, and a BS transports both K^+ and phosphate species in preference to H^+/OH^- . Therefore, with respect to pH splitting, any one of these membranes is suitable for an MFC with an aerobic biocathode. All three membranes had some O_2 mass transfer, which was of the same order of magnitude, although the AEM had 1.5 times the O_2 mass transfer coefficient of the other two membranes. Acetate diffusion was only detectable for the BS, although k_{Ac} for the BS was an order of magnitude lower than the k_{O_2} values determined for the three membranes. In terms of ohmic resistance, the membrane area resistance was approximately 1.5 times greater for the BS in comparison to the CEM and AEM, at $64 \Omega \text{ cm}^2$.

This is the first time that a battery separator has been characterised in by in-depth, abiotic membrane characterisation experiment to determine principal charge carriers in phosphate buffered media. The results presented here are therefore highly relevant as a comparison with other ion exchange membranes, and demonstrate how ion exchange groups are not important to overall membrane function in the conditions found in MFCs.

The membranes were tested in full MFCs, and the following was found;

1. All three aerobic biocathode MFCs with different membranes performed similarly in terms of cell voltage over time (approximately 600 mV cell voltage at 510Ω), and the peak power densities were 67, 59 and $80 \mu\text{W}/\text{cm}^2$ for the cells with the CEM, AEM and BS, respectively. Differences between peak powers were associated with different biocathode performance over time. The MFC with the BS performed well, comparatively.
2. Coulombic efficiencies were in the range between 26-46 % for the three membranes, and the AEM, which had the highest O_2 mass transfer coefficient, had the lowest CE of 26 %. This was a reduction of 13 % from the previous value for this MFC with an old AEM, which may have been associated with removal of the membrane biofouling on replacement with a new AEM. However, this is speculative, without replicate MFCs and controls. A non-negligible k_{Ac} value for the BS did not translate into a lower CE in the MFC. Further abiotic tests with acetate crossover examined under electrolysis conditions are required to further investigate this.

3. pH splitting occurred for all 3 cells with different membranes to a similar extent, regardless of membrane-type.
4. The aerobic biocathode MFC with a BS exhibited no noticeable drop in performance in comparison to the other two MFCs with ion exchange membranes, making it a suitable membrane for this MFC system, despite a higher acetate diffusion coefficient.

In practice, the BS compared favourably in terms of MFC performance in comparison to the CEM and AEM. Therefore, the BS appears to be a good choice for this system, given its significantly lower cost. Membrane biofouling, caused by O₂/acetate crossover, is predicted to be the principle cause of lower coulombic efficiency levels across all cells, and should be investigated in future studies. Further optimisation of the cell architecture is required to further improve the peak power density output from the device, and further investigations of acetate cross-over under electrolysis conditions are required in order to determine why the MFC performance did not drop significantly in comparison to the MFCs with the other two membranes. Critically, replicate MFCs are required for future studies to verify many of the experimental findings. Additionally, the MFC studies required an optimised system architecture to increase the ohmic resistance contribution from the membrane, and the study would have benefited from more consistency in batch mode operation (to eliminate this as a potential source of variation). Measurements of ohmic resistance could have been made over time, as this was likely changing due to the dynamic nature of the system. The abiotic experiments would have served as better controls for the MFC experiments if many of these things had been met. However, this study does explore, for the first time, the use of a simple BS as a separator material between an aerobic biocathode and a bioanode in an MFC.

Chapter 9. Conclusions

9.1 Summary

An initial materials investigation using carbon felt, allowed determination of the poised-potential over which growth was possible on this material, and was a necessary pre-requisite for the enrichment step in poised-potential half-cells. For carbon felt, this poised-potential window was determined to be 0.0 to +0.6 V (pH 7.0). Further to this, the performance of the aerobic biocathodes in this thesis was found to be dependent on pH and oxygen mass transfer. The optimum pH was 5.8, although the majority of the performance was still retained as this was increased to neutral pH. In terms of O₂ mass transfer, in the absence of air sparging, with the DO = 5.0 - 5.5 mg/L, the reduction current for a half-cell at -0.1 V poised-potential was less than 50 $\mu\text{A}/\text{cm}^2$, and this increased significantly from 180 to 300 $\mu\text{A}/\text{cm}^2$ when the DO was increased from 7.5 to 8.0 mg/L. The biofilm was found to reside primarily on the carbon felt surface, with a penetration depth of between 20-30 %.

In terms of fundamental understanding of aerobic biocathodes, there is strong evidence to show that a dominant group of unidentified *Gammaproteobacteria*, which had 23-44 % sequence abundance in the community on polarised electrodes and < 1 % of the community on non-polarised control electrodes, is involved in the ORR catalysis of aerobic biocathodes with an onset potential for ORR of +0.4 V. This is the first time that a connection has been made between ORR catalysis in high-performing aerobic biocathodes (E_{onset} for ORR of +0.4 V) and the bacteria likely responsible for this catalysis. These bacteria were found to be 96 % similar to the dominant DGGE band (assigned as *Proteobacteria*) of another aerobic biocathode grown on carbon felt with a high onset E_{onset} for ORR of +0.35 V recovered from a freshwater sediment MFC [83]. They were also found to be 96 % similar to 3 unidentified *Gammaproteobacteria* clones isolated from bacterial communities in steel waste [275], which is a strong indicator that they perform this catalysis as part of metal bio-corrosion processes in the natural environment. Future work should focus on isolating these organisms and their enzymes. The enzymes would be excellent ORR catalysis for use in enzyme fuel cells, for example.

The response of the aerobic biocathode to azide inhibition shows that the ORR catalysis is very likely coupled to an electron transport chain, and therefore direct. Through electrochemical investigations, the mechanism of this direct ORR catalysis appears to change with the applied potential, with the presence of a reversible, diffusive redox peak with $E_{1/2} = +0.1$ V when the electrode is polarised at -0.1 V, which is absent when the electrode is polarised at $+0.2$ V. This is believed to be an additional ET pathway which the bacteria utilise to make use of the additional energy available from the more negative electrode potential, and may be a MET mechanism, or DET mechanism which gives a diffusive like-response, such as for a network of cytochromes. Interestingly, no such peaks are observed when the electrode is held at $+0.2$ V poised-potential, and the non-turnover CV at this poised-potential are featureless. Additionally, in all of the poised-potential electrodes, there are no peaks observed in the non-turnover CV at potentials close to $+0.4$ V. The reasons for a lack of non-turnover CV peak features in some of these cases is not currently understood, but must indicate some type of DET mechanism.

From the MFC studies, external variables which have a big impact on MFC performance have been investigated. Light clearly had a detrimental impact on performance due to the proliferation of red planktonic cell mass, believed to be PNS, which reduced the MFC coulombic efficiency and performance significantly. In terms of external resistance, a high resistance of 5480Ω was found to lower MFC performance in comparison to external resistances of 100 and 1000Ω . However, the degree of pH splitting, caused by the membrane, increased significantly as the resistance was lowered. One of the major problems with this aerobic biocathode was found to be the mass transport of oxygen to the biofilm, making the system more costly to run in terms of energy, than the energy given out. For the MFC, an increase in the DO of the catholyte from 3.2 to 6.9 mg/L resulted in an increase in cell voltage from 45 to 300 mV, and a further increase from 7.5 to 8.0 mg/L, resulted in a cell voltage increase from 360 to 600 mV. Therefore, O_2 mass transfer to the biofilm had a huge impact on MFC performance, which was particularly apparent when the electrolyte was not sparged.

In terms of the membrane, pH splitting was found to occur for a CEM, AEM and BS used in the MFC system. In abiotic tests, this was shown as the membranes having significantly different affinities for different ions, dependent on the membrane-type;

1. For the CEM, 76 ± 7 % of the charge was transported by K^+ , with the deficit being H^+/OH^- , and some phosphate transfer.
2. For the AEM, 36 ± 7 to 71 ± 13 % of the charge was transferred by phosphate ions, depending on the assumed charge, with the remainder being H^+/OH^- . No K^+ was transferred.

3. For the BS, 48 ± 6 % of the charge was transferred by K^+ , with the other half consisting of phosphate species and H^+/OH^- .

This is the first time that the principal charge carriers in phosphate buffered media have been determined for a simple BS. This gives insight into how the functionality of ion exchange membranes is not important to separator function in phosphate buffered electrolyte at neutral pH. It therefore shows that microporous membranes, such as battery separators, can function just as well as ion exchange membranes in MFCs.

The diffusion of acetate was found to be significant for the BS, and non-detectable for the AEM and CEM, whilst all three membranes exhibited some O_2 mass transfer under abiotic runs. Despite differences in membrane properties, particularly for the BS, there were no significant differences in performance between the three membranes when incorporated into the aerobic biocathode MFC system. O_2 appears to be the most significant membrane property, given that the CE values were all less than 50 %, two of the membranes did not exhibit any detectable acetate cross-over, and much higher CE values have been observed in the literature for acetate-fed MFC systems. The low CE values are accompanied by significant membrane biofouling. Small differences in membrane ohmic resistance did not have an impact on performance, and in practice, the much cheaper BS was found to be as effective as the other two ion exchange membranes, despite it having a non-negligible acetate mass transfer coefficient. Additionally, the BS had a higher conductivity than the AEM, which is likely due to it having more selectivity for K^+ than the AEM, which transported primarily anions.

Therefore, aerobic biocathode MFCs should be operated at peak power or lower resistance (provided pH splitting is minimised using flow systems or by recirculating spent anolyte into the catholyte) and using cheap battery separators (which have similar performance to functionalised membranes). Additionally, all types of MFCs using acetate as substrate at the anode should be operated in complete darkness in order to increase the competitiveness of the ARB at the bioanode.

9.2 Materials Cost

The biocathode makes a big improvement on lowering MFC capital cost. In the H-cell setup used in this thesis, used for development of the MFC system, the anode and cathode electrodes faced each other, with a membrane in between. The bioanode, biocathode and membrane were all of equal area. The price of the carbon felt was 417 £/m^2 and the RhinoHide BS was 1.5 £/m^2 . Scaling of this system to 1 m^2 , the reactor cost per m^2 is therefore $£ 417 \times 2$ (anode plus cathode) + $£ 1.5 = £ 835$, producing a power of 0.62 W/m^2 (using the power density reported in Chapter 7). The capital cost of the system with just a plain carbon elec-

trode is the same, but this time the power output is 0.07 W/m^2 . The same analysis can be carried out for the carbon cathode with Pt at a loading of 0.57 mg/cm^2 (5.7 g/m^2 , at a price of 133 £/g), giving a cost for the same system of $£ 1593$, with a power density of 0.70 W/m^2 . Therefore, Pt almost doubles the capital cost of the system, whilst giving a similar performance to the biocathode, and the MFC performance is 9-fold lower with just the plain carbon felt electrode. This cost analysis is summarised in Table 9.1, along with a column giving the capital cost to power ratio, which is a simple measure of the energy per capital cost of the system.

MFC	Price per m^2 of reactor £/m^2	Power per m^2 of reactor W/m^2	Price/Power £/W
Biocathode	835	0.62	1347
Pt	1593	0.70	2276
Carbon	835	0.07	11926

Table 9.1: A simple comparative MFC capital cost analysis. The cost of the MFCs using a biocathode, Pt (5.7 g/m^2) cathode and a plain carbon cathode are given. Price/Power is a ratio used for comparison, in order to factor in power performance. The cost analysis is with a RhinoHide BS.

As can be seen from the above cost analysis, carbon felt is prohibitively expensive, greatly increasing the reactor cost. In comparison, carbon fiber veil is 6.70 £/m^2 [39]. Assuming that this material would have given the same performance as carbon felt (which is not an unreasonable assumption, given that carbon felt has limited activity), then this makes the reactor cost 14.90 £/m^2 , and reduces the price/power ratio to 24.03 £/W . Additionally, the low-cost battery separator used in this study could have been replaced with a ceramic separator, with the added advantage that the ceramic can also serve as the walls of the MFC. Like battery separators, ceramic materials can also be very cheap ($£ 0.06$ for an earthenware pot of 400 ml volume [104]). The price/power reported here is still much more expensive than e.g. photovoltaic cells (approximately 0.2 £/W), but MFCs are the only technology that produce electricity directly from wastewater. They should also be complimentary to the anaerobic digestion technology, which operates at much higher organic loadings.

One of the important things to point out with the cost analysis is that this MFC system, regardless of the cathode, requires energy-intensive aeration of the catholyte, which would add significant operational costs. To provide mass transport of oxygen to the cathode, systems using a flow of catholyte should be explored. Pumps would have to be used anyway, in order to transport anode substrate into the anode chamber, and the anode effluent could perhaps be recirculated to the cathode. A similar system to the one developed by Clauwaert *et al.*, a tubular MFC utilising a biocathode on the external face [76], could perhaps be used for this. Individual MFCs could also be stacked as a gravity cascade, with some of the energy

produced used to power the pumps for feeding [37]. Gas diffusion electrodes as biocathode supports are another alternative to these flow systems, of which there have been a couple of studies [81, 91]. These electrodes could be optimised for aerobic biocathodes (instead of for chemical catalysts), by increasing the porosity of the material in order to increase biofilm size, and by looking at ways to increase O_2 mass transfer to the biofilm (by e.g. reducing the number of PTFE layers on the GDE). With a proper system of aeration, mass transport of O_2 to the biocathode should not be an issue.

Despite the need for further optimisation, the data presented in table 9.1 does provide a useful comparison between the different cathode types, showing how the biocathode is an effective substitute for a chemical catalyst, and how the performance of the system with plain carbon is enhanced considerably on modification of the cathode with an aerobic biocathode. With the MFC system with a biocathode, the single biggest contributor to capital cost is the carbon felt support used for the bioanode and biocathode biofilms. This underlies the importance of research into suitable bioanode and biocathode supporting materials.

9.3 Recommendations for Further Work

More work needs to be done to identify the reversible redox peak with $E_{1/2} = +0.1$ V, and the mechanism of ET more generally. This could be possible through detailed electrochemical investigations on isolated bacteria and proteomics studies. From these investigations, the electron transport chain and mechanism of electron transport could be worked out. Isolation of the bacteria would be difficult, and an electrode-dependent culture method would be necessary.

From an engineering perspective, identification of the best performing ORR catalysts would be particularly useful, allowing the tailoring of mixed-community aerobic biocathodes in order to select for these groups of bacteria, for example, by chemical modification of the cathode electrode surface, or optimising various other conditions, such as pH, ammonium concentration and temperature. Both the bioanode and biocathode materials might be further developed in order to enhance selectivity for the desired bacteria. More fundamental investigations are clearly needed in order to understand all of the processes which affect biocathode performance.

For the MFC, the O_2 mass transport limitation problem must be solved. Gas diffusion electrodes are an obvious way to this, and could be incorporated into a stacked MFC system which powers the pumps for operation, whilst also supplying surplus energy [37]. Another way to solve the O_2 mass transport limitation problem might be to recirculate the spent anolyte over the cathode, using a minimal catholyte volume over an open-air cathode (similar to a trickling

filter) in order to allow for efficient diffusion of oxygen from the air. The cell architecture of the system reported in this thesis could be greatly improved. This should be done by decreasing the anode to cathode electrode spacing. Some recent novel architectures utilising ceramic materials could be used to do this effectively for individual MFCs [39, 143]. Additionally, considering the findings in this thesis, the MFCs should be constructed using cheap electrode and separator materials. The electrode materials could be easily replaced with cheaper alternatives (e.g. carbon veil), and there are many cheap options for separator materials (battery separators and ceramics). Any MFC system would also need to be tested using real wastewater at the anode, which is likely to give a lower power output.

9.4 Closing Comments

A more fundamental understanding of the biocathode catalysts is clearly now needed. However, the aerobic biocathode is already an excellent substitute for a chemical catalyst, and has the enormous advantage over a chemical catalyst of not degrading and maintaining its performance over long periods of time. Optimised architectures, cheap electrode/membranes, and gas diffusion electrodes, are already available for MFCs, and the next step should be to incorporate these. This system could then be used to produce sustainable electrical power from wastewater at low cost.

Appendix A. Additional material



Figure A.1: Image of a graticule slide taken at x100 magnification using an epifluorescence microscope (Olympus BX40) fitted with a digital camera (Olympus E-400). The rule has 1mm/0.01 divisions (10 μm). From this image, the image height has been determined as 0.55 mm.

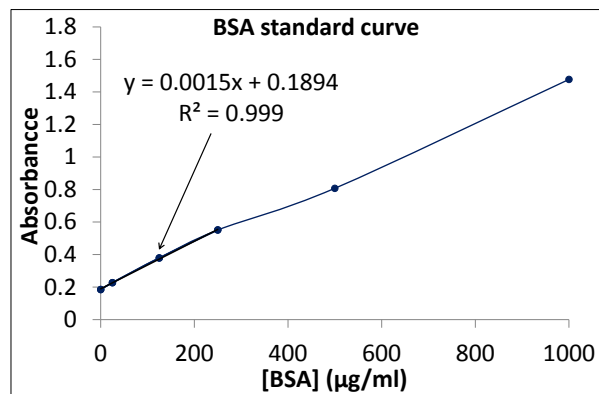


Figure A.2: BSA standard curve obtained using 0, 25, 125, 250, 500 and 1000 $\mu\text{g/ml}$ BSA dilutions from a 2 mg/ml BSA stock. The curve was fitted using a quadratic function. Absorbance was measured at 562 nm.

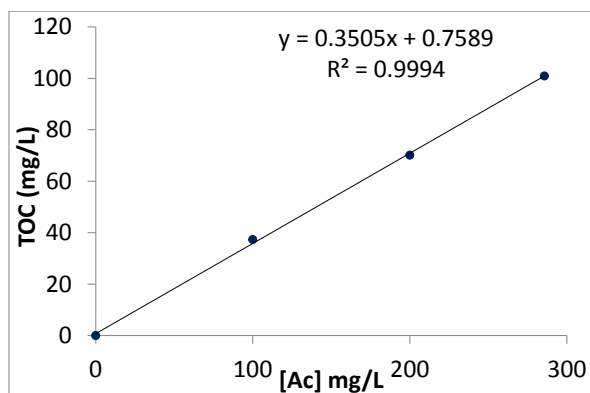
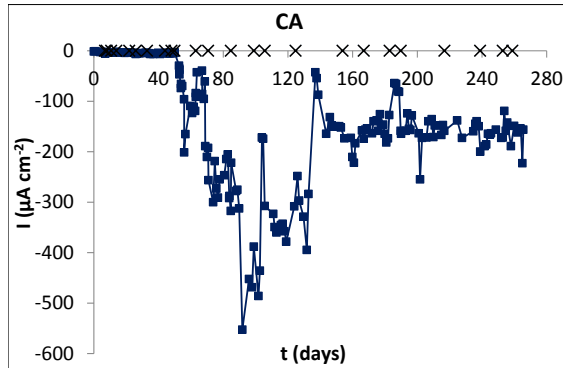
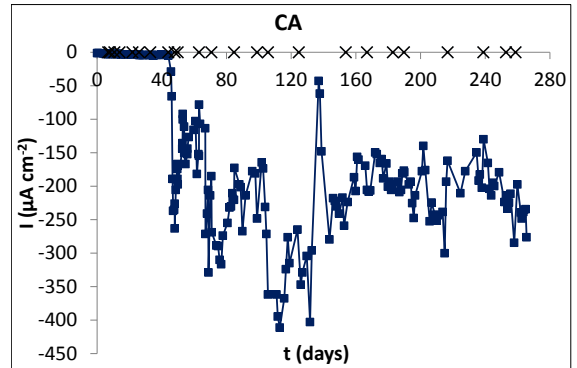


Figure A.3: TOC calibration using x 3.5, 5, 10 diluted bioanode medium (1 g/L sodium acetate, 50 mM pH 7.0 phosphate buffer, nutrient solutions) and DI water.

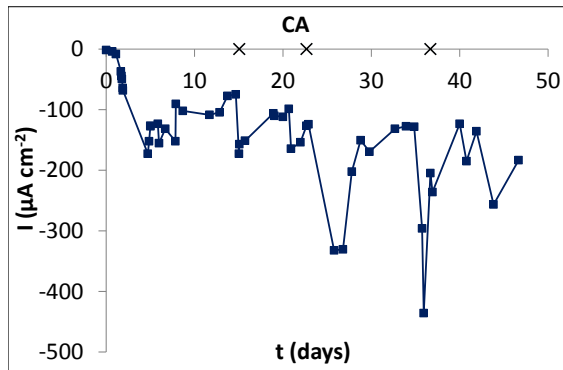
$$\begin{aligned} \frac{d[\text{H}_2\text{O}_2]}{dt} &= r - k[\text{H}_2\text{O}_2] & (\text{A.1}) \\ \frac{1}{k} \frac{d[\text{H}_2\text{O}_2]}{dt} &= \frac{r}{k} - [\text{H}_2\text{O}_2] \\ \int_0^{[\text{H}_2\text{O}_2]} \frac{1}{\frac{r}{k} - [\text{H}_2\text{O}_2]} d[\text{H}_2\text{O}_2] &= \int_0^t k dt \\ -\ln \left[\frac{r}{k} - [\text{H}_2\text{O}_2] \right]_0^{[\text{H}_2\text{O}_2]} &= kt \\ \ln \left(\frac{r}{k} - [\text{H}_2\text{O}_2] \right) - \ln \left(\frac{r}{k} \right) &= -kt \\ \ln \left(\left(\frac{r}{k} - [\text{H}_2\text{O}_2] \right) \left(\frac{k}{r} \right) \right) &= -kt \\ \left(\frac{r}{k} - [\text{H}_2\text{O}_2] \right) \left(\frac{k}{r} \right) &= e^{-kt} \\ [\text{H}_2\text{O}_2] &= \frac{r}{k} (1 - e^{-kt}) \end{aligned}$$



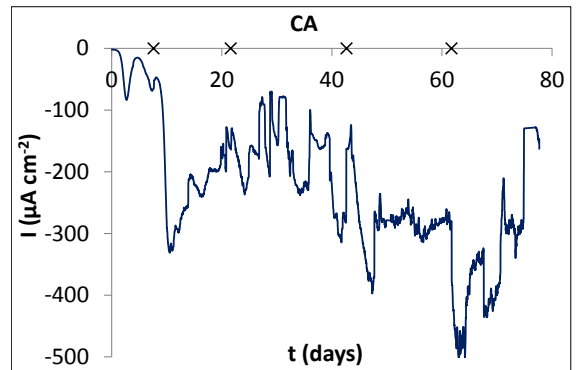
(a) -0.1 primary inoc. (A)



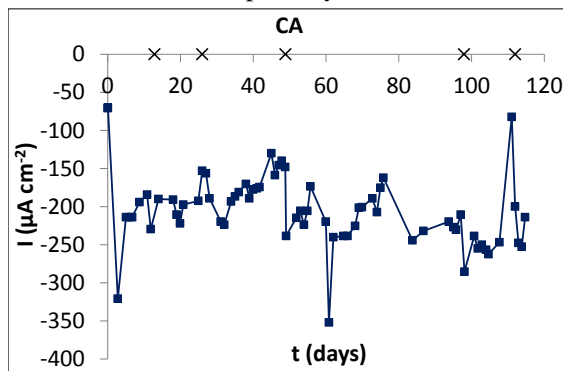
(b) -0.1 V primary inoc. (B)



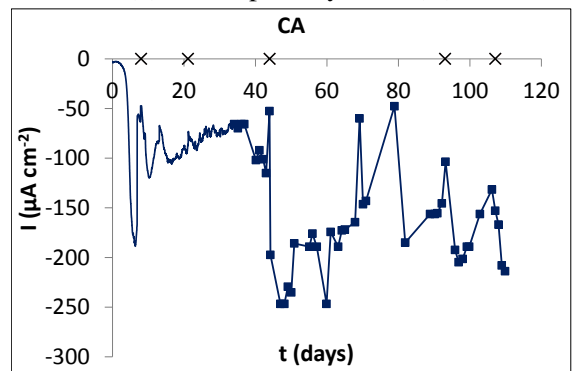
(c) -0.1 V primary inoc. (C)



(d) -0.1 V primary inoc. (D)

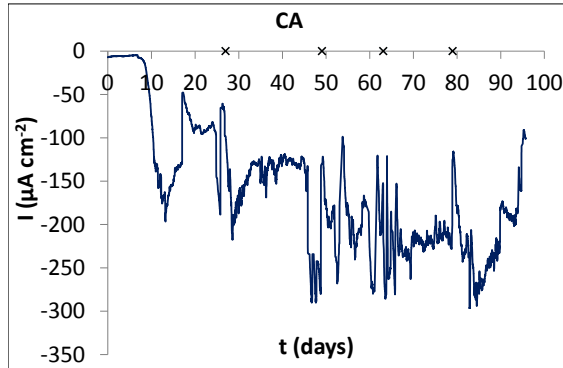


(e) -0.1 V primary inoc. (E)

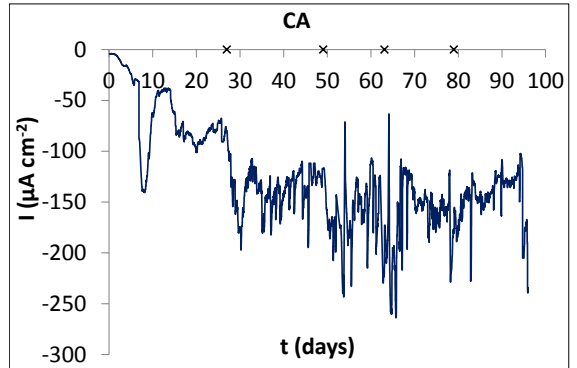


(f) -0.1 V primary inoc. (F)

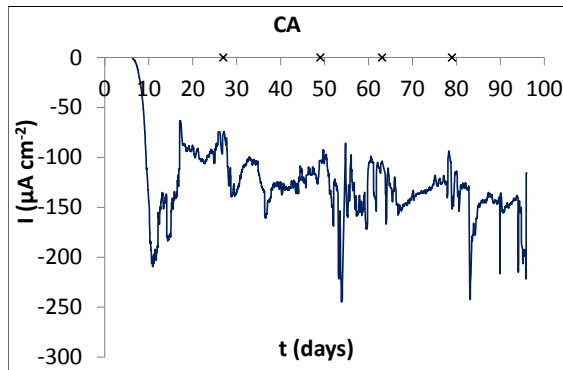
Figure A.4: CA data for half-cells A-F



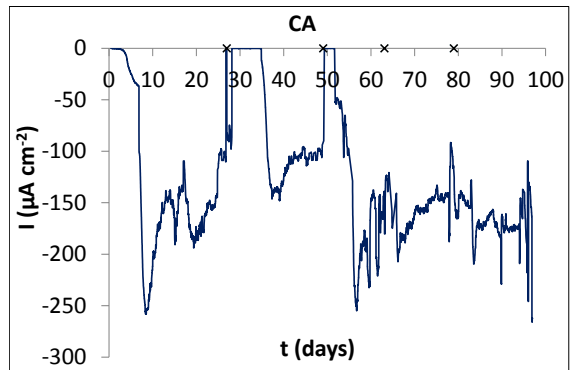
(a) -0.1 V secondary inoc. (G)



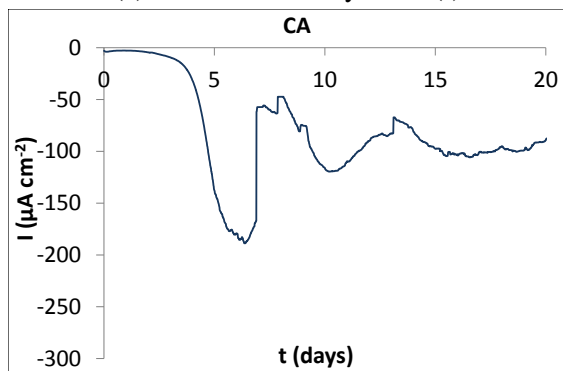
(b) -0.1 V secondary inoc. (H)



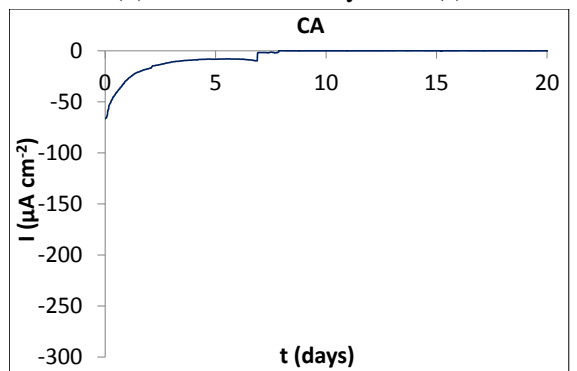
(c) +0.2 V secondary inoc. (I)



(d) +0.2 V secondary inoc. (J)

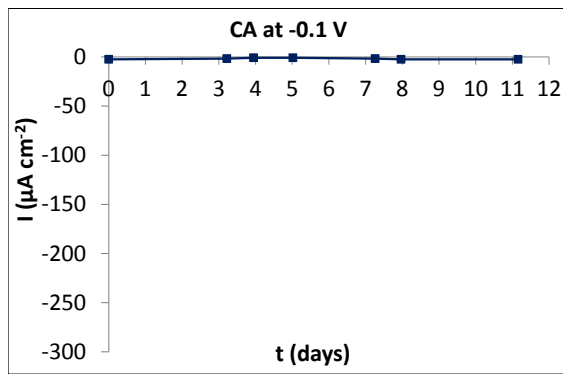


(e) -0.1 V secondary inoc. (K)

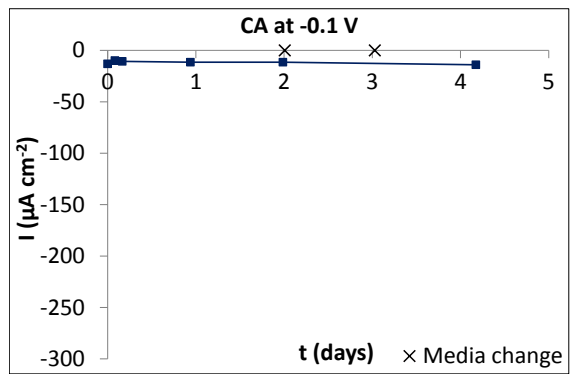


(f) -0.2 V secondary inoc. (L)

Figure A.5: CA data for half-cells G-L

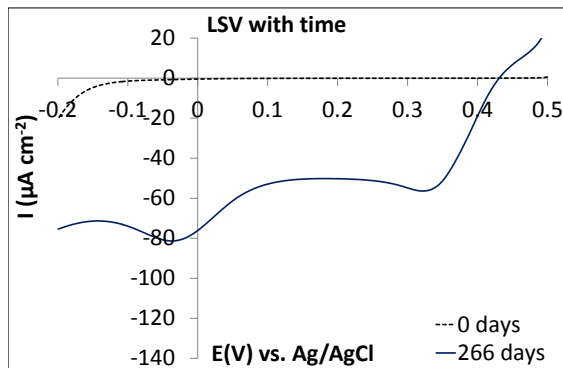


(a) CNT - no inoculum

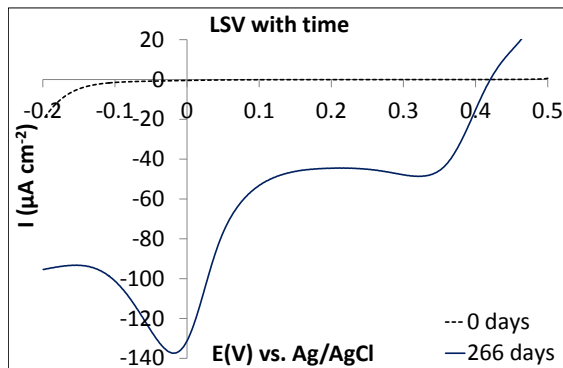


(b) CNT - x 10 [metals]

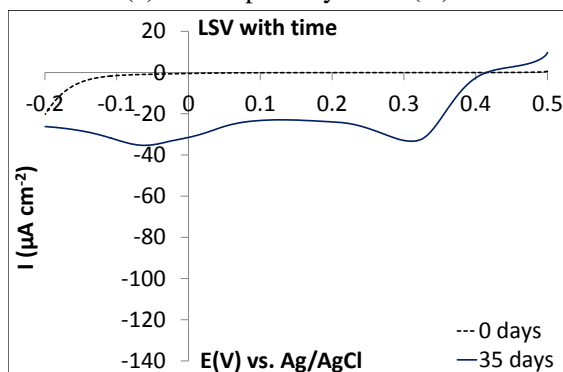
Figure A.6: CA data for control half-cells.



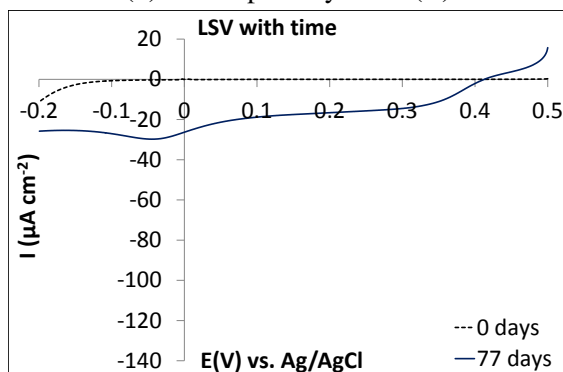
(a) -0.1 V primary inoc. (A)



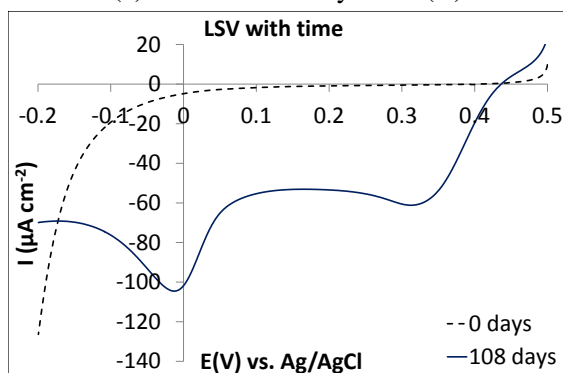
(b) -0.1 V primary inoc. (B)



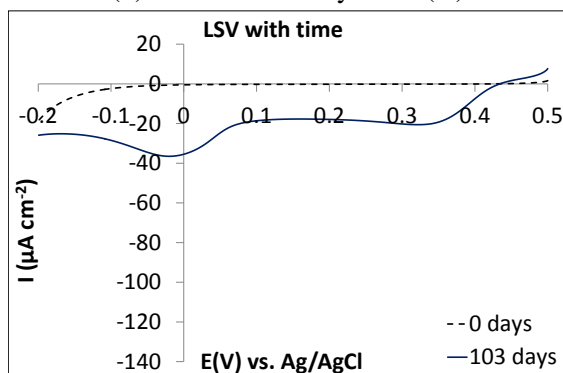
(c) -0.1 V secondary inoc. (C)



(d) -0.1 V secondary inoc. (D)

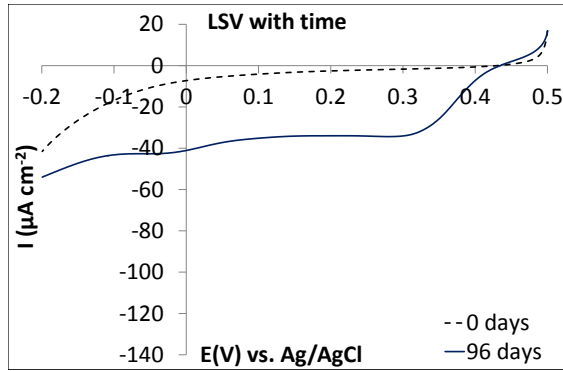


(e) -0.1 V secondary inoc. (E)

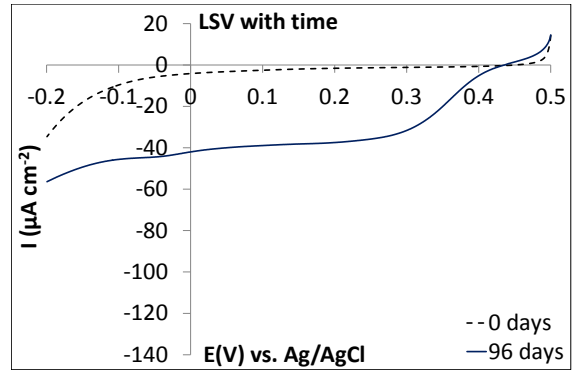


(f) -0.1 V secondary inoc. (F)

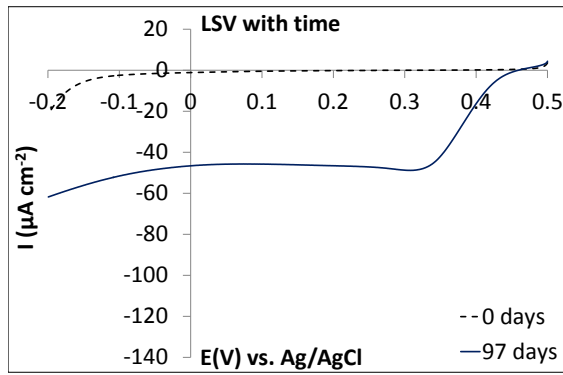
Figure A.7: LSV data for half-cells A-F



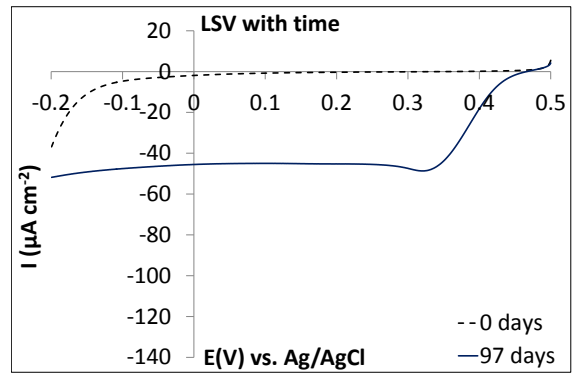
(a) -0.1 V secondary inoc. (G)



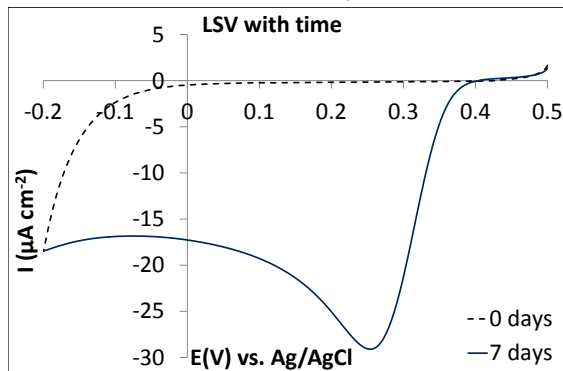
(b) -0.1 V secondary inoc. (H)



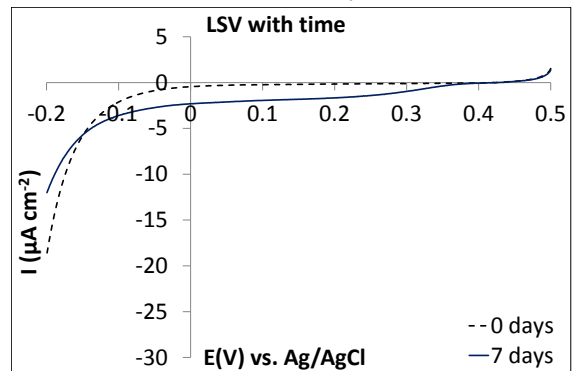
(c) +0.2 V secondary inoc. (I)



(d) +0.2 V secondary inoc. (J)

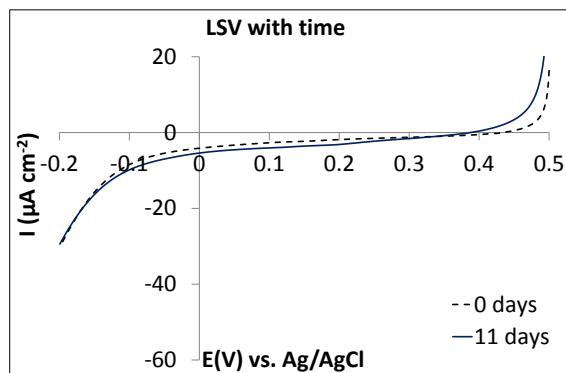


(e) -0.1 V secondary inoc. (K)



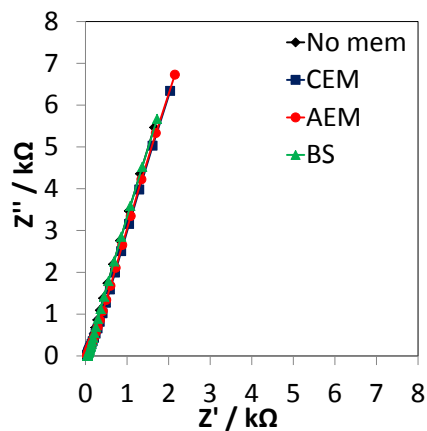
(f) -0.2 V secondary inoc. (L)

Figure A.8: LSV data for all half-cells G-L

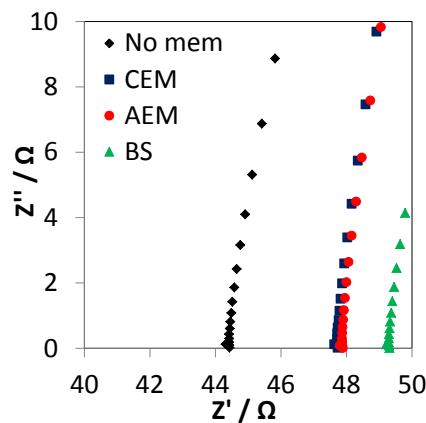


(a) CNT - no inoculum

Figure A.9: LSV data for the control half-cell



(a) 1-8 kΩ real impedance



(b) 40-50 Ω real impedance

Figure A.10: 2-electrode EIS spectra of the membrane ohmic resistance testing cell without a membrane, with a CEM (Nafion), with an AEM (Fumasep FAD) and with a BS (RhinoHide), using pH 7.0 anode medium as electrolyte (pH 7.0 phosphate buffer, 1 g/L sodium acetate, trace solutions). Graph (a) shows the EIS spectra over the complete frequency range (1-8 kΩ real impedance), whilst graph (b) gives the same EIS spectra between 40-50 Ω, real impedance.

References

- [1] Koen Wetser, Emilius Sudirjo, Cees J.N. Buisman, and David P.B.T.B. Strik. Electricity generation by a plant microbial fuel cell with an integrated oxygen reducing biocathode. *Applied Energy*, 137(0):151–157, 2015.
- [2] David P. B. T. B. Strik, H. V. M. Hamelers (Bert), Jan F. H. Snel, and Cees J. N. Buisman. Green electricity production with living plants and bacteria in a fuel cell. *International Journal of Energy Research*, 32(9):870–876, 2008.
- [3] M. Helder, D.P.B.T.B. Strik, H.V.M. Hamelers, A.J. Kuhn, C. Blok, and C.J.N. Buisman. Concurrent bio-electricity and biomass production in three plant-microbial fuel cells using *Spartina anglica*, *Arundinella anomala* and *Arundo donax*. *Bioresource Technology*, 101(10):3541 – 3547, 2010.
- [4] David P.B.T.B. Strik, Hilde Terlouw, Hubertus V.M. Hamelers, and Cees J.N. Buisman. Renewable sustainable biocatalyzed electricity production in a photosynthetic algal microbial fuel cell (PAMFC). *Applied Microbiology and Biotechnology*, 81(4):659–668, 2008.
- [5] Sharon B. Velasquez-Orta, Tom P. Curtis, and Bruce E. Logan. Energy from algae using microbial fuel cells. *Biotechnology and Bioengineering*, 103(6):1068–1076, 2009.
- [6] Avinash Shantaram, Haluk Beyenal, Raaja Raajan Angathevar Veluchamy, and Zbigniew Lewandowski. Wireless sensors powered by microbial fuel cells. *Environmental science & technology*, 39(13):5037–5042, 2005.
- [7] Conrad Donovan, Alim Dewan, Deukhyoun Heo, and Haluk Beyenal. Batteryless, wireless sensor powered by a sediment microbial fuel cell. *Environmental science & technology*, 42(22):8591–8596, 2008.
- [8] Conrad Donovan, Alim Dewan, Huan Peng, Deukhyoun Heo, and Haluk Beyenal. Power management system for a 2.5 w remote sensor powered by a sediment microbial fuel cell. *Journal of Power Sources*, 196(3):1171–1177, 2011.

- [9] Ioannis Ieropoulos, Chris Melhuish, John Greenman, and Ian Horsfield. Ecobot-ii: An artificial agent with a natural metabolism. *Journal of Advanced Robotic Systems*, 2(4):295–300, 2005.
- [10] Ioannis Ieropoulos, John Greenman, Chris Melhuish, and Ian Horsfield. Ecobot-iii-a robot with guts. In *ALIFE*, pages 733–740, 2010.
- [11] Chris Melhuish, Ioannis Ieropoulos, John Greenman, and Ian Horsfield. Energetically autonomous robots: food for thought. *Autonomous Robots*, 21(3):187–198, 2006.
- [12] Parliamentary Office of Science and Technology. *Energy and Sewage*, April 2007. Postnote 282.
- [13] B. E. Logan. Exoelectrogenic bacteria that power microbial fuel cells. *Nature Reviews Microbiology*, 7(5):375–381, 2009.
- [14] Bruce Logan. Effective wastewater treatment using microbial fuel cells and anaerobic fluidized bed membrane bioreactors. In *2nd European meeting of the International Society for Microbial Electrochemistry and Technology*, Aug 2014.
- [15] Korneel Rabaey, Nico Boon, Monica Höfte, and Willy Verstraete. Microbial phenazine production enhances electron transfer in biofuel cells. *Environmental science & technology*, 39(9):3401–3408, 2005.
- [16] Bruce E. Logan and John M. Regan. Microbial fuel cells - challenges and applications. *Environmental Science & Technology*, 40(17):5172–5180, 2006.
- [17] Feng Zhao, Falk Harnisch, Uwe Schröder, Fritz Scholz, Peter Bogdanoff, and Iris Herrmann. Application of pyrolysed iron(II) phthalocyanine and CoTMPP based oxygen reduction catalysts as cathode materials in microbial fuel cells. *Electrochemistry Communications*, 7(12):1405–1410, 2005.
- [18] Eileen Yu, Shaoan Cheng, Keith Scott, and Bruce Logan. Microbial fuel cell performance with non-Pt cathode catalysts. *Journal of Power Sources*, 171(2):275–281, 2007.
- [19] Kien Ben Liew, Wan Ramli Wan Daud, Mostafa Ghasemi, Jun Xing Leong, Swee Su Lim, and Manal Ismail. Non-Pt catalyst as oxygen reduction reaction in microbial fuel cells: A review. *International Journal of Hydrogen Energy*, 39(10):4870–4883, 2014.

- [20] Stefano Freguia, Korneel Rabaey, Zhiguo Yuan, and Jürg Keller. Non-catalyzed cathodic oxygen reduction at graphite granules in microbial fuel cells. *Electrochimica Acta*, 53(2):598–603, 2007.
- [21] Benjamin Erable, Narcis Duteanu, SM Kumar, Yujie Feng, Makarand M Ghangrekar, and Keith Scott. Nitric acid activation of graphite granules to increase the performance of the non-catalyzed oxygen reduction reaction (ORR) for MFC applications. *Electrochemistry communications*, 11(7):1547–1549, 2009.
- [22] B. E. Logan. *Microbial Fuel Cells*. John Wiley & Sons, Inc., 2008.
- [23] Michael C Potter. Electrical effects accompanying the decomposition of organic compounds. *Proceedings of the Royal Society of London. Series B, Containing Papers of a Biological Character*, pages 260–276, 1911.
- [24] Anthony Janicek, Yanzen Fan, and Hong Liu. Design of microbial fuel cells for practical application: a review and analysis of scale-up studies. *Biofuels*, 5(1):79–92, 2014.
- [25] Heming Wang, Jae-Do Park, and Zhiyong Jason Ren. Practical energy harvesting for microbial fuel cells: A review. *Environmental science & technology*, 49(6):3267–3277, 2015.
- [26] Deepak Pant, Anoop Singh, Gilbert Van Bogaert, Stig Irving Olsen, Poonam Singh Nigam, Ludo Diels, and Karolien Vanbroekhoven. Bioelectrochemical systems (bes) for sustainable energy production and product recovery from organic wastes and industrial wastewaters. *Rsc Advances*, 2(4):1248–1263, 2012.
- [27] Yonggang Yang, Guoping Sun, and Meiyong Xu. Microbial fuel cells come of age. *Journal of Chemical Technology and Biotechnology*, 86(5):625–632, 2011.
- [28] Kazuya Watanabe. Recent developments in microbial fuel cell technologies for sustainable bioenergy. *Journal of Bioscience and Bioengineering*, 106(6):528–536, 2008.
- [29] Peter Clauwaert, Peter Aelterman, The Hai Pham, Liesje Schampelaire, Marta Carballa, Korneel Rabaey, and Willy Verstraete. Minimizing losses in bio-electrochemical systems: the road to applications. *Applied Microbiology and Biotechnology*, 79(6):901–913, 2008.
- [30] Rene A Rozendal, Hubertus VM Hamelers, Korneel Rabaey, Jurg Keller, and Cees JN Buisman. Towards practical implementation of bioelectrochemical wastewater treatment. *Trends in biotechnology*, 26(8):450–459, 2008.

- [31] Derek R. Lovley. Bug juice: harvesting electricity with microorganisms. *Nature Reviews Microbiology*, 4(7):497–508, 2006.
- [32] Z. Du, H. Li, and T. Gu. A state of the art review on microbial fuel cells: A promising technology for wastewater treatment and bioenergy. *Biotechnology Advances*, 25(5):464–482, 2007.
- [33] Ashley E. Franks and Kelly P. Nevin. Microbial fuel cells, a current review. *Energies*, 3(5):899–919, 2010.
- [34] Hong Liu and Bruce E. Logan. Electricity generation using an air-cathode single chamber microbial fuel cell in the presence and absence of a proton exchange membrane. *Environmental Science & Technology*, 38(14):4040–4046, 2004.
- [35] Orianna Bretschger, Jason B Osterstock, William E Pinchak, ShunŃichi Ishii, and Karen E Nelson. Microbial fuel cells and microbial ecology: applications in ruminant health and production research. *Microbial ecology*, 59(3):415–427, 2010.
- [36] Hubertus VM Hamelers, Annemiek Ter Heijne, Tom HJA Sleutels, Adriaan W JeremiŃsse, David PBTB Strik, and Cees JN Buisman. New applications and performance of bioelectrochemical systems. *Applied microbiology and biotechnology*, 85(6):1673–1685, 2010.
- [37] Pablo Ledezma, Andrew Stinchcombe, John Greenman, and Ioannis Ieropoulos. The first self-sustainable microbial fuel cell stack. *Physical Chemistry Chemical Physics*, 15(7):2278–2281, 2013.
- [38] Bruce Logan. Scaling up microbial fuel cells and other bioelectrochemical systems. *Applied Microbiology and Biotechnology*, 85(6):1665–1671, 2010.
- [39] Iwona Gajda, Andrew Stinchcombe, John Greenman, Chris Melhuish, and Ioannis Ieropoulos. Ceramic mfcs with internal cathode producing sufficient power for practical applications. *International Journal of Hydrogen Energy*, 2015.
- [40] Ioannis A Ieropoulos, Pablo Ledezma, Andrew Stinchcombe, George Papaharalabos, Chris Melhuish, and John Greenman. Waste to real energy: the first mfc powered mobile phone. *Physical Chemistry Chemical Physics*, 15(37):15312–15316, 2013.
- [41] Folusho F Ajayi and Peter R Weigele. A terracotta bio-battery. *Bioresource technology*, 116:86–91, 2012.
- [42] Duncan Mara and Nigel J Horan. *Handbook of water and wastewater microbiology*. Academic press, 2003.

- [43] Lansing M. Prescott, John P. Harley, and Donald A. Klein. *Microbiology*. McGraw-Hill Higher Education, 5th edition, 2002.
- [44] Chaojie Song and JiuJun Zhang. *Electrocatalytic Oxygen Reduction Reaction*, chapter 2, pages 89–134. Springer London, 2008.
- [45] I Roche, K Katuri, and K Scott. A microbial fuel cell using manganese oxide oxygen reduction catalysts. *Journal of applied electrochemistry*, 40(1):13–21, 2010.
- [46] Valerie J Watson, Cesar Nieto Delgado, and Bruce E Logan. Improvement of activated carbons as oxygen reduction catalysts in neutral solutions by ammonia gas treatment and their performance in microbial fuel cells. *Journal of Power Sources*, 242:756–761, 2013.
- [47] H Wang, R Cote, G Faubert, D Guay, and JP Dodelet. Effect of the pre-treatment of carbon black supports on the activity of Fe-based electrocatalysts for the reduction of oxygen. *The Journal of Physical Chemistry B*, 103(12):2042–2049, 1999.
- [48] Qian Deng, Xinyang Li, Jiane Zuo, Alison Ling, and Bruce E Logan. Power generation using an activated carbon fiber felt cathode in an upflow microbial fuel cell. *Journal of Power Sources*, 195(4):1130–1135, 2010.
- [49] Korneel Rabaey and RenÅr A. Rozendal. Microbial electrosynthesis - revisiting the electrical route for microbial production. *Nature Reviews Microbiology*, 8(10):706–716, 2010.
- [50] Liping Huang, John M. Regan, and Xie Quan. Electron transfer mechanisms, new applications, and performance of biocathode microbial fuel cells. *Bioresource Technology*, 102(1):316–323, 2011.
- [51] Yi-cheng Wu, Ze-jie Wang, Yue Zheng, Yong Xiao, Zhao-hui Yang, and Feng Zhao. Light intensity affects the performance of photo microbial fuel cells with *Desmod-esmus sp.* A8 as cathodic microorganism. *Applied Energy*, 116:86–90, 2014.
- [52] X Alexis Walter, John Greenman, and Ioannis A Ieropoulos. Oxygenic phototrophic biofilms for improved cathode performance in microbial fuel cells. *Algal Research*, 2(3):183–187, 2013.
- [53] Iwona Gajda, John Greenman, Chris Melhuish, and Ioannis Ieropoulos. Photosynthetic cathodes for microbial fuel cells. *International Journal of Hydrogen Energy*, 38(26):11559–11564, 2013.

- [54] Botho Bowien and Hans G Schlegel. Physiology and biochemistry of aerobic hydrogen-oxidizing bacteria. *Annual Reviews in Microbiology*, 35(1):405–452, 1981.
- [55] Kenneth H. Nealson. The manganese-oxidizing bacteria. *Prokaryotes*, 5:222–231, 2006.
- [56] Derek R Lovley. The microbe electric: conversion of organic matter to electricity. *Current opinion in Biotechnology*, 19(6):564–571, 2008.
- [57] Sabrina Hedrich, Michael Schlömann, and D. Barrie Johnson. The iron-oxidizing proteobacteria. *Microbiology*, 157(6):1551–1564, 2011.
- [58] Cornelius G Friedrich, Dagmar Rother, Frank Bardischewsky, Armin Quentmeier, and Jörg Fischer. Oxidation of reduced inorganic sulfur compounds by bacteria: emergence of a common mechanism? *Applied and Environmental Microbiology*, 67(7):2873–2882, 2001.
- [59] Petr Vanysek. Electrochemical series. *CRC handbook of chemistry and physics*, 87, 1998.
- [60] Cindy Castelle, Marianne Guiral, Guillaume Malarte, Fouzia Ledgham, Gisèle Leroy, Myriam Brugna, and Marie-Thérèse Giudici-Ortoni. A new iron-oxidizing/O₂-reducing supercomplex spanning both inner and outer membranes, isolated from the extreme acidophile *Acidithiobacillus ferrooxidans*. *Journal of Biological Chemistry*, 283(38):25803–25811, 2008.
- [61] David L Nelson and Michael M Cox. *Lehninger Principles of Biochemistry Lecture Notebook*. Macmillan, 2004.
- [62] Marianne Ilbert and Violaine Bonnefoy. Insight into the evolution of the iron oxidation pathways. *Biochim. Biophys. Acta*, 1827:161–175, 2013.
- [63] DP Kelly. Biochemistry of the chemolithotrophic oxidation of inorganic sulphur. *Philosophical Transactions of the Royal Society of London. B, Biological Sciences*, 298(1093):499–528, 1982.
- [64] Zhen He and Largus T Angenent. Application of bacterial biocathodes in microbial fuel cells. *Electroanalysis*, 18(19-20):2009–2015, 2006.
- [65] A. Rhoads, H. Beyenal, and Z. Lewandowski. Microbial fuel cell using anaerobic respiration as an anodic reaction and biomineralized manganese as a cathodic reactant. *Environmental Science & Technology*, 39(12):4666–4671, 2005.

- [66] Annemiek Ter Heijne, Hubertus VM Hamelers, Vinnie De Wilde, René A Rozendal, and Cees JN Buisman. A bipolar membrane combined with ferric iron reduction as an efficient cathode system in microbial fuel cells. *Environmental science & technology*, 40(17):5200–5205, 2006.
- [67] Arantxa López-López, Eduardo Expósito, Josefa Antón, Francisco Rodríguez-Valera, and Antonio Aldaz. Use of *Thiobacillus ferrooxidans* in a coupled microbiological–electrochemical system for wastewater detoxification. *Biotechnology and bioengineering*, 63(1):79–86, 1999.
- [68] Annemiek ter Heijne, Hubertus V. M. Hamelers, and Cees J. N. Buisman. Microbial fuel cell operation with continuous biological ferrous iron oxidation of the catholyte. *Environmental Science & Technology*, 41(11):4130–4134, 2007.
- [69] Annemiek Ter Heijne, Fei Liu, Lucas S. van Rijnsoever, Michel Saakes, Hubertus V. M. Hamelers, and Cees J. N. Buisman. Performance of a scaled-up microbial fuel cell with iron reduction as the cathode reaction. *Journal of Power Sources*, 196(18):7572–7577, 2011.
- [70] Zarath M. Summers, Jeffrey A. Gralnick, and Daniel R. Bond. Cultivation of an obligate Fe(II)-oxidizing lithoautotrophic bacterium using electrodes. *mBio*, 4(1), 2013.
- [71] Sofía Carbajosa, Moustafá Malki, Renaud Caillard, María F. Lopez, F. Javier Palomares, José A. Martín-Gago, Nuria Rodríguez, Ricardo Amils, Victor M. Fernández, and Antonio L. De Lacey. Electrochemical growth of *Acidithiobacillus ferrooxidans* on a graphite electrode for obtaining a biocathode for direct electrocatalytic reduction of oxygen. *Biosensors and Bioelectronics*, 26(2):877–880, 2010.
- [72] Benjamin Erable, Damien Féron, and Alain Bergel. Microbial catalysis of the oxygen reduction reaction for microbial fuel cells: A review. *ChemSusChem*, 5(6):975–987, 2012.
- [73] Kenneth Lewis. Symposium on bioelectrochemistry of microorganisms. iv. biochemical fuel cells. *Bacteriological reviews*, 30(1):101, 1966.
- [74] Øistein Hasvold, Henrich Henriksen, Einar Melv, Gianfederico Citi, Bent Ø Johansen, Tom Kjøningsen, Robin Galetti, et al. Sea-water battery for subsea control systems. *Journal of Power Sources*, 65(1):253–261, 1997.
- [75] CE Reimers, P Girguis, HA Stecher, LM Tender, N Ryckelynck, and P Whaling. Microbial fuel cell energy from an ocean cold seep. *Geobiology*, 4(2):123–136, 2006.

- [76] Peter Clauwaert, David van der Ha, Nico Boon, Kim Verbeken, Marc Verhaege, Korneel Rabaey, and Willy Verstraete. Open air biocathode enables effective electricity generation with microbial fuel cells. *Environmental Science & Technology*, 41(21):7564–7569, 2007.
- [77] Korneel Rabaey, Suzanne T. Read, Peter Clauwaert, Stefano Freguia, Philip L. Bond, Linda L. Blackall, and Jurg Kelle. Cathodic oxygen reduction catalyzed by bacteria in microbial fuel cells. *ISME J*, 2(5):519–527, 2008.
- [78] Kyungmi Chung, Itto Fujiki, and Satoshi Okabe. Effect of formation of biofilms and chemical scale on the cathode electrode on the performance of a continuous two-chamber microbial fuel cell. *Bioresource Technology*, 102(1):355–360, 2011.
- [79] Shan Xie, Peng Liang, Yang Chen, Xue Xia, and Xia Huang. Simultaneous carbon and nitrogen removal using an oxic/anoxic-biocathode microbial fuel cells coupled system. *Bioresource Technology*, 102(1):348–354, 2011.
- [80] David P. B. T. B. Strik, Matthieu Picot, Cees J. N. Buisman, and Frédéric Barrière. pH and temperature determine performance of oxygen reducing biocathodes. *Electroanalysis*, 25(3):652–655, 2013.
- [81] Xue Xia, Justin C. Tokash, Fang Zhang, Peng Liang, Xia Huang, and Bruce E. Logan. Oxygen-reducing biocathodes operating with passive oxygen transfer in microbial fuel cells. *Environmental Science & Technology*, 47(4):2085–2091, 2013.
- [82] Jerome T Babauta, Lewis Hsu, Erhan Atci, Jeff Kagan, Bart Chadwick, and Haluk Beyenal. Multiple cathodic reaction mechanisms in seawater cathodic biofilms operating in sediment microbial fuel cells. *ChemSusChem*, 7(10):2898–2906, 2014.
- [83] Liesje De Schamphelaire, Pascal Boeckx, and Willy Verstraete. Evaluation of biocathodes in freshwater and brackish sediment microbial fuel cells. *Applied Microbiology and Biotechnology*, 87(5):1675–1687, 2010.
- [84] Annemiek Ter Heijne, David P. B. T. B. Strik, Hubertus V. M. Hamelers, and Cees J. N. Buisman. Cathode potential and mass transfer determine performance of oxygen reducing biocathodes in microbial fuel cells. *Environmental Science & Technology*, 44(18):7151–7156, 2010.
- [85] Annemiek Ter Heijne, Olivier Schaetzle, Sixto Gimenez, Francisco Fabregat-Santiago, Juan Bisquert, David P. B. T. B. Strik, Frederic Barriere, Cees J. N. Buisman, and Hubertus V. M. Hamelers. Identifying charge and mass transfer resistances of an oxygen reducing biocathode. *Energy & Environmental Science*, 4(12):5035–5043, 2011.

- [86] Jincheng Wei, Peng Liang, Xiaoxin Cao, and Xia Huang. Use of inexpensive semicoke and activated carbon as biocathode in microbial fuel cells. *Bioresource Technology*, 102(22):10431 – 10435, 2011.
- [87] C. Dumas, A. Mollica, D. Féron, R. Basséguy, L. Etcheverry, and A. Bergel. Marine microbial fuel cell: Use of stainless steel electrodes as anode and cathode materials. *Electrochimica Acta*, 53(2):468 – 473, 2007.
- [88] X. Xia, Y. Sun, P. Liang, and X. Huang. Long-term effect of set potential on biocathodes in microbial fuel cells: Electrochemical and phylogenetic characterization. *Bioresource Technology*, 120:26–33, 2012.
- [89] Sarah M Strycharz-Glaven, Richard H Glaven, Zheng Wang, Jing Zhou, Gary J Vora, and Leonard M Tender. Electrochemical investigation of a microbial solar cell reveals a nonphotosynthetic biocathode catalyst. *Applied and environmental microbiology*, 79(13):3933–3942, 2013.
- [90] Benjamin Erable, Rémy Lacroix, Luc Etcheverry, Damien Féron, Marie-Line Délia, and Alain Bergel. Marine floating microbial fuel cell involving aerobic biofilm on stainless steel cathodes. *Bioresource technology*, 142:510–516, 2013.
- [91] Zejie Wang, Yue Zheng, Yong Xiao, Song Wu, Yicheng Wu, Zhaohui Yang, and Feng Zhao. Analysis of oxygen reduction and microbial community of air-diffusion biocathode in microbial fuel cells. *Bioresource technology*, 144:74–79, 2013.
- [92] Yue Du, Yujie Feng, Yue Dong, Youpeng Qu, Jia Liu, Xiangtong Zhou, and Nanqi Ren. Coupling interaction of cathodic reduction and microbial metabolism in aerobic biocathode of microbial fuel cell. *RSC Adv.*, 4:34350–34355, 2014.
- [93] Yaping Zhang, Jian Sun, Yongyou Hu, Sizhe Li, and Qian Xu. Carbon nanotube-coated stainless steel mesh for enhanced oxygen reduction in biocathode microbial fuel cells. *Journal of Power Sources*, 239(0):169–174, 2013.
- [94] Alain Bergel, Damien Féron, and Alfonso Mollica. Catalysis of oxygen reduction in PEM fuel cell by seawater biofilm. *Electrochemistry Communications*, 7(9):900–904, 2005.
- [95] Yaping Zhang, Jian Sun, Yongyou Hu, Sizhe Li, and Qian Xu. Bio-cathode materials evaluation in microbial fuel cells: A comparison of graphite felt, carbon paper and stainless steel mesh materials. *International Journal of Hydrogen Energy*, 37(22):16935–16942, 2012.

- [96] Lilian Malaeb, Krishna P. Katuri, Bruce E. Logan, Husnul Maab, S. P. Nunes, and Pascal E. Saikaly. A hybrid microbial fuel cell membrane bioreactor with a conductive ultrafiltration membrane biocathode for wastewater treatment. *Environmental Science & Technology*, 47(20):11821–11828, 2013.
- [97] Fengling Xu, Jizhou Duan, and Baorong Hou. Electron transfer process from marine biofilms to graphite electrodes in seawater. *Bioelectrochemistry*, 78(1):92–95, 2010.
- [98] Li Zhuang, Yong Yuan, Guiqin Yang, and Shungui Zhou. In situ formation of graphene/biofilm composites for enhanced oxygen reduction in biocathode microbial fuel cells. *Electrochemistry Communications*, 21(0):69 – 72, 2012.
- [99] Elise Blanchet, Sophie Pécastaings, Benjamin Erable, Christine Roques, and Alain Bergel. Protons accumulation during anodic phase turned to advantage for oxygen reduction during cathodic phase in reversible bioelectrodes. *Bioresource Technology*, 173(0):224 – 230, 2014.
- [100] P. Cristiani, M.L. Carvalho, E. Guerrini, M. Daglio, C. Santoro, and B. Li. Cathodic and anodic biofilms in single chamber microbial fuel cells. *Bioelectrochemistry*, 92(0):6 – 13, 2013.
- [101] Ka Yu Cheng, Goen Ho, and Ralf Cord-Ruwisch. Anodophilic biofilm catalyzes cathodic oxygen reduction. *Environmental Science & Technology*, 44(1):518–525, 2010.
- [102] Jian Sun, Zhe Bi, Bin Hou, Yun qing Cao, and Yong you Hu. Further treatment of decolorization liquid of azo dye coupled with increased power production using microbial fuel cell equipped with an aerobic biocathode. *Water Research*, 45(1):283 – 291, 2011.
- [103] Z. Wang, J. Huang, C. Zhu, J. Ma, and Z. Wu. A bioelectrochemically-assisted membrane bioreactor for simultaneous wastewater treatment and energy production. *Chemical Engineering & Technology*, 36(12):2044–2050, 2013.
- [104] Manaswini Behera, Partha S. Jana, and M.M. Ghangrekar. Performance evaluation of low cost microbial fuel cell fabricated using earthen pot with biotic and abiotic cathode. *Bioresource Technology*, 101(4):1183–1189, 2010.
- [105] Zheng Chen, Yan-chao Huang, Jian-hong Liang, Feng Zhao, and Yong-guan Zhu. A novel sediment microbial fuel cell with a biocathode in the rice rhizosphere. *Bioresource technology*, 108:55–59, 2012.

- [106] Guo-Wei Chen, Soo-Jung Choi, Jae-Hwan Cha, Tae-Ho Lee, and Chang-Won Kim. Microbial community dynamics and electron transfer of a biocathode in microbial fuel cells. *Korean Journal of Chemical Engineering*, 27(5):1513–1520, 2010.
- [107] Guo-dong Zhang, Qing-liang Zhao, Yan Jiao, Jin-na Zhang, Jun-qiu Jiang, Nanqi Ren, and Byung Hong Kim. Improved performance of microbial fuel cell using combination biocathode of graphite fiber brush and graphite granules. *Journal of Power Sources*, 196(15):6036–6041, 2011.
- [108] Yanmei Sun, Jincheng Wei, Peng Liang, and Xia Huang. Microbial community analysis in biocathode microbial fuel cells packed with different materials. *AMB Express*, 2(1):1–8, 2012.
- [109] Guodong Zhang, Qingliang Zhao, Yan Jiao, Kun Wang, Duu-Jong Lee, and Nanqi Ren. Biocathode microbial fuel cell for efficient electricity recovery from dairy manure. *Biosensors and Bioelectronics*, 31(1):537 – 543, 2012.
- [110] Haiping Wang, Sunny C. Jiang, Yun Wang, and Bo Xiao. Substrate removal and electricity generation in a membrane-less microbial fuel cell for biological treatment of wastewater. *Bioresource Technology*, 138(0):109–116, 2013.
- [111] Stefano Freguia, Korneel Rabaey, Zhiguo Yuan, and Jürg Keller. Sequential anode-cathode configuration improves cathodic oxygen reduction and effluent quality of microbial fuel cells. *Water Research*, 42(6):1387–1396, 2008.
- [112] Jin-Na Zhang, Qing-Liang Zhao, Peter Aelterman, Shi-Jie You, and Jun-Qiu Jiang. Electricity generation in a microbial fuel cell with a microbially catalyzed cathode. *Biotechnology Letters*, 30(10):1771–1776, 2008.
- [113] Shaoqiang Yang, Boyang Jia, and Hong Liu. Effects of the Pt loading side and cathode-biofilm on the performance of a membrane-less and single-chamber microbial fuel cell. *Bioresource technology*, 100(3):1197–1202, 2009.
- [114] Jaehwan Cha, Soojung Choi, Hana Yu, Hyosoo Kim, and Changwon Kim. Directly applicable microbial fuel cells in aeration tank for wastewater treatment. *Bioelectrochemistry*, 78(1):72 – 79, 2010.
- [115] Yanping Mao, Lehua Zhang, Dongmei Li, Haifeng Shi, Yongdi Liu, and Lankun Cai. Power generation from a biocathode microbial fuel cell biocatalyzed by ferro/manganese-oxidizing bacteria. *Electrochimica Acta*, 55(27):7804–7808, 2010.
- [116] Xian-Wei Liu, Xue-Fei Sun, Yu-Xi Huang, Guo-Ping Sheng, Shu-Guang Wang, and Han-Qing Yu. Carbon nanotube/chitosan nanocomposite as a biocompatible biocath-

- ode material to enhance the electricity generation of a microbial fuel cell. *Energy & Environmental Science*, 4(4):1422–1427, 2011.
- [117] S. Venkata Mohan and S. Srikanth. Enhanced wastewater treatment efficiency through microbially catalyzed oxidation and reduction: Synergistic effect of biocathode microenvironment. *Bioresource Technology*, 102(22):10210–10220, 2011.
- [118] Guodong Zhang, Qingliang Zhao, Yan Jiao, Kun Wang, Duu-Jong Lee, and Nanqi Ren. Efficient electricity generation from sewage sludge using biocathode microbial fuel cell. *Water Research*, 46(1):43 – 52, 2012.
- [119] Peng Liang, Mingzhi Fan, Xiaoxin Cao, and Xia Huang. Evaluation of applied cathode potential to enhance biocathode in microbial fuel cells. *Journal of Chemical Technology & Biotechnology*, 84(5):794–799, 2009.
- [120] Guo-Wei Chen, Soo-Jung Choi, Tae-Ho Lee, Gil-Young Lee, Jae-Hwan Cha, and Chang-Won Kim. Application of biocathode in microbial fuel cells: cell performance and microbial community. *Applied Microbiology and Biotechnology*, 79(3):379–388, 2008.
- [121] Zheng Wang, Dagmar H Leary, Anthony P Malanoski, Robert W Li, W Judson Hervey, Brian J Eddie, Gabrielle S Tender, Shelley G Yanosky, Gary J Vora, Leonard M Tender, et al. A previously uncharacterized, nonphotosynthetic member of the chromatiaecae is the primary CO₂-fixing constituent in a self-regenerating biocathode. *Applied and environmental microbiology*, 81(2):699–712, 2015.
- [122] Mickaël Rimboud, Elie Desmond-Le Quemener, Benjamin Erable, Théodore Bouchez, and Alain Bergel. The current provided by oxygen-reducing microbial cathodes is related to the composition of their bacterial community. *Bioelectrochemistry*, 102:42–49, 2015.
- [123] Stefano Freguia, Seiya Tsujimura, and Kenji Kano. Electron transfer pathways in microbial oxygen biocathodes. *Electrochimica Acta*, 55(3):813–818, 2010.
- [124] Miriam Rosenbaum, Federico Aulenta, Marianna Villano, and Largus T. Angenent. Cathodes as electron donors for microbial metabolism: Which extracellular electron transfer mechanisms are involved? *Bioresource Technology*, 102(1):324–333, 2011.
- [125] Liang Shi, Thomas C Squier, John M Zachara, and James K Fredrickson. Respiration of metal (hydr) oxides by shewanella and geobacter: a key role for multihaem c-type cytochromes. *Molecular microbiology*, 65(1):12–20, 2007.

- [126] Benjamin Erable, Ilse Vandecandelaere, Marco Faimali, Marie-Line Delia, Luc Etcheverry, Peter Vandamme, and Alain Bergel. Marine aerobic biofilm as biocathode catalyst. *Bioelectrochemistry*, 78(1):51–56, 2010.
- [127] Sandrine Parot, Ilse Vandecandelaere, Amandine Cournet, Marie-Line Délia, Peter Vandamme, Mathieu Bergé, Christine Roques, and Alain Bergel. Catalysis of the electrochemical reduction of oxygen by bacteria isolated from electro-active biofilms formed in seawater. *Bioresource Technology*, 102(1):304–311, 2011.
- [128] Amandine Cournet, Marie-Line Délia, Alain Bergel, Christine Roques, and Mathieu Bergé. Electrochemical reduction of oxygen catalyzed by a wide range of bacteria including Gram-positive. *Electrochemistry Communications*, 12(4):505–508, 2010.
- [129] Pablo Sebastián Bonanni, German D Schrott, Luciana Robuschi, and Juan Pablo Busalmen. Charge accumulation and electron transfer kinetics in geobacter sulfurreducens biofilms. *Energy & Environmental Science*, 5(3):6188–6195, 2012.
- [130] Kelvin B. Gregory, Daniel R. Bond, and Derek R. Lovley. Graphite electrodes as electron donors for anaerobic respiration. *Environmental Microbiology*, 6(6):596–604, 2004.
- [131] Catarina M Paquete, Bruno M Fonseca, Davide R Cruz, Tiago M Pereira, Isabel Pacheco, Cláudio M Soares, and Ricardo O Louro. Exploring the molecular mechanisms of electron shuttling across the microbe/metal space. *Frontiers in microbiology*, 5, 2014.
- [132] Laura Klupfel, Annette Piepenbrock, Andreas Kappler, and Michael Sander. Humic substances as fully regenerable electron acceptors in recurrently anoxic environments. *Nature Geoscience*, 7(3):195–200, 2014.
- [133] Eric E Roden, Andreas Kappler, Iris Bauer, Jie Jiang, Andrea Paul, Reinhard Stoesser, Hiromi Konishi, and Huifang Xu. Extracellular electron transfer through microbial reduction of solid-phase humic substances. *Nature Geoscience*, 3(6):417–421, 2010.
- [134] Maria E. Hernandez, Andreas Kappler, and Dianne K. Newman. Phenazines and other redox-active antibiotics promote microbial mineral reduction. *Applied and Environmental Microbiology*, 70(2):921–928, 2004.
- [135] Enrico Marsili, Daniel B. Baron, Indraneel D. Shikhare, Dan Coursolle, Jeffrey A. Gralnick, and Daniel R. Bond. *Shewanella* secretes flavins that mediate extracellular electron transfer. *Proceedings of the National Academy of Sciences*, 105(10):3968–3973, 2008.

- [136] Yonggang Yang, Meiyong Xu, Jun Guo, and Guoping Sun. Bacterial extracellular electron transfer in bioelectrochemical systems. *Process Biochemistry*, 47(12):1707–1714, 2012.
- [137] César I Torres, Andrew Kato Marcus, Hyung-Sool Lee, Prathap Parameswaran, Rosa Krajmalnik-Brown, and Bruce E Rittmann. A kinetic perspective on extracellular electron transfer by anode-respiring bacteria. *FEMS microbiology reviews*, 34(1):3–17, 2010.
- [138] Kim Kinoshita. Carbon: electrochemical and physicochemical properties. 1988.
- [139] Xiuping Zhu, Matthew D Yates, Marta C Hatzell, Hari Ananda Rao, Pascal E Saikaly, and Bruce E Logan. Microbial community composition is unaffected by anode potential. *Environmental science & technology*, 48(2):1352–1358, 2014.
- [140] Xiuping Zhu, Matthew D Yates, and Bruce E Logan. Set potential regulation reveals additional oxidation peaks of *Geobacter sulfurreducens* anodic biofilms. *Electrochemistry Communications*, 22:116–119, 2012.
- [141] Catarina M Paquete and Ricardo O Louro. Molecular details of multielectron transfer: the case of multiheme cytochromes from metal respiring organisms. *Dalton Transactions*, 39(18):4259–4266, 2010.
- [142] Sung-Hee Roh. Microbial fuel cells as the real source of sustainable energy. In *Advanced Functional Materials*, pages 195–219. Springer, 2011.
- [143] Jonathan Winfield, Lily D Chambers, Jonathan Rossiter, and Ioannis Ieropoulos. Comparing the short and long term stability of biodegradable, ceramic and cation exchange membranes in microbial fuel cells. *Bioresource technology*, 148:480–486, 2013.
- [144] Lee F. Adams and William C. Ghiorse. Influence of manganese on growth of a sheathless strain of *Leptothrix discophora*. *Appl. Environ. Microbiol.*, 49(3):556–562, 1985.
- [145] Tatsuo Yagishita, Shigeki Sawayama, Ken ichiro Tsukahara, and Tomoko Ogi. Effects of intensity of incident light and concentrations of *Synechococcus sp.* and 2-hydroxy-1,4-naphthoquinone on the current output of photosynthetic electrochemical cell. *Solar Energy*, 61(5):347 – 353, 1997.
- [146] K.B. Lam, Mu Chiao, and Liwei Lin. A micro photosynthetic electrochemical cell. In *Micro Electro Mechanical Systems, 2003. MEMS-03 Kyoto. IEEE The Sixteenth Annual International Conference on*, pages 391–394, Jan 2003.

- [147] JohnM. Pisciotta, YongJin Zou, and IliaV. Baskakov. Role of the photosynthetic electron transfer chain in electrogenic activity of cyanobacteria. *Applied Microbiology and Biotechnology*, 91(2):377–385, 2011.
- [148] Alistair J. McCormick, Paolo Bombelli, Amanda M. Scott, Alexander J. Philips, Alison G. Smith, Adrian C. Fisher, and Christopher J. Howe. Photosynthetic biofilms in pure culture harness solar energy in a mediatorless bio-photovoltaic cell (BPV) system. *Energy Environ. Sci.*, 4:4699–4709, 2011.
- [149] Miriam Rosenbaum, Uwe Schröder, and Fritz Scholz. Utilizing the green alga *Chlamydomonas reinhardtii* for microbial electricity generation: a living solar cell. *Applied Microbiology and Biotechnology*, 68(6):753–756, 2005.
- [150] Miriam Rosenbaum, Uwe Schröder, and Fritz Scholz. In situ electrooxidation of photobiological hydrogen in a photobioelectrochemical fuel cell based on rhodobacter sphaeroides. *Environmental Science & Technology*, 39(16):6328–6333, 2005.
- [151] Y.K. Cho, T.J. Donohue, I. Tejedor, M.A. Anderson, K.D. McMahon, and D.R. Noguera. Development of a solar-powered microbial fuel cell. *Journal of Applied Microbiology*, 104(3):640–650, 2008.
- [152] Xiaoxin Cao, Xia Huang, Nico Boon, Peng Liang, and Mingzhi Fan. Electricity generation by an enriched phototrophic consortium in a microbial fuel cell. *Electrochemistry Communications*, 10(9):1392 – 1395, 2008.
- [153] Defeng Xing, Shaoan Cheng, John M. Regan, and Bruce E. Logan. Change in microbial communities in acetate- and glucose-fed microbial fuel cells in the presence of light. *Biosensors and Bioelectronics*, 25(1):105 – 111, 2009.
- [154] Hyung-Sool Lee, Wim F.J. Vermaas, and Bruce E. Rittmann. Biological hydrogen production: prospects and challenges. *Trends in Biotechnology*, 28(5):262 – 271, 2010.
- [155] Maria J Barbosa, Jorge M.S Rocha, Johannes Tramper, and René H Wijffels. Acetate as a carbon source for hydrogen production by photosynthetic bacteria. *Journal of Biotechnology*, 85(1):25–33, 2001.
- [156] Rajib Kumar Das, Yan Wang, Svetlana V. Vasilyeva, Evan Donoghue, Ilaria Pucher, George Kamenov, Hai-Ping Cheng, and Andrew G. Rinzler. Extraordinary hydrogen evolution and oxidation reaction activity from carbon nanotubes and graphitic carbons. *ACS Nano*, 8(8):8447–8456, 2014.

- [157] Delina Y. Lyon, Francois Buret, Timothy M. Vogel, and Jean-Michel Monier. Is resistance futile? changing external resistance does not improve microbial fuel cell performance. *Bioelectrochemistry*, 78(1):2 – 7, 2010.
- [158] Zhiyong Ren, Hengjing Yan, Wei Wang, Matthew M. Mench, and John M. Regan. Characterization of microbial fuel cells at microbially and electrochemically meaningful time scales. *Environmental Science & Technology*, 45(6):2435–2441, 2011.
- [159] Liang Zhang, Xun Zhu, Jun Li, Qiang Liao, and Dingding Ye. Biofilm formation and electricity generation of a microbial fuel cell started up under different external resistances. *Journal of Power Sources*, 196(15):6029 – 6035, 2011.
- [160] G.S. Jadhav and M.M. Ghangrekar. Performance of microbial fuel cell subjected to variation in pH, temperature, external load and substrate concentration. *Bioresource Technology*, 100(2):717 – 723, 2009.
- [161] Krishna P. Katuri, Keith Scott, Ian M. Head, Cristian Picioreanu, and Tom P. Curtis. Microbial fuel cells meet with external resistance. *Bioresource Technology*, 102(3):2758 – 2766, 2011.
- [162] Hamid Rismani-Yazdi, Ann D. Christy, Sarah M. Carver, Zhongtang Yu, Burk A. Dehority, and Olli H. Tuovinen. Effect of external resistance on bacterial diversity and metabolism in cellulose-fed microbial fuel cells. *Bioresource Technology*, 102(1):278 – 283, 2011. Special Issue: Biofuels - II: Algal Biofuels and Microbial Fuel Cells.
- [163] André Baudler, Igor Schmidt, Markus Langner, Andreas Greiner, and Uwe Schröder. Does it have to be carbon? metal anodes in microbial fuel cells and related bioelectrochemical systems. *Energy & Environmental Science*, 2015.
- [164] Alloy electrical properties. http://www.goodfellow.com/catalogue/GFCat2C.php?ewd_token=0RgiaE8JyTygxG1vYkHG0szw7tqrGf&n=Tpd07GvSz6hHyAfOAJ84gAmqiHhrQf&ewd_urlNo=GFCat26&type=01&prop=5. Accessed: 2015-08-03.
- [165] Metal electrical properties. http://www.goodfellow.com/catalogue/GFCat2C.php?ewd_token=j4ozUTRKiT0x1dOuDtR1o2QgHYGuHg&n=3M5InqAoY1UhXe1AqSP1U1WRdiIi71&ewd_urlNo=GFCat26&type=00&prop=5. Accessed: 2015-08-03.
- [166] Annemiek ter Heijne, Hubertus V.M. Hamelers, Michel Saakes, and Cees J.N. Buisman. Performance of non-porous graphite and titanium-based anodes in microbial fuel cells. *Electrochimica Acta*, 53(18):5697 – 5703, 2008.

- [167] Leonard M Tender, Clare E Reimers, Hilmar A Stecher, Dawn E Holmes, Daniel R Bond, Daniel A Lowy, Kanoelani Pilobello, Stephanie J Fertig, and Derek R Lovley. Harnessing microbially generated power on the seafloor. *Nature biotechnology*, 20(8):821–825, 2002.
- [168] Jincheng Wei, Peng Liang, and Xia Huang. Recent progress in electrodes for microbial fuel cells. *Bioresource Technology*, 102(20):9335–9344, 2011.
- [169] Xin Wang, Shaoan Cheng, Yujie Feng, Matthew D Merrill, Tomonori Saito, and Bruce E Logan. Use of carbon mesh anodes and the effect of different pretreatment methods on power production in microbial fuel cells. *Environmental science & technology*, 43(17):6870–6874, 2009.
- [170] Carbon fabric coil. <http://www.sigmaaldrich.com/catalog/product/aldrich/gf78271140?lang=en®ion=GB>. Accessed: 2015-08-02.
- [171] C0450 woven carbon fabric 204 g/m² plain. http://www.prfcomposites.com/store/index.php?route=product/product&path=97_63_64&product_id=66. Accessed: 2015-08-02.
- [172] Carbon fiber veil. http://www.fibreglast.com/product/Carbon_Fiber_Veil_1064/carbon_fiber_all. Accessed: 2015-08-02.
- [173] Ioannis Ieropoulos, John Greenman, and Chris Melhuish. Microbial fuel cells based on carbon veil electrodes: stack configuration and scalability. *International Journal of Energy Research*, 32(13):1228–1240, 2008.
- [174] Andrea Corti, Roberto Solaro, and Emo Chiellini. Biodegradation of poly (vinyl alcohol) in selected mixed microbial culture and relevant culture filtrate. *Polymer Degradation and stability*, 75(3):447–458, 2002.
- [175] H Schonberger, A Baumann, W Keller, and P Pogopetris. Study of microbial degradation of polyvinyl alcohol (pva) in wastewater treatment plants. *American dyestuff reporter*, 86(8):9–18, 1997.
- [176] Swades K Chaudhuri and Derek R Lovley. Electricity generation by direct oxidation of glucose in mediatorless microbial fuel cells. *Nature biotechnology*, 21(10):1229–1232, 2003.
- [177] Carbon felt, 6.35mm (0.25in) thick, 99.0 <http://www.alfa.com/en/catalog/43200>. Accessed: 2015-08-02.

- [178] Peter Aelterman, Mathias Versichele, Massimo Marzorati, Nico Boon, and Willy Verstraete. Loading rate and external resistance control the electricity generation of microbial fuel cells with different three-dimensional anodes. *Bioresource Technology*, 99(18):8895–8902, 2008.
- [179] Bruce Logan, Shaoan Cheng, Valerie Watson, and Garrett Estadt. Graphite fiber brush anodes for increased power production in air-cathode microbial fuel cells. *Environmental science & technology*, 41(9):3341–3346, 2007.
- [180] Yujie Feng, Qiao Yang, Xin Wang, and Bruce E Logan. Treatment of carbon fiber brush anodes for improving power generation in air-cathode microbial fuel cells. *Journal of Power Sources*, 195(7):1841–1844, 2010.
- [181] Vanessa Lanas, Yongtae Ahn, and Bruce E. Logan. Effects of carbon brush anode size and loading on microbial fuel cell performance in batch and continuous mode. *Journal of Power Sources*, 247(0):228–234, 2014.
- [182] Bradley R Ringeisen, Emily Henderson, Peter K Wu, Jeremy Pietron, Ricky Ray, Brenda Little, Justin C Biffinger, and Joanne M Jones-Meehan. High power density from a miniature microbial fuel cell using shewanella oneidensis dsp10. *Environmental science & technology*, 40(8):2629–2634, 2006.
- [183] María C Gutiérrez, Zaira Y García-Carvajal, María J Hortigüela, Luis Yuste, Fernando Rojo, María L Ferrer, and Francisco del Monte. Biocompatible mwcnt scaffolds for immobilization and proliferation of e. coli. *Journal of Materials Chemistry*, 17(29):2992–2995, 2007.
- [184] Yan Qiao, Shu-Juan Bao, Chang Ming Li, Xiao-Qiang Cui, Zhi-Song Lu, and Jun Guo. Nanostructured polyaniline/titanium dioxide composite anode for microbial fuel cells. *Acs Nano*, 2(1):113–119, 2007.
- [185] Yan Qiao, Shu-Juan Bao, and Chang Ming Li. Electrocatalysis in microbial fuel cells from electrode material to direct electrochemistry. *Energy & Environmental Science*, 3(5):544–553, 2010.
- [186] Jung Rae Kim, Booki Min, and Bruce E Logan. Evaluation of procedures to acclimate a microbial fuel cell for electricity production. *Applied microbiology and biotechnology*, 68(1):23–30, 2005.
- [187] Yanzhen Fan, Shoutao Xu, Rebecca Schaller, Jun Jiao, Frank Chaplen, and Hong Liu. Nanoparticle decorated anodes for enhanced current generation in microbial electrochemical cells. *Biosensors and Bioelectronics*, 26(5):1908–1912, 2011.

- [188] D Park and J Zeikus. Impact of electrode composition on electricity generation in a single-compartment fuel cell using shewanella putrefaciens. *Applied microbiology and biotechnology*, 59(1):58–61, 2002.
- [189] Shaoan Cheng and Bruce E Logan. Ammonia treatment of carbon cloth anodes to enhance power generation of microbial fuel cells. *Electrochemistry Communications*, 9(3):492–496, 2007.
- [190] K. Scott, G. A. Rimbu, K. P. Katuri, K. K. Prasad, and I. M. Head. Application of modified carbon anodes in microbial fuel cells. *Process Safety and Environmental Protection*, 85(5):481–488, 2007.
- [191] Korneel Rabaey, Peter Clauwaert, Peter Aelterman, and Willy Verstraete. Tubular microbial fuel cells for efficient electricity generation. *Environmental science & technology*, 39(20):8077–8082, 2005.
- [192] Shaoan Cheng, Hong Liu, and Bruce E Logan. Power densities using different cathode catalysts (pt and cotmpp) and polymer binders (nafion and ptfe) in single chamber microbial fuel cells. *Environmental science & technology*, 40(1):364–369, 2006.
- [193] Shaoan Cheng, Hong Liu, and Bruce E Logan. Increased performance of single-chamber microbial fuel cells using an improved cathode structure. *Electrochemistry Communications*, 8(3):489–494, 2006.
- [194] Fang Zhang, Tomonori Saito, Shaoan Cheng, Michael A Hickner, and Bruce E Logan. Microbial fuel cell cathodes with poly (dimethylsiloxane) diffusion layers constructed around stainless steel mesh current collectors. *Environmental science & technology*, 44(4):1490–1495, 2010.
- [195] Fang Zhang, Matthew D Merrill, Justin C Tokash, Tomonori Saito, Shaoan Cheng, Michael A Hickner, and Bruce E Logan. Mesh optimization for microbial fuel cell cathodes constructed around stainless steel mesh current collectors. *Journal of Power Sources*, 196(3):1097–1102, 2011.
- [196] Jung Rae Kim, Shaoan Cheng, Sang-Eun Oh, and Bruce E. Logan. Power generation using different cation, anion, and ultrafiltration membranes in microbial fuel cells. *Environmental Science & Technology*, 41(3):1004–1009, 2007.
- [197] Kyu Jung Chae, Mijin Choi, Folusho F. Ajayi, Wooshin Park, In Seop Chang, and In S. Kim. Mass transport through a proton exchange membrane (Nafion) in microbial fuel cells. *Energy & Fuels*, 22(1):169–176, 2008.

- [198] René A. Rozendal, Hubertus V. M. Hamelers, and Cees J. N. Buisman. Effects of membrane cation transport on pH and microbial fuel cell performance. *Environmental Science & Technology*, 40(17):5206–5211, 2006.
- [199] René A. Rozendal, T. H. J. A. Sleutels, H. V. M. Hamelers, and Cees J. N. Buisman. Effect of the type of ion exchange membrane on performance, ion transport, and pH in biocatalyzed electrolysis of wastewater. *Wastewater Science & Technology*, 57(11):1757–1762, 2008.
- [200] Tom H.J.A. Sleutels, Hubertus V.M. Hamelers, René A. Rozendal, and Cees J.N. Buisman. Ion transport resistance in microbial electrolysis cells with anion and cation exchange membranes. *International Journal of Hydrogen Energy*, 34(9):3612 – 3620, 2009.
- [201] Falk Harnisch, Uwe Schröder, and Fritz Scholz. The suitability of monopolar and bipolar ion exchange membranes as separators for biological fuel cells. *Environmental Science & Technology*, 42(5):1740–1746, 2008.
- [202] Falk Harnisch, Robert Warmbier, Ralf Schneider, and Uwe Schröder. Modeling the ion transfer and polarization of ion exchange membranes in bioelectrochemical systems. *Bioelectrochemistry*, 75(2):136–141, 2009.
- [203] ES Heidrich, J Dolfing, K Scott, SR Edwards, C Jones, and TP Curtis. Production of hydrogen from domestic wastewater in a pilot-scale microbial electrolysis cell. *Applied microbiology and biotechnology*, 97(15):6979–6989, 2013.
- [204] Elizabeth S Heidrich, Stephen R Edwards, Jan Dolfing, Sarah E Cotterill, and Thomas P Curtis. Performance of a pilot scale microbial electrolysis cell fed on domestic wastewater at ambient temperatures for a 12month period. *Bioresource technology*, 173:87–95, 2014.
- [205] Booki Min, Shaoan Cheng, and Bruce E Logan. Electricity generation using membrane and salt bridge microbial fuel cells. *Water research*, 39(9):1675–1686, 2005.
- [206] Fikret Kargi and Serkan Eker. Electricity generation with simultaneous wastewater treatment by a microbial fuel cell (mfc) with cu and cu–au electrodes. *Journal of Chemical Technology and Biotechnology*, 82(7):658–662, 2007.
- [207] Zhi-Dan Liu and Hao-Ran Li. Effects of bio-and abio-factors on electricity production in a mediatorless microbial fuel cell. *Biochemical Engineering Journal*, 36(3):209–214, 2007.

- [208] Y Mohan, S Manoj Muthu Kumar, and D Das. Electricity generation using microbial fuel cells. *International Journal of Hydrogen Energy*, 33(1):423–426, 2008.
- [209] Sunil A Patil, Venkata Prasad Surakasi, Sandeep Koul, Shrikant Ijmulwar, Amar Vivek, YS Shouche, and BP Kapadnis. Electricity generation using chocolate industry wastewater and its treatment in activated sludge based microbial fuel cell and analysis of developed microbial community in the anode chamber. *Bioresource technology*, 100(21):5132–5139, 2009.
- [210] Li Zhuang, Shungui Zhou, Yueqiang Wang, Chengshuai Liu, and Shu Geng. Membrane-less cloth cathode assembly (cca) for scalable microbial fuel cells. *Biosensors and Bioelectronics*, 24(12):3652–3656, 2009.
- [211] Xiaoyuan Zhang, Shaoan Cheng, Xin Wang, Xia Huang, and Bruce E Logan. Separator characteristics for increasing performance of microbial fuel cells. *Environmental science & technology*, 43(21):8456–8461, 2009.
- [212] Yanzhen Fan, Hongqiang Hu, and Hong Liu. Enhanced coulombic efficiency and power density of air-cathode microbial fuel cells with an improved cell configuration. *Journal of Power Sources*, 171(2):348–354, 2007.
- [213] Justin C Biffinger, Ricky Ray, Brenda Little, and Bradley R Ringeisen. Diversifying biological fuel cell designs by use of nanoporous filters. *Environmental science & technology*, 41(4):1444–1449, 2007.
- [214] Yi Zuo, Shaoan Cheng, Doug Call, and Bruce E Logan. Tubular membrane cathodes for scalable power generation in microbial fuel cells. *Environmental science & technology*, 41(9):3347–3353, 2007.
- [215] Jian Sun, Yongyou Hu, Zhe Bi, and Yunqing Cao. Improved performance of air-cathode single-chamber microbial fuel cell for wastewater treatment using micro-filtration membranes and multiple sludge inoculation. *Journal of Power Sources*, 187(2):471–479, 2009.
- [216] S Venkata Mohan, S Veer Raghavulu, and PN Sarma. Biochemical evaluation of bio-electricity production process from anaerobic wastewater treatment in a single chambered microbial fuel cell (mfc) employing glass wool membrane. *Biosensors and Bioelectronics*, 23(9):1326–1332, 2008.
- [217] Doo Hyun Park and J Gregory Zeikus. Improved fuel cell and electrode designs for producing electricity from microbial degradation. *Biotechnology and bioengineering*, 81(3):348–355, 2003.

- [218] Ha Na Seo, Woo Jin Lee, Tae Sik Hwang, Doo Hyun Park, et al. Electricity generation coupled with wastewater treatment using a microbial fuel cell composed of a modified cathode with a ceramic membrane and cellulose acetate film. *J Microbiol Biotechnol*, 19(9):1019–1027, 2009.
- [219] Manaswini Behera, Partha S Jana, Tanaji T More, and MM Ghangrekar. Rice mill wastewater treatment in microbial fuel cells fabricated using proton exchange membrane and earthen pot at different ph. *Bioelectrochemistry*, 79(2):228–233, 2010.
- [220] M Behera and MM Ghangrekar. Electricity generation in low cost microbial fuel cell made up of earthenware of different thickness. *Water Science & Technology*, 64(12):2468–2473, 2011.
- [221] Jonathan Winfield, John Greenman, David Huson, and Ioannis Ieropoulos. Comparing terracotta and earthenware for multiple functionalities in microbial fuel cells. *Bioprocess and biosystems engineering*, 36(12):1913–1921, 2013.
- [222] Anil N Ghadge, Mypati Sreemannarayana, Narcis Duteanu, and Makarand M Ghangrekar. Influence of ceramic separator's characteristics on microbial fuel cell performance. *Journal of Electrochemical Science and Engineering*, 4(4):315–326, 2014.
- [223] Qunyin Xu and Marc A Anderson. Synthesis of porosity controlled ceramic membranes. *Journal of materials research*, 6(05):1073–1081, 1991.
- [224] Iwona Gajda, John Greenman, Chris Melhuish, and Ioannis Ieropoulos. Simultaneous electricity generation and microbially-assisted electrosynthesis in ceramic mfc. *Bioelectrochemistry*, 104:58–64, 2015.
- [225] Leonard M Tender, Sam A Gray, Ethan Groveman, Daniel A Lowy, Peter Kauffman, Julio Melhado, Robert C Tyce, Darren Flynn, Rose Petrecca, and Joe Dobarro. The first demonstration of a microbial fuel cell as a viable power supply: powering a meteorological buoy. *Journal of Power Sources*, 179(2):571–575, 2008.
- [226] Daqian Jiang, Michael Curtis, Elizabeth Troop, Karl Scheible, Joy McGrath, Boxun Hu, Steve Suib, Dustin Raymond, and Baikun Li. A pilot-scale study on utilizing multi-anode/cathode microbial fuel cells (mac mfc) to enhance the power production in wastewater treatment. *international journal of hydrogen energy*, 36(1):876–884, 2011.
- [227] Shaoan Cheng and Bruce E Logan. Increasing power generation for scaling up single-chamber air cathode microbial fuel cells. *Bioresource technology*, 102(6):4468–4473,

2011.

- [228] Hong Liu, Shaoan Cheng, Liping Huang, and Bruce E Logan. Scale-up of membrane-free single-chamber microbial fuel cells. *Journal of Power Sources*, 179(1):274–279, 2008.
- [229] Alim Dewan, Haluk Beyenal, and Zbigniew Lewandowski. Scaling up microbial fuel cells. *Environmental science & technology*, 42(20):7643–7648, 2008.
- [230] Arjan Dekker, Annemiek Ter Heijne, Michel Saakes, Hubertus VM Hamelers, and Cees JN Buisman. Analysis and improvement of a scaled-up and stacked microbial fuel cell. *Environmental science & technology*, 43(23):9038–9042, 2009.
- [231] Peter Aelterman, Korneel Rabaey, Hai The Pham, Nico Boon, and Willy Verstraete. Continuous electricity generation at high voltages and currents using stacked microbial fuel cells. *Environmental science & technology*, 40(10):3388–3394, 2006.
- [232] Allen Bard and Larry Falkner. *Electrochemical Methods: Fundamentals and Applications*. Wiley, 2nd edition, 2001.
- [233] Feng Zhao, Robert CT Slade, and John R Varcoe. Techniques for the study and development of microbial fuel cells: an electrochemical perspective. *Chemical Society Reviews*, 38(7):1926–1939, 2009.
- [234] Fraser A Armstrong, Hendrik A Heering, and Judy Hirst. Reaction of complex metalloproteins studied by protein-film voltammetry. *Chem. Soc. Rev.*, 26(3):169–179, 1997.
- [235] B. E. Logan, B. Hamelers, R. A. Rozendal, U. Schröder, J. Keller, S. Freguia, P. Aelterman, W. Verstraete, and K. Rabaey. Microbial fuel cells: Methodology and technology. *Environmental Science & Technology*, 40(17):5181–5192, 2006.
- [236] Aswin K Manohar and Florian Mansfeld. The internal resistance of a microbial fuel cell and its dependence on cell design and operating conditions. *Electrochimica Acta*, 54(6):1664–1670, 2009.
- [237] Xochitl Dominguez-Benetton, Surajbhan Sevda, Karolien Vanbroekhoven, and Deepak Pant. The accurate use of impedance analysis for the study of microbial electrochemical systems. *Chemical Society Reviews*, 41(21):7228–7246, 2012.
- [238] Zhen He and Florian Mansfeld. Exploring the use of electrochemical impedance spectroscopy (EIS) in microbial fuel cell studies. *Energy & Environmental Science*, 2(2):215–219, 2009.

- [239] Rabiya S Tuma, Matthew P Beaudet, Xiaokui Jin, Laurie J Jones, Ching-Ying Cheung, Stephen Yue, and Victoria L Singer. Characterization of SYBR gold nucleic acid gel stain: a dye optimized for use with 300-nm ultraviolet transilluminators. *Analytical biochemistry*, 268(2):278–288, 1999.
- [240] John M Walker. The bicinchoninic acid (BCA) assay for protein quantitation. In *The Protein Protocols Handbook*, pages 11–15. Springer, 2009.
- [241] Jay Shendure and Hanlee Ji. Next-generation DNA sequencing. *Nature biotechnology*, 26(10):1135–1145, 2008.
- [242] Devin Dressman, Hai Yan, Giovanni Traverso, Kenneth W Kinzler, and Bert Vogelstein. Transforming single dna molecules into fluorescent magnetic particles for detection and enumeration of genetic variations. *Proceedings of the National Academy of Sciences*, 100(15):8817–8822, 2003.
- [243] Barry Merriman, Ion Torrent, Jonathan M Rothberg, R&D Team, et al. Progress in ion torrent semiconductor chip based sequencing. *Electrophoresis*, 33(23):3397–3417, 2012.
- [244] Nicholas J Loman, Raju V Misra, Timothy J Dallman, Chrystala Constantinidou, Saheer E Gharbia, John Wain, and Mark J Pallen. Performance comparison of benchtop high-throughput sequencing platforms. *Nature biotechnology*, 30(5):434–439, 2012.
- [245] J Gregory Caporaso, Justin Kuczynski, Jesse Stombaugh, Kyle Bittinger, Frederic D Bushman, Elizabeth K Costello, Noah Fierer, Antonio Gonzalez Pena, Julia K Goodrich, Jeffrey I Gordon, et al. QIIME allows analysis of high-throughput community sequencing data. *Nature methods*, 7(5):335–336, 2010.
- [246] Catherine Lozupone and Rob Knight. Unifrac: a new phylogenetic method for comparing microbial communities. *Applied and environmental microbiology*, 71(12):8228–8235, 2005.
- [247] Xiandeng Hou and Bradley T Jones. Inductively coupled plasma-optical emission spectrometry. *Encyclopedia of Analytical Chemistry*, 2000.
- [248] Claudia Eith, Maximilian Kolb, Andreas Seubert, and Kai Henning Viehweger. Practical ion chromatography. *Metrohm Ltd., Herisau, Switzerland*, 2001.
- [249] Heiner Strathmann. *Ion-exchange membrane separation processes*, volume 9. Elsevier, 2004.

- [250] S Slade, SA Campbell, TR Ralph, and FC Walsh. Ionic conductivity of an extruded nafion 1100 EW series of membranes. *Journal of the Electrochemical Society*, 149(12):A1556–A1564, 2002.
- [251] N. Duteanu, B. Erable, S. M. Senthil Kumar, M. M. Ghangrekar, and K. Scott. Effect of chemically modified vulcan XC-72R on the performance of air-breathing cathode in a single-chamber microbial fuel cell. *Bioresource Technology*, 101(14):5250–5255, 2010.
- [252] Emad Aldeen Khudaish. *The Electrochemical Oxidation of Hydrogen Peroxide on Platinum Electrodes at Phosphate Buffer Solutions*. Phd, Massey University, Palmerston North, New Zealand, 1999.
- [253] A. Rey, J. A. Zazo, J. A. Casas, A. Bahamonde, and J. J. Rodriguez. Influence of the structural and surface characteristics of activated carbon on the catalytic decomposition of hydrogen peroxide. *Applied Catalysis A: General*, 402:146–155, 2011.
- [254] W. G. Barb, J. H. Baxendale, P. George, and K. R. Hargrave. Reactions of ferrous and ferric ions with hydrogen peroxide. Part II.-The ferric ion reaction. *Transactions of the Faraday Society*, 47(0):591–616, 1951.
- [255] B. Khoumeri, N. Balbi, E. Leoni, N. Chiaramonti, and J. Balbi. The decomposition of hydrogen peroxide. a non-linear dynamic model. *Journal of Thermal Analysis and Calorimetry*, 59(3):901–911, 2000.
- [256] Tong Zhang, Ming-Fei Shao, and Lin Ye. 454 pyrosequencing reveals bacterial diversity of activated sludge from 14 sewage treatment plants. *The ISME journal*, 6(6):1137–1147, 2012.
- [257] R Maurício, CJ Dias, and F Santana. Monitoring biofilm thickness using a non-destructive, on-line, electrical capacitance technique. *Environmental monitoring and assessment*, 119(1):599–607, 2006.
- [258] Taeyoung Kim, Junil Kang, Joon-Hee Lee, and Jeyong Yoon. Influence of attached bacteria and biofilm on double-layer capacitance during biofilm monitoring by electrochemical impedance spectroscopy. *Water research*, 45(15):4615–4622, 2011.
- [259] David R. Lide. *CRC Handbook of Chemistry and Physics*. 81st edition, 2000.
- [260] James A. Imlay. Pathways of oxidative damage. *Annual Review of Microbiology*, 57(1):395–418, 2003.

- [261] Simon AQ Burton and Jim I Prosser. Autotrophic ammonia oxidation at low pH through urea hydrolysis. *Applied and environmental microbiology*, 67(7):2952–2957, 2001.
- [262] Daniel R Bond, Sarah M Strycharz-Glaven, Leonard M Tender, and César I Torres. On electron transport through geobacter biofilms. *ChemSusChem*, 5(6):1099–1105, 2012.
- [263] Mårten Wikström. Cytochrome c oxidase: 25 years of the elusive proton pump. *Biochimica et Biophysica Acta (BBA) - Bioenergetics*, 1655(0):241 – 247, 2004.
- [264] H. Michel, J. Behr, A. Harrenga, and A. Kannt. Cytochrome c oxidase: Structure and spectroscopy. *Annual Review of Biophysics and Biomolecular Structure*, 27(1):329–356, 1998.
- [265] A. Kleinhofs, W.M. Owais, and R.A. Nilan. Azide. *Mutation Research/Reviews in Genetic Toxicology*, 55(3–4):165 – 195, 1978.
- [266] Marshall L. Snyder and Herman C. Lichstein. Sodium azide as an inhibiting substance for Gram-negative bacteria. *The Journal of Infectious Diseases*, 67(2):113–115, 1940.
- [267] Herman C. Lichstein and Malcolm H. Soule. Studies of the effect of sodium azide on microbic growth and respiration: I. the action of sodium azide on microbic growth. *Journal of Bacteriology*, 47(3):221–230, 1944.
- [268] Daniel Baron, Edward LaBelle, Dan Coursolle, Jeffrey A. Gralnick, and Daniel R. Bond. Electrochemical measurement of electron transfer kinetics by *Shewanella oneidensis* mr-1. *Journal of Biological Chemistry*, 284(42):28865–28873, 2009.
- [269] Jared N. Roy, Sofia Babanova, Kristen E. Garcia, Jose Cornejo, Linnea K. Ista, and Plamen Atanassov. Catalytic biofilm formation by *Shewanella oneidensis* mr-1 and anode characterization by expanded uncertainty. *Electrochimica Acta*, 126(0):3 – 10, 2014.
- [270] Deboleena Chakraborty and Scott Calabrese Barton. Influence of mediator redox potential on fuel sensitivity of mediated laccase oxygen reduction electrodes. *Journal of The Electrochemical Society*, 158(4):B440, 2011.
- [271] Paul Kavanagh and Donal Leech. Mediated electron transfer in glucose oxidising enzyme electrodes for application to biofuel cells: recent progress and perspectives. *Physical Chemistry Chemical Physics*, 15(14):4859–4869, 2013.
- [272] James K. Fredrickson, Margaret F. Romine, Alexander S. Beliaev, Jennifer M. Auchtung, Michael E. Driscoll, Timothy S. Gardner, Kenneth H. Nealson, Andrei L. Osterman, Grigoriy Pinchuk, Jennifer L. Reed, Dmitry A. Rodionov, Jorge L. M. Rodrigues,

- Daad A. Saffarini, Margrethe H. Serres, Alfred M. Spormann, , Igor B. Zhulin, and James M. Tiedje. Towards environmental systems biology of *Shewanella*. *Nature Reviews Microbiology*, 6(8):592–603, 2008.
- [273] Hirosuke Tatsumi, Hiroshi Nakase, Kenji Kano, and Tokugi Ikeda. Mechanistic study of the autoxidation of reduced flavin and quinone compounds. *Journal of Electroanalytical Chemistry*, 443(2):236 – 242, 1998.
- [274] M.E. Lai and A. Bergel. Electrochemical reduction of oxygen on glassy carbon: catalysis by catalase. *Journal of Electroanalytical Chemistry*, 494(1):30 – 40, 2000.
- [275] Dulcecleide B Freitas, Mariana P Reis, Leandro M Freitas, Paulo S Assis, Edmar Chartone-Souza, and Andrea MA Nascimento. Molecular bacterial diversity and distribution in waste from a steel plant. *Canadian journal of microbiology*, 54(12):996–1005, 2008.
- [276] Hong Liu, Shaoan Cheng, and Bruce E Logan. Power generation in fed-batch microbial fuel cells as a function of ionic strength, temperature, and reactor configuration. *Environmental science & technology*, 39(14):5488–5493, 2005.
- [277] A Larrosa-Guerrero, K Scott, IM Head, F Mateo, A Ginesta, and C Godinez. Effect of temperature on the performance of microbial fuel cells. *Fuel*, 89(12):3985–3994, 2010.
- [278] Ioannis Ieropoulos, Chris Melhuish, and John Greenman. Artificial gills for robots: Mfc behaviour in water. *Bioinspiration & biomimetics*, 2(3):S83, 2007.
- [279] Falk Harnisch and Uwe Schröder. Selectivity versus mobility: separation of anode and cathode in microbial bioelectrochemical systems. *ChemSusChem*, 2(10):921–926, 2009.
- [280] Wen-Wei Li, Guo-Ping Sheng, Xian-Wei Liu, and Han-Qing Yu. Recent advances in the separators for microbial fuel cells. *Bioresource Technology*, 102(1):244–252, 2011.
- [281] AD Pethybridge, JDR Talbot, and WA House. Precise conductance measurements on dilute aqueous solutions of sodium and potassium hydrogenphosphate and dihydrogenphosphate. *Journal of solution chemistry*, 35(3):381–393, 2006.